

DISSERTATION

CHARACTERIZING FLOW RESISTANCE IN HIGH GRADIENT MOUNTAIN
STREAMS, FRASER EXPERIMENTAL FOREST, COLORADO

Submitted by

Gabrielle Catherine Leila David

Department of Geosciences

In partial fulfillment of the requirements

For the degree of Doctor of Philosophy

Colorado State University

Fort Collins, Colorado

Spring 2011

Doctoral Committee:

Advisor: Ellen Wohl

Brian P. Bledsoe

Daniel Cenderelli

Sandra Ryan-Burkett

ABSTRACT

CHARACTERIZING FLOW RESISTANCE IN HIGH GRADIENT MOUNTAIN STREAMS, FRASER EXPERIMENTAL FOREST, CO

High gradient mountain streams dissipate energy when water flows over poorly sorted grains in the bed and banks and over bedforms such as steps and pools, creating a constant alternation between supercritical and subcritical flow and causing energy dissipation through hydraulic jumps. Mountain streams (bed slope ranging between 0.02 and 0.19) differ from their low gradient counterparts by having large boulders that are of the same order of magnitude as the depth of flow, low values of relative grain submergence (R_h/D_{84} , where R_h is hydraulic radius and D_{84} is the 84th percentile of the cumulative grain-size distribution), armored beds, and wood that commonly spans the entire width of the channel. The complex interaction of the different forms of flow resistance in steep mountain streams has made it particularly challenging to quantify flow resistance, usually represented by the dimensionless Darcy-Weisbach friction factor (ff). This research focuses on studying controls and interactions among different forms of resistance in step-pool, cascade, and plane-bed reaches on two different streams, where a reach is a length of channel 10^0 - 10^1 m in length with consistent channel morphology. The project is divided into three parts: 1) identify specific controls on the total flow resistance throughout the channel network using statistical analysis; 2) investigate specific variations and controls in relation to stage within each reach by analyzing at-a-

station hydraulic geometry; and 3) quantify and evaluate interactions among the individual flow resistance components that contribute to total flow resistance.

Detailed channel and water surface surveys were conducted on 15 mountain stream reaches (nine step-pool channels, five cascade channels, and one plane-bed channel) using a tripod-mounted Light Detection and Ranging (LiDAR) scanner and laser theodolite. Reach-average velocities were measured at varying discharges with dye tracers and fluorometers. Results indicate that gradient is a dominant control for both total ff and the individual components of ff , which were divided into grain (ff_{grain}), form (ff_{step}), wood (ff_{wood}), and spill resistance (ff_{spill}). A second strong control on values of ff was discharge, with values of ff decreasing with increasing discharge. Spill and form resistance contributed the greatest amount towards total ff at low flows, whereas wood contributed a larger proportion at high discharges. The contribution of grain resistance was small at all flows, but generally decreased with increasing discharge. Methods for calculating the components of resistance were found to have large sources of error. Grain resistance was typically under-estimated at lower discharges, because methods assuming a semi-logarithmic velocity profile become invalid at base flows. A new method of calculating grain resistance is suggested for lower flows, by dividing the characteristic grain size between those elements that protrude above the water surface (D_{90}) and those that are still submerged (D_{50}).

Methods for calculating wood resistance were also found to have high sources of error and cause the values of ff_{wood} to be overestimated. An attempt is made to calculate form resistance created by adverse pressure gradients around the step bedforms at high flows. Commonly, this effect is ignored in favor of lumping the remaining component of

resistance into spill resistance. Although spill resistance still made up the largest amount of the total at the lowest flows, ff_{step} made a significant contribution at bank-filling discharges and further work in the flume and field needs to be done to understand the contribution of form drag around steps. Interactions between components of resistance also indicate that an additive method of resistance partitioning is not appropriate in these higher gradient streams.

Wood significantly affected the values of flow resistance throughout each channel type. The presence of wood increased resistance within each reach. Steps with wood are significantly wider and have greater drop heights than boulder steps. Wood also was significantly related to grain resistance, causing values of ff_{grain} to be smaller than in reaches without wood. The increase in resistance from wood, as well as the larger steps, caused reduced velocity, increased depth and therefore decreased ff_{grain} .

The detailed analysis of these high gradient reaches shows the large amount of complexity inherent in these channel types, which makes developing predictive equations of ff difficult. This analysis was undertaken to better understand the complexity and to help in determining appropriate methods for calculating ff . The dominance of gradient as a control on both total ff and its components is useful to understand because this is a metric that can be used to remotely predict these characteristics, as the resolution of remote data improves with time.

ACKNOWLEDGMENTS

I have many people to thank for their patience and help as I worked on my dissertation. First, I would like to thank my advisor, Ellen Wohl, for her constant patience and magical ability to read and review papers in a few hours. I would like to thank my committee, Dan Cenderelli, Sandra Ryan-Burkett, Brian Bledsoe for their constant flexibility in setting new defense dates. I would also like to thank the Forest Service for logistical support and NSF for fiscal support.

Steve Yochum was my research partner and provided constant support and advice both in the field and in the lab. I would like to thank him for spending long hours in the field setting survey-grade GPS points and collecting the LiDAR data, as well as spending time in the lab cleaning up point-clouds and developing a method and spreadsheets for calculating cross-section data. It was extraordinarily helpful to have someone to share the data processing with and to split the fieldwork up with.

I would like to thank my parents for their constant support through this process. Both have helped keep me afloat while I remained in grad school. I want to thank my father for helping me buy a house, so that I could live comfortably in one location while I remained in Fort Collins. I would like to thank my mom for helping me maintain my sanity by bringing me on extraordinary river trips on the Colorado River in the Grand Canyon.

I want to thank everyone that helped with fieldwork including Lina Polvi and Dan Dolan. I especially want to thank Dan Cadol who followed me up into the field one fall when I had a broken back and carried and hammered rebar into all of our reaches. Dan has also been a constant source of advice and has often helped in developing particular

methods in the lab. Dan and I both started our masters together here at CSU and continued through to our PhDs, so I want to thank him for always being such a good friend and for helping me through many difficult situations, including field work.

I want to thank my cats, Nicholas (who is no longer with me) and Jack and Emerson, who sat on my lap while I worked and attempted to eat my papers.

Most importantly, I want to thank my boyfriend Mark Hussey, who has put up with more than can be recounted here. Mark played an essential role as field assistant for two summers, as well as helping to keep me fed while I constantly worked on my dissertation. Mark helped keep me focused and provided me with constant and much needed support.

TABLE OF CONTENTS

CHAPTER 1	INTRODUCTION	1
1.1	STUDY OBJECTIVES.....	4
CHAPTER 2	BACKGROUND.....	6
2.1	CURRENT METHODS OF PREDICTING FLOW RESISTANCE.....	6
2.2	AT-A-STATION HYDRAULIC GEOMETRY	9
2.3	PARTITIONING.....	12
2.4	GRAIN RESISTANCE (FF_{GRAIN})	15
2.5	STEP (FF_{STEP}) AND SPILL RESISTANCE (FF_{SPILL}).....	19
2.6	WOOD RESISTANCE (FF_{WOOD})	22
2.7	OTHER FORMS OF RESISTANCE.....	25
CHAPTER 3	FIELD METHODS.....	26
3.1	SITE DESCRIPTION	26
3.2	FIELD METHODS	32
CHAPTER 4	CONTROLS ON SPATIAL VARIATIONS IN FLOW RESISTANCE ALONG STEEP MOUNTAIN STREAMS	36
4.1	ABSTRACT	36
4.2	INTRODUCTION	37
4.3	STATISTICAL METHODS	43
4.4	RESULTS	45
4.4.1	<i>Friction factor, gradient, relative submergence, wood load, channel type and drainage basin (H1 and H2).....</i>	<i>45</i>
4.4.2	<i>Friction factor and standard deviation of bed elevation (H2).....</i>	<i>53</i>
4.4.3	<i>Friction factor and channel type (H2).....</i>	<i>53</i>
4.4.4	<i>Friction factor, gradient and channel type (H3)</i>	<i>54</i>
4.4.5	<i>Friction factor, relative grain submergence and channel type (H4).....</i>	<i>56</i>
4.4.6	<i>Friction factor, relative grain submergence, wood load, gradient and dimensionless unit discharge for each channel type (H5).....</i>	<i>57</i>
4.5	DISCUSSION	61
4.5.1	<i>Gradient, dimensionless unit discharge, flow period, wood load and friction factor.....</i>	<i>61</i>
4.5.2	<i>Relative grain submergence, dimensionless unit discharge, standard deviation of bed elevation, relative step submergence and Darcy-Weisbach Friction Factor.....</i>	<i>69</i>
4.5.3	<i>Channel type and friction factor.....</i>	<i>74</i>
4.5.4	<i>Other sources of variability.....</i>	<i>78</i>
4.6	CONCLUSION.....	78
CHAPTER 5	CONTROLS ON AT-A-STATION HYDRAULIC GEOMETRY RELATIONSHIPS IN STEEP HEADWATER STREAMS	81
5.1	ABSTRACT	81
5.2	INTRODUCTION	82
5.3	STATISTICAL METHODS	89
5.4	RESULTS	92
5.4.1	<i>Summary of At-A-Station Hydraulic Geometry</i>	<i>96</i>
5.4.2	<i>Channel Type and At-A-Station Hydraulic Geometry</i>	<i>100</i>
5.4.3	<i>Potential Controls on At-A-Station Hydraulic Geometry.....</i>	<i>101</i>
5.5	DISCUSSION	109

5.5.1	<i>At-a-station hydraulic geometry and flow resistance</i>	111
5.5.2	<i>Hydraulic exponents vs. gradient</i>	121
5.5.3	<i>Problems with using reach-averaged hydraulic geometry</i>	121
5.6	CONCLUSION.....	122
CHAPTER 6 COMPARITIVE ANALYSIS OF BED RESISTANCE PARTITIONING IN HIGH GRADIENT STREAMS		124
6.1	ABSTRACT	124
6.2	INTRODUCTION	125
6.3	METHODS.....	136
6.3.1	<i>Field Methods</i>	136
6.3.2	<i>Partitioning Methods</i>	138
6.3.3	<i>Grain Resistance</i>	140
6.3.4	<i>Wood Resistance (ff_{wood})</i>	143
6.3.5	<i>Form Resistance (ff_{step})</i>	146
6.4	RESULTS	149
6.4.1	<i>Grain Resistance, ff_{grain}</i>	149
6.4.2	<i>Wood Resistance, ff_{wood}</i>	160
6.4.3	<i>Step Resistance, ff_{step} and ff_{spill}</i>	162
6.4.4	<i>Limitations in calculating total and component resistance in steep streams</i>	164
6.4.5	<i>Overview of total and component resistance</i>	180
6.4.6	<i>Relationship of ff_{grain}, ff_{spill}, and ff_{step} to Q, and S_o, and wood as well as interrelationship between components</i>	186
6.5	DISCUSSION	189
6.5.1	<i>Methods for calculating ff_{grain} and associated limitations</i>	190
6.5.2	<i>Methods for calculating ff_{wood} and associated limitations</i>	197
6.5.3	<i>Methods for calculating ff_{step} and associated limitations</i>	199
6.5.4	<i>Methods for calculating ff_{total} and associated limitations</i>	201
6.5.5	<i>Relationships between ff_{grain}, ff_{wood}, ff_{step}, and ff_{spill} and potential control variables</i>	201
6.6	CONCLUSION.....	204
CHAPTER 7 CONCLUSIONS		207
7.1	SUGGESTIONS FOR FUTURE RESEARCH	212
CHAPTER 8 REFERENCES		216
CHAPTER 9 APPENDICES.....		226
9.1	APPENDIX A: REACH-AVERAGE VALUES OF CHANNEL AND HYDRAULIC VARIABLE FOR EACH REACH AT EACH FLOW	227
9.2	APPENDIX B: GAGE FLOW DATA	230
9.3	APPENDIX C: DETAILED PICTURES AND DESCRIPTIONS OF EACH REACH	234
9.4	APPENDIX D: GRAIN SIZE DISTRIBUTION GRAPHS FOR EACH REACH	249
9.5	APPENDIX E: IN-CHANNEL WOOD PHOTOGRAPHS AND LOCATION IN EACH REACH.....	258
9.6	APPENDIX F: PLAN VIEW OF EACH REACH SHOWING LOCATION OF LARGE BOULDERS AND COBBLES USED TO CALCULATE FF_{GRAIN} WITH THE DRAG APPROACH.....	276
9.7	APPENDIX F: LONGITUDINAL PROFILES AND PLAN VIEW OF THALWEG FOR EAST ST. LOUIS, LOWER FOOL CREEK, AND UPPER FOOL CREEK.....	290

LIST OF TABLES

TABLE 1: DRAINAGE BASIN INFORMATION FOR EAST ST. LOUIS (ESL), UPPER FOOL CREEK (UFC) AND LOWER FOOL CREEK (LFC)	26
TABLE 2: DESCRIPTION OF THALWEG LENGTH, L_r , GRADIENT, S_0 , AVERAGE CROSS-SECTIONAL AREA, A , AVERAGE HYDRAULIC RADIUS, R_H , STEP STEEPNESS, H/L_s , PARTICLE SIZE, D_{50} AND D_{84} , AVERAGE VELOCITY, V , AVERAGE DISCHARGE, Q , DIMENSIONLESS UNIT DISCHARGE, Q^* , FROUDE NUMBER, FR, REYNOLDS NUMBER, RE AND DARCY-WEISBACH FRICTION FACTOR, FF FOR EACH REACH. VALUES ON TOP ARE MINIMUM VALUES AND VALUES ON BOTTOM ARE MAXIMUM VALUES OVER THE FOUR FLOW PERIODS. A MINIMUM SLOPE VALUE DOES NOT NECESSARILY CORRELATE WITH A MINIMUM F VALUE. SEE APPENDIX A FOR FULL TABLE.....	30
TABLE 3: LINEAR REGRESSIONS OF $(8/F)^{0.5}$ AND FF VERSUS INDEPENDENT VARIABLES AND CATEGORICAL VARIABLES. MODELS 1 – 4B AND 6 – 12 USE $(8/F)^{0.5}$ AS THE DEPENDENT VARIABLE. MODELS 5A – 5B USE FF AS THE DEPENDENT VARIABLE. THE NUMBERS IN EACH COLUMN UNDER THE MODEL NUMBER SHOWS WHICH VARIABLES WERE USED IN EACH REGRESSION. THE MALLOW'S CP IS NOT SHOWN FOR REGRESSIONS THAT HAD OUTLIERS REMOVED.	47
TABLE 4: LINEAR REGRESSIONS OF $(8/F)^{0.5}$ AND FF VERSUS INDEPENDENT VARIABLES SEPARATED BY CHANNEL TYPE. MODEL 13 – 15 ONLY INCLUDE CASCADE REACHES. MODEL 16 – 19 ONLY INCLUDE STEP-POOL REACHES.	60
TABLE 5: SUMMARY TABLE SHOWING SIGNIFICANT REACH AVERAGED VALUES FOR EACH REACH.	91
TABLE 6: SUMMARY TABLE SHOWING THE POWER RELATIONSHIPS BETWEEN Q VS. w ($w = aQ^b$), Q VS. d ($d = cQ^f$), Q VS. v ($v = kQ^m$), AND Q VS. FF ($ff = oQ^x$). THE MINIMUM AND MAXIMUM VALUES OF $w:d$, FF , AND R_H/D_{84} THAT WERE FOUND OVER THE FOUR FLOW PERIODS OF MEASUREMENT. THE NUMBER OF CROSS-SECTIONS USED TO DETERMINE AVERAGE VALUES FOR WIDTH AND DEPTH ARE ALSO SHOWN. THE NUMBER OF CROSS-SECTIONS VARIED BASED ON REACH LENGTHS. FOR ALL THE MEASURED VALUES FROM EACH FLOW PERIOD SEE APPENDIX A.	98
TABLE 7: RESULTS OF BEST SUBSETS REGRESSIONS FOR PCA AXIS 1 SCORES, THE VELOCITY EXPONENT (M) AND FRICTION EXPONENT (X) VERSUS SIGNIFICANT EXPLANATORY VARIABLES. THERE WERE NO SIGNIFICANT REGRESSIONS FOUND USING THE WIDTH AND DEPTH EXPONENTS.....	99
TABLE 8: CORRELATION MATRIX SHOWING CORRELATIONS AMONG FOUR VARIABLES: D_{84} , WOOD VOLUME PER CHANNEL AREA, POOL VOLUME PER CHANNEL AREA, AND GRADIENT.....	108
TABLE 9: MINIMUM AND MAXIMUM VALUES USED FOR EACH LOG IN EACH REACH.....	145
TABLE 10: REGRESSION FOR FF_{TOTAL} VS. FF_{GRAIN} . REGRESSED AGAINST SQRT (FF_{TOTAL}) TO MEET NORMALITY ASSUMPTIONS (DF = 53). FC3 JULY 2008 WAS AN OUTLIER AND REMOVED FROM REGRESSION. ADDITIONALLY FC3 AUGUST 2007 AND FC6 AUGUST 2007 WERE FOUND TO BE OUTLIERS FOR PARKER AND PETERSON EQUATION AND REMOVED FROM THOSE REGRESSIONS. PARKER AND PETERSON = 51 DF. $A = 0.05$ **; $A = 0.10$ *	156
TABLE 11: EACH GRAIN RESISTANCE EQUATION VS. F_{DRAG} . ESL3 AND ESL4 OUTLIERS FOR BATHURST (TREAD). ESL4 REMOVED AS OUTLIER IN KEULEGAN (ST). IN EVERY REGRESSION ESL3, ESL4 AND FC4 SEEM TO HAVE HIGHER LEVERAGE THAN OTHER REACHES. FOR AUGUST 2007 REGRESSIONS ESL9 AND FC6 WERE OUTLIERS.....	156
TABLE 12: LINEAR REGRESSION OF FF_{TOTAL} VS. FF_{STEP1} FOR JUNE 2008 FLOWS. THE RELATIONSHIP IS A POWER FUNCTION WITH 10 DEGREES OF FREEDOM.	164
TABLE 13: MULTIPLE REGRESSION FOR LOG (FF), 52 DF.	169
TABLE 14: MULTIPLE REGRESSION FOR FF_{GRAIN} , N=59, DF = 55, DISCHARGE LOG TRANSFORMED TO MEET NORMALITY ASSUMPTIONS.	186
TABLE 15: LINEAR REGRESSION FOR FF_{STEP1} VS. WOOD DENSITY (WOOD SURFACE AREA/REACH SURFACE AREA).	187
TABLE 16: MULTIPLE REGRESSION OF FF_{STEP1} . REACHES WITHOUT STEPS ARE EXCLUDED (ESL6, ESL7) AND ESL3	187
TABLE 17: MULTIPLE REGRESSION FOR FF_{SPILL} (ALL REACHES INCLUDED, N=59)	187
TABLE 18: MULTIPLE REGRESSION WITH FF_{WOOD} (ALL REACHES INCLUDED, N=59)	188
TABLE 19: SUMMARY OF CHANNEL AND HYDRAULIC VARIABLES USED FOR EACH REACH, WHERE L_r = REACH LENGTH; S_0 = BED GRADIENT; A = CROSS-SECTIONAL AREA; R = HYDRAULIC RADIUS; L_s = STEP	

LENGTH; D_{50} = GRAIN SIZE IN WHICH 50% IS SMALLER; D_{84} = GRAIN SIZE IN WHICH 84% ARE SMALLER; V = REACH-AVERAGE VELOCITY; Q = DISCHARGE; U^* = SHEAR VELOCITY; Fr = FROUDE NUMBER; Re = REYNOLDS NUMBER; FF = DARCY-WEISBACH FRICTION FACTOR.....227

TABLE 20: SUMMARY TABLE FOR WOOD: NO. CYL = NUMBER OF PIECES COUNTED IN EACH REACH AS AN INDIVIDUAL CYLINDER THAT INFLUENCES ROUGHNESS; L_w = AVERAGE LENGTH OF INDIVIDUAL CYLINDERS IN EACH REACH; D_w = AVERAGE DIAMETER OF INDIVIDUAL CYLINDERS; V_T = TOTAL VOLUME OF WOOD COUNTING BOTH WOOD AS INDIVIDUAL PIECES AND WOOD IN STEPS; V_c = TOTAL VOLUME OF INDIVIDUAL CYLINDERS IN EACH REACH; V_{WS} = TOTAL VOLUME OF WOOD IN STEPS IN EACH REACH; % STEPS = PERCENT OF WOOD IN STEPS; % CYL. = PERCENT OF WOOD AS INDIVIDUAL CYLINDERS; FF_{WOOD} = PARTITIONED FRICTION FACTOR FOR WOOD (ONLY USING WOOD AS INDIVIDUAL CYLINDERS IN EACH REACH).....273

LIST OF FIGURES

FIGURE 1: LOCATION MAP FOR EAST ST. LOUIS AND FOOL CREEK IN FRASER EXPERIMENTAL FOREST	27
FIGURE 2: PHOTOGRAPH OF A STEP-POOL, CASCADE REACH IN EACH BASIN AND THE PLANE-BED REACH IN ESL: A) STEP-POOL REACH ON EAST ST. LOUIS CREEK (ESL4) DURING AUGUST 2007 SURVEY; B) STEP-POOL REACH ON LOWER FOOL CREEK (FC3) DURING JULY 2008 SURVEY; C) CASCADE REACH ON UPPER FOOL CREEK (FC5) DURING AUGUST 2007 SURVEY; D) CASCADE REACH ON EAST ST. LOUIS (ESL3) DURING AUGUST 2007 SURVEY; E) PLANE-BED REACH ON EAST ST. LOUIS (ESL6) DURING JUNE 2008 SURVEY.....	31
FIGURE 3: EXAMPLE OF THE RESULTS OF A LIDAR SCAN OF ESL9. THE ARROW IS POINTING TO THE SAME LOG ON THE PHOTOGRAPH (LEFT) AND THE POINT CLOUD (RIGHT). THE PHOTOGRAPH AND SCAN IMAGE ARE BOTH SHOWING A WOOD STEP IN ESL9.....	34
FIGURE 4: $(8/F)^{0.5}$ VERSUS GRADIENT (S_0) FOR EACH CHANNEL TYPE: A) SHOWS TREND LINE AND POINTS FOR AUGUST 2007 FLOW FOR CASCADE AND STEP-POOL CHANNELS; B) SHOWS TREND LINES AND POINTS FOR JULY 2007 AND 2008 FLOWS FOR CASCADE AND STEP-POOL CHANNELS; C) SHOWS TREND LINE AND POINTS FOR JUNE 2008 FLOW FOR CASCADE AND STEP-POOL CHANNELS.	48
FIGURE 5: BOX-PLOTS OF FF VERSUS CHANNEL TYPE (A) AND FF VERSUS CHANNEL TYPE FOR EACH BASIN (B). THE CONTRASTING LETTERS (A AND B) ABOVE THE BOXES SHOW THE RESULTS OF THE SIGNIFICANT ($P <$ 0.05) PAIRWISE DIFFERENCES IN MEANS FROM TUKEY'S TEST FOLLOWING AN ANOVA. BOX-PLOTS WITH THE SAME LETTER DO NOT HAVE SIGNIFICANTLY DIFFERENT MEANS, BOX-PLOTS WITH DIFFERENT LETTERS DO HAVE SIGNIFICANTLY DIFFERENT MEANS.....	51
FIGURE 6: COMPARISON OF THE AUGUST 2007 (LOW) FLOW PERIOD AND JUNE 2008 (HIGH) FLOW PERIOD IN THE STEP-POOL REACHES FC3 AND ESL4. THE LONGITUDINAL PROFILES ARE SHOWN FOR EACH LOW FLOW AND HIGH FLOW SURVEY FOR EACH REACH. THE PHOTOGRAPHS AND GRAPHS SHOW THE DIFFERENCES IN DEPTHS AND RELATIVE SUBMERGENCE AT THE TWO FLOWS FOR EACH REACH.	52
FIGURE 7: BOX-PLOTS OF GRADIENT VERSUS CHANNEL TYPE (A) AND GRADIENT VERSUS CHANNEL TYPE AND BASIN (B). THE LETTERS A, B, C AND D OVER EACH BOXPLOT SHOW THE RESULTS OF THE TUKEY'S TEST FOLLOWING AN ANOVA. BOX-PLOTS WITH THE SAME LETTER DO NOT HAVE SIGNIFICANTLY DIFFERENT MEANS ($P > 0.05$), BOX-PLOTS WITH DIFFERENT LETTERS DO HAVE SIGNIFICANTLY DIFFERENT MEANS ($P < 0.05$).	55
FIGURE 8: BOX-PLOTS OF RELATIVE GRAIN SUBMERGENCE (R_H/D_{84}) VERSUS CHANNEL TYPE (A) AND RELATIVE GRAIN SUBMERGENCE VERSUS CHANNEL TYPE AND BASIN (B). THE LETTERS A, B AND C OVER EACH BOXPLOT SHOW THE RESULTS OF THE TUKEY METHOD FOLLOWING AN ANOVA. BOX-PLOTS WITH THE SAME LETTER DO NOT HAVE SIGNIFICANTLY DIFFERENT MEANS, BOX-PLOTS WITH DIFFERENT LETTERS DO HAVE SIGNIFICANTLY DIFFERENT MEANS ($P < 0.05$).	58
FIGURE 9: A) RELATIVE GRAIN SUBMERGENCE VERSUS $(8/F)^{0.5}$ FOR EACH CHANNEL TYPE. TRENDLINE SHOWS RELATIONSHIP BETWEEN RELATIVE SUBMERGENCE AND FRICTION FACTOR FOR ALL SITES (EXCLUDING ESL6, THE PLANE-BED REACH). B) RELATIVE GRAIN SUBMERGENCE VERSUS FRICTION FACTOR FOR CASCADE REACHES.	59
FIGURE 10: TWO CASCADE REACHES AT LOW (AUGUST 2007) AND HIGH (JUNE 2008) FLOWS. ARROWS POINT TO THE SAME LOCATION ON BOTH IMAGES. IMAGES SHOW THAT AT HIGH FLOW THE MAJORITY OF GRAINS ARE SUBMERGED IN FC6 WHILE IN ESL7 THE LOCATION OF THE GRAINS IS STILL VISIBLE. .	63
FIGURE 11: PREDICTED VERSUS OBSERVED $(8/F)^{0.5}$ FOR A) MODEL 7 (S_0) ; B) MODEL 8 (R/D_{84}) ; C) MODEL 9 (Q^*); D) MODEL 5A (Q^* , S_0 AND CHANNEL TYPE).	66
FIGURE 12: WOOD LOAD VERSUS S_0 FOR STEP-POOL AND CASCADE CHANNEL TYPES. REACHES IN OVAL ARE LINEARLY CORRELATED WITH S_0 EXCEPT FOR ESL2.....	72
FIGURE 13: EXAMPLE OF A ROUGH CROSS-SECTION AND SIMPLIFIED CROSS-SECTION FOR ESL2. THE SHADED AREA IS THE ROUGHNESS AREA, USED IN THE STATISTICAL ANALYSIS.	87
FIGURE 14: AT-A-STATION HYDRAULIC GEOMETRY OF EACH REACH. THE POWER RELATIONSHIPS BETWEEN DISCHARGE AND VELOCITY (M), DEPTH (F), WIDTH (B) AND THE DARCY-WEISBACH FRICTION FACTOR (X).....	93
FIGURE 15: AT-A-STATION HYDRAULIC GEOMETRY OF EACH CASCADE REACH AND THE PLANE-BED REACH (ESL6). THE POWER RELATIONSHIPS BETWEEN DISCHARGE AND VELOCITY (M), DEPTH (F), WIDTH (B) AND THE DARCY-WEISBACH FRICTION FACTOR (X) ARE SHOWN ON EACH GRAPH.	94

FIGURE 16: $B - F - M$ TERNARY DIAGRAMS, SHOWING STEP-POOL AND CASCADE REACHES IN COMPARISON TO REID'S (2005) STUDY (A); SHOWING WHERE REACHES WITH PARTICULAR RATES OF CHANGE OF THE DARCY-WEISBACH FRICTION FACTOR (x) PLOT (B); SHOWING WHERE REACHES WITH A PARTICULAR COEFFICIENT OF VARIATION OF R_H/D_{84} PLOT (C); SHOWING WHERE REACHES WITH A PARTICULAR WIDTH:DEPTH RATIO PLOT (D). 95

FIGURE 17: PRINCIPAL COMPONENT ANALYSIS (PCA) OF ALL REACHES USING M , F , AND B . THE SHADED AREA SHOWS THE REACHES THAT HAVE THE MOST SIMILAR CHARACTERISTICS BOTH IN THE TERNARY DIAGRAM AND ARE INTERPRETED TO BE DOMINATED BY GRAIN RESISTANCE. 102

FIGURE 18: BOXPLOTS SHOWING THE RANGE OF VALUES OF THE WIDTH EXPONENTS (B) FOR STEP-POOL AND CASCADE REACHES (A); THE RANGE OF VALUES FOR THE VELOCITY EXPONENTS (M) FOR STEP-POOL AND CASCADE REACHES (B); THE RANGE OF VALUES FOR THE DEPTH EXPONENTS (F) FOR STEP-POOL AND CASCADE REACHES (C); AND THE RANGE OF VALUES FOR THE FRICTION FACTOR EXPONENTS (x) FOR STEP-POOL AND CASCADE REACHES (D). THE LETTERS A AND B ABOVE THE BOXES SHOW THE RESULTS OF THE ANOVA AND TUKEY HSD TEST. IF THE SAME LETTERS ARE ABOVE THE BOXES THEN THE AVERAGE VALUE OF THE EXPONENTS FOR THOSE TWO CHANNEL TYPES ARE NOT SIGNIFICANTLY DIFFERENT FROM EACH OTHER, IF DIFFERENT LETTERS ARE ABOVE THE BOXES THEN THEY ARE SIGNIFICANTLY DIFFERENT FROM EACH OTHER. 103

FIGURE 19: THE PCA AXIS 1 SCORES AGAINST THE DARCY-WEISBACH FRICTION FACTOR EXPONENT (x) DIVIDED BY DRAINAGE BASINS (LEFT) AND CHANNEL TYPE (RIGHT). 106

FIGURE 20: PCA AXIS 1 SCORES VERSUS AVERAGE ROUGHNESS AREA (A), COEFFICIENT OF VARIATION OF R_H/D_{84} (B), COEFFICIENT OF VARIATION OF POOL VOLUME (C), AND WOOD VOLUME PER CHANNEL AREA (D) FOR THE TWO DRAINAGE BASINS (EAST ST. LOUIS AND FOOL CREEK). 107

FIGURE 21: BARPLOTS SHOWING VALUES FOR EACH REACH OF WOOD VOLUME PER CHANNEL AREA (A), BED GRADIENT (B), D_{84} (C), AND POOL VOLUME PER CHANNEL AREA (D). 108

FIGURE 22: EXAMPLE OF LONGITUDINAL PROFILE AND CROSS-SECTION OF ESL2. THE LONGITUDINAL PROFILE SHOWS BOTH THE BED PROFILE AND WATER SURFACE WITH FITTED LINEAR TREND LINES AND EQUATIONS SHOWN FOR BOTH. THE PHOTOGRAPH IN THE BOTTOM LEFT SHOWS THE ENTIRE REACH, LOOKING UPSTREAM DURING THE JUNE 2008 HIGH FLOW. THE CROSS-SECTION SHOWS THE WATER SURFACE AT THREE STAGES (AUGUST 2007, JULY 2008, JUNE 2008). THE PHOTOGRAPH ON THE BOTTOM RIGHT SHOWS THE APPROXIMATE LOCATION OF THE CROSS-SECTION AT AUGUST 2007 LOW FLOW. 117

FIGURE 23: PHOTOGRAPHS AND CROSS-SECTIONS FOR THREE CASCADE REACHES: FC5, FC6 AND ESL7. THE WHITE ARROWS SHOW THE SAME LOCATION IN EACH PHOTOGRAPH AND THE PHOTOGRAPHS ARE OF THE APPROXIMATE LOCATION OF EACH OF THE CROSS-SECTIONS SHOWN AT THE RIGHT. THE CROSS-SECTIONS SHOW THE WATER SURFACE OVER THREE FLOW PERIODS (AUGUST 2007, JULY 2008 AND JUNE 2008) FOR FC5 AND FC6 AND JUNE 2008 AND JULY 2008 FOR ESL7. 118

FIGURE 24: PCA AXIS 1 SCORES VERSUS WOOD VOLUME PER CHANNEL AREA (LEFT) AND $\log(D_{84}/D_{50})$ (RIGHT). THE REACHES ARE DIVIDED BY THOSE INTERPRETED TO BE DOMINATED BY GRAIN RESISTANCE (OPEN CIRCLES) AND THOSE THAT ARE DOMINATED BY FORM AND SPILL RESISTANCE (CLOSED CIRCLES). 120

FIGURE 25: EXAMPLE OF LARGE AND SMALL BOULDER STEPS IN ESL4 AND FC1. EXAMPLE OF WHAT IS CHARACTERIZED AS A WOOD1 STEP IN ESL1 AND A WOOD2 STEP IN FC3. 137

FIGURE 26: EXAMPLE OF WOOD AS INDIVIDUAL PIECE (1) AND WOOD AS PART OF STEP (2). LEFT IS A PLANFORM VIEW OF ESL1 SHOWING INDIVIDUAL WOOD PIECE (1) AND WOOD JAM THAT IS PART OF A STEP (2). ALL PICTURES ARE LOOKING UPSTREAM EXCEPT FOR THE TOP RIGHT PHOTO. YELLOW ARROWS ARE POINTING TO THE SAME LOCATION IN PHOTOS GOING FROM LEFT TO RIGHT. 144

FIGURE 27: SCHEMATIC OF A WOOD AND BOULDER STEP-POOL REACH. 147

FIGURE 28: DIMENSIONLESS SURFACE AREA FOR EACH STEP SHOWING DIVISIONS OF THE DRAG COEFFICIENT FOR STEPS. 148

FIGURE 29: SEPARATED D_{50} AND D_{84} FOR EACH REACH, ILLUSTRATING THE RANGE IN VALUES, DEPENDING ON THE PORTION OF THE BED MEASURED. STEP D_{84} RMSE = 0.061; DOWNSTREAM POOL D_{84} RMSE = 0.079; UPSTREAM POOL D_{84} RMSE = 0.045; STEP TREAD D_{84} RMSE = 0.025. STEP D_{50} RMSE = 0.014; DOWNSTREAM POOL D_{50} RMSE = 0.018; UPSTREAM POOL D_{50} RMSE = 0.018; STEP TREAD D_{50} RMSE = 0.010. 150

FIGURE 30: SENSITIVITY ANALYSIS USING REACH D_{50} AND D_{84} VS. STEP TREAD D_{50} AND D_{84} . KEULEGAN (D_{50}) RMSE = 0.012; KEULEGAN (D_{84}) RMSE = 0.018; PARKER AND PETERSON (D_{84}) RMSE = 0.06; BATHURST (D_{84}) RMSE = 0.115. ESL4 IS THE LARGEST SOURCE OF ERROR IN EACH EQUATION. 151

FIGURE 31: PERCENT CONTRIBUTION OF EACH GRAIN RESISTANCE EQUATION OF TOTAL RESISTANCE. TOP SHOWS AUGUST 2007 (LOW) FLOWS AND BOTTOM SHOWS JUNE 2008 (HIGH) FLOWS..... 154

FIGURE 32: BOXPLOT OF GRAIN RESISTANCE EQUATIONS AGAINST STEP TYPE, FLOW PERIOD AND CHANNEL TYPE. STEP CATEGORIES: BOULDER = REACHES WITH ONLY BOULDER STEPS, MIXED = REACHES WITH BOTH WOOD AND BOULDER STEPS, NONE = REACHES WITH NO STEPS (ONLY ESL6 AND ESL7), WOOD = REACHES WITH ONLY WOOD STEPS. LOWER CASE LETTERS, A, B, AND C SHOW WHICH MEANS ARE SIGNIFICANTLY DIFFERENT FROM EACH OTHER BASED ON TUKEY HSD TEST IN AN ANOVA. 155

FIGURE 33: BOXPLOT OF STEP DIMENSIONS FOR EVERY INDIVIDUAL STEP IN EVERY REACH BASED ON STEP COMPOSITION. BOULDER = STEPS ONLY MADE UP OF LARGE GRAINS, WOOD1 = STEPS MADE UP OF A KEYSTONE BOULDER AND WOOD, WOOD2 = STEPS ONLY MADE UP OF WOOD. LOWER CASE LETTERS A AND B INDICATE WHICH MEANS ARE SIGNIFICANTLY DIFFERENT FROM EACH OTHER USING A TUKEY HSD TEST IN AN ANOVA. 159

FIGURE 34: EXAMPLE OF WOOD IN ESL 5 (A - C) AND ESL6 (D - F). A) PICTURE OF LOG IN ESL5 DURING HIGH FLOW. B AND C) PLAN VIEW OF ESL5 SHOWING LOCATION OF LOGS AND LIDAR SCAN OF ESL5. D AND E) PLAN VIEW OF ESL6 SHOWING LOGS AND LIDAR SCAN WITH MEASURED THALWEG IN THE CENTER. F) PHOTOGRAPH OF ESL6 IN JULY 2008. 161

FIGURE 35: EXAMPLE OF SENSITIVITY ANALYSIS FOR FF_{STEP} . EACH NUMBER IN THE KEY (1 - 6) INDICATES THAT A DIFFERENT DRAG COEFFICIENT WAS USED FOR EACH ITERATION. ONE IS RELATED TO THE SMALLEST VALUES OF C_D USED AND SIX ARE THE MAX VALUES. DEPENDING ON THE REACH, THE LARGER DRAG COEFFICIENTS COULD DOUBLE THE PERCENT CONTRIBUTION OF FF_{STEP} : ESL9 RANGED FROM 28 TO 52% AT HIGH FLOWS AND 18 TO 32% AT LOW FLOWS. FC3 WENT FROM 61 TO 89% AT HIGH FLOWS TO 5 TO 7% AT LOW FLOWS, FC6 GOES FROM 33 TO 66% AT HIGH AND 7 TO 14% AT LOW FLOWS. 163

FIGURE 36: EXAMPLE OF WATER SURFACE AND BED SLOPE REGRESSION LINES FOR ESL2. 165

FIGURE 37: SENSITIVITY ANALYSIS FOR CALCULATING FF_{TOTAL} . THE Y-AXIS SHOWS THE VALUES OF FF_{TOTAL} USED ALL OTHER ANALYSES, THE X-AXIS SHOWS VALUES OF FF_{TOTAL} CALCULATED USING OTHER METHODS. RMSE FOR S_o REGRESSION = 0.406; RMSE S_o CALC = 1.103; RMSE FOR S_w CALC = 1.451; RMSE STEP GRADIENT = 8.513; RMSE FOR R_{EFF} = 3.642; RMSE FOR S_f = 2.061; RMSE FOR S_w AVG = 1.263. 167

FIGURE 38: COMPARISON OF VELOCITIES MEASURED USING TRACER AND VELOCITIES CALCULATED FROM GAGE DISCHARGE. GRAY DOTTED LINE IS 1:1 LINE. RMSE FOR ALL DATA = 0.235; RMSE FOR STEP-POOL = 0.120; RMSE FOR CASCADE = 0.149; RMSE FOR PLANE-BED = 0.764. 168

FIGURE 39: FF_{GRAIN} REGRESSED AGAINST BOULDER CONCENTRATION FOR HIGH (JUNE 2008) AND LOW (AUGUST 2007) FLOWS AS A MEASURE OF EVALUATING APPLICABILITY OF EACH GRAIN RESISTANCE METHOD. BOTTOM TWO REGRESSION LINES ARE FOR KEULEGAN D_{50} , AND KEULEGAN D_{84} , RESPECTIVELY, IN EACH PLOT. TOP TWO LINES ARE FOR BATHURST AND PARKER AND PETERSON, RESPECTIVELY, FOR THE JUNE 2008 FLOWS AND THE OPPOSITE FOR THE AUGUST 2007 FLOWS. NEITHER THE PARKER AND PETERSON EQUATION NOR THE BATHURST EQUATION IS SIGNIFICANT AT THE LOWER FLOWS AT $\alpha = 0.05$. ESL3 IS EXCLUDED BECAUSE IT IS AN OUTLIER WITH A MUCH LARGER BOULDER CONCENTRATION THAN ANY OTHER REACH (~ 0.20)..... 171

FIGURE 40: FF_{GRAIN} FROM DRAG APPROACH VS. BOULDER CONCENTRATION AT AUGUST 2007 AND JUNE 2008 FLOWS (R^2 SIGNIFICANT AT THE $\alpha = 0.05$ LEVEL)..... 172

FIGURE 41: FLOW MOVING OVER BOULDERS IN A CASCADE REACH (ESL7) AT HIGH (A) AND LOW (B) FLOWS. THE SIDE AND PLAN VIEW ARE IDEALIZED VERSIONS OF HOW FLOW IS MOVING AROUND BOULDERS IN THE PHOTOGRAPH ABOVE AND DOES NOT ACTUALLY REPRESENT THE LOCATION OF BOULDERS IN ESL7. 173

FIGURE 42: DRAG COEFFICIENT VERSUS THE LOG ORIENTATION AND THE BLOCKAGE RATIO. THESE PLOTS INDICATE THAT DRAG COEFFICIENT, AS CALCULATED HERE, IS NOT SENSITIVE TO ANGLE OR BLOCKAGE RATIO. 176

FIGURE 43: SENSITIVITY ANALYSIS OF DRAG COEFFICIENT FOR CALCULATING FF_{WOOD} 179

FIGURE 44: MEASURING DISTANCE, X, BETWEEN LOGS AND OTHER OBJECTS IN ESL4. A) PLAN VIEW OF ESL4 SHOWING JUNE 2008 BANK OUTLINE AND THALWEG. THE ARROW POINTS IN THE DIRECTION OF FLOW AND THE WHITE BARS INDICATE THE LOCATION OF IN-CHANNEL WOOD. B) LIDAR SCAN OF ESL4

SHOWING THE JUNE DISTANCE (X) BETWEEN THE LOG AND THE NEXT LOG OBJECT UPSTREAM AND THE AUGUST DISTANCE (BETWEEN THE LOG AND THE BOULDER). C) PHOTOGRAPH OF JUNE 2008 FLOW IN ESL4. BLACK CIRCLE SHOWS WHERE LOG IN QUESTION IS SUBMERGED IN WATER. D) PHOTOGRAPH OF JULY 2008 FLOW; CIRCLED AREA SHOWS BOULDER AND LOG. E) AUGUST 2007 FLOW IN ESL4; CIRCLED AREA SHOWS BOULDER AND LOG.....	180
FIGURE 45: CONTRIBUTION OF PARTITIONED FRICTION FACTOR TO TOTAL. DOTTED WHITE LINES INDICATE DIVISION BETWEEN REACHES. THE FF_{SPILL} WERE MADE TO BE ZERO WHERE NEGATIVE VALUES EXISTED, BECAUSE ADDITIVE COMPONENTS EXCEEDED THE VALUE OF FF_{TOTAL} . FIGURE SHOWS PARTITIONED VALUES FOR EACH REACH OVER EACH FLOW PERIOD. A) STEP-POOL REACHES B) CASCADE REACHES AND PLANE BED REACH.....	181
FIGURE 46: BOXPLOTS OF PERCENTAGE CONTRIBUTION OF EACH COMPONENT OF RESISTANCE FOR EACH FLOW PERIOD. ESL3 IS EXCLUDED FROM THE BOXPLOTS. BOXES WITH THE SAME LETTER (A, B, C) HAVE MEANS SIMILAR AT $\alpha = 0.05$	183
FIGURE 47: BOXPLOTS SHOWING THE % OF TOTAL RESISTANCE DOMINATED BY GRAIN, WOOD, STEP AND SPILL FOR EACH CHANNEL TYPE. % FF_{STEP} HAS SIGNIFICANTLY DIFFERENT MEANS FOR CASCADE VERSUS STEP-POOL REACHES. LETTERS A AND B INDICATE SIGNIFICANTLY DIFFERENT MEANS USING TUKEY HSD TEST IN AN ANOVA.	184
FIGURE 48: BOXPLOT OF % CONTRIBUTION OF EACH PARTITIONED COMPONENT DIVIDED BY DOMINANT STEP COMPOSITION WITHIN THE REACH. BOULDER = REACH DOMINATED BY BOULDER STEPS; MIX = REACH HAS A COMBINATION OF WOOD AND BOULDER STEPS; NONE = REACH HAS NO STEPS (ONLY ESL7); WOOD = REACH ONLY HAS WOOD STEPS. ESL6 EXCLUDED FROM THESE GROUPINGS, BUT INCLUSION ONLY INCREASES DIFFERENCE BETWEEN NONE AND OTHER CATEGORIES. ESL3 IS EXCLUDED BECAUSE OF THE LARGE DEVIATION FROM FF_{TOTAL} DUE TO THE LARGE NUMBER CALCULATED FOR FF_{STEP} . BOXES WITH THE SAME LETTER (A, B, C) HAVE MEANS SIMILAR AT $\alpha = 0.05$	185
FIGURE 49: FF_{WOOD} VS. D_{84} FROM THE STEP TREAD FOR EACH FLOW PERIOD, JUNE AND JULY 08 (TOP); JULY AND AUGUST 07 (BOTTOM).	189
FIGURE 50: FC6 AT LOW (1 - 2) AND HIGH (3 -4) FLOWS. PICTURE AT TOP LEFT SHOWS REACH OUTLINE WITH SMALL LINES TO INDICATE LOCATION OF BOULDERS. ARROWS INDICATE SAME LOCATION ON EACH IMAGE. PHOTOGRAPH AND LIDAR IMAGE SHOW EXPOSURE OF MORE GRAINS AT LOW FLOWS, AS WELL AS INCREASED SINUOSITY OF THALWEG (LIGHT YELLOW LINE IN CENTER OF CHANNEL).	194
FIGURE 51: BOULDERS AND WOOD ON FC3 (1) AND ESL9 (2). BOULDERS ARE SHOWN IN WHITE AND WOOD IN GREY. BANKS AND THALWEG ALSO SHOWN IN GREY. THE $\Gamma = 0.008$ FOR FC3 AND 0.083 FOR ESL9.	196
FIGURE 52: EXAMPLES OF INDIVIDUAL PIECES OF WOOD IN THE STUDY REACHES. NOTE THAT THESE PIECES ARE ONLY IN THE FLOW DURING HIGH FLOW. A) ESL5 JUNE 2008 – LOG THAT CROSSES OVER STREAM AND CREATES A SLIGHT BACKWATER ON LEFT BANK SIDE OF LOG. B) ESL5 AUGUST 2007 – SAME LOG, BUT NOW WATER GOES COMPLETELY UNDERNEATH THE WOOD. C) ESL2 JUNE 2008 – BROKEN LOG WITH WATER CASCADING OVER THE TOP. D) ESL2 AUGUST 2007 – SAME LOG, BUT WATER NOW FLOWS COMPLETELY UNDERNEATH.....	199
FIGURE 53: REYNOLDS NUMBER AND FROUDE NUMBER VERSUS DARCY-WEISBACH FRICTION FACTOR (A AND C) AND S_o (B AND D); A AND C SHOW ALL THE REACHES DURING ALL MEASURED FLOWS. THE CIRCLED REACHES HAVE THE LOWEST VALUE OF BOTH Fr AND Re DURING AUGUST 2007 FLOW PERIOD. PORTIONS C AND D SHOW REACHES ONLY DURING AUGUST 2007 FLOWS. THE R^2 FOR THE BEST-FIT LINE IN A IS 0.54 AND IN B IS 0.85.	203
FIGURE 54: DAILY MEAN FLOW AND MINIMUM AND MAXIMUM INSTANTANEOUS FLOW FOR EAST ST. LOUIS IN 2007. RED, ORANGE, AND YELLOW INDICATE DAYS DATA WERE COLLECTED IN THE FIELD.....	230
FIGURE 55: DAILY MEAN FLOW AND MINIMUM AND MAXIMUM FLOW DATA FOR LOWER FOOL CREEK IN 2007. RED, ORANGE, AND YELLOW INDICATE DAYS FIELD DATA WERE COLLECTED IN STREAM.	231
FIGURE 56: DAILY MEAN FLOW AND MINIMUM AND MAXIMUM FLOW FOR EAST ST. LOUIS IN 2008. RED, YELLOW, AND ORANGE SECTIONS INDICATE DAYS FIELD WORK WAS COMPLETED IN THE CHANNEL...	232
FIGURE 57: DAILY MEAN FLOW AND MINIMUM AND MAXIMUM FLOW FOR LOWER FOOL CREEK IN 2008. RED AND ORANGE SECTIONS INDICATE DAYS FIELD WORK WAS COMPLETED IN THE STREAM.	232
FIGURE 58: DAILY MEAN FLOW AND MINIMUM AND MAXIMUM FLOW FOR UPPER FOOL CREEK IN 2008. RED AND ORANGE DOTS INDICATE DAYS THAT FIELD WORK WAS COMPLETED IN THE CHANNEL.....	233
FIGURE 59: PHOTOGRAPHS AND SUMMARY OF MEASURED AND CALCULATED HYDRAULIC VARIABLES FOR ESL1. RED ARROW INDICATES SAME LOCATION IN THE REACH IN EACH PHOTOGRAPH.	234

FIGURE 60: PHOTOGRAPHS AND MEASURED AND CALCULATED HYDRAULIC VARIABLES FOR EACH FLOW PERIOD IN ESL2. RED ARROWS INDICATE SAME LOCATION IN EACH PHOTOGRAPH.....	235
FIGURE 61: PHOTOGRAPHS AND MEASURED AND CALCULATED HYDRAULIC VARIABLES FOR ESL3. RED ARROWS INDICATE SAME LOCATION IN EACH PHOTOGRAPH.	236
FIGURE 62: PHOTOGRAPHS AND MEASURED AND CALCULATED HYDRAULIC VARIABLES FOR ESL4. RED ARROWS INDICATE SAME LOCATION IN EACH PHOTOGRAPH.	237
FIGURE 63: PHOTOGRAPH AND MEASURED AND HYDRAULIC VARIABLES FOR ESL5. RED ARROWS INDICATE SAME LOCATION IN EACH PHOTOGRAPH.....	238
FIGURE 64: PHOTOGRAPH AND MEASURED AND HYDRAULIC VARIABLES FOR ESL6. RED ARROWS INDICATE SAME LOCATION IN EACH PHOTOGRAPH.....	239
FIGURE 65: PHOTOGRAPH AND MEASURED AND HYDRAULIC VARIABLES FOR ESL7. RED ARROWS INDICATE SAME LOCATION IN EACH PHOTOGRAPH.....	240
FIGURE 66: PHOTOGRAPH AND MEASURED AND HYDRAULIC VARIABLES FOR ESL8. RED ARROWS INDICATE SAME LOCATION IN EACH PHOTOGRAPH.....	241
FIGURE 67: PHOTOGRAPH AND MEASURED AND HYDRAULIC VARIABLES FOR ESL9. RED ARROWS INDICATE SAME LOCATION IN EACH PHOTOGRAPH.....	242
FIGURE 68: PHOTOGRAPH AND MEASURED AND HYDRAULIC VARIABLES FOR FC1. RED ARROWS INDICATE SAME LOCATION IN EACH PHOTOGRAPH.....	243
FIGURE 69: PHOTOGRAPH AND MEASURED AND HYDRAULIC VARIABLES FOR FC2. RED ARROWS INDICATE SAME LOCATION IN EACH PHOTOGRAPH.....	244
FIGURE 70: PHOTOGRAPH AND MEASURED AND HYDRAULIC VARIABLES FOR FC3. RED ARROWS INDICATE SAME LOCATION IN EACH PHOTOGRAPH.....	245
FIGURE 71: PHOTOGRAPH AND MEASURED AND HYDRAULIC VARIABLES FOR FC4. RED ARROWS INDICATE SAME LOCATION IN EACH PHOTOGRAPH.....	246
FIGURE 72: PHOTOGRAPH AND MEASURED AND HYDRAULIC VARIABLES FOR FC5. RED ARROWS INDICATE SAME LOCATION IN EACH PHOTOGRAPH.....	247
FIGURE 73: PHOTOGRAPH AND MEASURED AND HYDRAULIC VARIABLES FOR FC6. RED ARROWS INDICATE SAME LOCATION IN EACH PHOTOGRAPH.....	248
FIGURE 74: GRAIN SIZE DISTRIBUTION FOR ENTIRE REACH AND SEPARATED BY SECTION FOR ESL1.	249
FIGURE 75: GRAIN SIZE DISTRIBUTION FOR ENTIRE REACH AND SEPARATED BY SECTION FOR ESL2.	249
FIGURE 76: GRAIN SIZE DISTRIBUTION FOR ENTIRE REACH AND SEPARATED BY SECTION FOR ESL3.	250
FIGURE 77: GRAIN SIZE DISTRIBUTION FOR ENTIRE REACH AND SEPARATED BY SECTION FOR ESL4.	250
FIGURE 78: GRAIN SIZE DISTRIBUTION FOR ENTIRE REACH AND SEPARATED BY SECTION FOR ESL5.	251
FIGURE 79: GRAIN SIZE DISTRIBUTION FOR ENTIRE REACH FOR ESL6.....	251
FIGURE 80: GRAIN SIZE DISTRIBUTION FOR ENTIRE REACH FOR ESL7.....	252
FIGURE 81: GRAIN SIZE DISTRIBUTION FOR ENTIRE REACH AND SEPARATED BY SECTION FOR ESL8.	252
FIGURE 82: GRAIN SIZE DISTRIBUTION FOR ENTIRE REACH AND SEPARATED BY SECTION FOR ESL9.	253
FIGURE 83: GRAIN SIZE DISTRIBUTION FOR ENTIRE REACH AND SEPARATED BY SECTION FOR FC1.....	253
FIGURE 84: GRAIN SIZE DISTRIBUTION FOR ENTIRE REACH AND SEPARATED BY SECTION FOR FC2.....	254
FIGURE 85: GRAIN SIZE DISTRIBUTION FOR ENTIRE REACH AND SEPARATED BY SECTION FOR FC3.....	254
FIGURE 86: GRAIN SIZE DISTRIBUTION FOR ENTIRE REACH AND SEPARATED BY SECTION FOR FC4.....	255
FIGURE 87: GRAIN SIZE DISTRIBUTION FOR ENTIRE REACH AND SEPARATED BY SECTION FOR FC5.....	255
FIGURE 88: GRAIN SIZE DISTRIBUTION FOR ENTIRE REACH AND SEPARATED BY SECTION FOR FC6.....	256
FIGURE 89: CUMULATIVE GRAIN SIZE DISTRIBUTION FOR ALL FOOL CREEK REACHES.	256
FIGURE 90: CUMULATIVE GRAIN SIZE DISTRIBUTION FOR ALL EAST ST. LOUIS REACHES.	257
FIGURE 91: LOCATION AND PHOTOGRAPHS IF WOOD IN ESL1.....	258
FIGURE 92: LOCATION AND PHOTOGRAPHS IF WOOD IN ESL2.....	259
FIGURE 93: LOCATION AND PHOTOGRAPHS IF WOOD IN ESL3.....	260
FIGURE 94: LOCATION AND PHOTOGRAPHS IF WOOD IN ESL4.....	261
FIGURE 95: LOCATION AND PHOTOGRAPHS IF WOOD IN ESL5.....	262
FIGURE 96: LOCATION AND PHOTOGRAPHS IF WOOD IN ESL6.....	263
FIGURE 97: LOCATION AND PHOTOGRAPHS IF WOOD IN ESL7.....	264
FIGURE 98: LOCATION AND PHOTOGRAPHS IF WOOD IN ESL8.....	265
FIGURE 99: LOCATION AND PHOTOGRAPHS IF WOOD IN ESL9.....	266
FIGURE 100: LOCATION AND PHOTOGRAPHS IF WOOD IN FC1.....	267
FIGURE 101: LOCATION AND PHOTOGRAPHS IF WOOD IN FC2.....	268

FIGURE 102: LOCATION AND PHOTOGRAPHS IF WOOD IN FC3.....	269
FIGURE 103: LOCATION AND PHOTOGRAPHS IF WOOD IN FC4.....	270
FIGURE 104: LOCATION AND PHOTOGRAPHS IF WOOD IN FC5.....	271
FIGURE 105: LOCATION AND PHOTOGRAPHS IF WOOD IN FC6.....	272
FIGURE 106: PLAN VIEW OF ESL1 SHOWING EACH BOULDER MEASURED FOR THE DRAG APPROACH AND FOR CALCULATING THE BOULDER CONCENTRATION (LEFT). THE VALUE OF FF_{GRAIN} SHOWN ABOVE WAS CALCULATED USING THE DRAG APPROACH. THE CROSS-SECTIONS ON THE RIGHT INDICATE THE LOCATIONS WHERE THE REACH WAS TRAVERSED FOR PEBBLE COUNTS, WHICH ARE SHOWN IN .APPENDIX D.	276
FIGURE 107: ESL2 BOULDERS (LEFT) AND PEBBLE COUNT CROSS-SECTIONS (RIGHT).....	277
FIGURE 108: ESL3 BOULDERS (LEFT) AND PEBBLE COUNT CROSS-SECTIONS (RIGHT).....	278
FIGURE 109: ESL4 BOULDERS (LEFT) AND PEBBLE COUNT CROSS-SECTIONS (RIGHT).....	279
FIGURE 110: ESL5 BOULDERS (LEFT) AND PEBBLE COUNT CROSS-SECTIONS (RIGHT).....	280
FIGURE 111: ESL6 BOULDERS (LEFT) AND PEBBLE COUNT CROSS-SECTIONS (RIGHT).....	281
FIGURE 112: ESL7 BOULDERS (LEFT) AND PEBBLE COUNT CROSS-SECTIONS (RIGHT).....	282
FIGURE 113: ESL8 BOULDERS (LEFT) AND PEBBLE COUNT CROSS-SECTIONS (RIGHT).....	283
FIGURE 114: ESL9 BOULDERS (LEFT) AND PEBBLE COUNT CROSS-SECTIONS (RIGHT).....	284
FIGURE 115: FC1 BOULDERS (LEFT) AND PEBBLE COUNT CROSS-SECTIONS (RIGHT).....	285
FIGURE 116: FC2 BOULDERS (LEFT) AND PEBBLE COUNT CROSS-SECTIONS (RIGHT).....	286
FIGURE 117: FC3 BOULDERS (LEFT) AND PEBBLE COUNT CROSS-SECTIONS (RIGHT).....	287
FIGURE 118: FC4 BOULDERS (LEFT) AND PEBBLE COUNT CROSS-SECTIONS (RIGHT).....	288
FIGURE 119: PLAN VIEW OF FC5 (RIGHT) AND FC6 (LEFT) SHOWING EACH BOULDER MEASURED FOR THE DRAG APPROACH AND FOR CALCULATING THE BOULDER CONCENTRATION. CROSS SECTIONS WERE NOT USED FOR PEBBLE COUNTS IN THESE REACHES, SINCE THE REACHES WERE SO SMALL THAT ALMOST EVERY PEBBLE WAS COUNTED.	289
FIGURE 120: PLAN VIEW OF THALWEG TRACE OF EAST ST. LOUIS CREEK SHOWING THE LOCATION OF ESL1 TO ESL9.	290
FIGURE 121: LONGITUDINAL PROFILE OF EAST ST. LOUIS CREEK. POINTS WERE COLLECTED EVERY 0.5 TO 1 M.	291
FIGURE 122: PLAN VIEW OF THALWEG TRACE OF LOWER FOOL CREEK SHOWING THE LOCATION OF FC1 TO FC3. FC4 IS MUCH FURTHER UPSTREAM FROM THESE REACHES.	291
FIGURE 123: CORRESPONDING LONGITUDINAL PROFILE OF LOWER FOOL CREEK.....	292
FIGURE 124: PLAN VIEW OF UPPER FOOL CREEK, SHOWING THE LOCATIONS OF FC5 AND FC6.....	293
FIGURE 125: CORRESPONDING LONGITUDINAL PROFILE FOR UPPER FOOL CREEK.	294

CHAPTER 1 INTRODUCTION

Quantifying flow resistance is an essential part of understanding hydraulics of streams. The interaction between stream flow and its boundaries dissipates energy as water moves around objects such as boulders and wood and over bedforms. Predictions of flow resistance are used for flood estimation, habitat assessment and prediction, design of fish passageways, and stream rehabilitation projects [Buffington and Montgomery, 1999; Bathurst, 2002; Ferguson, 2007]. Flow resistance is a quantity that relates the depth-averaged velocity to the shear velocity in the following way:

$$\frac{V}{u^*} = \left(\frac{8}{ff} \right)^{1/2} = \frac{R_h^{1/6}}{ng^{1/2}} = \frac{C}{g^{1/2}} \quad (1.1)$$

where, V = mean velocity (m/s); u^* = shear velocity (m/s); ff = Darcy-Weisbach friction factor; n = Manning coefficient; C = Chezy coefficient; g = acceleration due to gravity (m/s^2); R_h = hydraulic radius (m). The coefficients in each of these equations express the total resistance to flow, but the focus in this dissertation will be on the Darcy-Weisbach equation:

$$ff = \frac{8gR_h S_f}{V^2} \quad (1.2)$$

where, S_f = friction slope (m/m). The Darcy-Weisbach friction factor is sometimes preferred over the other two coefficients because it is non-dimensional and is physically interpretable as a drag coefficient if resistance is equated with gravitational driving forces per unit bed area [Ferguson, 2007].

High gradient mountain streams dissipate energy when water flows over poorly sorted grains in the bed and banks and over bedforms such as steps and pools, creating an alternating pattern between supercritical and subcritical flow and causing energy dissipation through hydraulic jumps. Mountain streams differ from their low gradient counterparts by having large boulders that are of the same order of magnitude as the depth of flow, low values of relative grain submergence (R_h/D_{84} , where R_h is hydraulic radius and D_{84} is the 84th percentile of the cumulative grain-size distribution), armored beds, and wood that commonly spans the entire width of the channel [Bathurst, 1993; Wohl, 2000]. The complex interaction of the different forms of flow resistance in steep mountain streams has made it particularly challenging to quantify ff . Form drag and skin friction around grains and bedforms dissipate energy through differential pressure and viscous effects on each object. Energy losses are also related to changes in acceleration and deceleration in the flow, known as spill resistance. Energy dissipated by these components of resistance is called grain (ff_{grain}), form (ff_{form}) and spill (ff_{spill}) resistance. The amount of momentum lost because of the presence of each individual roughness element can change based on the interaction of these roughness elements, making it difficult to quantify the total effect of the combined objects. Also, the contribution made by each of these sources of resistance can differ in relation to other factors such as gradient and channel morphology [Ferguson, 2007].

Steep gradient mountain streams are characterized by three distinct channel morphologies: step-pools, cascades and plane-beds [Montgomery and Buffington, 1997]. Step-pools have alternating plunging supercritical flow over steps and subcritical flows in the pools below [Zimmerman and Church, 2001; Church and Zimmerman, 2007]. Step-

pools generally form at gradients between 0.03 to 0.10 m/m [*Montgomery and Buffington, 1997*]. Steps create flow resistance by skin friction over large particles and wood, form drag from pressure differences around the upstream and downstream sides of protruding objects, and spill resistance created from flow acceleration and deceleration over the steps. Cascades form at $S_0 > 0.06$ m/m (where S_0 is bed gradient) and are characterized by tumbling flow over large, randomly arranged clasts [*Montgomery and Buffington, 1997*] that can create substantial grain resistance, dependent on stage. Skin friction and form drag around individual grains dissipate much of the mechanical energy. Occasional steps may be found in cascade reaches, creating a limited amount of spill resistance. Plane-bed channels have a uniform topography and lack any regular bedforms [*Montgomery and Buffington, 1997; Chartrand and Whiting, 2000*]. The dominant form of resistance in these reaches is skin friction and form drag around individual grains.

Equations developed for predicting flow resistance in low gradient streams have high errors ($\pm 25\%$ to $\pm 35\%$) when applied to high gradient mountain streams [*Bathurst, 1985; Thorne and Zevenbergen, 1985; Mussetter, 1989; Lee and Ferguson, 2002*]. The high errors in these equations reveal that the hydraulics of high gradient channels are still poorly understood. Flow resistance governs the energy available for the transport of water, sediment and other materials through the stream system. An improved understanding of both the driving and resisting forces in mountain channels will help advance understanding of transport processes, channel form and stability, stage-discharge relations and aquatic habitat [*Wilcox et al., 2006*].

1.1 Study Objectives

The following project focuses on studying controls and interactions among different forms of resistance in step-pool, cascade and plane-bed reaches on two different streams, where a reach is a length of channel 10^0 - 10^1 m in length with consistent channel morphology. The project is divided into three parts: 1) identify specific controls on the total flow resistance throughout the channel network using statistical analysis; 2) investigate specific variations within each reach by analyzing at-a-station hydraulic geometry; and 3) quantify and evaluate interactions among the individual flow resistance components that contribute to total flow resistance.

To improve predictions of resistance and estimation of discharge, it is important to obtain a better understanding of resistance throughout a channel network, including variations in flow resistance for specific channel characteristics within each type of channel morphology. Therefore, the following two objectives are used to: 1) examine how resistance varies with gradient, channel morphology, and relative submergence of grains, steps and the bed among various channel types; and 2) examine how resistance varies with gradient, relative grain submergence and discharge within each channel type. The latter objective reflects our understanding that the influence of each variable on total resistance may differ based on gross morphologic differences between each channel type.

The next part of the study is designed to examine controls on flow resistance within each reach in relation to stage. The following two objectives are addressed in this component of the study: 1) report at-a-station hydraulic geometry values for cascade, step-pool, and plane-bed reaches and determine whether there are significantly different

values for cascade versus step-pool reaches; and 2) explore what influences the variability in the rate of change of width, depth and velocity with discharge.

The final section evaluates methods for dividing total resistance into its individual components and investigates interactions and potential controls on these components. The following three objectives are addressed in this section: 1) evaluate methods for calculating ff_{grain} , ff_{wood} , and ff_{step} ; 2) identify limitations in the existing methods of calculating total and component resistance when these methods are applied to steep streams; and 3) analyze interrelationships among component resistance and other independent variables such as stage and discharge.

All of the above objectives are addressed using detailed measurements of nine step-pool reaches, five cascade reaches, and one plane-bed reach in Fraser Experimental Forest, Colorado. The velocity, water-surface elevation and channel geometry were all measured using a combination of tracers, a laser theodolite and tripod-mounted LiDAR (Light Detection and Ranging). The study site and methods are described in CHAPTER 3, after an extensive literature review of our current state of knowledge on flow resistance in high-gradient streams. The remaining chapters are subdivided based on the three main components of the project: 1) controls on flow resistance; 2) at-a-station hydraulic geometry; and 3) partitioning total flow resistance into its components of ff_{grain} , ff_{wood} , ff_{step} , and ff_{spill} . The last chapter then integrates the conclusions drawn from all three components of the project.

CHAPTER 2 BACKGROUND

2.1 Current methods of predicting flow resistance

In mountain streams, where $S_0 > 0.02$, bedforms, grains and wood are commonly on the same order of magnitude as the flow depth. Equations used to predict flow resistance are based on the concepts and theories developed for low-gradient streams. Many equations that have been used to predict ff are based on some iteration of the *Keulegan* [1938] relation, which integrates the logarithmic law of the wall throughout the flow depth:

$$\left(\frac{8}{f}\right)^{1/2} = \frac{1}{\kappa} \ln\left(\frac{R_h}{k_s}\right) + 6 = \frac{1}{\kappa} \ln\left(\frac{11R_h}{k_s}\right) \quad (2.1)$$

where, κ = von Karman constant (~ 0.4); k_s = representative roughness height, usually related to a multiple (C_m) of a representative grain diameter (D_m). These equations are based on the boundary-layer theory, that near the boundary the velocity is influenced by boundary effects and scales with depth [*Bathurst*, 1993]. The assumptions of a logarithmic velocity profile and resistance dominated by grain roughness may not be valid in channels where the relative roughness (R_h/D_{84}) is less than 4 and the velocity profile is better approximated with an s-shape [*Wiberg and Smith*, 1991; *Bathurst*, 1993; *Comiti et al.*, 2007; *Ferguson*, 2007]. However, *Wiberg and Smith* [1991] found that the logarithmic equation can adequately represent mean velocity because velocity primarily depends on flow depth and the D_{84} of the vertically-oriented axis. *Ferguson* [2007] found that all submergence-based equations had high errors, where velocity was incorrectly estimated by a factor of two at least 15% of the time.

Another approach, developed by *Jarrett* [1984], is to equate resistance to channel slope and hydraulic radius through a power law equation:

$$n = 0.39S^{0.38}R_h^{-0.16} \quad (2.2)$$

The problem with this and other power law equations is that the best fit is based on the data used to calibrate the equation [*Ferguson*, 2007]. Therefore, the equations can only be employed for the specific range of data that were used to develop the equation. *Lee and Ferguson* [2002] found that this equation performed poorly in step-pool streams, particularly in comparison to a modified *Keulegan* [1938] relation by *Thompson and Campbell* [1979]. *Comiti et al.* [2007] developed a power relationship between dimensionless velocity and unit discharge:

$$v^* = aq^{*b} S^c \quad (2.3)$$

$$v^* = \frac{v}{\sqrt{gD_c}} \quad (2.4)$$

$$q^* = \frac{q}{\sqrt{gD_m^3}} \quad (2.5)$$

where, q = unit discharge; a = empirically derived coefficient; b and c = empirically derived exponents; D_m = roughness parameter. *Ferguson* [2007] found that this approach reduced the velocity error from being greater than a factor of 2 for 15% of the cases in submergence-based equations to 8%.

Most equations rely heavily on determining a characteristic grain size [*Keulegan*, 1938; *Limerinos*, 1970; *Hey*, 1979; *Thompson and Campbell*, 1979; *Bray*, 1982; *Bathurst*, 1985; *Bathurst*, 1993], even though these approaches have been shown to have high error rates when applied to steep mountain streams [*Thorne and Zevenbergen*, 1985]. The

values for k_s have ranged from $2D_{90}$ [Parker and Peterson, 1980], to $3.5D_{84}$ [Hey, 1989], $3D_{84}$ [Whiting and Dietrich, 1990], D_{84} [Prestegard, 1983], and D_{50} [Griffiths, 1989; Millar, 1999]. Bray [1982] found no significant difference between using D_{50} , D_{84} , and D_{90} as the characteristic grain diameter. Millar [1999] showed that values of C_{50} (from $k_s = C_{50}D_{50}$) could range between 0.4 and 55.7. Although Wiberg and Smith [1991] showed that the values of k_s and C_{50} increased as the bed became more poorly sorted, no such relationship was found by Millar [1999]. Comiti et al. [2007] showed that D_{84} was significantly related to flow velocity and therefore chose that grain size. Lee and Ferguson [2002] found that step D_{84} performed well in predicting total resistance in reaches without any wood. Aberle and Smart [2003] rejected any use of a characteristic grain size and proposed using the standard deviation of the bed elevation as the roughness parameter. In a review of the state of current step-pool research, Church and Zimmerman [2007] noted that researchers other than Aberle and Smart have had limited success with this roughness parameter and no one had tested whether this parameter could be used at low flows. The large amount of variation in predictive equations and the lack of ability to apply equations developed for one dataset to another, without large errors, signify that the spatial and temporal variability in ff is still poorly understood in these high gradient systems.

Gradient is another defining characteristic of any stream channel. Gradient coupled with flow governs the amount of energy available for transporting material or eroding the banks and bed. Reach-scale gradient can be an independent variable in mountain streams and typically correlates well with channel morphology [Montgomery and Buffington, 1997; Wohl and Merritt, 2005], grain size [Wohl et al., 2004], and step

height (H_s) and length (L_s) [Abrahams *et al.*, 1995; Comiti *et al.*, 2005]. One difficulty in quantifying flow resistance in mountain streams is that V , R_h , and S_f exhibit large spatial and temporal variability. Many empirical equations have been developed that relate ff to these and other channel variables, but these typically perform poorly when extrapolated to other steep channels and in some cases have been shown to have errors as high as 66% [Bathurst, 1985, 1986, 2002; Wohl, 2000; Katul *et al.*, 2002; Aberle and Smart, 2003; Curran and Wohl, 2003; Ferguson, 2007]. Part of the uncertainty in applying empirically-based equations to new sites is that the relative importance of different sources of resistance can vary between sites. Total resistance is typically partitioned into grain (form drag on individual particles and viscous/skin friction on their surfaces), form (dunes, bars, steps), and spill (flow transitions and wave drag on elements protruding above the water surface) resistance [Einstein and Barbarossa, 1952; Parker and Peterson, 1980; Wilcox *et al.*, 2006; Ferguson, 2007]. The contribution made by each of these sources of resistance can differ in relation to gradient, channel morphology, or other factors [Ferguson, 2007]. To better understand the various controls on total flow resistance it is important to recognize both local controls at a specific point and reach as well as methods of quantifying each source of resistance.

2.2 At-a-station hydraulic geometry

At-a-station hydraulic geometry (AHG) is an important tool to use to help in our understanding of resistance in steep mountain streams. AHG characterizes how changes in discharge affect specific hydraulic variables such as width, depth, velocity and friction. Leopold and Maddock [1953] first coined the term “hydraulic geometry” to describe

systematic changes both downstream and at a cross-section for each of the above hydraulic variables. They proposed three power relations to describe how width ($w = aQ^b$), depth ($d = cQ^f$), and velocity ($v = kQ^m$) vary with discharge both downstream and at a given cross-section in a channel, where Q is discharge; w is water-surface width, d is mean depth; and v is velocity. These power relations are bound by the continuity equation ($Q = wdv$), indicating that the coefficients a , c , and k have a product equal to one and the exponents b , f , and m sum to one. *Leopold and Maddock* [1953] found that the rates of change of width, depth and velocity with discharge were related to the shape of the channel, the slope of the water surface, and the roughness of the wetted perimeter. They also found the sediment load to be an important control on the rates of change of both velocity and depth [*Leopold and Maddock*, 1953].

Park [1977] ascertained that a wide range of the three hydraulic geometry exponents exists throughout the world, which suggests the need for an improved understanding of the sources of variation. Other controls on at-a-station values that have been identified include differences between braided, meandering, and straight reaches [*Knighton*, 1975; *Ferguson*, 1986]; differences based on bank composition [*Knighton*, 1974]; variations between pool and riffle sections [*Knighton*, 1975; *Richards*, 1976]; and differences based on irregularities in resistance in relation to stage [*Richards*, 1976; *Ferguson*, 1986]. *Ferguson* [1986] also noted that at-a-station hydraulic geometry may vary over the course of a flood cycle as both scour and fill occur during this time period. The heterogeneous nature of high gradient mountain streams may cause there to be even greater variations in AHG.

The use of power relations in hydraulic geometry is based on empirical evidence and does not have a solid foundation in theory [Park, 1977; Richards, 1973; Ferguson, 1986]. Further work has been done using extremal hypotheses to develop a theoretical framework for predicting AHG values [Langbein, 1964; Huang and Nanson, 2000; Singh and Zhang, 2008a]. Langbein [1964] proposed the minimum variance hypothesis in which the most probable state is found by minimizing the variance of the dependent variables (width, depth, and velocity). Huang and Nanson [2000] proposed combining the maximum sediment transport capacity [Kirkby, 1977; White et al., 1982], minimum unit stream power [Yang, 1976], and minimum stream power [Chang, 1980] into the principle of least action to describe channel adjustment in alluvial rivers. Singh and Zhang [2008a] took the concepts of minimum energy dissipation rate and the principle of maximum entropy to derive AHG values. Singh and Zhang [2008a] propose a weighting factor to represent the unequal distribution of stream power among the variables width, depth, velocity, roughness, and slope, which all adjust with increasing discharge. In alluvial rivers, they found that the change in stream power is most often accomplished with a change in width and flow depth, and to a lesser extent, a change in roughness [Singh and Zhang, 2008b]. Although these extremal hypotheses are important in the attempts to predict AHG, the objective of my work is to describe and understand differences in AHG among reaches and not to predict the actual values. The examination of differences in AHG may help in the eventual development of a predictive equation and of the theory behind AHG.

In AHG the rate of change of mean velocity with water depth is controlled by hydraulic laws and frictional characteristics, which may not follow power-law trends

[*Ferguson*, 1986]. *Ferguson* concludes that the wide scatter in AHG is related to the wide variety of channel shapes and frictional characteristics. *Lawrence* [2007] further supports *Ferguson's* [1986] work by showing that an exponent which reflects cross-section form (r) and depth in a hydraulic relation drives the values for the AHG exponents. *Lawrence* [2007] concludes that the values of the coefficients depend on a combination of the physical characteristics of the section including width, depth, hydraulic conductance and energy slope.

Few studies have reported AHG values for steep mountain channels [*Lee and Ferguson*, 2002; *Reid*, 2005; *Comiti et al.*, 2007]. A better understanding of at-a-station changes in each of the above hydraulic variables can improve our understanding of the sources and magnitude of hydraulic roughness in these channels, which tend to have values of flow resistance as reflected in Manning's n or Darcy-Weisbach ff that are much higher than values for channel reaches with gradient $< 1\%$ [*Jarrett*, 1984; *Bathurst*, 1985, 1993]. An examination of AHG, as presented in Chapter 5, will further our understanding of sources of variability in flow resistance and the interaction among hydraulic variables as discharge increases.

2.3 Partitioning

The complex interaction of the different forms of flow resistance in steep mountain streams makes it difficult to quantify the Darcy-Weisbach friction factor. *Einstein and Barbarossa* [1952] proposed that despite interactions of different components of resistance, the individual components could be quantified and summed. The bed shear stress, friction slope and Darcy-Weisbach friction factor are all common hydraulic variables that are commonly partitioned in attempts to understand different

forms of resistance [*Einstein and Barbarossa*, 1952; *Millar*, 1999; *Maxwell and Papanicolaou*, 2001]. The Darcy-Weisbach friction factor can be partitioned into its individual components of grain, wood, form (from step bedforms) and spill resistance:

$$ff_{total} = ff_{grain} + ff_{wood} + ff_{step} + ff_{spill} \quad (2.6)$$

where, ff_{grain} = friction factor caused by grains in the absence of bedforms; ff_{wood} = friction factor caused by individual pieces of wood in the absence of bedforms; ff_{step} = pressure/form drag around bedforms and other objects; and ff_{spill} = energy dissipation from flow acceleration and deceleration, usually over steps. *Bathurst* suggests that in mountain rivers there should be three scales of roughness: large-scale ($R_h/D_{84} < 1$), intermediate-scale ($1 < R_h/D_{84} < 4$) and small-scale ($R_h/D_{84} > 4$). It is important to note the varying methods and definitions of partitioning between ff_{grain} and ff_{form} . Some methods are based on partitioning specifically between form drag and skin friction [*Julien*, 1998]. Both types of resistance can be applied to one object, therefore these methods partition the total resistance created by each object. Other methods more generally partition resistance created by each object. For instance, with large-scale roughness, large grains create as much form drag as skin friction, therefore the combination of form drag and skin friction is considered the total grain resistance; i.e., the grain resistance is not divided between form drag and skin friction. *Einstein and Barbarossa* [1953] were some of the first to propose a method for partitioning resistance and a division between grain and form roughness, where grain roughness is defined as the frictional losses created by grains in the absence of bedforms and form roughness is the frictional losses from the inclusion of bedforms. *Leopold et al.* [1960] first defined the third component, ff_{spill} , as the sudden forced reduction in velocity as in the case of a sudden expansion beyond a

partially opened valve, or from a waterfall. Both *Millar* [1999] and *Comiti et al.* [2009] include the effect of grain and boulder protrusions in the quantification of ff_{form} along with bedforms and bars. On the other hand, *Parker and Peterson* [1980], *Wilcox et al.* [2006], and *Ferguson* [2007] all consider ff_{grain} to represent both viscous effects and form drag around individual grains. Form resistance is related to pressure drag around bedforms and other objects that cause significant amounts of flow separation and turbulence [*Leopold et al.*, 1964; *Wilcox et al.*, 2006]. *Wilcox et al.* [2006] chose to define form resistance as the combined ff_{spill} and ff_{wood} . Although spill resistance can be considered part of ff_{form} , it is most commonly considered as the separate unmeasured component unless changes in ff_{total} are measured directly in a flume [*Wilcox et al.*, 2006; *Comiti et al.*, 2009]. When ff_{spill} is the leftover component, it may be encompassing other unmeasured components such as bank resistance (ff_{bank}), bend resistance (ff_{bend}), and resistance related to bed load transport (ff_{bl}). In this dissertation, form resistance is divided into step resistance (ff_{step} from pressure drag around the step bedforms) and wood resistance (ff_{wood}). Spill resistance is still the unmeasured component.

Each type of resistance may be the dominant component depending on the location of the reach in the channel network [*Bathurst*, 1993]. *Bathurst* [1993] summarized the changes in the dominant components of resistance throughout a channel network. In low gradient sand-bed reaches, the bedforms and suspended load dominate the individual contributions to total resistance. In gravel-bed rivers, the total resistance is dominated by the relative submergence of the grains and the ponding effect of pool/riffle sequences and bars. In boulder-bed streams, where $R_h/D_{84} < 4$, the total resistance is dominated by the combined effects of drag around individual boulders. In step-pool

streams, flow resistance is dominated by spill resistance and ponding in the pools [Curran and Wohl, 2003; Comiti *et al.*, 2009]. Resistance related to bends may be more significant in lower gradient channels [Leopold *et al.*, 1960, Parker and Peterson, 1980, Bathurst, 1993], whereas wood can make an important contribution towards resistance at all gradients [Shields and Gippel, 1995; Manga and Kirchner, 2000; Curran and Wohl, 2003; Wilcox and Wohl, 2006].

Additive approaches have been used to investigate the contribution of grains [Einstein and Barbarossa, 1952; Parker and Peterson, 1980, Millar and Quick, 1994; Millar, 1999], wood and spill resistance [Shields and Gippel, 1995; Curran and Wohl, 2003; McFarlane and Wohl, 2003], and bar resistance in gravel-bed rivers [Parker and Peterson, 1980; Prestegard, 1983]. In a flume study, however, Wilcox *et al.* [2006] demonstrated that the unmeasurable component was always the largest contributor to total resistance, meaning that an additive approach always inflates the leftover component. Thus, the first challenge to understanding flow resistance in streams is to quantify the relative contribution of different sources of resistance. Understanding the relative contribution of each roughness element along with the interactions among these elements and slope and discharge can help in predicting total ff . Therefore, the available methods for calculating each type of resistance are described below.

2.4 Grain Resistance (ff_{grain})

The contribution of grain resistance in high gradient channels has varied depending on whether the study was carried out in a flume or in a natural channel and whether wood was present in the reach. In boulder-dominated step-pool reaches, the grain resistance has been found to contribute anywhere from 20 to 40 % of the total flow

resistance. In step-pool reaches with a significant contribution from wood, grain resistance contributed anywhere from 8 to 32% to ff_{total} [Curran and Wohl, 2003; Wilcox et al., 2006]. Wilcox et al. [2006] concluded that grain resistance made up the smallest percentage of total resistance in step-pool streams.

The methods used to calculate ff_{grain} are typically related to using some form of the Keulegan [1938] equation (Equation 2.1) and determining some characteristic grain size, as discussed above. Millar and Quick [1994] proposed using D_{50} as the characteristic grain size because they found that any large grain size causes both form and grain resistance to be combined in the value of ff_{grain} . In their study, the larger clasts that created flow separation and pressure differences were part of form resistance and only the viscous friction was part of grain resistance. A variant on Equation (2.1) proposed by Parker and Peterson [1980] is:

$$ff_{grain} = 8 * \left[2.5 \ln \left(\frac{11d}{2D_{90}} \right) \right]^{-2} \quad (2.7)$$

where d = mean flow depth (m). Bathurst [2002] proposed the use of a power relationship rather than a logarithmic function:

$$ff_{grain} = 8 * \left[3.1 \left(\frac{d}{D_{84}} \right)^{0.93} \right]^{-2} \quad (2.8)$$

Bathurst [2002] found that D_{84} was a preferred characteristic grain size because it accounted for the primary grain roughness effects of wave drag, roughness concentration and velocity profile without being able to explain these effects mathematically. Each of these two equations was developed for lower gradient channels than are found in this study, but they are the only equations currently available for calculating ff_{grain} .

The size, shape, spacing and sorting of the bed material in boulder-bed channels cause the velocity profiles to be closer to s-shaped than semi-logarithmic. The distortion of the profile is also dependent on the submergence of the boulders, but generally can be partitioned into two sections. The flow around the boulders is retarded by drag and other resistance effects, whereas the flow above the boulders can be unimpeded by these effects, depending on submergence [Bathurst, 1993]. Therefore, the flow above the boulder has a rapid increase in velocity with depth, creating a shear layer between the two sections and a greater amount of resistance from internal distortions of the flow field. *Wiberg and Smith* [1991] found that although the velocity profiles deviated significantly from the log-law form, the mean velocity can still be predicted from the log-law-based calculations. For this to work, the roughness height has to be set to a large multiple of the average grain size.

Bathurst [1993] also proposed that when depth is on the same order of magnitude as the bed material height ($R_b/D_{84} < 4$), flow resistance has to be determined from drag forces on boulders rather than from the boundary layer theory, which is dependent on the semi-logarithmic velocity profile. The value of the drag coefficient around an object depends on its Reynolds number (Re), Froude number (Fr) and relative submergence. The position of flow separation and size of the wake around an object are dependent on whether the boundary layer is laminar or turbulent and hence the Reynolds number [Bathurst, 1993]. On the other hand, boulders have irregular shapes that have a greater effect on the position of flow separation than the Re . In shallow flows, the C_D is more closely related to the Fr and relative submergence. The Fr is used to account for energy losses from the distortion of the free surface when boulders protrude through the surface

[Bathurst, 1993]. *Flammer et al.* [1970] found that for a relative submergence < 4 , the C_D generally decreased with increasing Fr . Above relative submergence values of 4 the C_D does not vary with the Fr . Unfortunately, drag coefficients have mainly been measured for fully submerged grains and not partially submerged grains, as is commonly found in mountain channels, particularly at lower flows.

Form drag around a particle scales with bed-roughness length scale and the concentration of roughness elements, since it is more closely related to local velocity profiles than to the depth-averaged velocity [*Nelson et al.*, 1991; *Wiberg and Smith*, 1991; *Canovaro et al.*, 2007]. Because of this, the particle form drag is not necessarily a function of relative roughness (R_h/D_m) or bed slope. On the other hand, *Lamb et al.* [2008] determined that eddy viscosity and turbulent fluctuations seem to depend more strongly on relative roughness than on form drag around particles or morphologic structures, similar to *Bathurst's* [2002] findings in streams with gradients between 0.2 to 4%. *Buffington and Montgomery* [1999a] established that in channels with slopes between 0.0017 and 0.027, the form drag increased as slope increased, which decreased shear stress. The competent D_{50} could be overpredicted by 2 to 32% when form drag is not accounted for in the quantification of flow resistance.

The arrangement of grains and spacing between boulders can also have a significant effect on the total flow resistance. As the spacing decreases, the total drag force per unit area of bed can increase, although eventually the spacing is reduced to a point at which the objects are affected by the wake of the neighbor and the total flow resistance is reduced. *Canovaro et al.* [2007] found that randomly arranged boulders resulted in smaller values of flow resistance than boulders set in transverse stripes,

similar to steps. Consequently, the effect of an individual grain on flow resistance is related to a number of variables including the concentration of boulders (Γ), the Fr , Re , spatial arrangement, and relative submergence (R_H/D_m).

The various methods available for calculating ff_{grain} are analyzed in CHAPTER 6 to understand both the benefits and limitations of these methods in high gradient systems. Along with an examination of these methods is an analysis of the interaction between ff_{grain} and other sources of resistance as well as potential controls on values of ff_{grain} . The large variability in mountain streams between the interaction of grains with flow based on relative submergence, and the spatial arrangement of grains, has made it difficult to find one method that is the preferred method for calculating ff_{grain} . An understanding of each method, along with how ff_{grain} varies based on other hydraulic controls such as slope and discharge, will help in future development of predictive equations.

2.5 Step (ff_{step}) and Spill Resistance (ff_{spill})

In mountain streams, a major proportion of flow resistance is attributed to the step-pool reaches [Abrahams *et al.*, 1995]. Energy is dissipated both by roller eddies, as water plunges over the steps, and by form resistance from the rapid changes from pool to step riser [Chartrand and Whiting, 2000]. The total resistance in step-pool channels is dominated by form and spill resistance, which vary with wood amount and location [Comiti *et al.*, 1999; Curran and Wohl, 2003; Wilcox *et al.*, 2006; Comiti *et al.*, 2008]. Form resistance is related to pressure differences around the step bedform (ff_{step}) and spill resistance (ff_{spill}) is the energy loss from flow acceleration and deceleration as flow plunges over the steps. Spill resistance can also be found in cascading reaches where

hydraulic jumps form as flow moves over larger bed elements or goes from a constricted area to an expanded section of channel [Leopold *et al.*, 1960]. Plane-bed reaches are considered to be dominated only by ff_{grain} .

Spill resistance is most often studied in step-pool reaches, therefore this section focuses on spill resistance in step-pool channels. The flow regime in step-pool channels is subdivided into nappe, submerged and skimming flows [Chanson, 1994; Church and Zimmerman, 2007]. Nappe flow regime proceeds when flow is a free-falling jet over a series of steps [Chanson, 1994]. Energy is dissipated by the breakup and mixing of the jet on the step tread. The skimming flow regime is characterized by a smooth free-surface over the steps. The flow is cushioned by a re-circulating fluid trapped between the steps. In a skimming flow regime, the upstream steps do not have air entrainment, but flow becomes rapidly aerated downstream because of turbulence at the boundaries [Chanson, 1994]. Chanson [1994] deduced that skimming flow occurs at a critical value defined by the following equation:

$$\frac{(d_c)_{onset}}{H_s} = 1.057 - 0.465 \frac{H_s}{L_s} \quad (\text{for } 0.2 < H_s/L_s < 1.3) \quad (2.9)$$

where, d_c = characteristic critical depth; H_s = step height, and L_s = step length. This is similar to Comiti *et al.*'s [2009] results where skimming flow occurred when h_c/z (ratio of critical depth to drop height) > 1.2 and $Fr > 0.9$. The re-circulating vortices that occur during skimming flows play a major role in dissipating energy in step-pool channels and change some of the characteristics of how the reach dissipates energy [Chanson, 1994]. Comiti *et al.* [2009] found that in the nappe regime grain resistance only accounts for ~5 to 15% of total resistance, whereas in the skimming flow regime the contribution of grain resistance increased to ~25 to 30%. The contribution towards ff_{total} from spill resistance

correspondingly drops as grain resistance increases. *Comiti et al.* [2009] hypothesize that the remaining fraction is related to flow recirculation in pools. Wood was not included in this study.

Zimmerman and Church [2001] established that the step height is more closely related to the pool just downstream than to the upstream pool. Therefore, the effect of scour from the plunging flow is more significant than the damming effect from the step [*Comiti et al.*, 2005]. The size of the pool is significant in determining the effect of the jet on the bed. A smaller pool has more intense turbulent circulation in comparison to a large pool [*Zimmerman and Church*, 2001]. More turbulence leads to larger pressure differences, thus creating greater lift forces capable of moving larger sediment. *Wohl and Thompson* [2000] found that the jet is most effective in the immediate vicinity of the plunge, where wake turbulence dominates.

Likewise, the step height and length have a significant influence on flow resistance in the nappe flow regime. *Abrahams et al.* [1995] established that maximum flow resistance existed when $1 < (H_s/L_s)/S_0 < 2$ (where H_s = step height, L_s = step length, S_0 = bed gradient). *Wilcox and Wohl* [2006] showed in a flume study that the effectiveness of step-pool sequences to dissipate energy is maximized at low discharges when the distance from the step lip to the pool is greatest. At high discharges, when the profile becomes less stepped, the amount of energy that can dissipate decreases [*Chin*, 2003].

The interaction of each component of resistance is significant and is not represented by the additive partitioning equation [*Wilcox et al.*, 2006; *Wilcox and Wohl*, 2006]. *Wilcox et al.* [2006] showed that the presence of grains on the step tread could

increase the flow resistance, causing depth to increase and fully submerging wood that had not previously been submerged. The drag force around the submerged logs then increased, further increasing the flow resistance. Another interaction found by *Wilcox et al.* [2006] and *Wilcox and Wohl* [2006] was that the effect of spill resistance was much larger when wood was present in the steps, versus when there was no wood in the steps.

Despite the fact that spill resistance is often cited as contributing the largest component to total resistance in step-pool reaches, there are no adequate methods that have been developed to calculate spill resistance in a natural stream. Understanding the various controls on ff_{total} , the variations in at-a-station in hydraulic variables with discharge, and the methods for calculating other sources of resistance will contribute to our understanding of the relative importance of spill resistance in these reaches and particularly the relative importance of spill resistance when discharge increases but the flow still remains below a skimming regime.

2.6 Wood Resistance (ff_{wood})

Wood is an important component of any stream channel, influencing channel morphology, flow hydraulics, and aquatic habitat [*Keller and Swanson*, 1979; *Montgomery et al.*, 1996; *Manners and Doyle*, 2007]. In-channel wood increases roughness, creating micro-environments of low-velocity zones for both terrestrial and aquatic organisms, and influences sediment transport and nutrient cycling [*Dudley et al.*, 1998]. The inclusion of in-channel wood has been shown by a number of researchers to increase the total resistance in a reach [*Dudley et al.*, 1998; *Curran and Wohl*, 2003; *Wilcox and Wohl*, 2006], but the influence of the wood may be smaller at higher flows

[Dudley *et al.*, 1998]. Buffington and Montgomery [1999a] concluded that reaches that are wood-rich have significant textural fining from increased hydraulic roughness.

Scour can occur around wood where the flow converges, causing coarse-grained pools at the outer tips of wood pieces or jams [Cherry and Bescheta, 1989]. Buffington and Montgomery [1999] found that wood repartitions the boundary shear stress, resulting in an overall finer bed. The presence of individual logs or a wood jam alters the spatial distribution of shear stress [Manga and Kirchner, 2000].

Wood is typically dealt with as an individual log [Gippel *et al.*, 1992; Wilcox *et al.*, 2006], rather than as the accumulated pieces in a jam. Manners and Doyle [2007] attempted to understand the hydraulics and drag effects of wood jams, rather than individual pieces.

Individual pieces of wood, as well as entire jams, have a drag force applied to them:

$$F_D = C_D \rho \frac{\bar{v}^2}{2} A_F \quad (2.8)$$

where, F_D = total drag force (N); C_D = coefficient of drag, ρ = density of water (kg/m^3); \bar{v} = mean free-stream velocity (m/s); A_F = submerged frontal area of object (m^2).

Manners *et al.* [2007] determined that C_D and A_F are too closely interrelated to separate into individual terms. Manners *et al.* [2007] studied three bank deflector jams on a stream with a gradient of 0.01. Manners *et al.* [2007] look at the difference between assuming a non-porous jam, which is assumed when using an individual cylinder model, versus a porous jam. Manners *et al.* [2007] found that adjacent to jams there is high excess shear stress. When jams were wrapped to make them non-porous, the downstream shear stress decreased significantly. With increased porosity there was increased flow

through the jam and increased shear stress applied to the bed downstream from the jam. As porosity increased, the core of excess shear moved from being adjacent to the jam to downstream of the jam. The highest drag force was associated with the greatest amount of material and lowest porosity. The magnitude of C_D did not change systematically in their experiments with stage of removal. *Manners et al.* [2007] suggest that erosion and deposition around a jam are dependent on the degree of porosity, which is dependent on the age of the jam. They found that C_D values around jams in the field range from 0.7 to 9.0. Values ranged from 0.4 to 4.5 in the flume [*Gippel et al.*, 1996] to 1.0 to 3.3 in the field [*Hygelund and Manga*, 2003]. The drag coefficient around individual cylinders has also been found to change with log submergence, log slenderness, blockage, orientation, distance from bed and Reynolds number and Froude number [*Gippel et al.*, 1996; *Wallerstein et al.*, 2001; *Hygelund and Manga*, 2003; *Wilcox et al.*, 2006]. *Manners et al.* [2007] did not find a clear relationship between C_D and jam porosity, but this may have partly to do with the placement of the key member in the water column and the location of the removed material, which was mainly under the key member. The surface area was determined to be significantly related to the $(C_D A_F)_{\text{calc}}$ variable. $(C_D A_F)_{\text{calc}}$ was found to be a better representation of hydraulics than attempting to calculate the individual numbers, since it is difficult to quantify both jam geometry and the drag coefficient. The jam geometry and surface area could both be used to predict $(C_D A_F)_{\text{calc}}$; the greater the surface area, the greater the roughness [*Manners et al.*, 2007].

Wood adds a lot of complexity to high-gradient channels as individual pieces throughout the channels and as jams that are most often a component of steps. The work of *Manners et al.* [2007] signifies that the flow resistance around a wood step may be

even more complex than the flow resistance around a boulder step. Wood interacts with other sources of resistance by either creating increased resistance and causing textural fining [Buffington and Montgomery, 1999] and thus a decrease in the influence of grains, or by causing backwaters which also submerge grains and decrease their relative importance [Wilcox and Wohl, 2006]. Understanding the relative importance of wood among high-gradient reaches (CHAPTER 4), as well as within each reach (Chapter 5) is essential for computing values of ff in mountain streams.

2.7 Other forms of resistance

Bedload transport is another source of resistance in these channels, although transport is limited even when water fills to the top of banks. *Buffington and Montgomery* [1999] found that sediment supply influences bed-surface textures and vice versa, leading to a feedback between rates and supply. *Shields and Gippel* [1995] also included the effects of banks and bends in their partitioning of resistance. These other forms of resistance may also be significant in these streams, but the focus of this research is on the contributions from the bed. Also, bedload transport is considered negligible under the flows studied in this project. The importance of bedload transport and bank resistance may vary with discharge, such that bedload transport becomes increasingly important for very high discharges. The importance of banks may vary with discharge, depending on how rough the banks are and whether bank characteristics change with flow. Inclusion of these sources of resistance would add much more complexity to the analysis. Consequently, the analysis is limited to resistance of a static bed, similar to what previous investigators have done.

CHAPTER 3 FIELD METHODS

3.1 Site Description

East St. Louis Creek (ESL) and Fool Creek are located in Fraser Experimental Forest in the Colorado Rockies 112 km west-northwest of Denver (Figure 1). Elevation varies from 3925 m a.s.l. at the top of the Fool Creek basin to 2895 m a.s.l. at the bottom of East St. Louis Creek (Table 1). The Fool Creek basin is subdivided into Lower Fool Creek (LFC) and Upper Fool Creek (UFC) (Figure 1). Vegetation varies from Engelmann spruce and subalpine fir at higher elevations to lodgepole pine at lower elevations. Alpine tundra can also be found at the higher elevations in both basins. Runoff is dominated by snowmelt with small contributions by summer convective storms [Trayler and Wohl, 2000]. Average annual precipitation over the entire forest is 787 mm [USDA Forest Service, 2009]. Historically, peak discharges occur in mid-June, with 80% of the total flows occurring between April and October [Wilcox and Wohl, 2007].

Table 1: Drainage basin information for East St. Louis (ESL), Upper Fool Creek (UFC) and Lower Fool Creek (LFC)

Drainage Basin Name	Drainage Area (km²)	Elevation Range of Basin (m a.s.l.)	No. of Step-pool Reaches	No. of Cascade Reaches	No. of Plane-bed Reaches	Total No. of Reaches
ESL	8.73	2895 to 3850	5	3	1	9
LFC ^a	2.89	2910 to 3925	4	0	0	4
UFC	0.69	3212 to 3925	0	2	0	2

^a The drainage area and elevation ranges include UFC

Each creek is in a confined valley surrounded by Pleistocene and Holocene lateral moraines and underlain by Pre-Cambrian biotite schist and gneiss and Silver Plume granite [Taylor, 1975]. Both basins have shallow soils with low silt/clay content that are mainly derived from gneiss and schist [USDA Forest Service, 2009].

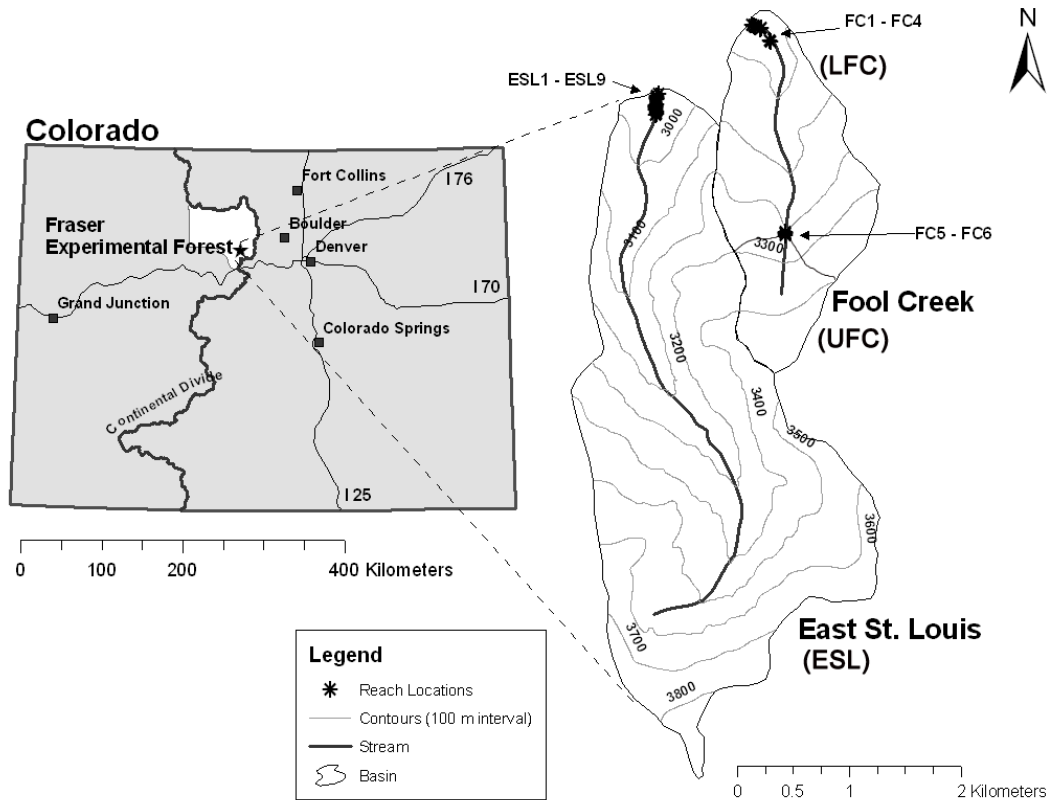


Figure 1: Location map for East St. Louis and Fool Creek in Fraser Experimental Forest

ESL drains approximately 8.73 km^2 and has been gaged since 1943. LFC, including UFC, drains 2.89 km^2 and has been gaged since 1941. UFC is a 0.69 km^2 basin with a gage installed circa 1986. All of the basins are dominated by cascade and step-pool morphologies above the gages, with limited plane-bed reaches (Table 1).

Fifteen channel reaches on East St. Louis Creek (ESL) and Fool Creek (FC) were selected in the field based on visual assessment of morphology (Table 2). Upper and lower boundaries of each reach were chosen to ensure consistent morphology and

gradient within the reach. Reaches are labeled in order from downstream to upstream on each basin. Step-pool reaches in both ESL and LFC include large amounts of wood (Figure 2). Over 95% of the wood in the step-pool reaches is found in the steps. ESL4 and FC1 are the only two step-pool reaches where 100% of the steps are boulder steps. The rest of the step-pool reaches are more varied, with half the steps being boulder steps and the other half having steps created by a wood jam around one large keystone boulder. FC3 is the only reach where all the steps are wood steps. The cascade reaches in both basins contain a small number of steps and, except for ESL5, these steps are mainly boulder steps. These reaches are still identified as cascade since the pools are not as wide as channel and the majority of the reach has tumbling flow over large boulders [Zimmerman and Church, 2001]. In ESL3 and ESL8, large bars of boulders, wood and herbaceous vegetation exist above the mean annual peak flow line in the middle of the reach, separating the flow into two paths. ESL2, ESL5, and FC3 each have a large and complex wood jam that causes a greater deceleration of the water than in other reaches and deposition of a relatively large amount of fine sediment just upstream of the step. ESL6, the lone plane-bed reach (Figure 2), can be found just upstream of the large wood step at the upstream end of ESL5.

Field surveys were conducted at all fifteen reaches during the summers of 2007 and 2008. Only ESL5 and ESL7 had changes in the wood load between 2007 and 2008. ESL5 had the largest change with an additional log in the reach in 2008. ESL7 has the largest amount of logs bridging the reach and some of these broke before the 2008 survey. FC3 had overbank flow during the 2008 high flow, which notably widened the reach and allowed a small island to develop in the middle of the channel. The flow went

back to the main channel once the snowmelt period was complete. ESL1 and ESL4 also had some slight overbank flow during the peak runoff period, but the majority of the water remained within the main channel.

Further descriptions of reaches with photographs and tables can be found in the Appendixes. Appendix A contains tables with summaries of hydraulic variables that were either measured or calculated for each reach, as well as reach descriptors such as wood load. Appendix B shows graphs of the flow measured at each of the gages. Appendix C contains photographs and descriptions of each reach. Appendix D contains graphs of the grain size distribution for each reach. Appendix E contains photographs and location of wood in each reach.

Table 2: Description of thalweg length, L_r , gradient, S_0 , average cross-sectional area, A , average hydraulic radius, R_h , step steepness, H/L_s , particle size, D_{50} and D_{84} , average velocity, V , average discharge, Q , dimensionless unit discharge, q^* , Froude number, Fr , Reynolds number, Re and Darcy-Weisbach friction factor, ff for each reach. Values on top are minimum values and values on bottom are maximum values over the four flow periods. A minimum slope value does not necessarily correlate with a minimum f value. See Appendix A for full table.

Reach	Channel Type	L_r (m)	S_0 (m/m)	A (m ²)	R (m)	H/L_s	D_{50} (m)	D_{84} (m)	V (m/s)	Q (m ³ /s)	q^*	Fr	Re	f
ESL1	Step-pool	27.3	0.086	0.29	0.12	0.13	0.05	0.16	0.22	0.06	0.16	0.21	2.2E+04	4.23
		31.6	0.104	0.99	0.25	0.18			0.66	0.66	1.16	0.42	1.5E+05	16.32
ESL2	Step-pool	13.7	0.085	0.45	0.15	0.14	0.01	0.07	0.25	0.11	0.76	0.20	3.4E+04	4.35
		14.7	0.095	1.00	0.25	0.20			0.63	0.63	3.34	0.42	1.4E+05	16.84
ESL3	Cascade	10.1	0.124	0.42	0.14	0.31	0.06	0.13	0.39	0.16	0.46	0.33	4.8E+04	3.75
		11.3	0.140	0.87	0.18	0.66			0.73	0.64	1.18	0.55	1.2E+05	9.15
ESL4	Step-pool	15.6	0.102	0.50	0.17	0.19	0.07	0.17	0.54	0.16	0.31	0.25	5.0E+04	5.17
		16.5	0.128	0.99	0.26	0.24			0.73	0.68	1.05	0.43	1.6E+05	13.15
ESL5	Cascade	12.5	0.136	0.59	0.15	0.21	0.05	0.14	0.25	0.15	0.26	0.21	3.3E+04	10.66
		15.1	0.160	1.20	0.24	1.03			0.52	0.63	0.90	0.34	1.1E+05	22.85
ESL6	Plane-Bed	5.9	0.017	0.44	0.15	N/A	0.02	0.09	0.42	0.18	0.88	0.35	5.5E+04	0.10
		6.5	0.023	0.89	0.26				2.07	1.85	7.92	1.30	3.8E+05	1.31
ESL7	Cascade	22.1	0.083	0.42	0.15	N/A	0.08	0.17	0.43	0.18	0.33	0.35	5.7E+04	3.34
		24.3	0.099	0.97	0.25				0.73	0.71	1.04	0.46	1.6E+05	5.26
ESL8	Step-pool	30.7	0.082	0.48	0.16	0.07	0.07	0.17	0.36	0.17	0.30	0.29	5.1E+04	4.22
		35.5	0.099	0.91	0.23	0.09			0.62	0.57	0.80	0.41	1.3E+05	8.05
ESL9	Step-pool	16.1	0.095	0.47	0.17	0.14	0.06	0.15	0.34	0.16	0.38	0.26	5.0E+04	5.60
		18.6	0.117	0.92	0.25	0.18			0.62	0.57	1.09	0.40	1.4E+05	10.78
FC1	Step-pool	22.3	0.058	0.09	0.06	0.06	0.03	0.08	0.20	0.02	0.18	0.25	1.1E+04	1.07
		25.1	0.062	0.38	0.16	0.08			0.86	0.33	2.18	0.68	1.2E+05	7.58
FC2	Step-pool	14.2	0.071	0.08	0.06	0.06	0.03	0.08	0.19	0.01	0.18	0.25	1.0E+04	2.23
		15.1	0.077	0.39	0.18	0.11			0.68	0.26	2.21	0.52	1.0E+05	9.59
FC3	Step-pool	11.9	0.079	0.12	0.07	0.09	0.01	0.05	0.11	0.01	0.28	0.13	6.9E+03	7.24
		14.9	0.095	0.55	0.19	0.15			0.43	0.24	3.27	0.32	7.2E+04	42.13
FC4	Step-pool	18.9	0.130	0.14	0.09	0.11	0.05	0.10	0.15	0.02	0.19	0.16	1.2E+04	3.82
		19.8	0.136	0.49	0.20	0.17			0.75	0.37	2.42	0.53	1.3E+05	39.89
FC5	Cascade	11.9	0.143	0.05	0.05	0.33	0.03	0.09	0.12	0.01	0.10	0.17	5.5E+03	4.64
		14.2	0.163	0.20	0.13	0.86			0.60	0.12	1.32	0.54	6.6E+04	39.22
FC6	Cascade	19.1	0.166	0.04	0.05	0.21	0.05	0.09	0.13	0.01	0.09	0.19	5.7E+03	4.73
		22.1	0.195	0.17	0.12	0.30			0.61	0.10	1.06	0.58	6.2E+04	36.16



$Q = 0.16 \text{ m}^3/\text{s}; ff = 13.15; S_0 = 0.102$



$Q = 0.04 \text{ m}^3/\text{s}; ff = 26.92; S_0 = 0.092$



$Q = 0.01 \text{ m}^3/\text{s}; ff = 39.22; S_0 = 0.143$



$Q = 0.16 \text{ m}^3/\text{s}; ff = 9.15; S_0 = 0.131$



$Q = 1.13 \text{ m}^3/\text{s}; ff = 0.14; S_0 = 0.017$

Figure 2: Photograph of a step-pool, cascade reach in each basin and the plane-bed reach in ESL: a) Step-pool reach on East St. Louis Creek (ESL4) during August 2007 survey; b) Step-pool reach on Lower Fool Creek (FC3) during July 2008 survey; c) Cascade reach on Upper Fool Creek (FC5) during August 2007 survey; d) Cascade reach on East St. Louis (ESL3) during August 2007 survey; e) Plane-bed reach on East St. Louis (ESL6) during June 2008 survey.

3.2 Field Methods

A laser theodolite was used to collect bed and water surface data every 15 cm along the thalweg and banks of each reach. All measurements were made over two summers in 2007 and 2008. The water surface was surveyed during a high flow (June 2008), two intermediate flows (July 2007, 2008) and one low flow (August 2007). These four measurement periods are referred to as flow periods in the rest of the paper and used as a categorical variable in the statistical analysis. The two intermediate flows are treated as separate flow periods. During each of these surveys the reach-average mean velocity was measured using Rhodamine WT dye tracer and fluorometers attached to rebar. The Rhodamine WT dye tracer was used in place of a salt tracer because of the requirements of the USDA Forest Service, which administers the study site. The rebar were fixed in the thalweg of the streambed at the upstream and downstream end of each reach. The fluorometers were placed at 0.6 of the water depth (h) for each measurement. Previous studies have shown that despite the lack of a logarithmic velocity profile, the reach-average mean velocity can still be approximated by placing probes at $0.6h$ or $0.2h$ and $0.8h$ [Wiberg and Smith, 1991; Legleiter et al., 2007; Wilcox and Wohl, 2007]. The probes recorded values at one second intervals and continued to record until the values returned to background levels. The measurements were repeated four times in each reach at each flow period. The differences between the centroids of the mass of dye were used rather than the difference between peaks for determining the time difference between the two probes [Lee and Ferguson, 2002; Curran and Wohl, 2003]. The centroid method was preferred because large amounts of noise in some of the measurements made a peak

arrival time difficult to read. Also, previous researchers have found that peak times may vary based on reach length, whereas the centroid method is more consistent [*Calkins and Dunne, 1970*].

A *Wolman* [1954] pebble count of 300 pebbles was conducted to determine particle-size distribution in each reach. Usually, 100 pebbles are counted in a *Wolman* pebble count, but it has been shown that increasing the sample size can reduce the error [*Thorne and Zevenbergen, 1985*]. The intermediate axis of each clast was measured with a ruler. Many of the largest boulders (0.5 – 1 m) were partly embedded, therefore the length of the intermediate axis was approximated. The pebble counts were done at evenly spaced cross-sections throughout the reach, which were anywhere from 0.5 to 1 m apart. Separate particle-size distributions were not determined for the steps and pools, only a composite value was used for the reach. A pebble count was repeated in one step-pool, cascade and plane-bed reach and average errors of 13, 8 and 4%, respectively, were determined for each channel type. A 13% error for step-pool reaches is well within the range of $\pm 10\%$ to $\pm 20\%$ reported by Ferguson (2007).

A tripod-mounted Light Detection and Ranging (LiDAR) Leica HDS Scanstation was used during the August 2007 low flow period to capture bank and bed topography (Figure 3). Each individual scan was merged within a tolerance of 1 cm at the control points. Figure 3 shows both a photograph and an example of the resulting pointcloud of ESL9. The pointcloud density varied substantially in each reach. The LiDAR scans were coupled with a feature-based survey with variable gridding that depended upon the underwater features, which was completed with a laser theodolite. The water surface data were imported into the scans and used together with cross-

sections created in Cyclone 5.8.1 [Leica Geosystems, 2008] using the LiDAR scans to calculate channel geometry data; i.e., width (w), depth (h), hydraulic radius (R_h), cross-sectional area (A). Values of these variables were reach averages based on multiple cross-sections. The cross-sections were evenly spaced (0.5 to 1.5 m) in each reach depending on the reach length. The cross-sections were surveyed in Cyclone 5.8.1 and then imported into Microsoft Excel. A spreadsheet was created that allowed calculation of channel geometry data (e.g., cross-sectional area, wetted perimeter, top width, average depth, hydraulic radius) after importing the water surface elevation for each flow period.



Figure 3: Example of the results of a LIDAR scan of ESL9. The arrow is pointing to the same log on the photograph (left) and the point cloud (right). The photograph and scan image are both showing a wood step in ESL9.

The water-surface slope (S_w) and bed slope (S_0) were calculated for each reach using a linear regression on the longitudinal profile of the thalweg, collected with the laser theodolite data. The S_w is used to calculate ff and S_0 is used in the statistical analyses. The average percent difference between S_w and S_0 is 4.2%, with the highest percent difference in the plane-bed reach, which had an average difference of 22.9% over the four flow periods. The average percent difference between S_0 and S_w in the step-pool and cascade reaches is 2.8 and 2.6%, respectively.

The standard deviation of bed elevation (s_{bed}) was calculated using the residuals of a planar regression of the elevation on the northing and easting axes. The northing and easting axes were taken from the laser theodolite survey of the thalweg. The relative step submergence, R_r/H_s , where H_s is step height, was calculated for step-pool reaches from thalweg and LiDAR data. The ratio of step steepness to gradient $(H_s/L_s)/S_0$ was also measured using the same data (where L_s = step length). Table 2 lists the minimum and maximum values for a selection of variables, which changed as a function of discharge, for each reach. Table 2 is presented to show the range of values that exist in each reach, but the minimum values in each row do not necessarily all correspond to each other, therefore the full data set is shown in Appendix A.

Wood length and diameter was measured for each flow period using a combination of the LiDAR scans, a tin of the water surface created in Cyclone 5.8.1, and photographs. The wood volume was calculated from these measurements and divided by the plan area of the reach (L_r*w). The wood volume includes pieces of wood found as single unattached pieces in the reach as well as in the steps. The total surface area of wood was found for each reach as well and dimensionalized by dividing by the plan area of the reach. ESL2 and FC3 have the largest wood load of any of the reaches. Photographs showing the location of the wood and a summary table of the data collected can be found in Appendix E.

CHAPTER 4 CONTROLS ON SPATIAL VARIATIONS IN FLOW RESISTANCE ALONG STEEP MOUNTAIN STREAMS

4.1 Abstract

Detailed channel and water surface surveys were conducted on 15 mountain stream reaches (nine step-pool channels, five cascade channels and one plane-bed channel) using a tripod-mounted Light Detection and Ranging (LiDAR) scanner and laser theodolite. Reach-average velocities were measured at varying discharges with dye tracers and fluorimeters. Multiple regressions and ANOVAs were used to test hypothesized correlations between Darcy-Weisbach friction coefficient, ff , and potential control variables. Gradient (S_0) and relative grain submergence (R_h/D_{84}) individually explained a low proportion of the variability in ff ($R^2 = 0.18$), where R_h is hydraulic radius, D_{84} is the 84th percentile of the cumulative grain size distribution, and R^2 is equal to the coefficient of determination. Because channel type, grain size and S_0 are interrelated, we tested the hypothesis that ff is highly correlated with all three of these variables or a combination of the above variables with flow period (a categorical variable) or dimensionless unit discharge (q^*). Total resistance correlated strongly ($\text{adj-}R^2 = 0.74, 0.69, \text{ and } 0.64$) with S_0 , flow period, wood load (volume of wood/m² of channel), q^* and channel type (step-pool, cascade, plane-bed). Total resistance differed between step-pool and plane-bed reaches and between cascade and plane-bed reaches. Significant differences in ff in step-pool and cascade reaches were found at the same values of flow and S_0 . The regression analyses indicate that discharge explains the most variability in ff , followed by S_0 when discharge is similar among channel reaches, and that R_h/D_{84} is not an appropriate variable

in these steep mountain streams to represent variations in both resistance and discharge. Results also indicate that the forms of resistance among channel types are sufficiently different to change the relationship of the control variables with ff in each channel type. These results can be used to further the development of predictive equations for high gradient mountain streams.

4.2 Introduction

Gradient is a defining characteristic of any stream channel. Gradient coupled with flow governs the amount of energy available for transporting material or eroding the banks and bed. Reach-scale gradient can be an independent variable in mountain streams, and typically correlates well with channel morphology [*Montgomery and Buffington, 1997; Wohl and Merritt, 2005*] and with grain size [*Wohl et al., 2004*].

Energy is dissipated in channels through resistance to flow from interactions with the bed and banks and formation of waves at the free surface [*Bathurst, 1982*]. In low gradient channels, resistance to flow and subsequent dissipation of energy occur when water is forced around channel bends or over bedforms such as ripples and dunes and from grain resistance. High gradient mountain streams dissipate energy when water flows over poorly sorted grains in the bed and banks and over bedforms such as steps and pools, creating an alternating pattern between supercritical and subcritical flow and causing energy dissipation through hydraulic jumps. Mountain streams differ from their low gradient counterparts by having large boulders that are of the same order of magnitude as the depth of flow, low values of relative grain submergence (R_h/D_{84} , where R_h is hydraulic radius and D_{84} is the 84th percentile of the cumulative grain-size

distribution), armored beds, and wood that commonly spans the entire width of the channel [Bathurst, 1993; Wohl, 2000].

The relationship of gradient on flow velocity and resistance is expressed in the three primary resistance equations developed by Chezy, Darcy and Weisbach, and Manning:

$$V = C(R_h S_f)^{1/2} = \left(\frac{8gR_h S_f}{ff} \right)^{1/2} = \frac{R_h^{2/3} S_f^{1/2}}{n} \quad (4.1)$$

where, V = mean flow velocity (m/s); C = Chezy coefficient; R_h = hydraulic radius (m); S_f = friction slope (m/m); ff = Darcy-Weisbach friction factor; g = acceleration due to gravity (m/s^2); and n = Manning coefficient. The coefficients in each of these equations express the total resistance to flow. For the remainder of this chapter I will focus on the Darcy-Weisbach equation and use ff to express total flow resistance because it is non-dimensional and is physically interpretable as a drag coefficient if resistance is equated with gravitational driving forces per unit bed area [Ferguson, 2007].

One difficulty in quantifying flow resistance in mountain streams is that V , R_h , and S_f exhibit large spatial and temporal variability. Many empirical equations have been developed that relate ff to these and other channel variables, but these typically perform poorly when extrapolated to other steep channels and in some cases have been shown to have errors as high as 66% [Bathurst, 1985, 1986, 2002; Wohl, 2000; Katul *et al.*, 2002; Aberle and Smart, 2003; Curran and Wohl, 2003; Ferguson, 2007].

Part of the uncertainty in applying empirically-based equations to new sites is that the relative importance of different sources of resistance can vary between sites. Total resistance is typically partitioned into grain (form drag on individual particles and viscous/skin friction on their surfaces), form (dunes, bars, steps), and spill (flow

transitions and wave drag on elements protruding above the water surface) resistance [Einstein and Barbarossa, 1952; Parker and Peterson, 1980; Wilcox et al., 2006; Ferguson, 2007]. The contribution made by each of these sources of resistance can differ in relation to gradient, channel morphology, or other factors [Ferguson, 2007]. Previous studies have typically focused on quantifying and/or partitioning resistance within a particular channel morphology [Lee and Ferguson, 2002; Wilcox and Wohl, 2007; Comiti et al, 2009, 2007; Reid and Hickin, 2008]. I propose that, because gradient is such an important influence on form and process in steep channels, spatial patterns of relative total resistance in mountain streams vary consistently in relation to gradient, and thus channel morphology.

The morphology of mountain streams is typically characterized as cascade, step-pool and plane-bed [Montgomery and Buffington, 1997]. Cascades form at $S_0 > 0.06$ m/m (where S_0 is bed gradient) and are characterized by tumbling flow over large, randomly arranged clasts [Montgomery and Buffington, 1997] that can create substantial grain resistance, dependent on stage. Skin friction and form drag around individual grains dissipate much of the mechanical energy. Occasional steps may be found in cascade reaches, creating a limited amount of spill resistance.

Step-pool channels form at gradients of $0.03 < S_0 < 0.10$ m/m [Montgomery and Buffington, 1997]. These reaches alternate between supercritical flow over steps transverse to flow and plunge pools with subcritical flow [Zimmerman and Church, 2001; Church and Zimmerman, 2007]. Steps create flow resistance by skin friction over large particles and wood, form drag from pressure differences around the upstream and downstream sides of an object, and spill resistance created from flow acceleration and

deceleration. The total resistance in step-pool channels is dominated by spill resistance, which varies with wood amount and location [Curran and Wohl, 2003; Wilcox et al., 2006; Comiti et al., 1999]. Comiti et al. [2008] found that the presence of wood dams in the Southern Andes can increase flow resistance up to one order of magnitude in step-pool channels.

Plane-bed channels lack well-defined, rhythmically occurring bedforms and occur at gradients of 0.01 to 0.03 m/m. This channel type is considered a transition between supply-limited cascade and step-pool reaches and transport-limited pool-riffle reaches [Montgomery and Buffington, 1997; Wohl, 2000]. The bed surface of the plane-bed reach is armored and has a threshold mobility near bankfull [Montgomery and Buffington, 1997].

Previous studies have demonstrated that discharge exerts an important influence on resistance; at-a-site variation in ff can be up to 100% as discharge and flow depth vary [Lee and Ferguson, 2002; Reid and Hickin, 2008]. Some investigators incorporate a measure of discharge such as R_h [Jarrett, 1984], discharge per unit width, q [Bjerklie et al., 2005], or dimensionless unit discharge, $q^* = q / \sqrt{gD_{84}^3}$ [Comiti et al., 2007; Ferguson, 2007]. Others use a ratio of flow depth to boundary roughness such as relative submergence of grains (R_h/D_{84}) or relative submergence of the bed (R_h/s_{bed}), where s_{bed} is equal to the standard deviation of the bed elevation [Aberle and Smart, 2003]. Bathurst [1985], for example, characterized roughness based on the relative grain submergence value as large- ($0 < R_h/D_{84} < 1$), intermediate- ($1 < R_h/D_{84} < 4$), or small-scale ($R_h/D_{84} > 4$), and Ferguson [2007] proposed resistance equations with different parameters for deep and shallow flows. Based on this, I also propose that spatial patterns of relative total

resistance in mountain streams vary consistently in relation to discharge, expressed via relative submergence of grains, steps and the bed.

To improve predictions of resistance and estimation of discharge, it is important to obtain a better understanding of resistance throughout a channel network, including variations in resistance within each type of channel morphology. My primary objective is to understand how resistance varies with gradient, channel morphology and relative submergence of grains, steps and the bed throughout a channel network. I hypothesize that predictable patterns of relative magnitude of total resistance exist throughout a channel network and that simple variables such as gradient can be used to predict these patterns. Because each morphologic type of cascade, step-pool and plane-bed channel spans a range of values for gradient and grain size, a secondary objective is to examine how resistance varies with gradient, relative grain submergence and discharge within each channel type. This objective reflects our understanding that the influence of each variable on total resistance may differ based on gross morphology differences within each channel type.

I address the first objective by testing two hypotheses with respect to flow resistance across a channel network. The null hypotheses are not explicitly listed for any of the hypotheses expressed below. H1: Total resistance correlates most strongly with a combination of potential control factors, which include S_0 , R_h/D_{84} , q^* , R_h/s_{bed} , wood load (m^3/m^2) and the categorical variables flow period and channel type, rather than with any single potential control factor. Relative grain submergence, q^* , R_h/s_{bed} and flow period all represent changes in discharge in each reach. Relative submergence of D_{84} and s_{bed} represent variations in discharge under the assumption that R_h changes with discharge,

but D_{84} and s_{bed} remain relatively constant. An alternative hypothesis is H2: Total resistance correlates most strongly with a single variable. Both hypotheses test differences in ff between sites rather than at-a-site. The choice of potential control variables reflects past work in this research field [*Bathurst, 2002; Aberle and Smart, 2003; Wohl and Merritt, 2005; Comiti et al., 2007; Ferguson, 2007*].

I also address the second objective by testing three hypotheses with respect to resistance between channel types and resistance within each channel type. H3: For a given gradient, there is a consistent difference in total resistance between step-pool and cascade channels. This hypothesis reflects the fact that an overlap occurs in the gradient range at which each channel type can form, and tests the possibility that channel morphology rather than gradient exerts the strongest influence on ff . H4: For a given R_h/D_{84} , there is a consistent difference in total resistance between step-pool and cascade reaches. This hypothesis provides another means of examining the possibility that channel type exerts the strongest influence on ff . H5: For each individual channel type, there is a consistent difference in which variables control variations in ff . This final hypothesis reflects our understanding that total resistance in each channel type may result from grain, form or spill resistance. The separate contributions from each of these components of resistance may result in different control variables being significantly related to total resistance in each channel type. For instance, in step-pool reaches the relationship between relative step submergence (R_h/H , where H is step height) and ff is investigated.

4.3 Statistical Methods

Both regression analysis and analysis of variance (ANOVA) were used in the program R to investigate which independent variables significantly influence ff [Jongman *et al.*, 1995; Kutner *et al.*, 2005; R Core Development Team, 2007]. Therefore, the major goal of this analysis and the results presented in Table 3 are not prediction and should not be used outside the range of values shown in Appendix A. The friction factor was used in the form of $(8/f)^{0.5}$ and related to gradient, relative grain submergence and channel type. The function, $(8/f)^{0.5}$, is easily related to dimensionless velocity (V/u^*), where u^* is shear velocity $(ghS_f)^{1/2}$, and the two other flow resistance coefficients,

$$\left(\frac{8}{f}\right)^{1/2} = \frac{C}{g^{1/2}} = \frac{R^{1/6}}{ng^{1/2}} \quad (4.2)$$

[Bathurst, 1985; Thorne and Zevenbergen, 1985]. The only time the friction factor is used in its regular form, as ff , is when it is used in a regression with q^* . The results of these regression models are presented so that they can be compared with the values calculated by Comiti *et al.* [2007]. The variables $(8/f)^{0.5}$, S_0 , R_h/D_{84} , wood load, and q^* were log-transformed to meet regression assumptions of homoscedacity [Jongman *et al.*, 1995; Kutner *et al.*, 2005]. All regressions and variables were significant at an $\alpha = 0.05$ level.

The plane-bed reach was removed as an outlier in the regression analysis and the ANOVA. Because there is only one plane-bed reach, it often drives the model by increasing the R^2 (coefficient of determination) value and causing heteroscedacity of the residuals. Therefore, the plane-bed reach is only included in the ANOVA testing the relationship between channel type and ff , S_0 , and R/D_{84} respectively. A Tukey HSD method was used to gage significant differences between means in the ANOVAs. The

Tukey HSD method adjusts for differences in sample sizes, so appropriate comparisons can be made between means [Kutner *et al.*, 2005; R Core Development Team, 2007].

Both the Mallows' C_p and adjusted- R^2 were used to compare models. The C_p is calculated by comparing a reduced model to a model with all the variables. The minimum C_p is sought to determine the best model with the smallest mean squared error and the smallest bias [Kutner *et al.*, 2005]. The adjusted- R^2 is adjusted for the number of variables in the model. The best model is associated with the maximum adjusted- R^2 and all values reported in the results, below, are adjusted- R^2 . Flow period is used as a categorical variable because repeat measures were taken in the same reaches, meaning that those values are not independent of each other. A benefit of using the categorical variable flow period is to understand how ff varies at-a-site with discharge. To reduce autocorrelation variables such as stream power, Froude number and Reynolds number were not used in the analysis even though it is understood that each of these variables have an effect on ff . Discharge (Q) is not included as a predictor of ff since the ultimate goal of this type of research is to find variables that will help in prediction of ff and subsequently Q and V in these high-gradient channels. I chose to include one variable, q^* , that includes Q in the calculation of the variable, because of the success in using this variable from previous work on high gradient streams [Comiti *et al.*, 2007; Ferguson, 2007] and the understanding that the goal of some applications is to predict V when Q is known. It is also noted that in any regression models that include S_0 there may be issues with autocorrelation because of the collinearity between S_0 and S_w .

4.4 Results

4.4.1 Friction factor, gradient, relative submergence, wood load, channel type and drainage basin (H1 and H2)

H1 tests whether $(8/f)^{0.5}$ is significantly related to a combination of control variables which include S_0 , R_h/D_{84} , q^* , wood load, flow period and channel type. Table 3 shows seven models that combine S_0 with each flow variable (R_h/D_{84} , q^* , flow period) and channel type. The values in Table 3 for each of the continuous variables are all exponents that indicate the rate of change of each independent variable with the dependent variable. Gradient, R_h/D_{84} , q^* , flow period and channel type all explain a significant amount of the variation in $(8/f)^{0.5}$ and ff at the $\alpha = 0.05$ level. Gradient and channel type combined with either flow period or q^* are the models that explain the greatest amount of variability in both $(8/f)^{0.5}$ and ff (Table 3). Models 3 and 5a have the highest adjusted- R^2 (0.69 and 0.64) and lowest Mallows' C_p values (8.16 and 12.47). Models that include wood load (Model 1, 4b, and 5b) also have an improved adj- R^2 . The rate of change of S_0 with $(8/f)^{0.5}$ varies between -0.45 to -0.89 for Models 1 through 4b. As S_0 increases the value of $(8/f)^{0.5}$ decreases, indicating that ff is highest at steeper gradients.

Model 1 tests whether there is a consistent difference in $(8/f)^{0.5}$ for each flow period for a given S_0 and wood load. The model is improved with this categorical variable (adjusted- $R^2 = 0.64$) and the intercepts for each flow period are significantly different from each other (Figure 4). Model 1 shows that for high- and intermediate-flow period, $(8/f)^{0.5}$ is significantly greater than the August low flow period (Table 3). Therefore, $(8/f)^{0.5}$ is lowest for the higher flows for a given S_0 and wood load. The interaction term

between S_0 and flow period was tested, but found to be not significant. Therefore, the rate of change of $(8/f)^{0.5}$ with S_0 is not significantly different at each flow period (Figure 4). If the rate of change was significantly different it would mean that the slope of the regression line is significantly different for each flow period. The relationship between $(8/f)^{0.5}$ and wood load was also found to be significant at a given S_0 and flow period. As wood load increases $(8/f)^{0.5}$ decreases. The interaction term was not significant between wood load and flow period, therefore the rate of change does not vary with flow period.

Model 2 tests whether there are significant differences in $(8/f)^{0.5}$ between the two basins, East St. Louis and Fool Creek, while holding gradient constant. The cascade reaches in UFC and step-pool reaches in LFC are combined in the Fool Creek basin. The two basins have some distinct characteristics relative to each other, therefore we tested whether for a given S_0 there is a consistent difference in $(8/f)^{0.5}$ in East St. Louis versus Fool Creek, holding the flow period constant. The regression shows that there is a significant difference between the two (Table 3). For a given S_0 and flow period, $(8/f)^{0.5}$ in Fool Creek is higher than in East St. Louis. The interaction term between S_0 and drainage basin was found to be not significant. Therefore, the overall value of $(8/f)^{0.5}$ is affected by differences in each basin, but the rate of change of $(8/f)^{0.5}$ with S_0 is not affected by the basin. Because of the small number of reaches, it is not appropriate to also separate by channel type in the multiple regression, but the differences in $(8/f)^{0.5}$ between channel type and basin are further explored in the ANOVAs in section 4.4.

The variation in ff between high and low flow is much greater in Fool Creek than in East St. Louis (Figure 5). Figure 5b displays the differences in the at-a-site variation in $(8/f)^{0.5}$ for both Fool Creek and East St. Louis. The greater variability in $(8/f)^{0.5}$ in Fool

Table 3: Linear regressions of $(8/f)^{0.5}$ and ff versus independent variables and categorical variables. Models 1 – 4b and 6 – 12 use $(8/f)^{0.5}$ as the dependent variable. Models 5a – 5b use ff as the dependent variable. The numbers in each column under the model number shows which variables were used in each regression. The Mallow's Cp is not shown for regressions that had outliers removed.

Dependent Variable ²	Independent Variables ¹														
	Model 1 ³	Model 2	Model 3	Model 4a	Model 4b	Model 5a	Model 5b	Model 6	Model 7	Model 8	Model 9	Model 10	Model 11	Model 12	
	H1	H1	H1	H1	H1	H1	H2	H2	H2	H2	H2	H2 ⁴	H3	H4	
$(8/f)^{0.5}$	Intercept	0.12*	0.17*	0.11*	0.22*	0.19*			0.89*	0.29*	0.88*		0.51*	0.23*	0.88
ff	Intercept						84.95*	242.64*				5.97*			
	S_0^5	-	-0.66*	-0.89*	-	-0.45*	1.32*	0.79*		-0.54*				-0.69*	
	R/D_{84}^*	0.63*			0.69*	0.39*	0.56*				0.39*				0.41*
	R/s_{bed}								0.72*						
	wood load	-0.05*					-0.09*		0.13*				-0.10*		
	July07 ⁶	1.39*	1.46*	1.47*											
	July08 ³	1.36*	1.36*	1.38*											
	June08 ³	2.02*	2.10*	2.16*											
	August 07 ³	1.00*	1.00*	1.0*											
	Step-Pool ⁷			0.79*	0.76*	0.87	1.62*	1.09						0.86	0.98
	Cascade			1.00*	1.00*	1.00	1.00*	1.00						1.00	1.00
	FC ⁸		0.86*												
	ESL		1.00*												
F-statistic		30.76	23.71	25.01	9.59	18.08	33.57	21.84	96.38	11.88	11.32	51.89	10.6	6.76	6.84
p-value⁹		0.001	0.001	0.001	0.001	0.001	0.001	0.001	0.001	0.001	0.001	0.001	0.002	0.002	0.002
R²		0.77	0.71	0.72	0.36	0.60	0.66	0.65	0.65	0.18	0.18	0.49	0.18	0.21	0.21
Adj. R²		0.74	0.68	0.69	0.32	0.57	0.64	0.62	0.64	0.17	0.16	0.49	0.16	0.18	0.18
Mallow Cp			10.04	8.16	56.23		12.47		58.52	82.29	82.83	25.66		79.92	84.79

¹ Variables with * indicate that value is significant at the $\alpha = 0.05$ level.

² Variables in **bold** were transformed using the natural log.

³ FC3 Aug 2007 and FC3 July 2008 were both outliers when wood load is included in the regression. Therefore, both of these were removed.

⁴ All ESL2 data were removed as outliers.

⁵ Numbers shown are exponents of independent variables, if it is a categorical variable and that category is true than the number should be multiplied with the intercept.

⁶ Part of Flow Period categorical variable with four levels that include July 07, July 08, June 08 and August 07.

⁷ Part of Channel Type categorical variable that includes two levels in all models except for Model 7. The two levels are step-pool and cascade channel types.

⁸ Part of drainage basin categorical variable that has two levels FC and ESL. FC includes both UFC and LFC.

⁹ Where 0.001 is indicated, the value is actually < 0.001 .

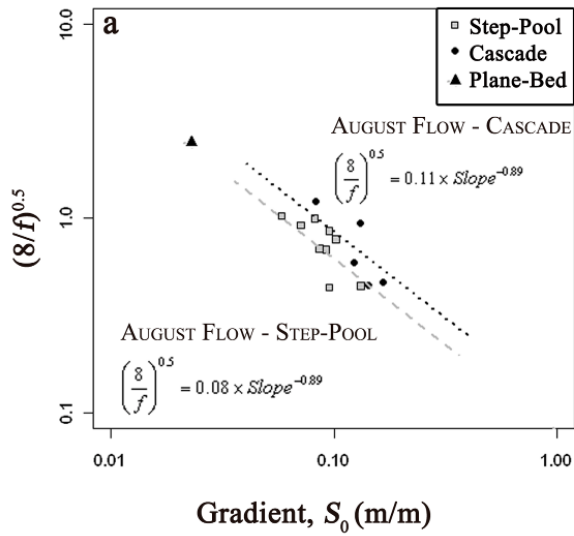
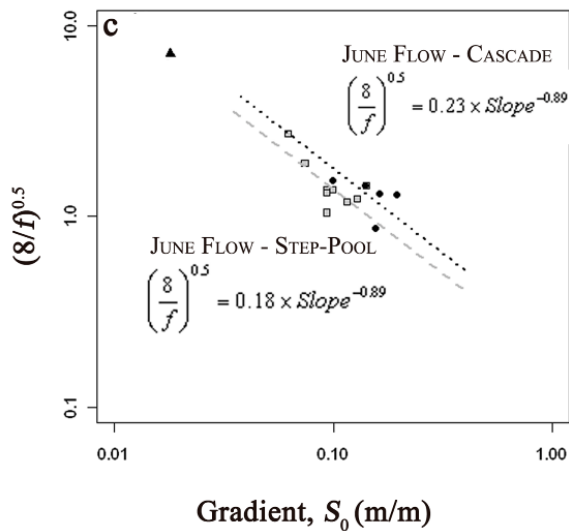
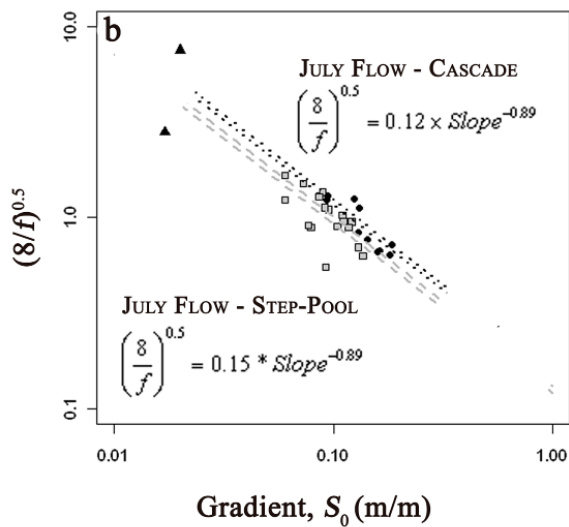


Figure 4: $(8/f)^{0.5}$ versus gradient (S_0) for each channel type: a) shows trend line and points for August 2007 flow for cascade and step-pool channels; b) shows trend lines and points for July 2007 and 2008 flows for cascade and step-pool channels; c) shows trend line and points for June 2008 flow for cascade and step-pool channels.



Creek is most likely related to the greater variation in flow depth and wetted width at the high versus low flows (Figure 6). The baseflow remains much higher in East St. Louis after snowmelt than in Fool Creek. Therefore, the relatively small flow in Fool Creek has a much higher friction than the lowest surveyed flow in East St. Louis, causing an increased variability in $(8/f)^{0.5}$ in Fool Creek. Models 1 and 2 show that $(8/f)^{0.5}$ is correlated with S_0 throughout a channel network and that correlation is better explained by holding flow period and drainage basin constant.

Models 5a and 5b show that ff decreases as q^* increases while holding both S_0 and channel type constant. The dimensionless unit discharge is used in place of flow period and R_h/D_{84} . Wood load is included in Model 5b, causing the channel type to no longer be significant. All variables (S_0 , q^* , channel type) are found to explain a significant proportion of the variability in ff while holding all other variables constant. The significance of q^* and improved model fits indicate that R_h/D_{84} does not completely encompass the effects of different flows in these steep mountain streams. The results shown in Table 3 therefore support H1; ff correlates most strongly with a combination of potential control factors, rather than with any single potential control factor.

The relationship between $(8/f)^{0.5}$ and individual control variables is shown with Models 6 through 10 (Table 3). These models are shown to better understand the relationship between individual control variables and $(8/f)^{0.5}$ rather than between combinations of control variables and $(8/f)^{0.5}$. For all reaches at all flow periods, $(8/f)^{0.5}$ correlates positively with R_h/D_{84} and negatively with S_0 . The relative grain submergence explains the same proportion of the variability in $(8/f)^{0.5}$ as does S_0 and wood load (Models 7, 8, and 10). These results partially support the second hypothesis, that $(8/f)^{0.5}$

correlates with individual control variables (Table 3), but do not suggest that $(8/f)^{0.5}$ correlates most strongly with an individual control variable.

The friction factor was found to be significantly related to q^* ; as q^* increases, ff decreases (Model 9). In this case q^* is related to ff rather than $(8/f)^{0.5}$. The relationship was found to explain more of the variability in ff (adjusted- $R^2 = 0.49$) than R/D_{84} (Model 8, adjusted- $R^2 = 0.16$). These results are re-emphasized in Model 4a, where S_0 combined with R_f/D_{84} and channel type explains a much smaller proportion of the variability in $(8/f)^{0.5}$ than a model with either flow period (Model 4) or q^* (Model 5). A model with wood load also explains a greater proportion of the variability, particularly when combined with S_0 and q^* or flow period. These results do not support H2 that ff correlates most strongly with an individual variable. Therefore, the best model that explains the most variability in the dataset is a model with a combination of control variables.

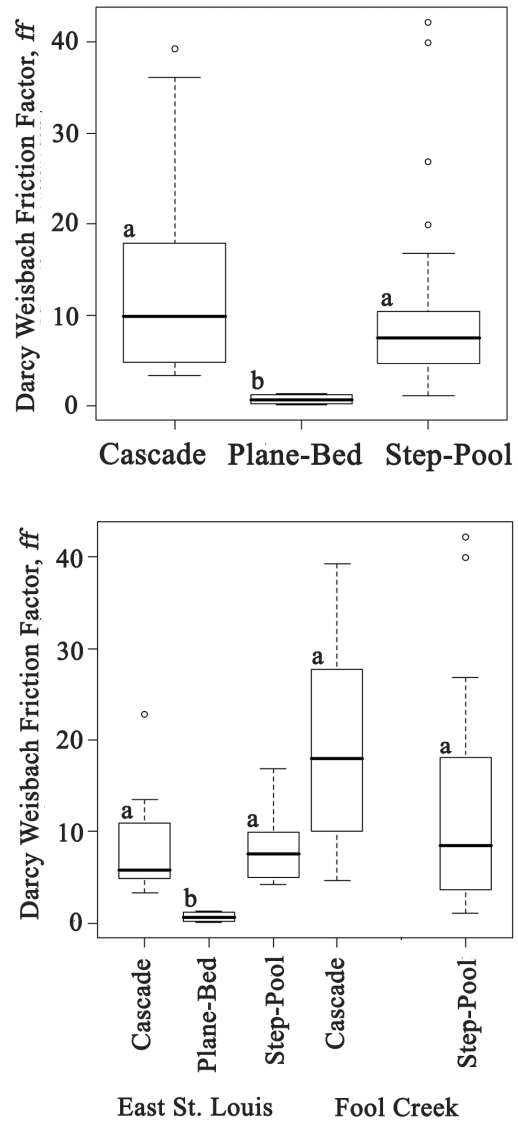


Figure 5: Box-plots of ff versus channel type (a) and ff versus channel type for each basin (b). The contrasting letters (a and b) above the boxes show the results of the significant ($p < 0.05$) pairwise differences in means from Tukey's test following an ANOVA. Box-plots with the same letter do not have significantly different means, box-plots with different letters do have significantly different means.

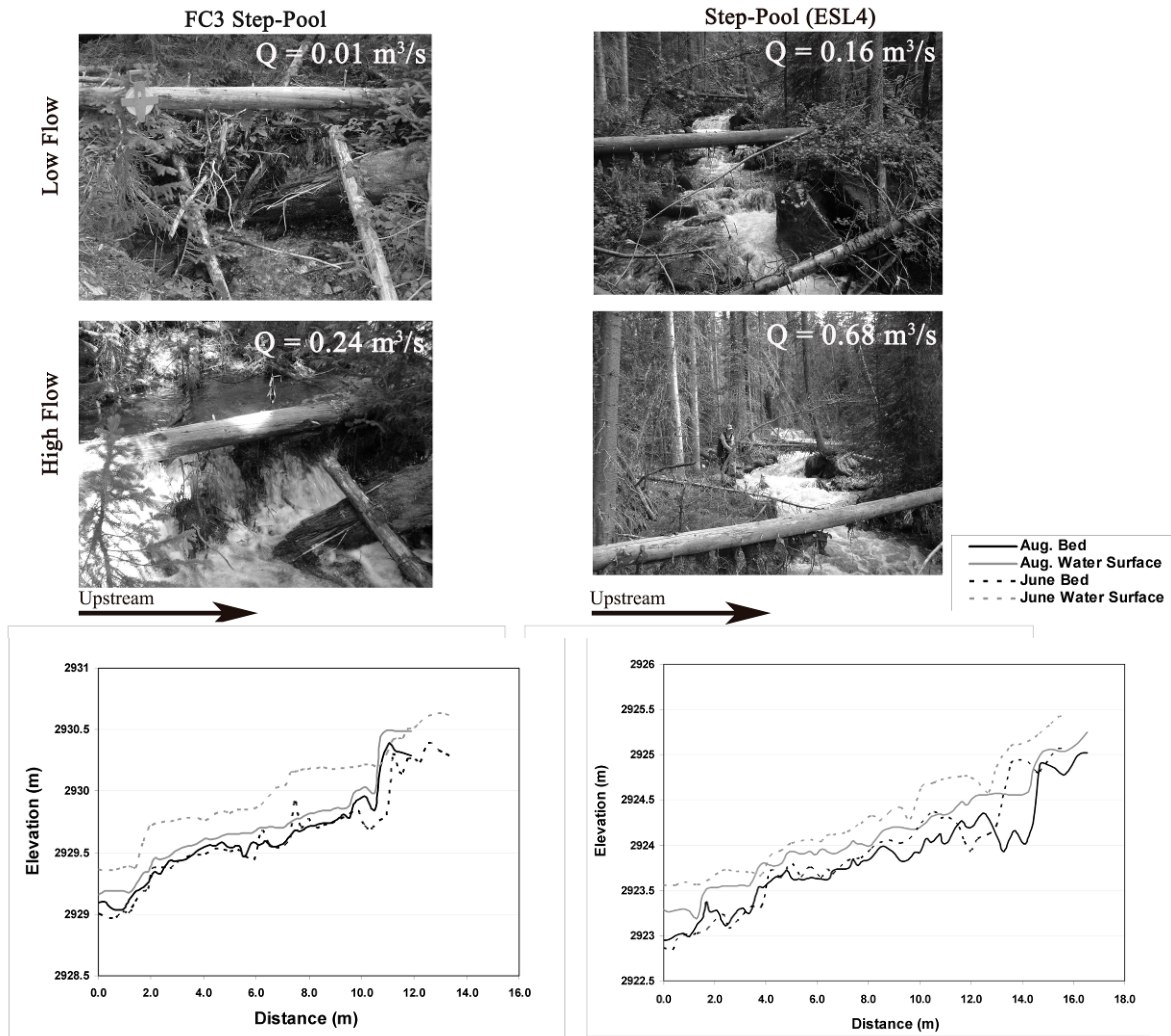


Figure 6: Comparison of the August 2007 (low) flow period and June 2008 (high) flow period in the step-pool reaches FC3 and ESL4. The longitudinal profiles are shown for each low flow and high flow survey for each reach. The photographs and graphs show the differences in depths and relative submergence at the two flows for each reach.

4.4.2 Friction factor and standard deviation of bed elevation (H2)

The D_{84} , D_{50} , $\log(D_{84}/D_{50})$ and s_{bed} were each regressed against velocity to determine which variable is the most appropriate roughness parameter. These roughness parameters are on the same order of magnitude as the flow depth, and the variation in each may be larger than the variation in flow depth. Therefore, I expect that the individual roughness parameters will be related to flow velocity without accounting for flow depth. Both D_{84} and D_{50} were significantly related to velocity, but no significant relationship could be found between velocity and s_{bed} or velocity and $\log(D_{84}/D_{50})$.

There is a significant relationship between R_h/s_{bed} and velocity, which is reflected in the significant relationship shown in Model 6 between R_h/s_{bed} and $(8/f)^{0.5}$ (Table 3). R_h/s_{bed} as a relative submergence parameter explains more of the variation of $(8/f)^{0.5}$ than R_h/D_{84} (Model 8). The improved relationship may result partially from the spurious correlation between R_h and $(8/f)^{0.5}$. The strong relationship supports the second hypothesis that $(8/f)^{0.5}$ correlates with R_h/s_{bed} despite the lack of correlation between s_{bed} and velocity.

4.4.3 Friction factor and channel type (H2)

Channel type, S_o and grain size are all interrelated, therefore I investigated how ff varies by channel type. Figure 5 shows a box-plot of the three channel types versus ff , determined for the different flow periods. An ANOVA and a Tukey's test were used to compare significant differences between means of ff . The friction factor was log transformed to meet normality assumptions of the ANOVA and Tukey's test. Means for cascade and step-pool channels were found to be significantly different from the plane-bed channel, but not significantly different from each other. The Tukey HSD method takes account of the smaller sample size of 4 in the plane-bed versus 20 for the cascade

and 35 for the step-pool reaches while gaging differences between means. How well this plane-bed reach represents plane-beds in mountain streams will be discussed further in a subsequent paper.

Figure 5b shows the channel types separated by drainage basin. The box-plot re-emphasizes that the plane-bed reach is significantly different from all other channel types in both basins. The main difference between Fool Creek and East St. Louis is that the standard deviation of ff is much broader for cascade and step-pool reaches in Fool Creek than in East St. Louis. Therefore, ff does not vary significantly between cascade and step-pool reaches over all flow periods, but does vary significantly between the cascade and plane-bed and between the step-pool and plane-bed reaches. Thus, the results do not support hypothesis 2, that ff correlates most strongly with the individual control variable of channel type.

4.4.4 Friction factor, gradient and channel type (H3)

Figure 7 displays a significant variation in S_0 among channel types and among channel types in each basin. Once the channel types are differentiated by basin, the mean S_0 values between the step-pool and cascade reaches in East St. Louis are not significantly different, but are significantly different in Fool Creek. Model 11 shows that, holding S_0 constant, there is no consistent difference in $(8/f)^{0.5}$ between cascade and step-pool channels (Table 3). The lack of relationship in Model 11 may reflect the large at-a-site variability in these reaches (Figure 6) that is accounted for when flow period or q^* is held constant (Model 3 and Model 5a). The results therefore do not support the third hypothesis that while holding S_0 constant there is a consistent difference in $(8/f)^{0.5}$ between cascade and step-pool channels.

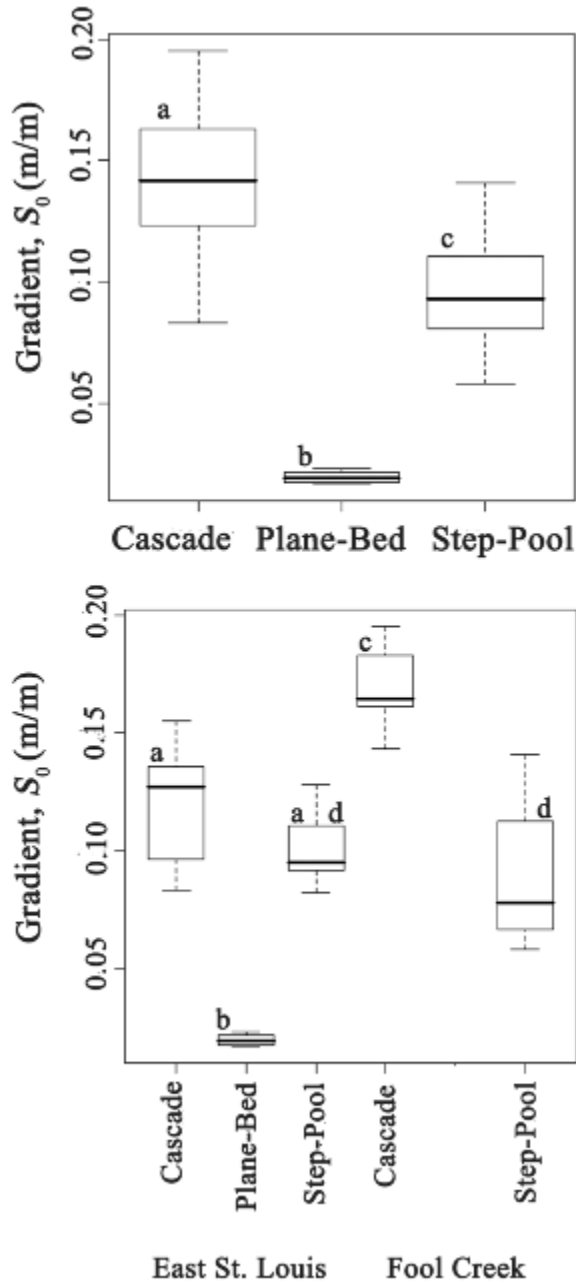


Figure 7: Box-plots of gradient versus channel type (a) and gradient versus channel type and basin (b). The letters a, b, c and d over each boxplot show the results of the Tukey's test following an ANOVA. Box-plots with the same letter do not have significantly different means ($p > 0.05$), box-plots with different letters do have significantly different means ($p < 0.05$).

4.4.5 Friction factor, relative grain submergence and channel type (H4)

R_h/D_{84} was found to be significantly related to $(8/f)^{0.5}$. Table 3 shows the regression of R_h/D_{84} and channel type on $(8/f)^{0.5}$ in Model 12. The channel type is not significantly related to $(8/f)^{0.5}$ when R_h/D_{84} is held constant. The interaction terms were not tested because there was no significant relationship between $(8/f)^{0.5}$ and channel type. Figure 8a indicates that there are significant differences in R_h/D_{84} between cascade and plane-bed and between step-pool and plane-bed reaches. The variation in $(8/f)^{0.5}$ between plane-bed and other channel types may be better explained by R_h/D_{84} but cannot be further explored because there is only one plane-bed reach. Figure 8b indicates that the difference in standard deviation between cascade and step-pool channels is greater in Fool Creek than in East St. Louis.

R_h/D_{84} is plotted against $(8/f)^{0.5}$ for cascade and step-pool reaches in Figure 9a. The scatter in $(8/f)^{0.5}$ is much broader for the step-pool than for the cascade reaches. A regression using only the cascade reaches (Figure 9b) indicates that there is a significant power relationship between R_h/D_{84} and $(8/f)^{0.5}$. Therefore, holding R_h/D_{84} constant, there is no consistent difference in ff between channel types, but a regression restricted to only cascade reaches indicates that a high proportion of the variability in $(8/f)^{0.5}$ is explained by R_h/D_{84} in that channel type. The results thus do not support the fourth hypothesis, that for a given R_h/D_{84} there is a consistent difference in $(8/f)^{0.5}$ between step-pool and cascade reaches. Instead, the significant relationship is between R_h/D_{84} and $(8/f)^{0.5}$ for cascade reaches.

4.4.6 Friction factor, relative grain submergence, wood load, gradient and dimensionless unit discharge for each channel type (H5)

The final hypothesis examines how the significance of the relation of each of these control variables and $(8/f)^{0.5}$ may vary depending on the channel type. Table 4 shows three multiple regressions using only the cascade reaches and four multiple regressions using only the step-pool reaches. The results re-emphasize that Model 13 using only the cascade reaches with both S_0 and R_h/D_{84} is much better than Model 16 which only uses step-pool reaches. The highest proportion of the variability is explained in both channel types when q^* is included in the regression (Model 14 and Model 19). The regression with the step-pool reaches is greatly improved (adjusted- $R^2 = 0.68$) when the variable of relative step submergence (R_h/H) is included, but no relationship was found by including $(H/L_s)/S_0$ (Model 18). Including wood load improved both the cascade model (Model 15) and the step-pool model (Model 18).

Table 4 also shows that the rate of change of q^* with ff is different for the two channel types. Both q^* and S_0 have exponents close to -1.0 and 1.0 for the cascade reaches, whereas the exponents for q^* and S_0 are equal to -0.59 and 1.40, respectively, for step-pool reaches. Most likely these differences were not apparent when the interaction terms were tested in Table 3, because the larger variability in the step-pool reaches may have made it difficult to examine the relationships with the cascade reaches. These results support H5, that the components of resistance are sufficiently different in each channel type to change the relationship of the control variables with ff in each channel type. This suggests that different control variables should be used when considering the different channel types.

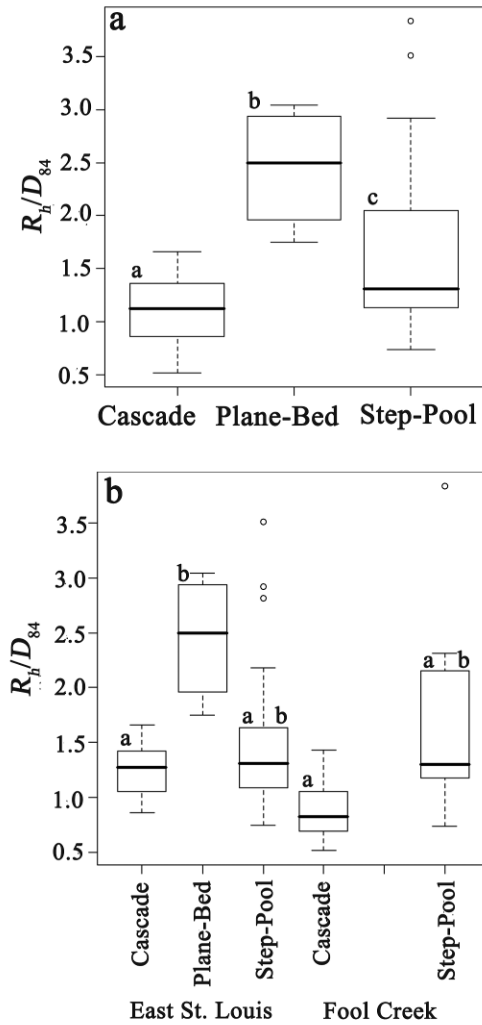


Figure 8: Box-plots of relative grain submergence (R_h/D_{84}) versus channel type (a) and relative grain submergence versus channel type and basin (b). The letters a, b and c over each boxplot show the results of the Tukey method following an ANOVA. Box-plots with the same letter do not have significantly different means, box-plots with different letters do have significantly different means ($p < 0.05$).

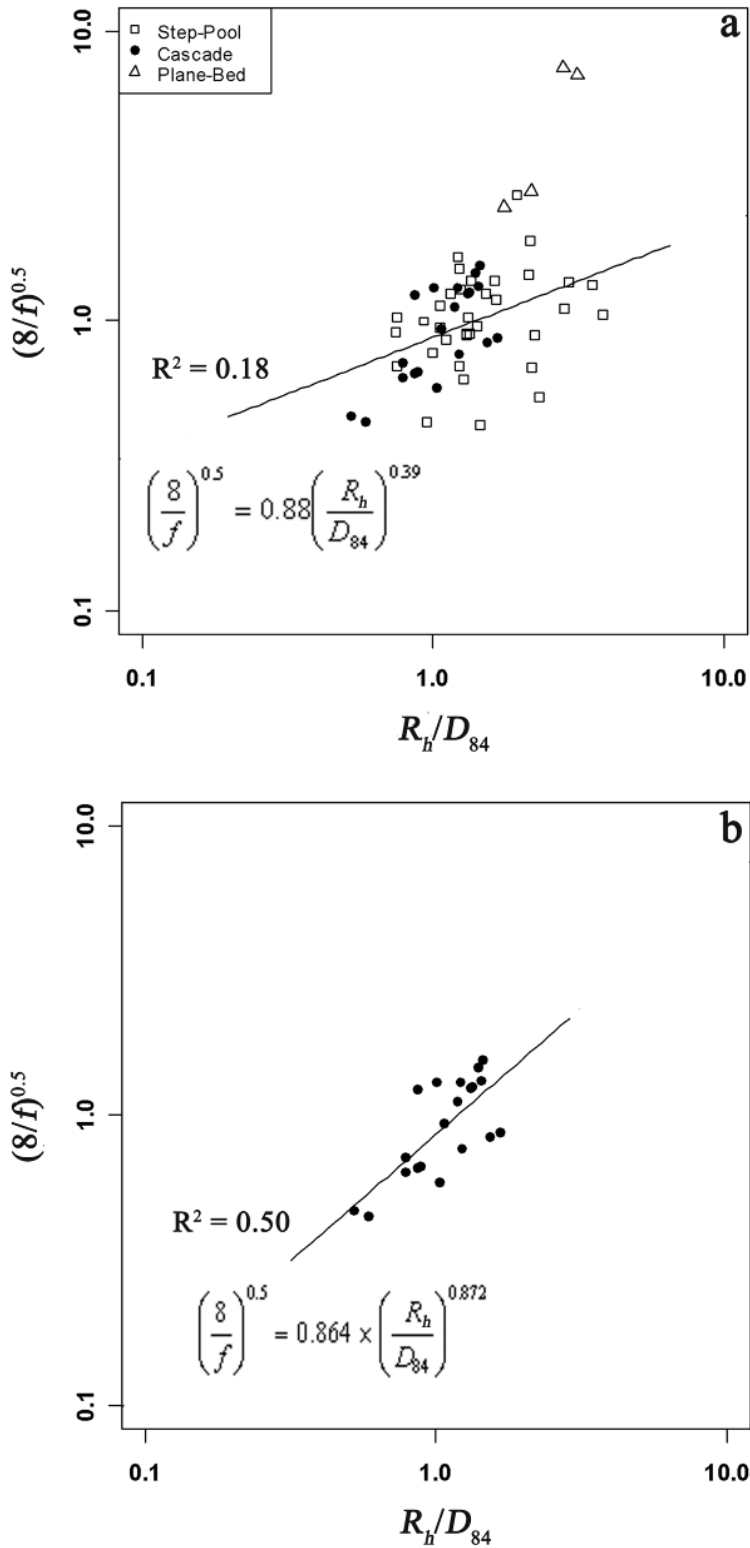


Figure 9: a) Relative grain submergence versus $(8/f)^{0.5}$ for each channel type. Trendline shows relationship between relative submergence and friction factor for all sites (excluding ESL6, the plane-bed reach). b) Relative grain submergence versus friction factor for cascade reaches.

Table 4: Linear regressions of $(8/f)^{0.5}$ and ff versus independent variables separated by channel type. Model 13 – 15 only include cascade reaches. Model 16 – 19 only include step-pool reaches.

		Independent Variables ^a						
Dependent Variables ^b		Cascade Model 13	Cascade Model 14	Cascade Model 15	Step-Pool Model 16	Step-Pool Model 17	Step-Pool Model 18	Step-Pool Model 19
$(8/f)^{0.5}$	Intercept ^c	0.32*			0.17*			
ff	Intercept		40.53*	162.06*		6.20*	39.33*	156.00 *
	S_0	-0.50*	1.04*		-0.53*	0.57*		1.40*
	R_p/D_{84}	0.78*			0.42*			
	q		-0.90*	-1.10*			-0.73*	-0.59*
	R_p/H^d					-1.75*		
	wood load			0.25*	-0.09*		0.15*	
	$(H/L_s)/S_0$						0.38	
F-statistic		13.62	41.31	19.81	6.57	36.37	11.98	35.74
p-value		< 0.001	< 0.001	< 0.001	0.001	< 0.001	< 0.001	< 0.001
R²		0.62	0.83	0.70	0.39	0.69	0.55	0.71
Adj. R²		0.57	0.81	0.66	0.32	0.68	0.51	0.69

^a Variables with * indicate that value is significant at the $\alpha = 0.05$ level.

^b Variables in **bold** were transformed using natural log.

^c Numbers shown are exponents of independent variables, if it is a categorical variable and that category is true than the number should be multiplied with the intercept.

^d R_p/H is equivalent to the relative submergence of the step-height where H is equal to the average step height from the lowest point in the pool to the top of the step.

4.5 Discussion

4.5.1 Gradient, dimensionless unit discharge, flow period, wood load and friction factor

Gradient explains a significant proportion of the variability in $(8/f)^{0.5}$ through the channel network, particularly when used in conjunction with the categorical variable of flow period. The relationship shows that ff is higher at higher S_0 (Figure 4). The higher the S_0 , the more energy is likely dissipated from cascading flow and abrupt transitions from supercritical to subcritical. Therefore, S_0 is a significant explanatory variable that is greatly improved when paired with flow period, q^* , or wood load (Model 1, 5a, and 11).

Many studies have recognized the important correlation between S_0 , grain size, step steepness, and channel type [Bathurst, 1993; Abrahams *et al.*, 1995; Montgomery and Buffington, 1997; Zimmerman and Church, 2001; Wohl *et al.*, 2004; Wohl and Merritt, 2005; Wohl and Merritt, 2008], and my results plus some additional analysis indicate that bed-gradient is related to each of these variables (Figure 7). Conversely, a significant difference in ff was not found to exist between step-pool and cascade channels for a given S_0 (Model 11). The channel types represent the bed morphology and the potential variability in flow resistance from spill resistance in step-pool channels to grain resistance in cascade reaches, with form resistance being prominent in both [Curran and Wohl, 2003; Wilcox *et al.*, 2006; Comiti *et al.*, 2007]. Both Model 11 and 12 show that $(8/f)^{0.5}$ is not significantly different for step-pool and cascade reaches. Therefore, the type of resistance (i.e., grain, form, or spill) may vary based on channel type, but the total flow resistance is similar for both.

The effect of bed-gradient is likely related to its relationship to other explanatory variables such as D_{84} , H/L_s and the Froude number (Fr) [Abrahams *et al.*, 2005; Church and Zimmerman, 2007; Comiti *et al.*, 2009]. All of these variables are highly interrelated. At higher slopes, the flow depth is shallower and the boulders larger in relation to the flow depth. An object that protrudes through the surface creates greater surface drag, which varies with Fr [Bathurst, 1982]. The Fr is highly variable throughout the reach as localized areas of supercritical flow and hydraulic jumps develop. There is greater energy dissipation and turbulence at low flows as flow separates around individual boulders [Wohl and Thompson, 2000]. As flow increases, these larger elements may become quickly submerged, creating localized skimming flows, where the water surface flattens between successive objects [Chanson, 1994]. The larger change in depth between low and high flows at steeper gradients may cause a much larger reduction in the total flow resistance, in comparison with the lower gradient reaches, as boulders are quickly submerged [Pagliara and Chiavaccini, 2005]. Also, as flow increases, the number of particles that influence the surface are reduced as smaller cobbles and boulders are submerged (Figure 10).

Flow period, q^* and other relative submergence variables (R_f/D_{84} , R_f/H , R_f/s_{bed}) were all significant explanatory variables and represent the influence of discharge on total ff (Table 3 and Table 4). As discharge increases in each channel type, the flow patterns vary and total ff decreases. The drop from the step lip to the pool is larger at low flows, therefore more energy is lost from larger steps and spill resistance dominates [Comiti *et al.*, 2009]. Conversely, at high flows there are larger hydraulic jumps and more

turbulence through the velocity profile [Wilcox and Wohl, 2007], which dissipates a large amount of energy. Comiti et al. [2009] identified nappe and skimming flow regimes as

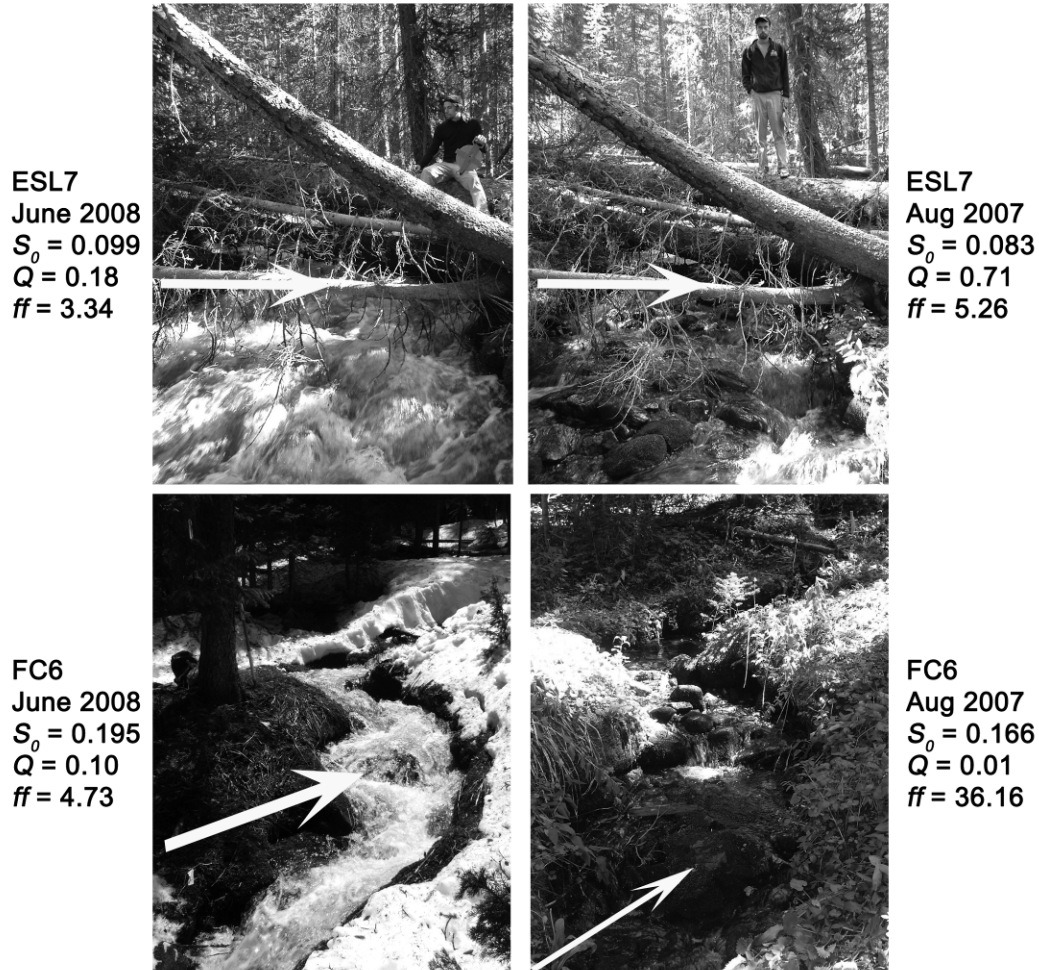


Figure 10: Two cascade reaches at low (August 2007) and High (June 2008) flows. Arrows point to the same location on both images. Images show that at high flow the majority of grains are submerged in FC6 while in ESL7 the location of the grains is still visible.

two distinct regimes in step-pool channels. Additionally Comiti et al., [2009] found that the type of resistance that dominates in step-pool reaches (i.e., grain, form, or spill) depends on the flow regime. In step-pool reaches, flow transitions from nappe flow at low discharges to skimming and submerged flow at the highest flows [Church and Zimmerman, 2007; Comiti et al., 2009]. Nappe flow is free-falling flow over steps into a

pool [Chanson, 1994]. Skimming flow is where flow becomes more planar over the step and air pockets disappear. Flow in this regime becomes supercritical [Comiti *et al.*, 2009]. Submerged flow occurs when flow over the step is affected by the downstream tailwater [Church and Zimmerman, 2007]. Nappe flow existed in a majority of the steps in the current research over all flow periods. Skimming flow was observed over a limited number of steps during June 2008 flows, particularly over the boulder steps at lower S_0 . Submerged flow was only observed over the smaller steps identified in FC1. An added component in many of these reaches is flow over and through the porous wood steps versus flow over large boulder steps. When flow drops over wood steps at low flows, the drop is higher and the jet does not plunge immediately from the wood step lip to the pool. At higher flows the water more easily flows from the wood step lip to the pool. Once skimming flow occurs, form and grain resistance increase as spill resistance decreases with the drop height. Form resistance increases as the water surface gradient steepens in the pools [Comiti *et al.*, 2009]. The large variability in step type and flow regime over the step-pool reaches explains the greater variability in $(8/f)^{0.5}$ over all flow periods and reaches (Figure 9).

In cascade reaches at lower flows, larger grains protrude through the surface, creating wave drag and increasing the total ff in a reach [Smart *et al.*, 2002]. One or two steps and pools exist in some of the cascade reaches, but the variability in these reaches is not as large as in the step-pool reaches (Figure 9), therefore the total resistance in cascade reaches is more easily explained by a small number of control variables (Table 4, Model 13 to 15). Overall, the results of the regressions show that the total ff is highest at low

flows and lowest at high flows for all the reaches, indicating that individual grains and bedforms more effectively retard the flow at lower discharges.

Dimensionless unit discharge, q^* , provides another way to represent relative grain submergence and differences in flow. The reason for the improved relationship between q^* and ff versus the R_h/D_{84} is not completely understood. *Ferguson* [2007] proposed that there is a reduction in measurement error when q^* is used, rather than R_h/D_{84} , because any error in D_{84} , Q , or V affects both the observed and predicted values of velocity.

Alternatively, any error in R_h/D_{84} will affect either predicted or observed velocities, but not both at the same time. It is also possible that in using q^* , the inclusion of width ($q = Q/W$) in the relative submergence variable improves its explanatory power. Therefore, q^* was found to be an improved metric for representing both flow and relative submergence in these steep gradient streams, but more work needs to be done to understand why it explains so much more variability than R_h/D_{84} .

The differences in the ability of individual control variables (S_0 , R_h/D_{84} , and q^*) to explain the variability in $(8/f)^{0.5}$ are demonstrated in Figure 11. Figure 11a and 11b show that the error in predicting ff by using S_0 and R_h/D_{84} is greatest at the lowest flows, which correlates to the highest values of $(8/f)^{0.5}$ (FC1 and FC2). Figure 11c shows that a model with q^* (Model 9, Table 3) greatly improves the prediction of $(8/f)^{0.5}$, but the FC1 and FC2 are still under-predicted. Figure 11d shows the prediction of a combined multiple regression (Model 5a, Table 3) which includes q^* , S_0 and channel type. The inclusion of S_0 and channel type greatly improves the overall error, but values of $(8/f)^{0.5}$

are over-predicted for step-pool reaches and under-predicted for cascade reaches. The highest error in Figure 11d is in the prediction of $(8/f)^{0.5}$ for ESL2 and FC3, which were often distinguished as outliers.

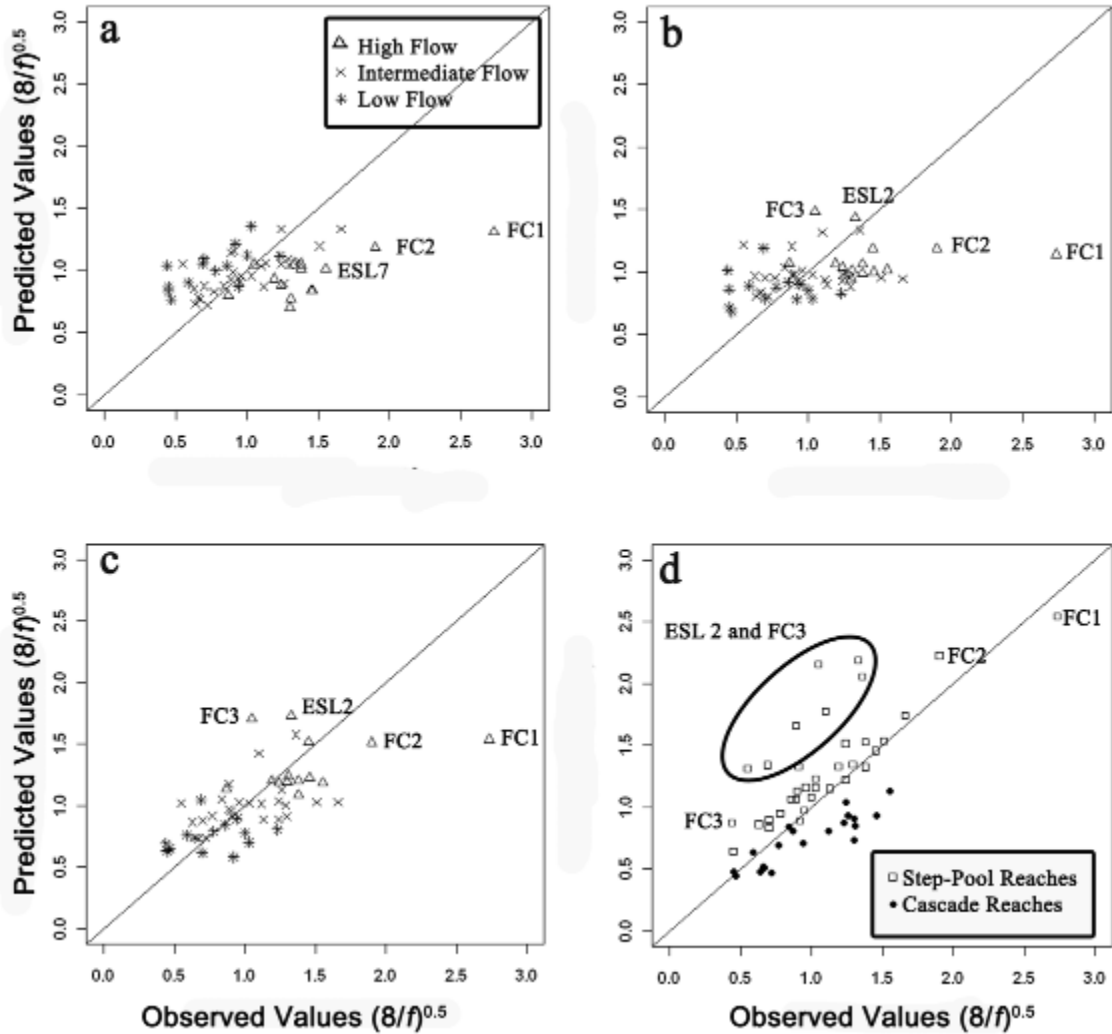


Figure 11: Predicted versus observed $(8/f)^{0.5}$ for a) Model 7 (S_0); b) Model 8 (R/D_{84}); c) Model 9 (q^*); d) Model 5a (q^* , S_0 and channel type).

Although these regressions are meant for explanatory purposes and not for prediction, Figure 11, Table 3 and Table 4 help to demonstrate which variables may be useful for developing new predictive equations in these higher gradient streams.

Inclusion of a flow variable (q^*), gradient and channel type increase the ability to explain

the variability in FC1 and FC2 (Figure 11d), but do not explain the variability as well in ESL2 and FC3. FC1 and FC2 have some of the smallest grain sizes, smallest amounts of wood and lowest S_0 (Table 2). FC1 may even be a transition reach between a plane-bed and step-pool. The values of total flow resistance in both reaches are the lowest (Table 2), except for the plane-bed reach (ESL6). In Model 5a, S_0 is a proxy for both grain size and step steepness, which combines with q^* and channel type to better explain the variability in these two reaches. On the other hand, S_0 , q^* and channel type can not account for the higher values of total flow resistance in ESL2 and FC3 because wood load dominates in these reaches, meaning that form drag and spill resistance dominate and including only a grain submergence variable (q^*) does not help explain the greater variability.

Wood load was found to be significantly related to total ff for all reaches (Table 3) and for regressions evaluating only step-pool or cascade reaches (Table 4). The importance of wood in step-pool channels has been noted by other researchers in both flume studies [Wilcox *et al.*, 2006] and field studies [Curran and Wohl, 2003; Manners *et al.*, 2007; Comiti *et al.*, 2008]. Wilcox *et al.* [2006] found that wood located at the step lip contributed both to the structure of the step and increased the step height, which subsequently increased the spill resistance. Both Manga and Kirchner [2000] and Hygelund and Manga [2003] determined that the presence of wood increases the depth of flow in a channel, increasing the total shear stress, but that the shear stress acting on the bed decreases as wood density increases. The wood increases the resistance, decreasing the total shear stress available for bed or bank erosion and reducing sediment transport. Curran and Wohl [2003] also concluded that step-forming wood contributes more to total

flow resistance than wood found as individual pieces throughout the reach. *Wilcox et al.* [2006] showed that grain roughness was greatly reduced once steps or wood were present. The flume study done by *Wilcox et al.* [2006] did not include the boulder steps found in reaches in the current study and the more heterogeneous grain size distribution. Variables related to grain roughness (R/D_{84} and q^*) and wood were both significant explanatory variables (Table 3, Model 4b, and 5b). The majority of the wood is found in steps, therefore the significance of wood load on ff is related to the significance of steps. The greater heterogeneity in grain size and step types (boulder and wood) probably accounts for the greater significance of variables related to grain roughness. S_0 is a significant explanatory variable in all regressions and is another variable that is correlated with both grain size and is slightly correlated with wood (Figure 12). For all reaches, except for ESL2, which has a significant amount of wood, wood load increases with S_0 . Most likely, this is related to an increase in step steepness as log steps increase step height, therefore creating steeper gradients [*Comiti et al.*, 2008]. The positive correlation between S_0 and wood load is even greater in the channel type regressions (Table 4), therefore S_0 is left out of regressions that include wood load. Wood load is positively related with ff and is a better explanatory variable in cascade reaches versus step-pool reaches. The cascade reaches have higher variability in the amount of wood in each reach and where the wood is located, which may account for the better relationship between the wood load and ff . The step-pool reaches all have a large amount of wood, except for ESL4 and FC1, and most of that wood is found in the steps. The wood load in these reaches mainly represents the size of the steps, which is better represented by R_s/H .

There was not a significant difference in the variability in ff between channel types holding S_0 constant (Model 11), signifying that grain, form and spill resistance may vary based on the channel type, but that total ff varies in predictable ways with S_0 and flow, despite the differences between step-pool and cascade reaches. The differences between individual reaches may be more significant than the differences between channel types. Also, channel type was found to only be significant in regression models that included S_0 and did not include wood, suggesting that channel type cannot be used as a proxy for S_0 . Gradient, R_h/D_{84} , and ff overlap for the cascade and step-pool reaches, because some of these reaches overlap in characteristics. Some of the cascade reaches have steps and pools, which may indicate that these reaches are transitional between step-pool and cascades rather than distinct cascading reaches. Despite similarities, Table 4 indicates that different control variables explain a greater proportion of the variability in step-pool versus cascade reaches.

4.5.2 Relative grain submergence, dimensionless unit discharge, standard deviation of bed elevation, relative step submergence and Darcy-Weisbach Friction Factor

Relative grain submergence is a measure that is commonly equated with grain resistance in a channel [Wilcox *et al.*, 2006]. I found that R_h/D_{84} correlated positively with $(8/f)^{0.5}$, meaning that at high values of R_h/D_{84} , ff is at its lowest value in the channel. There is significant correlation between these variables, but the low adjusted- R^2 (0.16) indicates that the proportion of variability explained by the relationship is minimal. The use of R_h/D_{84} in equations to estimate both the friction and velocity in a stream is based on turbulent boundary layer theory, where the flow is affected by the friction at the

boundary of the channel and varies with distance from the boundary [Bathurst, 1993]. Many relations were developed that equate R_h/D_{84} to ff for lower gradient channels using either the logarithmic law of the wall or an empirical power-law equation [Keulegan, 1938; Bathurst, 1993, 2002; Katul et al., 2002]. Comiti et al. [2007], along with others [Wiberg and Smith, 1991; Ferguson, 2007], also found that for large-scale roughness, which was defined as $R_h/D_{84} < 1.8$, resistance equations based on the approach of the law of the wall may be invalid. Most of the reaches in this study remain within the range of large-scale roughness, therefore the use of R_h/D_{84} may be inappropriate for these reaches.

Lee and Ferguson [2002] concluded that a power law gives the best fit when the roughness height, k_s , is estimated by the step D_{50} rather than a reach-average grain size. The use of a reach-average grain size in this paper may be another explanation for the poor correlation between R_h/D_{84} and ff , particularly in the step-pool reaches (Table 4). Baiamonte and Ferro [1997] showed that a scale parameter, size distribution parameter and particle arrangement parameter should be used together to more appropriately account for coarser bed elements. More work needs to be done to determine if any of these parameters would be appropriate for representing grain resistance in these reaches.

The relationship between $(8/f)^{0.5}$ and R_h/D_{84} has a lot of scatter at all flows, but the largest error is in the prediction of $(8/f)^{0.5}$ for FC1 and FC2 at the August 2007 low flow (Figure 11b). Ferguson [2007] showed that equations split between shallow flows and deep flows were the best predictors of velocity, although all submergence-based equations had a high error in predicting the velocity, particularly at lower flows ($R_h/D_{84} < 1$). Bathurst [2002] found that the relationship between $(8/f)^{0.5}$ and R_h/D_{84} changed with S_0 . Model 4a (Table 3) shows that including both R_h/D_{84} and S_0 together improves the

regression, but the low adjusted- R^2 indicates that other combination of variables are needed to explain a greater proportion of the variability in $(8/f)^{0.5}$.

A model with R_H/D_{84} is greatly improved by including wood load (Model 4b) instead of channel type, suggesting that wood load is a better predictor than channel type (Model 4a). Wood is related to both form drag around individual pieces and spill resistance over steps [Curran and Wohl, 2003]. The majority of the wood found in both channel types is located in the steps, creating an interrelationship between wood load and bed morphology. There is also a slight positive relationship between wood load and S_0 (Figure 12), which is described in Section 4.5.1. Model 4a indicates that R_H/D_{84} is a poor surrogate for flow (Figure 11b), but inclusion of a wood parameter accounts for a much larger proportion of the variability in total flow resistance. Buffington and Montgomery [1999] found that pool-riffle and plane-bed reaches with increased wood caused increased hydraulic roughness and textural fining of the particle-size distribution. In the current study, no significant relationship was found between wood load and D_{84} . However, the reaches with the largest wood loads, ESL2 and FC3, have the smallest particle size in both basins. The interrelationship between wood load, particle size and S_0 may account for the difficulty in describing the variability in ESL2 and FC3. Localized fining was also noted behind some of the larger wood steps in ESL1, ESL8, ESL9 and FC4, but these localized areas were not large enough to noticeably influence the reach-average values. The same effect of localized fining was not observed upstream of boulder steps. The wood load represents both form and spill resistance and together with R_H/D_{84} the grain resistance is encompassed in the multiple regression.

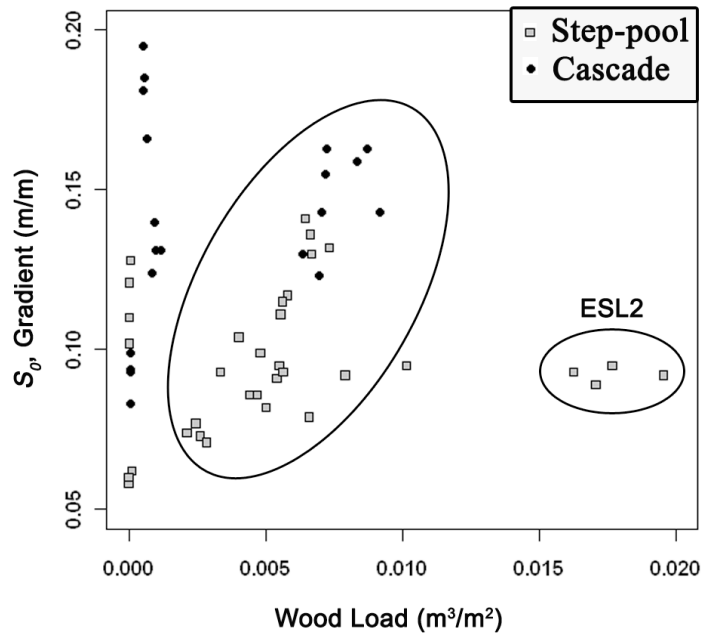


Figure 12: Wood load versus S_0 for step-pool and cascade channel types. Reaches in oval are linearly correlated with S_0 except for ESL2.

Comiti et al. [2007], *Aberle and Smart* [2003], and *Rickenmann* [1991] proposed using dimensionless unit discharge (q^*) in place of R_h/D_{84} for steep gradient streams. This approach was initially developed to relate q^* with a dimensionless velocity ($v^* = V/(gD_{84})^{0.5}$), but in this study, as well as the study by *Comiti et al.* [2007], it is used to understand the variability in ff . Model 9 (Table 3) demonstrates that this parameter explains a greater proportion of the variability in ff than either R_h/D_{84} or S_0 . *Ferguson* [2007] also found that q^* has the lowest error for predicting velocity in a reach. Figure 11c and Figure 11d demonstrate that including q^* has a similar effect in predicting ff as including a categorical variable for flow period, therefore q^* is effectively representing the changes in roughness that occur as flow increases. Unfortunately, this parameter is only useful if the Q is already known and V is being predicted. If both Q and V need to be predicted, some other measure of the effect of flow variation should be considered.

Another measure of bed roughness, R_h/s_{bed} , was proposed by *Aberle and Smart* [2003] to be a more appropriate measure of the roughness structure in a steep gradient channel than the grain size. *Aberle and Smart* [2003] argued that beds armored with the same mean grain diameter may have a completely different roughness structure. *Baiamonte and Ferro* [1997] also showed the importance of the spatial arrangement of particles. Therefore, the s_{bed} is used as a measure of the roughness structure. I used a similar methodology as *Comiti et al.* [2007] by regressing the two grain size parameters (D_{84} , D_{50}) and s_{bed} against velocity to determine which variable explains a greater proportion of the variability in velocity. These roughness parameters are all on the same order of magnitude as the water depth, therefore each is expected to have some relationship with ff . The most significant relationship was between D_{84} and velocity. There was no significant relationship between s_{bed} and velocity, although R_h/s_{bed} was found to be a better measure for predicting flow resistance than R_h/D_{84} or q^* (Table 3, Models 4a, 6 and 9). Some spurious correlations exist between R_h and ff , since R_h is used in the calculation of ff , but that does not account for the high adj- R^2 when relating R_h/s_{bed} to ff . Although R_h/s_{bed} is a significant variable and may be a preferred variable for developing an equation to predict ff , the physical significance of this relationship is unclear since s_{bed} was not found to be related to V . The lack of correlation between s_{bed} and V may be because the measurement spacing was not narrow enough (~15 to 20 cm). Also, s_{bed} represents the standard deviation of the bed elevation along the thalweg and not over the entire bed. *Church and Zimmerman* [2007] suggest that the s_{bed} does not

adequately describe how velocity may vary over a step-pool reach during lower flows. The poor correlation between s_{bed} and ff agrees with *Comiti et al.*'s [2007] analysis of high gradient channels.

The multiple regressions in Table 4 indicate that a greater proportion of the variability can be explained by including relative step submergence (R_t/H) in step-pool reaches and relative grain submergence (R_t/D_{84}) in cascade reaches if q^* cannot be used. These results suggest that, despite similarities in ff and even S_0 , the types of resistance (i.e., grain, form, or spill) are sufficiently different in these two channel types that other control variables should be considered when attempting to predict V . *Comiti et al.* [2009] found in a flume study of step-pool channels that, in order to predict total flow resistance, there must be some differentiation between low and high flows or, in the step-pool reaches, between nappe and skimming flows. The results of the regression analysis in the present study support that conclusion (Table 3). R_t/H can be a measure of flow regime; as steps become more submerged, the flow will move from nappe to skimming flow. Wood load is not used in a model with R_t/H because the two variables are interrelated since wood load is related to step height.

Jarrett [1984] found that S_0 is a better parameter than R_t/D_{84} for predicting ff in high gradient channels. The results of the present study indicate that both relationships are significant, but neither works better than the other, although a more appropriate flow parameter (q^* , flow period) and wood load can be coupled with S_0 for an improved model.

4.5.3 Channel type and friction factor

A significant difference in total ff exists between the plane-bed reach and both step-pool and cascade channel types (Figure 5). Only one plane-bed reach is used in this

study and although it is significantly different from the two other channel types, more work needs to be done to determine if this reach appropriately represents all plane-bed reaches. The step-pool and cascade reaches were not found to have significantly different means. The step-pool and cascade channel types were only found to be significantly different while holding both S_0 constant together with a flow variable (Table 3).

Although cascade and step-pool channel types may vary in terms of S_0 and D_{84} , the values of total ff are high for both of these channel types in these high-gradient streams.

The greatest variability between channel types is the type of flow resistance that dominates and therefore the parameters that best explain the variability in ff differ.

R_h/D_{84} better explains the variability in ff in cascade reaches versus step-pool reaches (Figure 9 and Table 4). Many other researchers have noted the lack of correlation

between R_h/D_{84} and ff in step-pool streams [Aberle and Smart, 2003; Church and Zimmerman, 2007; Comiti et al., 2007; Wohl and Merritt, 2008]. The correlation

between R_h/D_{84} and ff in the cascade reaches may indicate that grain roughness dominates in these reaches, leading to the closer correlation with a variable that includes the grain size. Wood load is also a significant source of variability in these cascade reaches and together with another grain submergence variable, q^* , explains the largest proportion of variability (Table 4, Model 15). Model 15 shows that for a given q^* , wood load increases with ff . Therefore, form resistance is still a significant source of resistance in these cascade reaches.

Form and spill resistance most likely dominate in the step-pool reaches [Curran and Wohl, 2003; Church and Zimmerman, 2007; Ferguson, 2007; Comiti et al., 2009], therefore R_h/D_{84} is not appropriate for describing the variability in ff in this channel type.

Despite the dominance of form and spill resistance, a different form of grain roughness, q^* , does work for step-pool reaches (Model 19). The models that explain the greatest proportion of variability in ff in step-pool reaches are the ones with either R_h/H or q^* (Table 4, Model 17 and 19). R_h/H represents spill resistance over steps by representing the height that the water falls over each step. Larger values of R_h/H mean that steps are becoming more submerged and the drop from the step lip to the pool is reduced, causing a reduction in the contribution of spill resistance to total flow resistance [Comiti *et al.*, 2009]. Skimming flow occurred over a proportion of the steps in each reach during high flows, causing a reduction in spill resistance from these steps. Form and grain resistance would then begin to dominate at higher flows [Comiti *et al.*, 2009]. Wood load does not greatly improve the explanatory power of any of the step-pool models (Table 4, Model 16 and 18). The high correlation between wood load and S_0 in step-pool reaches mean that when S_0 is included in a regression, it also represents wood load. Therefore, the regressions with S_0 and R_h/H or q^* better explain the variability in step-pool reaches than the regressions that include wood load (Table 4).

The step steepness (H/L_s) is positively related to S_0 through a power function, meaning that as S_0 increases the H increases in relation to L_s . H/L_s represents the three distinct sections that make up a step-pool channel, where velocity varies from critical to supercritical to subcritical: the step lip, the pool, and the run. Flow over the step lip is critical right before the water plunges into the pool. In the pool, there is a sharp velocity reduction as water goes from supercritical to subcritical [Leopold *et al.*, 1964]. Therefore, pools are dominated by hydraulic jumps and wake turbulence [Wohl and Thompson, 2000; Church and Zimmerman, 2007]. The greatest amount of energy is

dissipated as flow plunges over the steps and decelerates in the pools [Wohl and Thompson, 2000]. The runs, also known as the step treads, are the areas just upstream of the step. Flow accelerates through the runs and just as it plunges over the step lips, reducing turbulence in these sections. Wohl and Thompson [2000] concluded that the higher average velocities in the runs means that grain resistance is not as effective an energy dissipater as form drag around the steps and wake-generated turbulence in the pools. The relationship between S_0 and H/L_s means that at higher gradients there are steeper steps with shorter runs and thus a higher elevation difference between the step lip and the pool. Therefore, more energy may be dissipated by the steps at these higher gradients. In Model 18 the steepness factor $(H/L_s)/S$ was not found to be significantly related to ff in step-pool reaches, but wood load, R_h/H and S_0 were both significant and both are related to step geometry. No significant relationship was found between ff and individual step geometry variables (H , L_s , and H/L_s). These results support Curran and Wohl's [2003] conclusion that step geometry may not be an appropriate measure for estimating ff . Conversely, R_h/H is significant in step-pool reaches, despite the lack of significance of H and, just like R_h/s_{bed} , may still be an important variable when considering developing a predictive equation in high gradient channels. Furthermore, the regression results support the idea that each of these control variables represents a different form of resistance in these reaches. Therefore, if Q is unknown, then ff and subsequently V can be better approximated by R_h/D_{84} in cascade reaches and R_h/H in step-pool reaches.

4.5.4 Other sources of variability

Bathurst [1985] noted that at-a-site variability in ff was much greater than between-site variability for his data. Figure 6 shows the large differences in at-a-site and between-site variability in $(8/f)^{0.5}$ for each channel type and in each drainage basin. There are many other sources of variability in these channels that are not accounted for with the simple parameters tested in the above regressions. For instance, expansions and contractions of the channel banks can be an important source of resistance [*Bathurst*, 1985; *Kean and Smith*, 2006]. The purpose of the above analysis was to find simple reach-average variables that may eventually be used to develop a predictive equation for high-gradient streams, but these other sources of variability will be explored further in subsequent analyses.

4.6 Conclusion

Past work suggests that gradient and discharge are the dominant controls on ff in steep mountain streams. S_0 , coupled with one or two other explanatory variables, greatly improved the proportion of variability explained in any model. It is important to understand how S_0 is related to ff and other stream characteristics, since this is a metric that can be used to remotely predict these characteristics, as the resolution of remote data improves with time [*Wohl et al.*, 2007]. Further work needs to be completed to couple the results of these regressions with development of a predictive equation for high gradient channels. The regression analysis supports the conclusions of *Comiti et al.* [2009] developed from a flume study on step-pool channels, in that a parameter that

represents the flow regime needs to be included for the best predictive models of ff . Both q^* and flow period coupled with S_0 had the greatest explanatory power and would most likely have the best predictive capabilities.

The different forms of resistance that dominate in each channel type were mirrored by the different independent variables that were significant in the regressions for each channel type. The R_f/D_{84} was thought to be an appropriate measure of both the variation in flow and the roughness created by larger grains in a channel and was found to be a more appropriate measure of explaining the variability in total flow resistance in cascade reaches. A more appropriate relative submergence control variable in step-pool reaches is R_f/H . The significance of R_f/D_{84} in cascade reaches is most likely related to the dominance of grain resistance in these reaches, whereas R_f/H better represents spill and form resistance in step-pool reaches.

Wood load is also a significant explanatory variable, particularly when combined with S_0 and flow period or q^* . There is some correlation between wood load and S_0 , but overall the variable wood load seems to represent both form drag and spill resistance that is related to the amount of wood in each reach [Curran and Wohl, 2003; Comiti et al., 2008]. The total wood load explains more of the variability in ff in cascade reaches, most likely because there is much larger variation in wood load in these reaches versus step-pool reaches.

Channel type is a significant explanatory variable only if flow period, q^* , and S_0 are held constant in the regression. Therefore, at particular flows and S_0 there are significant differences between step-pool and cascade reaches. The overall values of total ff in step-pool reaches were higher than in cascade reaches for a given S_0 and flow

period. The plane-bed reach was consistently different from all other channel types. These differences suggest that each channel type may need to be accounted for separately when developing equations to predict ff . The interrelationship between S_0 , D_{84} , H/L_s , wood load and channel type means that S_0 may be used to remotely determine channel features. Further work should be done to consider if separate resistance equations could then be applied to those channel types, determined from remote data.

Returning to the original, most general hypothesis that predictable patterns of relative magnitude of total resistance exist throughout a channel network and that simple variables such as gradient can be used to predict these patterns, I conclude that gradient is a useful predictor of spatial variations in flow resistance at a given time (i.e., when flow varies only spatially as a function of drainage area). Spatial and temporal variations in resistance are more effectively predicted by combining gradient with q^* or flow period.

CHAPTER 5 CONTROLS ON AT-A-STATION HYDRAULIC GEOMETRY RELATIONSHIPS IN STEEP HEADWATER STREAMS

5.1 Abstract

At-a-station hydraulic geometry can be used to improve our understanding of the relationship between flow resistance and variations in velocity, width and depth with discharge. Detailed hydraulic measurements were made in nine step-pool reaches, five cascade reaches, and one plane-bed reach in Fraser Experimental Forest, Colorado. Water surface, bed and velocity measurements were conducted at four different stages in each reach using a laser theodolite, LiDAR (Light Detection and Ranging), and Rhodamine WT dye tracer. Average values for at-a-station hydraulic geometry exponents, m (0.49), f (0.39), and b (0.16), were well within the range found by other researchers working in steep gradient channels. A Principal Component Analysis (PCA) is used to compare the combined variations in all three exponents against five potential control variables: wood, D_{84} , grain size distribution (σ), coefficient of variation of pool volume, average roughness area (projected wetted area) and bed gradient. The gradient and average roughness area were found to be significantly related to the PCA Axis scores, indicating that both driving and resisting forces influence the rates of change of velocity, depth and width changes with discharge. Further analysis of the exponents showed that reaches with $m > b + f$ are most likely dominated by grain resistance and reaches below this value are dominated by form resistance.

5.2 Introduction

At-a-station hydraulic geometry (AHG) characterizes how changes in discharge affect specific hydraulic variables such as width, depth, velocity and friction. *Leopold and Maddock* [1953] first coined the term “hydraulic geometry” to describe systematic changes both downstream and at a cross-section for each of the above hydraulic variables. They proposed three power relations to describe how width ($w = aQ^b$), depth ($d = cQ^f$) and velocity ($v = kQ^m$) vary with discharge both downstream and at a given cross-section in a channel, where Q is discharge; w is water-surface width; d is mean depth; and v is velocity. These power relations are bound by the continuity equation ($Q = wdv$), indicating that the coefficients a , c , and k have a product equal to one and the exponents b , f , and m sum to one. *Leopold and Maddock* [1953] found that the rates of width, depth and velocity changes with discharge were related to the shape of the channel, the slope of the water surface, and the roughness of the wetted perimeter. They also found the sediment load to be an important control on the rates of change of both velocity and depth [*Leopold and Maddock*, 1953].

Subsequent investigators have confirmed that cross-sectional shape and flow resistance are significant in determining how width and velocity vary with depth [*Knighton*, 1974, 1975; *Richards*, 1976; *Ferguson*, 1986; *Ridenour and Giardino*, 1995; *Wohl*, 2007]. *Ferguson* [1986] showed that depth would increase faster than width in a rectangular channel, but in a more triangular channel width may increase faster than depth. The variation in velocity with depth is related to the frictional characteristics of the channel. In a channel where increasing flow depth quickly drowns out the effects of

roughness elements, velocity would increase quickly with depth. *Knighton* [1975] proposed that a channel dominated by grain resistance would have the highest rates of decrease in resistance as discharge increases.

Park [1977] found that a wide range of the three hydraulic geometry exponents exists throughout the world, which suggests the need for an improved understanding of the sources of variation. Other controls on at-a-station values that have been identified include differences between braided, meandering, and straight reaches [*Knighton*, 1975; *Ferguson*, 1986]; differences based on bank composition [*Knighton*, 1974]; variations between pool and riffle sections [*Knighton*, 1975; *Richards*, 1976]; and differences based on irregularities in resistance in relation to stage [*Richards*, 1976; *Ferguson*, 1986]. *Ferguson* [1986] also noted that at-a-station hydraulic geometry may vary over the course of a flood cycle as both scour and fill occur during this time period.

The use of power relations in hydraulic geometry is based on empirical evidence and does not have a solid foundation in theory [*Park*, 1977; *Richards*, 1973; *Ferguson*, 1986]. Further work has been done using extremal hypotheses to develop a theoretical framework for predicting AHG values [*Langbein*, 1964; *Huang and Nanson*, 2000; *Singh and Zhang*, 2008a]. *Langbein* [1964] proposed the minimum variance hypothesis in which the most probable state is found by minimizing the variance of the dependent variables (width, depth, and velocity). *Huang and Nanson* [2000] proposed combining the maximum sediment transporting capacity [*Kirkby*, 1977; *White et al.*, 1982], minimum unit stream power [*Yang*, 1976] and minimum stream power [*Chang*, 1980] into the principle of least action to describe channel adjustment in alluvial rivers. *Singh and Zhang* [2008a] took the concepts of minimum energy dissipation rate and the

principle of maximum entropy to derive AHG values. *Singh and Zhang* [2008a] propose a weighting factor to represent the unequal distribution of stream power among the variables width, depth, velocity, roughness and slope, which all adjust with increasing discharge. In alluvial rivers, they found that the change in stream power is most often accomplished with a change in width and flow depth, and to a lesser extent the change in roughness [*Singh and Zhang*, 2008b]. Although these extremal hypotheses are important in the attempts to predict AHG, the objective of this paper is to describe and understand differences in AHG among reaches and not to predict the actual values.

Ferguson [1986], *Lawrence* [2007] and *Singh and Zhang* [2008b] all emphasize the importance of the change in depth and channel shape in their analyses of AHG. *Singh and Zhang* [2008b] describe a channel shape factor (α) which is most sensitive for $w:d < 10$. If $w:d > 10$, then channels can be approximated as rectangular reaches. *Ferguson* [1986] points out that the shape of the channel, and therefore the rate of change of width and depth with discharge, is largely controlled by the last flood. This may be particularly true in higher gradient streams where the beds are armored and the channel form is thought to have developed during large events [*Grant et al.*, 1990; *Church and Zimmerman*, 2007]. *Ferguson* [1986] argues that width, depth and velocity will only vary with discharge as power laws if width varies with depth and velocity varies with depth as power laws. In AHG the rate of change of mean velocity with water depth is controlled by hydraulic laws and frictional characteristics, which may not follow power-law trends [*Ferguson*, 1986]. *Ferguson* concludes that the wide scatter in AHG is related to the wide variety of channel shapes and frictional characteristics. *Lawrence* [2007] further supports *Ferguson's* [1986] work by showing that an exponent which reflects

cross-section form (r) and depth in a hydraulic relation drives the values for the AHG exponents. *Lawrence* [2007] concludes that the values of the coefficients depend on a combination of the physical characteristics of the section including width, depth, hydraulic conductance and energy slope. Other statistical models have been proposed for representing AHG including a log-quadratic model [*Richards*, 1973] and piecewise linear regression approach [*Bates*, 1990], but neither of these is as widely used as the power law relations. Unfortunately, statistical models are limited by the range of data used, and cannot often be extended outside that range. Despite these drawbacks, these models can be used to further understand differences in AHG values and to find previously unrecognized relationships between variables [*Rhoads*, 1992].

Few studies have reported AHG values for steep mountain channels [*Lee and Ferguson*, 2002; *Reid*, 2005; *Comiti et al.*, 2007]. A better understanding of at-a-station changes in each of the above hydraulic variables can improve our understanding of the sources and magnitude of hydraulic roughness in these channels, which tend to have values of flow resistance, as reflected in Manning's n or Darcy-Weisbach ff , that are much higher than values for channel reaches with gradient $< 1\%$ [*Jarrett*, 1984; *Bathurst*, 1985, 1993].

Steep mountain channels are divided into cascade, step-pool and plane-bed channel morphologies [*Montgomery and Buffington*, 1997]. Cascade morphologies are characterized by tumbling flow over individual randomly arranged clasts and form at $S_0 > 0.06$ m/m (where S_0 is bed gradient). Step-pools have a consistent step and pool morphology ($0.03 < S_0 < 0.10$ m/m) and plane-bed channels ($0.01 < S_0 < 0.03$) have no distinctive variations in the bed [*Montgomery and Buffington*, 1997]. Many at-a-station

studies have focused on lower gradient pool-riffle channels, which have significantly different hydraulic relations between pools and riffles [Richards, 1976]. Few studies have focused specifically on differences between cascade, step-pool and plane-bed reaches, which might be expected to exhibit differences in at-a-station relations because of the differences in channel configuration and primary source of roughness.

The relationship between resistance and stage ($ff = oQ^x$) is also important in understanding how width, depth and velocity vary with stage. Leopold et al. [1960] showed that resistance may not vary continuously with discharge. Knighton [1974] and Richards [1976] suggest that the sources of resistance vary in an irregular cross-section as point bars and island deposits are inundated with increasing discharge. Others have reported inflection points in data: as flow increases and water begins to spill over bars [Hogan and Church, 1989]; where the bed begins to mobilize [Knighton, 1998; Hickin, 1995]; and when larger grains are submerged, decreasing flow resistance [Knighton, 1998; Bathurst, 1982]. Wohl [2007] found a decreased rate of change in velocity and water-surface gradient at higher discharges in a pool-riffle channel and surmised that the inflection point reflected a transition from decreasing grain roughness to increasing form roughness. Therefore, resistance does not necessarily vary as a power relationship with discharge.

Sources of resistance in step-pool and cascade reaches include wood, individual grains, and the channel form. Resistance in these channels is most often subdivided into spill, form and grain resistance [Ferguson, 2007; Wilcox and Wohl, 2006]. Spill resistance is created from sharp flow transitions as flow plunges over steps or from wave drag over elements protruding above the water surface. Grain resistance is from skin

friction and form drag around individual grains. Form resistance is created from dunes, steps and bars in the channel [Wilcox and Wohl, 2006]. Each of these types of resistance varies as discharge varies in a reach. At higher flows, protruding grains occupy a smaller proportion of the total flow depth and form resistance may become the dominant type of resistance. Spill resistance is significant at both low flows, when the step heights are the largest, and high flows, when larger waves cause greater energy dissipation [Comiti et al., 2009; Church and Zimmerman, 2007]. Resistance associated with wood can be both from grain resistance around individual logs and form resistance around larger log jams and steps. Wood in the channels may also be inundated at different flow levels, causing the amount of resistance associated with the wood to vary with discharge. Therefore, the rate of change of resistance depends on the water depth and the different forms of resistance at that cross-section [Knighton, 1975]. Changes in width, depth and velocity at a cross section are intertwined with these variations in resistance; therefore, examining at-a-station hydraulic geometry is essential to understanding the interactions between all five variables (wood load, sediment size, pool size, gradient, roughness area (Figure 13)) and flow.

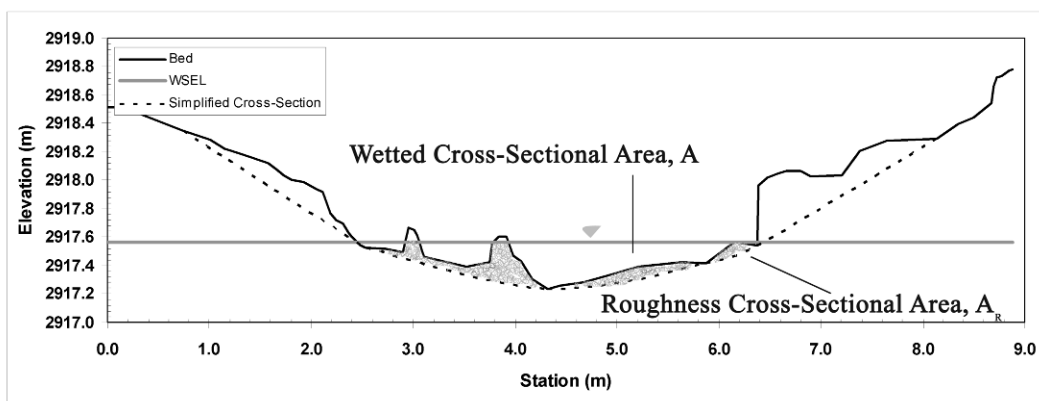


Figure 13: Example of a rough cross-section and simplified cross-section for ESL2. The shaded area is the roughness area, used in the statistical analysis.

Ridenour and Giardino [1991] proposed that because hydraulic geometry data are unit-sum constrained, they should be analyzed as a composition in order to understand how other parameters such as wood influence the combined variations in the three hydraulic geometry exponents. Compositional data are best represented by ternary diagrams, which were simultaneously introduced by *Park* [1977] and *Rhodes* [1977]. The exponents, b , f , and m are all dependent on each other, therefore *Ridenour and Giardino* [1991] argue that they should be analyzed simultaneously. Therefore, I use principal component analysis to describe the combined rates of change of width, depth and velocity for each segment of channel, and use the axis scores in a multiple regression analysis to better understand what influences the variability in these exponents.

Another method of understanding the simultaneous variability in the hydraulic exponents is by analyzing the ternary diagrams. *Rhodes* [1977] proposed five subdivisions of the diagram which represented width-depth ratio ($b = f$), competence ($m = f$), Froude number ($m = f/2$), velocity-cross-sectional area ratio ($m = b + f$), and slope-roughness ratio ($m = 2/3 f$). The latter two subdivisions are related to the Darcy-Weisbach friction factor (ff) and Manning equation (n), respectively. *Rhodes'* [1977] five divisions delineated ten areas in the diagram where each point plotted in similar areas would experience similar responses to changes in discharge. *Park* [1977], on the other hand, found a large range of AHG values over varying climatic regions. *Park* [1977] concluded that local controls may have a larger influence on AHG values than climatic controls.

The objectives of this study are to 1) report at-a-station values for cascading, step-pool and plane-bed reaches and determine whether there are significantly different values

for cascade versus step-pool reaches (plane-bed not included in statistical comparison since sample size = 1); and 2) explore what influences the variability in the rate of change of width, depth and velocity with discharge. These objectives can be separated into two hypotheses: i) there is a significant difference between hydraulic geometry exponents for cascade versus step-pool reaches; and ii) the variability in the hydraulic geometry exponents are significantly related to the following potential control variables: bed gradient, channel roughness, wood, and pools. The AHG for the single plane-bed reach is used for comparison with data collected from plane-bed reaches in British Columbia [Reid, 2005].

5.3 Statistical Methods

A Principal Component Analysis (PCA) was used in Multivariate Statistical Package (MVSP) [Kovach Computing System, 2002]. Principal Component Analysis (PCA) is an ordination technique that rearranges the data into a smaller set of composite variables [McCune and Grace, 2002]. This method uses an orthogonal linear transformation of the data, in which the greatest variation in the data lies on the first axis, or principal component. Each principal component minimizes the total residual sum of squares of the eigenvector (taken from the covariance matrix), after passing through the means of the eigenvalues. The greatest amount of variation in the data set is found in the first few principal components [McCune and Grace, 2002].

A best subsets regression was performed using the program R [R Core Development Team, 2007; Kutner et al., 2005] to determine which independent variables best explained the variability in hydraulic exponents. The roughness area, gradient, coefficient of variation of the pool volume (CVPoolV), pool volume/m² of reach, wood

volume/m² of reach, D_{84} , bed material size distribution (σ) and standard deviation of bed elevation (Table 5) were all regressed against the PCA Axis 1 scores in a best subsets regression. A best subsets was also used in a regression for the individual exponents and each of the above explanatory variables, to explore whether the same explanatory variables are significantly related to individual exponents. A Tukey HSD method was used to test for significant differences between means in the ANOVAs comparing the exponents for step-pool versus cascade reaches. The Tukey HSD method adjusts for differences in sample sizes, so appropriate comparisons can be made between means [R Core Development Team, 2007].

Ternary diagrams are used as a means of comparing the exponents (m, f, b) for each reach and each channel type. The AHG values found in this study are compared against the AHG values found by Reid's [2005] study on streams in British Columbia. All three AHG exponents are interrelated, therefore the ternary diagram has been found to be a useful format for investigating simultaneous variations in the exponents [Park, 1977; Rhodes, 1977]. The sum of the exponents do not equal one for a majority of the reaches, therefore the values were equally adjusted so that all reaches could be plotted on the diagram.

Roughness area was calculated using a macro in Microsoft Excel. For each cross-section during each flow period, a simplified, or smoothed, cross-section was created by finding the maximum slope between points in the cross-section (Figure 13). The macro was then used to find the area between the smoothed cross section and the rough cross section by subtracting the cross-sectional area from the simplified cross-sectional area.

Table 5: Summary table showing significant reach averaged values for each reach.

Reach*	Channel Type	Avg.	Gradient	D_{84}	σ^\dagger	CV of	Avg.	CV	Wood	Pool	CV [‡] of Pool
		Q				R_h/D_{84}	Roughness	Roughness	Volume/Area	Volume/Area	Volume
		(m ³ /s)	(m/m)	(m)			Area (m ²)		(m ³ /m ²)	(m ³ /m ²)	
ESL1	step-pool	0.34	0.09	0.16	0.51	0.36	0.51	0.80	0.0051	0.27	0.06
ESL2	step-pool	0.37	0.09	0.07	0.85	0.19	0.37	0.62	0.0169	0.22	0.35
ESL3	cascade	0.40	0.13	0.13	0.34	0.12	0.77	0.56	0.0014	0.05	0.33
ESL4	step-pool	0.38	0.12	0.17	0.39	0.20	0.33	0.90	0.0017	0.22	0.28
ESL5	cascade	0.39	0.14	0.14	0.45	0.21	0.52	0.86	0.0093	0.09	0.31
ESL6	plane-bed	0.88	0.02	0.09	0.65	0.24	0.11	0.56	0.0028	--	--
ESL7	cascade	0.41	0.09	0.17	0.33	0.23	0.29	0.65	0.0084	--	--
ESL8	step-pool	0.36	0.09	0.17	0.39	0.16	0.37	0.88	0.0118	0.13	0.07
ESL9	step-pool	0.33	0.11	0.15	0.40	0.16	0.37	0.72	0.0067	0.24	0.10
FC1	step-pool	0.12	0.06	0.08	0.43	0.39	0.07	0.72	0.0007	0.09	0.28
FC2	step-pool	0.10	0.07	0.08	0.43	0.43	0.08	0.67	0.0029	0.12	0.59
FC3	step-pool	0.09	0.09	0.05	0.70	0.41	0.15	0.86	0.0090	0.08	0.89
FC4	step-pool	0.13	0.13	0.10	0.30	0.37	0.21	0.67	0.0058	0.12	0.37
FC5	cascade	0.04	0.16	0.09	0.48	0.38	0.06	1.11	0.0074	0.03	0.14
FC6	cascade	0.04	0.18	0.09	0.26	0.35	0.06	0.92	0.0006	0.04	0.29

* ESL = East St. Louis Creek and FC = Fool Creek, ESL1 and FC1 are both the furthest downstream reach and ESL9 and FC6 are the furthest upstream

[†] $\sigma = \log(D_{84}/D_{50})$ = bed material size distribution

[‡] CV = coefficient of variation

5.4 Results

At-a-station hydraulic geometry is not significantly different among step-pool, cascade and plane-bed reaches at East St. Louis and Fool Creeks (Figure 14, Figure 15, Figure 16, and Table 6). These results do not support the hypothesis that there is a significant difference in hydraulic exponents for cascade and step-pool reaches. For all reaches except two, the at-a-station values show that $m > f > b$ (Table 6 and Figure 16). Therefore, the rate of change of velocity with discharge is greater than the rate of change of width or depth. The mean values of 0.49 for m , 0.35 for f and 0.16 for b are within the mean and range found by *Comiti et al.* [2007] and other researchers [*Lee and Ferguson, 2002; Bathurst, 1993*] who have studied step-pool and cascading systems. The at-a-station values are significantly related to average roughness area and the bed gradient in each reach (Table 7), supporting the second hypothesis that channel roughness and bed gradient explain the variability in at-a-station values. A more detailed presentation of the results follows in three sections: i) a summary of the at-a-station values found in these reaches; ii) channel type versus at-a-station hydraulic geometry; and iii) controls on at-a-station hydraulic geometry.

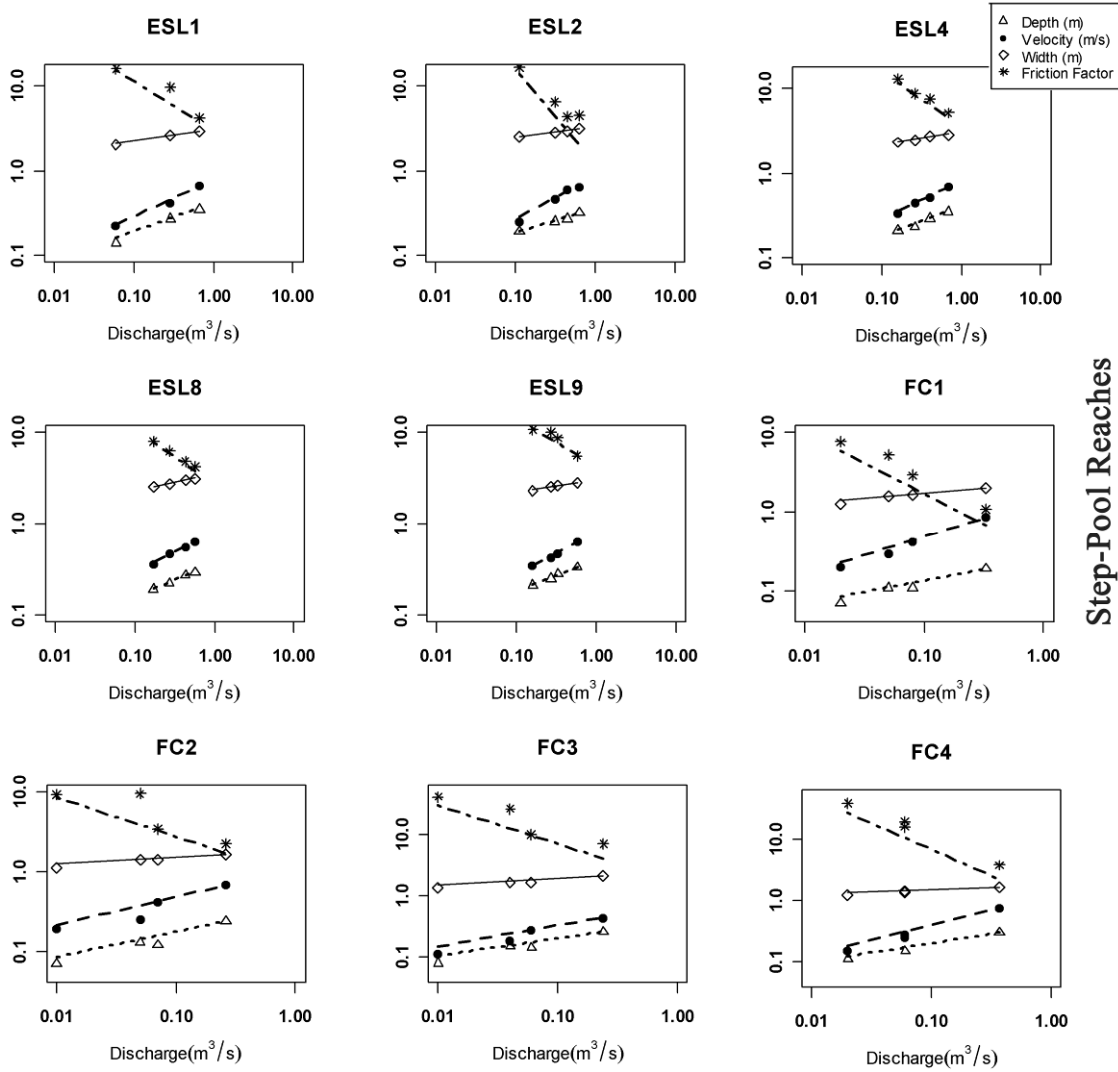


Figure 14: At-a-station hydraulic geometry of each reach. The power relationships between discharge and velocity (m), depth (f), width (b) and the Darcy-Weisbach Friction Factor (x).

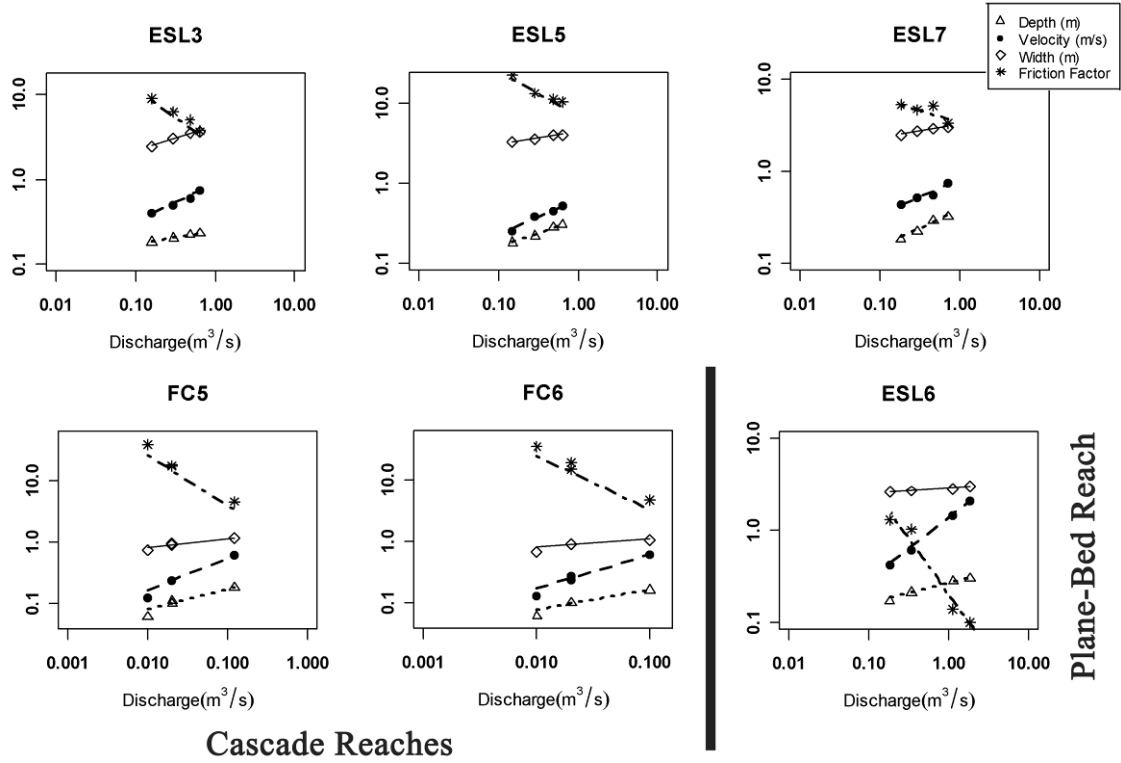


Figure 15: At-a-station hydraulic geometry of each cascade reach and the plane-bed reach (ESL6). The power relationships between discharge and velocity (m), depth (f), width (b) and the Darcy-Weisbach friction factor (x) are shown on each graph.

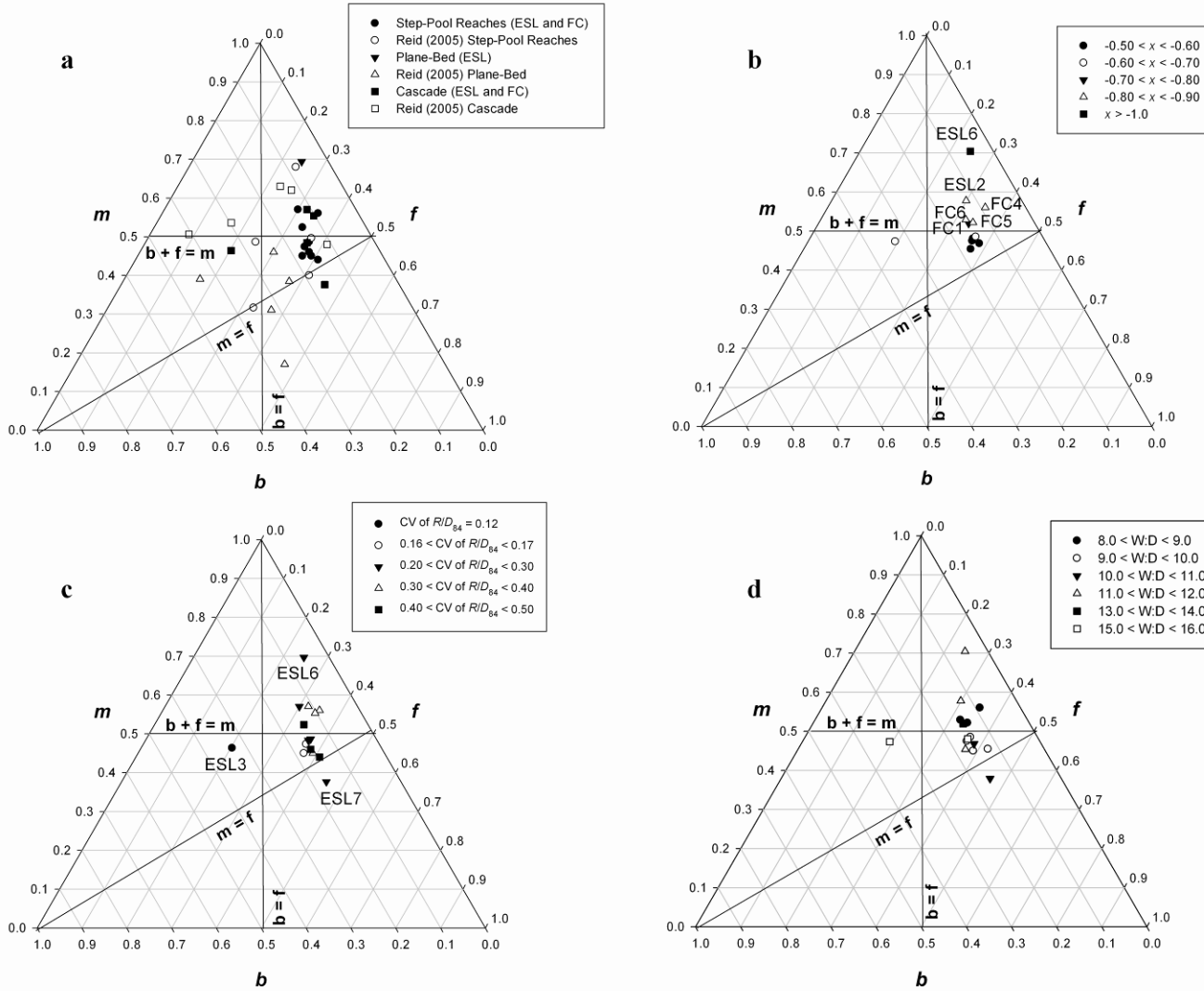


Figure 16: $b - f - m$ ternary diagrams, showing step-pool and cascade reaches in comparison to Reid's (2005) study (a); showing where reaches with particular rates of change of the Darcy-Weisbach Friction Factor (x) plot (b); showing where reaches with a particular coefficient of variation of R_h/D_{84} plot (c); showing where reaches with a particular width:depth ratio plot (d).

5.4.1 Summary of At-A-Station Hydraulic Geometry

The mean values of each of the exponents are 0.49 for m , 0.35 for f and for 0.16 for b (Table 6). All exponents were significant at the $\alpha = 0.05$ level except for the b value in FC6. All regressions were significant at the $\alpha = 0.05$ level, but some of the intercepts were not significant. Most likely the lack of significance of some of the coefficients is related to the low degrees of freedom in each regression. Because of the lack of significance of many of the coefficients, these were not analyzed separately. Despite the low degrees of freedom, the coefficient of determination is high for almost all the regressions, indicating a good fit of the data (Figure 14 and Figure 15). In most cases $m + f + b$ does not equal 1, but this is most likely an artifact of using average reach cross-sections rather than individual cross-sections for the analysis.

The mean, standard deviation and range of values for m are similar to the values found for step-pool and cascade reaches in the Rio Cordon [Comiti *et al.*, 2007] and other step-pool and cascade streams [Lee and Ferguson, 2002; Bathurst, 1993]. The range of values found in Colorado was also similar to the range found by Reid (2005) for lower gradient step-pool, cascade and plane-bed reaches in British Columbia (Figure 16a), although there was a larger amount of scatter in Reid's data and the means differed ($m = 0.51, f = 0.29, b = 0.20$).

Differences in the rate of change of depth and width with discharge may be related to differences in channel shape and roughness. For ESL2, ESL6, FC1, FC4, FC5, and FC6, m is greater than $b + f$, indicating that the velocity is increasing faster than the flow area in these reaches. The width exponent signifies that there is not a large variation

in width between low and high flows for a majority of the reaches despite changes in some reaches because of bank undercutting.

The at-a-station values indicate that for a majority of the reaches $m > f > b$. Therefore, the velocity increases faster with discharge than does depth, and depth increases faster than width for all reaches except ESL3 ($b > m > f$) and ESL7 ($f > m > b$). ESL3 is the only reach that has a width:depth ratio that increases with discharge (Table 6). The shape of the channel is very different from the other reaches because of a bar the length of the reach which has large boulders and even some herbaceous vegetation that splits the flow. The left bank of this reach is also noticeably steep and unstable, with most of the wood being input from this bank. An increasing width:depth ratio with discharge means that the flow is primarily accommodated by an increase in width rather than an increase in depth in this reach.

All reaches except ESL7 have $m > f$, which can be interpreted as increasing stream competence with increasing discharge [Rhodes, 1977; Reid, 2005]. However, this subdivision is related to low-gradient streams and does not account for bed armoring in these higher gradient channels. ESL7 is the only reach that has depth increasing faster with discharge than velocity. The increase in depth may be related to increased roughness from wood as discharge increases in this reach. Much of the roughness associated with wood in this reach is from overhanging branches that become submerged at higher flows. The channel shape in this reach is also different from the other reaches, with nearly vertical banks on both sides that enhance stage changes with increasing discharge.

Table 6: Summary table showing the power relationships between Q vs. w ($w = aQ^b$), Q vs. d ($d = cQ^f$), Q vs. v ($v = kQ^m$), and Q vs. ff ($ff = oQ^x$). The minimum and maximum values of $w:d$, ff , and R_h/D_{84} that were found over the four flow periods of measurement. The number of cross-sections used to determine average values for width and depth are also shown. The number of cross-sections varied based on reach lengths. For all the measured values from each flow period see Appendix A.

Reach	Channel Type	Width ^a			Depth			Velocity			Friction Factor			$w:d^\dagger$	ff	R_h/D_{84}	No. of Cross-Sections
		a	b	R^2	c	f	R^2	k	m	R^2	o	x	R^2				
ESL1	step-pool	3.13	0.16	0.99	0.42	0.39	0.99	0.76	0.45	0.99	3.98	-0.53	0.90	8.43	4.23	1.62	27
ESL2	step-pool	3.33	0.12	0.97	0.35	0.29	0.98	0.26	0.56	0.98	2.64	-0.82	0.95	9.95	4.35	3.51	18
ESL3	cascade	4.30	0.31	0.98	0.25	0.18	0.99	0.86	0.44	0.99	3.00	-0.62	0.98	15.54	3.75	1.39	13
ESL4	step-pool	3.04	0.15	0.99	0.40	0.37	0.97	0.15	0.49	0.98	4.09	-0.62	0.98	8.22	5.17	1.52	15
ESL5	cascade	4.37	0.16	0.99	0.36	0.37	0.99	0.66	0.49	0.98	7.80	-0.53	0.94	13.40	10.66	1.66	16
ESL6	plane-bed	2.86	0.05	0.96	0.27	0.24	0.99	1.33	0.69	0.99	0.20	-1.22	0.96	9.88	0.10	3.04	9
ESL7	cascade	3.24	0.15	0.96	0.38	0.44	0.98	0.78	0.36	0.92	3.45	-0.27	0.58	15.99	1.31	1.75	17
ESL8	step-pool	3.48	0.17	0.99	0.36	0.36	0.99	0.80	0.44	0.99	3.09	-0.54	0.99	9.32	3.34	1.45	20
ESL9	step-pool	3.09	0.16	0.98	0.41	0.36	0.99	0.79	0.47	0.99	4.54	-0.52	0.88	13.56	5.26	0.86	17
FC1	step-pool	2.36	0.15	0.97	0.28	0.34	0.97	1.53	0.53	0.99	0.50	-0.72	0.98	10.84	4.22	1.35	22
FC2	step-pool	1.91	0.11	0.98	0.37	0.37	0.96	1.08	0.40	0.90	1.35	-0.46	0.71	13.44	8.05	0.93	14
FC3	step-pool	2.53	0.14	0.97	0.43	0.36	0.97	0.82	0.44	0.97	2.91	-0.58	0.86	8.45	5.60	1.64	15
FC4	step-pool	1.83	0.09	0.96	0.41	0.35	0.99	1.28	0.56	0.99	1.76	-0.81	0.99	10.93	10.78	1.11	17
FC5	cascade	1.66	0.16	0.90	0.45	0.40	0.90	2.32	0.61	0.96	0.76	-0.83	0.99	10.21	1.07	1.95	15
FC6	cascade	1.68	0.18	0.77	0.42	0.39	0.91	2.82	0.64	0.96	0.63	-0.86	0.98	18.46	7.58	1.15	19

* Numbers in bold are significant at the level of $\alpha = 0.05$

† The values for $W:D$, f and R/D_{84} are the values at high flow (top) and low flow (bottom) for each reach

Table 7: Results of best subsets regressions for PCA Axis 1 scores, the velocity exponent (m) and friction exponent (x) versus significant explanatory variables. There were no significant regressions found using the width and depth exponents.

Dependent Variables*	Independent Variables†						
	Intercept	Roughness Area	Gradient	CV of Pool Volume‡	D_{84}	p-value	adj. R^2
PCA Axis 1 Scores§	0.14	-0.05	0.36	n.s.	n.s.	0.0007	0.68
Velocity Exponent (m)†, **	0.42	n.s.	1.60	n.s.	-0.82	0.005	0.59
Friction Exponent (e)††	-0.65	0.43	n.s.	-0.67	n.s.	0.04	0.59

* No significant regressions were found using the width and depth exponents (b, f) as dependent variables.

† Wood Volume/m², $\log(D_{84}/D_{50})$ and $w:d$ were all not significant in any regressions

‡ CV = Coefficient of Variation of Pool Volume

§ ESL3 and ESL6 both removed from regression as outliers

** FC1 and FC3 may have high leverage in this regression and could be driving the results

†† ESL1, ESL7, FC2 excluded because exponents not significant in at-a-station regressions. ESL6 and FC3 excluded because both are outliers and have high leverage on regression.

The rate of change of the friction factor with discharge (x) is higher than all other exponent values ($x > m > f > b$). The values of the friction factor exponents were not significant for ESL1, ESL7 and FC2, therefore the rate of change of friction factor with discharge may not be the same power relationship for these three reaches as for the other 12 reaches (Figure 14 and Figure 15). The rate of change of the friction factor is highest for the plane-bed reach and lowest for ESL5 and ESL9. Figure 14 and Figure 15 and the ternary diagrams (Figure 16b) indicate a relationship between the rate of change of the friction factor and the combined hydraulic geometry exponents. In particular, as the rate of change of velocity and depth increase, the friction factor decreases more rapidly.

Figure 16c and Figure 16d, respectively, show the CV of R/D_{84} and the $W:D$ for the same reaches. The CV of R/D_{84} is used as a measure of the variability in the protrusion of roughness elements over the four flow periods. Generally, reaches with lower variability (CV of $R/D_{84} < 0.17$) plotted below the $b + f = m$ line, but reaches with a higher coefficient of variation (CV of $R/D_{84} > 0.20$) plotted over a larger range. In Figure 16d, reaches with similar $W:D$ generally plotted together, but there was no particular trend for where those plotted on the ternary diagram.

5.4.2 Channel Type and At-A-Station Hydraulic Geometry

The ternary diagrams (Figure 16), PCA (Figure 17) and boxplots (Figure 18) indicate that there is no significant difference among hydraulic exponents between step-pool and cascade channel types. The width exponent (b) is significantly different between step-pool and cascade reaches. In all probability the width exponents are significantly different because of the much larger rate of change of width with discharge for ESL3.

Therefore, these results do not support the first hypothesis that the hydraulic geometry exponents are significantly different between step-pool and cascade reaches.

5.4.3 Potential Controls on At-A-Station Hydraulic Geometry

A principal component analysis (PCA) was conducted using the three at-a-station hydraulic geometry exponents. The axis scores for each reach represent the combined width, depth and velocity exponents for that reach. The scores on Axis 1 (Figure 17) explain the majority of the variability in the dataset (~97%) and are mainly related to the velocity and depth exponent. Very little of the variability is explained by the width exponent.

The regression of PCA Axis 1 scores shows that roughness area and gradient are significantly related to the rates of change of width, depth and velocity with discharge (Table 7). ESL3 and ESL6 were consistently outliers and removed from the regression.

The individual exponents were examined in separate regressions to determine whether individual exponents were similarly related to the explanatory variables (Table 7). Roughness area is also significantly related to the friction exponent. Wood volume/m² of reach is not significant in any regression. The D_{84} particle size and gradient are both significantly related to the velocity exponent. These results support the hypothesis that the exponent values are significantly related to control variables that represent both resisting forces (roughness area) and driving forces (gradient). Table 7 also shows that the friction exponent is significantly related to roughness area and the variability in pool volume (CVPoolV). These regressions indicate that roughness area may be a better measure of bed roughness than grain size. PCA Axis 1 scores were also significantly related to the friction exponent (Figure 19). The rate of change of the

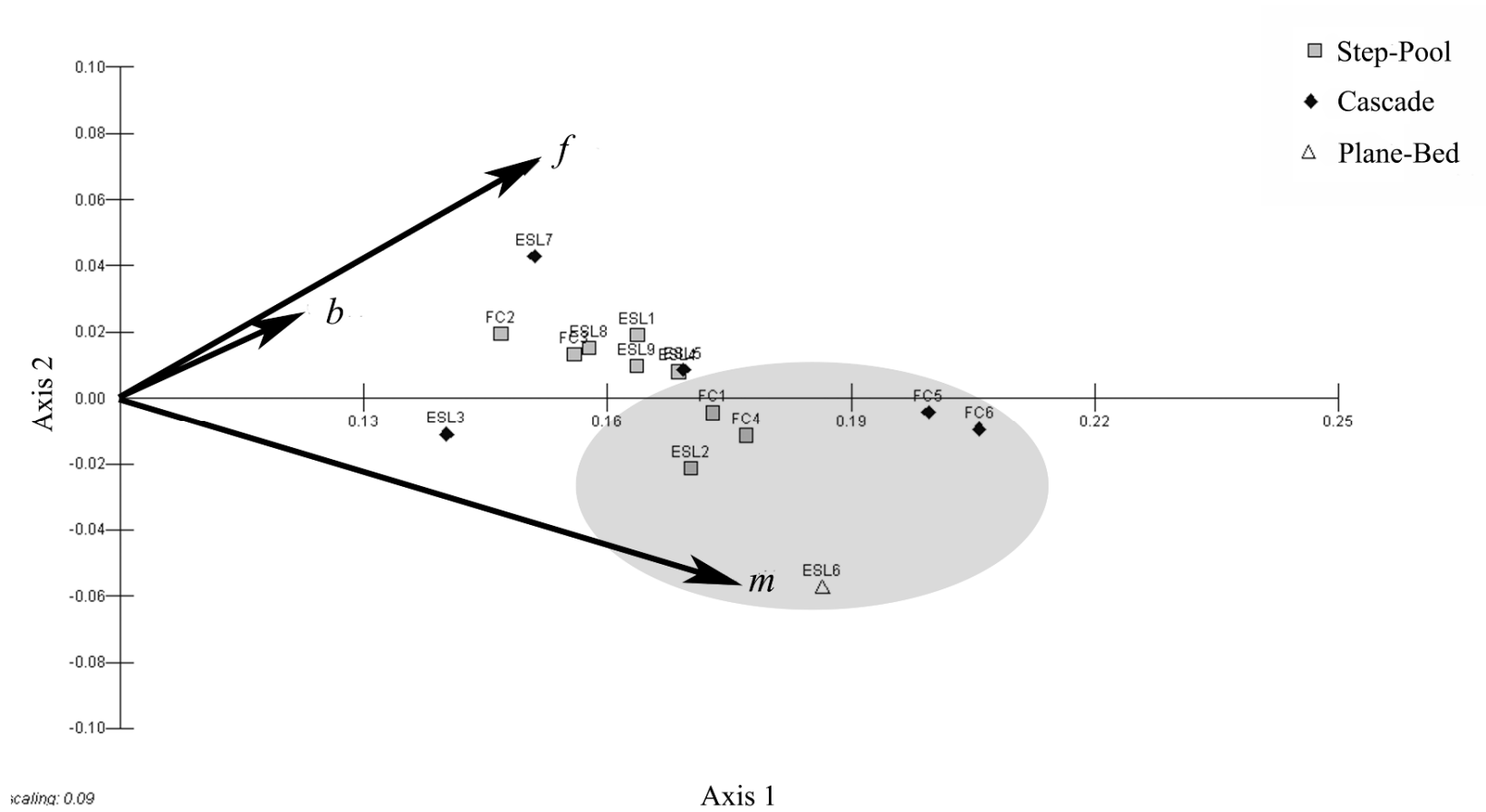


Figure 17: Principal Component Analysis (PCA) of all reaches using m , f , and b . The shaded area shows the reaches that have the most similar characteristics both in the ternary diagram and are interpreted to be dominated by grain resistance.

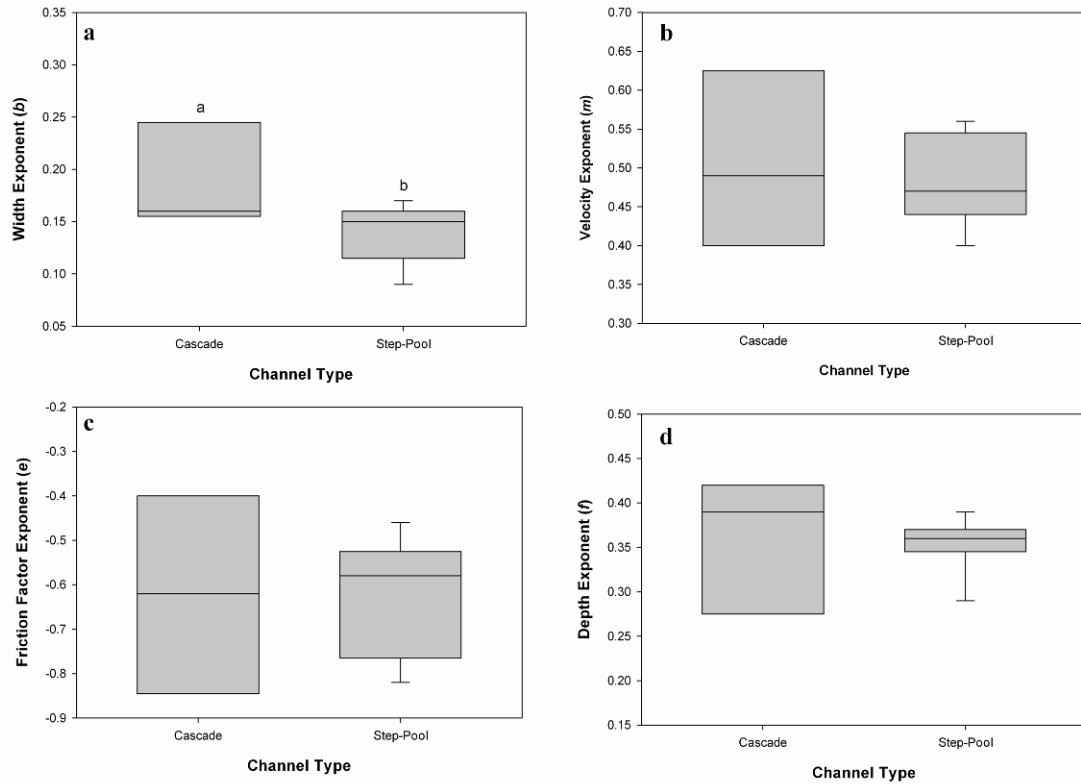


Figure 18: Boxplots showing the range of values of the width exponents (b) for step-pool and cascade reaches (a); the range of values for the velocity exponents (m) for step-pool and cascade reaches (b); the range of values for the depth exponents (f) for step-pool and cascade reaches (c); and the range of values for the friction factor exponents (x) for step-pool and cascade reaches (d). The letters a and b above the boxes show the results of the ANOVA and Tukey HSD test. If the same letters are above the boxes then the average value of the exponents for those two channel types are not significantly different from each other, if different letters are above the boxes then they are significantly different from each other.

friction exponent is larger for higher PCA Axis 1 scores, which is related to higher m values. Although there may be differences in this relationship based on the differences between basins or channel types (Figure 19), more cascade reaches would need to be included in the analysis to determine whether there is in fact a significantly different relationship. The steeper slope for both the cascade reaches and the Fool Creek reaches in the scatter plot is probably related to the steeper gradient of both FC5 and FC6.

Scatter plots (Figure 20) of PCA Axis 1 versus roughness area, wood volume/m², coefficient of variation of R_h/D_{84} , and CVPoolV show that the relationships between each

variable and the PCA axis scores may not be best represented by a log-linear regression. As the roughness area increases, the variability in PCA Axis1 scores decreases (Figure 20a). Therefore, there is more variability in the rates of change at a lower average roughness area. The relationship between the coefficient of variation of R_h/D_{84} and PCA Axis 1 is positive for the East St. Louis reaches, except for ESL1, and negative for the Fool Creek reaches (Figure 20b). The coefficient of variation is much higher for the Fool Creek reaches than for the East St. Louis reaches. This means that there is a larger standard deviation and lower mean value of relative submergence over the four flow periods in Fool Creek than in East St. Louis.

The coefficient of variation of pool volume represents the variability in pool size as flow changes for each reach. There is no significant relationship between this variable and PCA Axis1 score (Figure 20c), although a relationship may exist between $CVPoolV$ and the Fool Creek reaches. Both Figure 20b and Figure 20c underscore the differences between basins and the variability in these relationships even in adjacent basins.

The variability in PCA Axis1 scores is reduced at higher values of wood volume/ m^2 (Figure 20d); for both low values of roughness area and wood volume/ m^2 , there is much higher variability in rates of change of velocity and depth with discharge. At higher values the total friction factor increases and the velocity and depth do not vary as much between low and high flows. In reaches with higher values of wood volume/ m^2 , the roughness would increase with flow, as more and more wood becomes submerged. Therefore, the contribution of roughness from wood may either increase, or remain the same between low and high flows.

Figure 21 shows each of these variables in a bar plot for a better understanding of the magnitude of differences among reaches. The wood load and pool volume/m² vary the most among reaches, with FC1 through FC4 having similar values of pool volume/m². The average gradient gradually increases moving upstream from FC1 to FC6. The ESL reaches do not follow such a consistent trend and are much more similar in gradients except for the one plane-bed reach (ESL6). The D_{84} is similar for most of the FC reaches except for FC3. The same is true for the ESL reaches, except for ESL2 and ESL6. These bar plots and a correlation matrix (Table 8) also help in understanding the interactions between these variables. The two reaches in each basin with the highest wood load (ESL2, FC3) also have the lowest values of D_{84} . Table 8 displays a slight correlation between wood load and pool volume/m². The majority of the wood found in the step-pool reaches is located in the steps. Since each pool is associated with a step, it is expected that there would be some interrelationship between pools, steps and wood. There is also a slight correlation between pool volume/m² and D_{84} , but no correlation exists between D_{84} and wood volume per channel area.

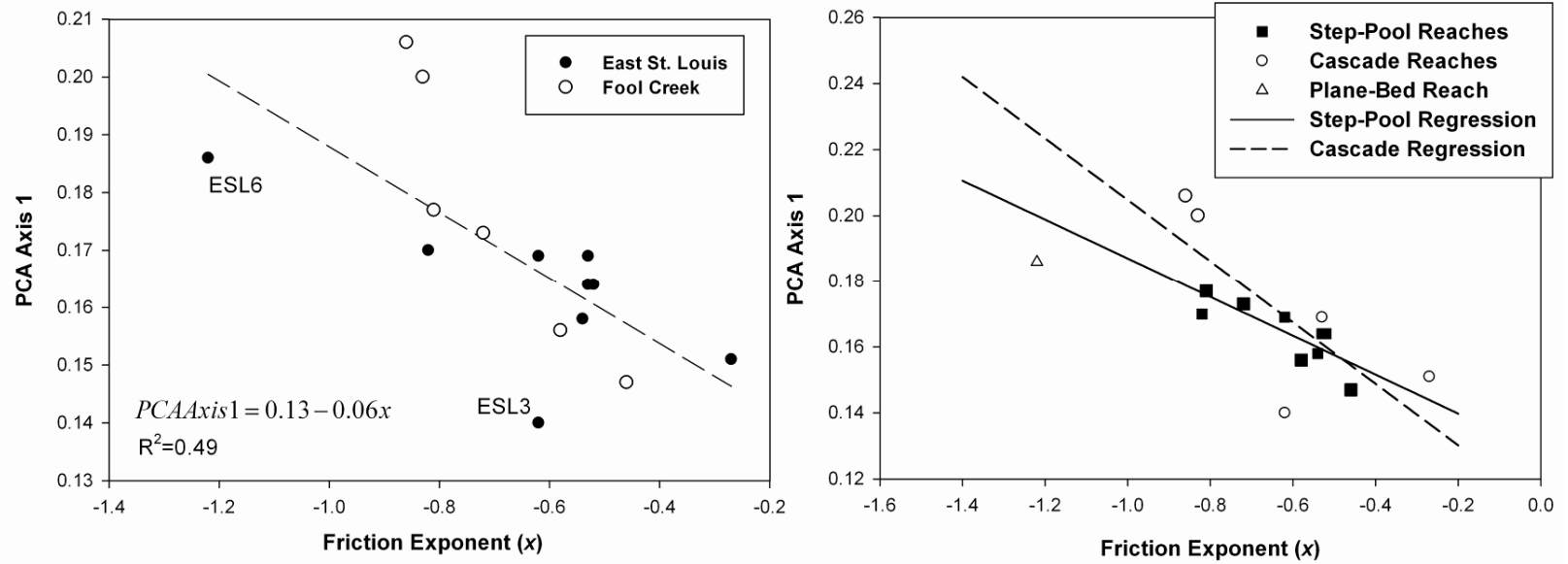


Figure 19: The PCA Axis 1 scores against the Darcy-Weisbach Friction Factor exponent (x) divided by drainage basins (left) and channel type (right).

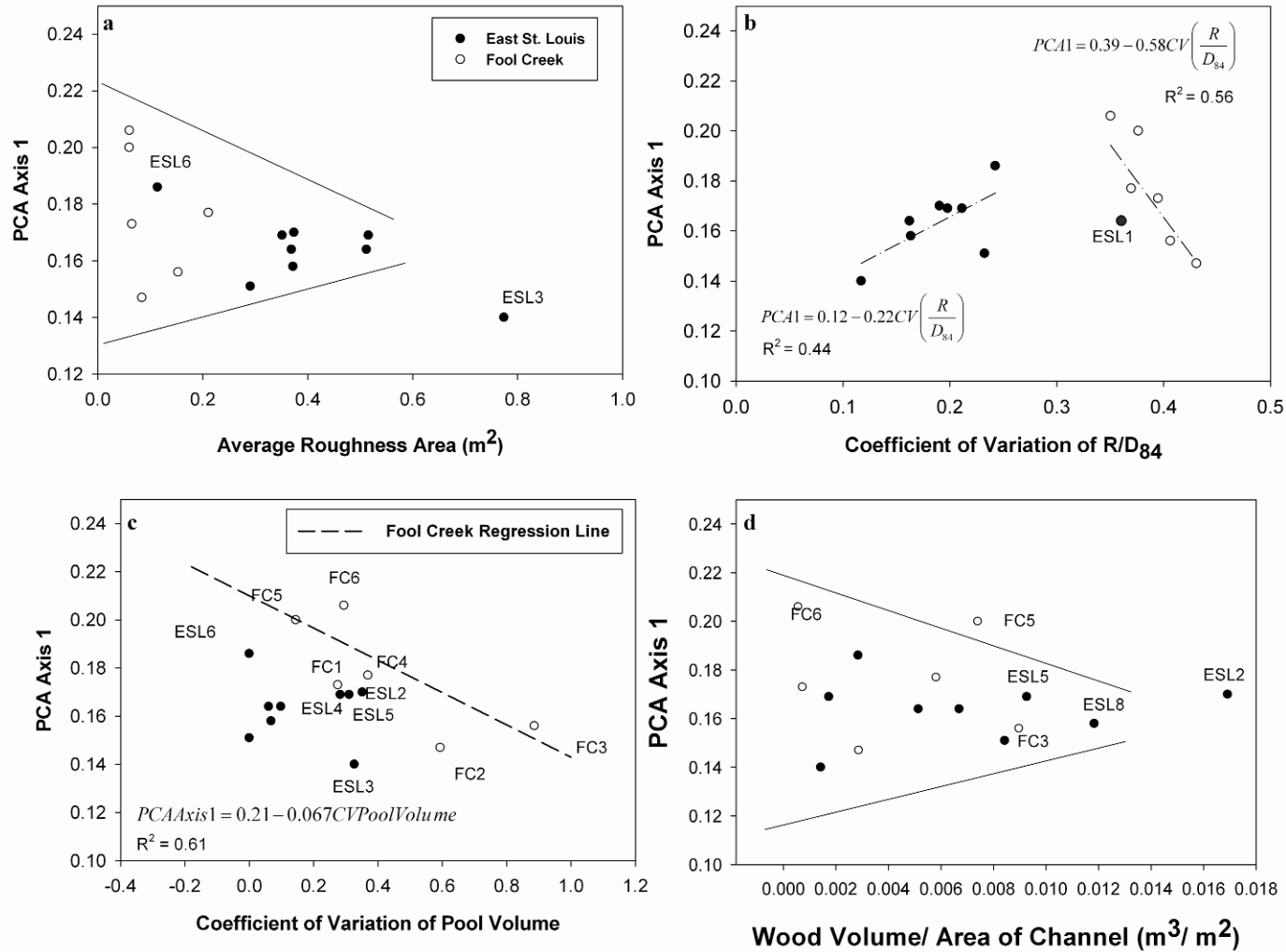


Figure 20: PCA Axis 1 scores versus average roughness area (a), coefficient of variation of R_h/D_{84} (b), coefficient of variation of pool volume (c), and wood volume per channel area (d) for the two drainage basins (East St. Louis and Fool Creek).

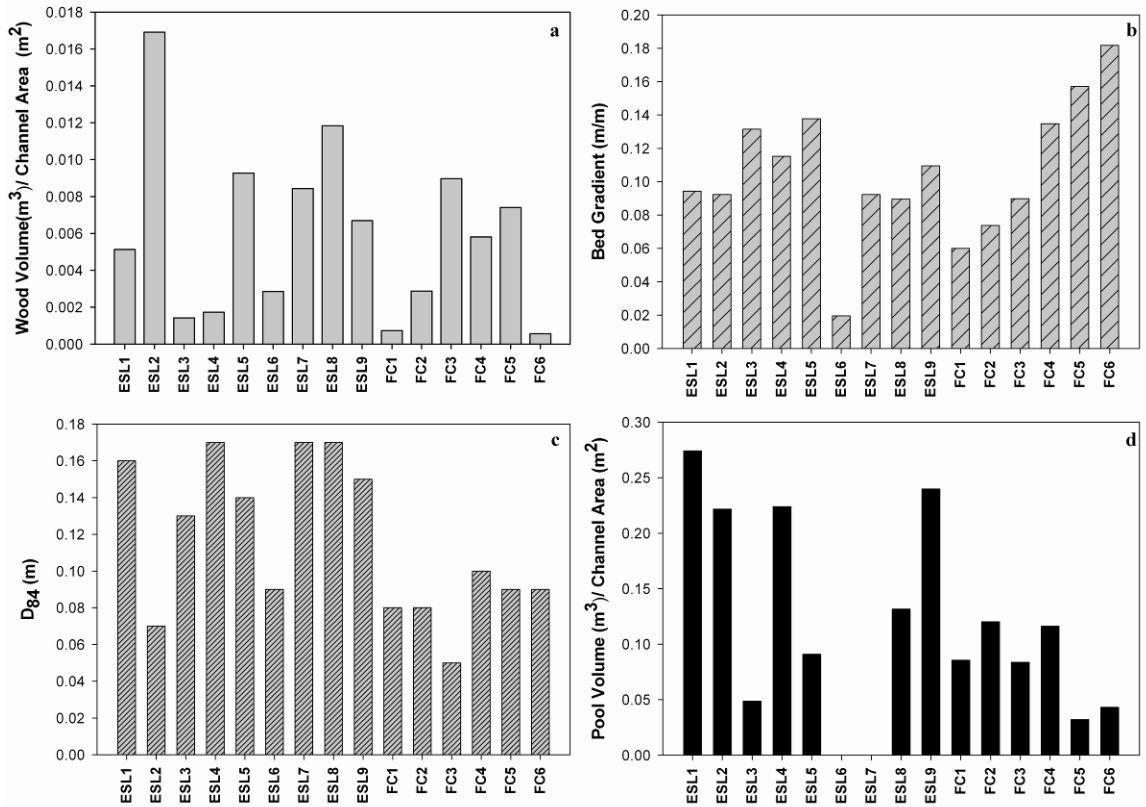


Figure 21: Barplots showing values for each reach of wood volume per channel area (a), bed gradient (b), D_{84} (c), and pool volume per channel area (d).

Table 8: Correlation matrix showing correlations among four variables: D_{84} , wood volume per channel area, pool volume per channel area, and gradient.

	D_{84} (m)	Wood Volume per channel area m^3/m^2	Pool Volume per channel area m^3/m^2	Gradient (m/m)
D_{84} (m)	--	0.00	0.30	0.12
Wood Volume per channel area m^3/m^2	0.00	--	0.24	-0.04
Pool Volume per channel area m^3/m^2	0.30	0.24	--	-0.03
Gradient (m/m)	0.12	-0.04	-0.03	--

5.5 Discussion

There are systematic variations of width, depth, velocity and friction factor with discharge in each of the study reaches, but there is no significant difference between channel types. The first hypothesis was based on the understanding that controls on roughness, which presumably influences width, depth, and velocity, may vary based on the channel type. Cascade reaches generally have steeper gradients and the major source of resistance is large boulders protruding in the flow. There are often some pools in a cascade channel, but these are not as well-developed as in a step-pool reach (Figure 21). The resistance is mainly related to skin friction and form drag around large boulders. Wood is present in both cascade and step-pool reaches (Figure 21). The major source of energy dissipation in a step-pool reach occurs when flow tumbles over each step and enters into the pool [Wilcox and Wohl, 2006; Curran and Wohl, 2003]. Wood is present in the steps and as individual pieces along the reach. The amount of wood in each of these reaches varies depending on the flow depth. Some of the wood is present as branches that reach down into the channel like a comb. I hypothesized that these various sources of resistance would contribute to differences in the rates of change of velocity, width and depth in each of the channel reaches, but there was not a significant difference between channel types. I concluded in Chapter 4 that total resistance in both East St. Louis and Fool Creek is significantly related to gradient, wood load, and temporal variations in discharge. In cascade reaches, relative submergence of grains (R_b/D_{84}) was a significant explanatory variable, but in step-pool reaches relative submergence of steps (R_b/H) was the significant explanatory variable, indicating a difference in the type of resistance that dominates in these channel types. Although different forms of resistance

may dominate in each channel type, the rates of velocity, width and depth change with discharge are related to a number of variables that are not solely dependent on channel type and the type of resistance present.

Richards [1976] found a significant difference in exponent values between pools and riffles, but an analogous difference does not appear to be present for reach-averaged values of different steep channel morphologies. The ternary diagram (Figure 16) and the PCA (Figure 17) indicate that the plane-bed reach is different from the other channel types, but once the data from British Columbia were included, the plane-bed reaches did not plot together. The plane-bed reach in this study (ESL6) has the highest increase in both velocity and friction factor with discharge (Table 6) and was most closely related to FC1, FC4, FC5, FC6, and ESL2. These six reaches all plotted above the $m = b + f$ line in the ternary diagram, indicating that for these six reaches the velocity is increasing faster than the flow area [*Rhodes*, 1977; *Reid*, 2005]. All six of these reaches also have a high rate of decreasing resistance with increasing discharge and velocity. *Knighton* [1975] found that the highest rates of decrease in resistance were related to cross-sections where grain resistance dominated. Therefore, grain resistance is probably the dominant form of resistance in these six reaches in relation to the rate of change of width, depth and velocity with discharge. For the step-pool reaches, the form resistance may control the value of total resistance, but the contribution of form resistance to total resistance probably does not change over all four flows. The contribution of grain resistance drastically decreases with increasing discharge, meaning that grain resistance actually has a larger influence on the rate of change of width, depth and velocity with discharge.

5.5.1 At-a-station hydraulic geometry and flow resistance

The flow resistance characteristics were represented by roughness area, wood load, coefficient of variation of pool volume, sediment sorting (σ), sediment size (D_{84}), standard deviation of bed elevation, and width:depth ratio. Both f and m are expected to be dependent on flow resistance characteristics, whereas b is dependent on channel shape [Ferguson, 1986; Bathurst, 1993]. The only resistance characteristic that was significantly related to the PCA Axis 1 scores was the average roughness area. The roughness area can include both boulders and logs that make up part of the bed as well as portions of the overhanging bank that become submerged as flow increases.

It is expected that smaller roughness elements would become submerged at higher flows, allowing a marked decrease in resistance and a much higher velocity [Knighton, 1975]. At lower flows, water is forced around boulders where form drag is high. As discharge increases, the boulders become submerged and form drag decreases and mean velocity increases rapidly [Bathurst, 1993]. If the boulders are an equivalent height as the flow at all flows, then they are never submerged and form drag will remain dominant in that reach. This is why D_{84} and R/D_{84} are commonly found to be good representations of roughness in a reach [Bathurst, 1993]. Sediment size and sediment sorting can play a role in influencing the velocity profile [Wiberg and Smith, 1991], but in these streams neither was found to be significantly related to the hydraulic exponents. Ferguson [1986] showed theoretically that hydraulic geometry should vary with bed particle size, but Ridenour and Giardino [1995] found no correlation between median grain size and hydraulic geometry for pool-riffle channels. The results of this study agree with Ridenour and Giardino [1995], in that there is no significant relationship between the PCA Axis

scores and D_{84} or sediment sorting for cascade and step-pool channels. In Chapter 4, bed material size distribution was shown to not be significantly related to resistance throughout the channel network in East St. Louis or Fool. *Bathurst* [1985] established that the relative roughness area (roughness area/simplified cross-sectional area) was significantly related to the relative submergence (R_f/D_{84}). There was no such relationship here, but the average roughness area was found to better represent the bed topography relation to flow resistance. *Lee and Ferguson* [2002] found that the velocity exponent (m) was related to the proportion of bankfull width that is occupied by protruding clasts at low flow. The velocity exponent (m) was found to be significantly related to the D_{84} and gradient for this study. Areas with protruding clasts cause the flow field to separate and wake turbulence to increase. As discharge increases, the smaller clasts become submerged and skimming flow may develop over the tops of the boulders. Table 7 shows that m is smaller in reaches with a larger range of clast sizes. At high flows the boulders are probably not submerged, maintaining a similar structure to the flow field over all flows and causing the rate of change of velocity with discharge to be much lower.

There are six reaches that have high friction exponents and have velocity exponents greater than $b + f$. Four of these are step-pool reaches, but the results indicate that these are still dominated by grain resistance [*Knighton*, 1975]. All the reaches are at different gradients, but have similar values of D_{84} . ESL2 has localized sections of very shallow gradients behind the large log step in the reach (Figure 22). The high wood load is related to this large log step, which is probably the cause for the local reduction in gradient and deposition of fine sediment [*Buffington and Montgomery*, 1999]. The log

step most likely increases the total friction in the reach, but is never completely submerged, so the rates of change of velocity, width and depth are not altered with discharge. On the other hand, the finer sediments behind the step are quickly submerged at high flows, meaning that the values of the exponents are influenced mainly by the grain size. There is also a small amount of bedrock exposed in the upstream portion of this reach. FC1 and FC4 are both step-pool reaches as well, but they are narrow reaches with local reductions in gradient and grain size that are quickly submerged as discharge increases. FC5 and FC6 are narrow, somewhat rectangular cascade reaches (Figure 23). The high wood load in FC5 is related to one log that is embedded in the channel bottom and creates one large step in the reach. Again, the resistance related to this step probably does not change with discharge since it is not submerged at the higher flows. As flow increases in both reaches, the larger clasts are quickly submerged, allowing velocity to increase and resistance to decrease quickly with discharge. Figure 23 shows how quickly the flow submerges the roughness elements in the flow for these two reaches versus ESL7.

ESL6 is the last reach in this category. The plane-bed reach is already expected to be dominated by grain resistance, although plane-bed reaches from *Reid's* study [2005] did not necessarily plot in the same part of the ternary diagram. The reaches in *Reid's* [2005] study had some previous modification, which may be why there was so much variability in this channel type.

The regression with the velocity exponent as the dependent variable (Table 7) was included to show that gradient is significant whether the PCA axis scores or the individual exponents are used. Because the values of the exponents are interrelated, it is

more appropriate to use some value that represents all three exponents rather than analyzing them individually [*Ridenour and Giardino, 1991*].

The relative submergence (R_h/D_{84}) has been shown to be an important representation of grain resistance, particularly in pool-riffle channels and boulder bed streams with gradients $< 4\%$ [*Bathurst, 1993; Bathurst, 2002; Reid and Hickin, 2008*]. The average relative submergence was not found to be significantly related to the PCA axis scores, but Figure 20b shows the complexity of the relationship between R/D_{84} and the axis scores. Except for ESL1, there is a division between the Fool Creek reaches and the East St. Louis reaches around a value of 0.3. The axis scores of East St. Louis reaches increase with increasing CV of R/D_{84} and the Fool Creek axis scores decrease. The differences here may represent a difference in both channel shape and resistance in the Fool Creek reaches.

Ridenour and Giardino [1995] found that Manning's roughness, drag resistance and median grain size were not correlated with the hydraulic exponents. They conclude that although roughness elements are related to velocity and depth, this does not mean that the rates of change of velocity and depth with discharge are related to these same roughness elements [*Ridenour and Giardino, 1995*]. Alternatively, the rates of change of velocity and depth were found to be significantly related to the rate of change of the friction factor (Figure 19) [*Richards, 1973; Ridenour and Giardino, 1995*]. The results of this study indicate that m is negatively correlated with x . Again, the reaches that are probably dominated by grain resistance have the highest values of x [*Knighton, 1975*]. Reaches that have boulders or logs the same order of magnitude as the flow depth do not have as high a rate of change in resistance or velocity with depth. The differences

between reaches that are dominated by grain resistance and those dominated by form or spill resistance may also indicate a need to evaluate the controls on the hydraulic exponents for these reaches separately.

Wood is an important source of flow resistance that can affect the hydraulics and geometry at both a cross-sectional and reach scale [Gippel *et al.*, 1996; Buffington and Montgomery, 1999; Manga and Kirchner, 2000; Hygelund and Manga, 2003; Wilcox and Wohl, 2006; Manners *et al.*, 2007]. The wood volume per m² of channel was used to determine whether there was a significant relationship between wood and the at-a-station hydraulic exponents, but no significant relationship was found (Table 7). The lack of significance in the regression could be either related to the complexity of the relationship or to the fact that, although wood is probably related to velocity in the reach, it is not necessarily related to the rate of change of velocity [Ridenour and Giardino, 1995]. Another possibility is that wood load does not sufficiently characterize the effect of wood in the reach on the overall roughness.

Variability in the value of the exponents appears to decrease with increasing wood load (Figure 20d). This suggests that when there is a smaller amount of wood in the reach the exponent values vary more, but at higher roughness the rates of change of velocity and depth with discharge may be limited. We expect that wood would reduce the average velocity and locally elevate the water surface, but the interaction between wood, other roughness elements such as boulders, and the hydraulic exponents is probably very complex. Wilcox and Wohl [2006] found that interactions between steps, grains and wood have a significant effect on how resistance varies with discharge in step-

pool streams, so we expect that the same interactions influence how velocity and depth vary with discharge in these same streams.

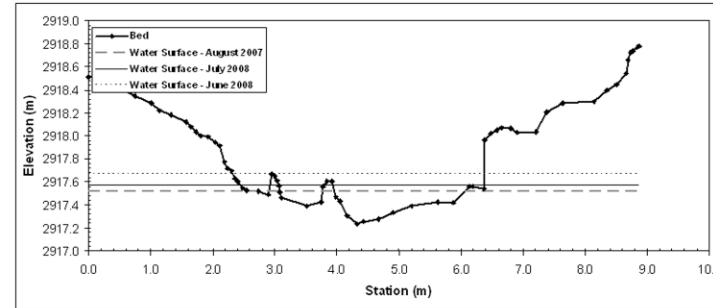
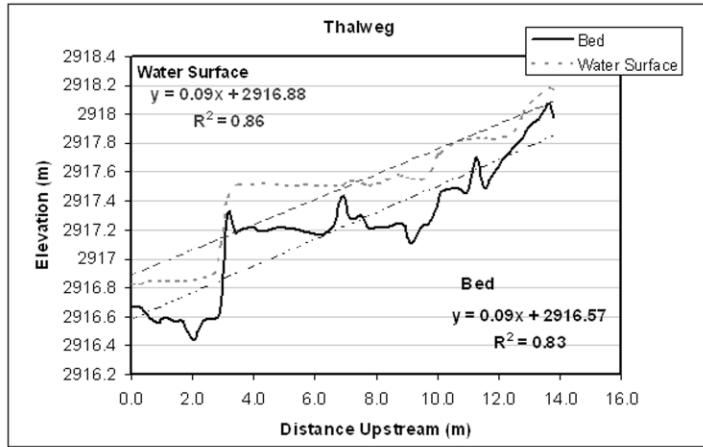
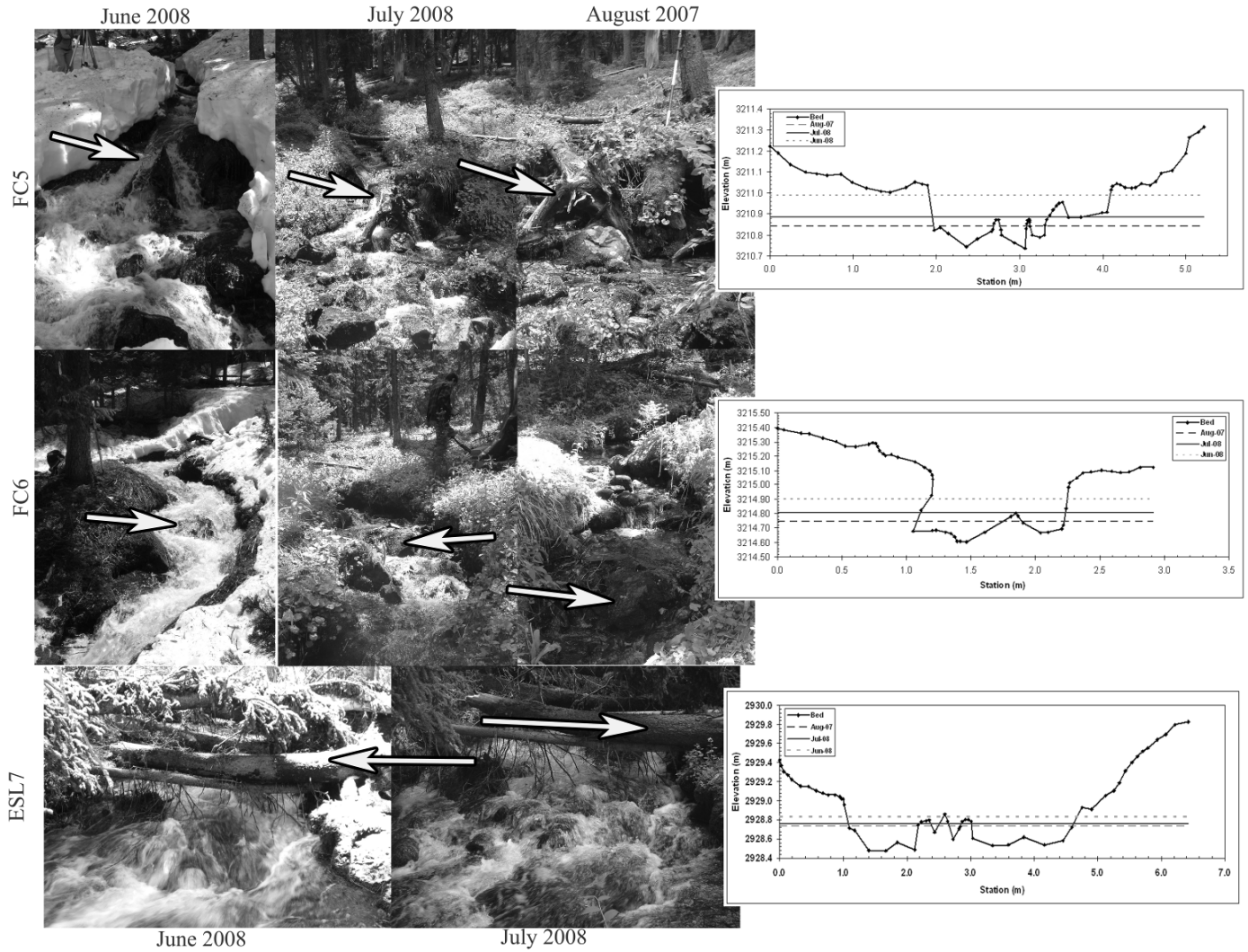


Figure 22: Example of longitudinal profile and cross-section of ESL2. The longitudinal profile shows both the bed profile and water surface with fitted linear trend lines and equations shown for both. The photograph in the bottom left shows the entire reach, looking upstream during the June 2008 high flow. The cross-section shows the water surface at three stages (August 2007, July 2008, June 2008). The photograph on the bottom right shows the approximate location of the cross-section at August 2007 low flow.



for ESL7.

Figure 23: Photographs and cross-sections for three cascade reaches: FC5, FC6 and ESL7. The white arrows show the same location in each photograph and the photographs are of the approximate location of each of the cross-sections shown at the right. The cross-sections show the water surface over three flow periods (August 2007, July 2008 and June 2008) for FC5 and FC6 and June 2008 and July 2008

The friction exponent (x) was not significantly related to the wood load (Table 7). The lack of a relationship is probably because the individual pieces of wood need to be categorized differently. *Wilcox and Wohl* [2006] found that the position of wood in the channel can have a greater effect on resistance than the density. Wood located at step lips increased the height of the step and dammed the flow. Another important characteristic is the size of the debris relative to water depth [*Gippel et al.*, 1996]. The resistance may not change around a large log that is submerged at all flows, but as a smaller log becomes submerged it may cause a change in resistance as flow increases. Also, a log that was not within the water column at low flow may change the resistance characteristics as it becomes submerged at higher flows. *Hygelund and Manga* [2003] found that drag did not vary with depth around logs that had diameters greater than one-third the channel depth. Therefore, large individual pieces in the flow would not have a large effect on how friction and velocity change with discharge. Reaches that had large single pieces of wood in the flow include ESL5, ESL9, FC1 and FC5. FC1 and FC5 both have one large log in the flow, which probably does not cause a significant difference in drag between low and high flows.

ESL5 and ESL9 both have larger log jams associated with large steps in the reach. *Manners et al.* [2007] found that the frontal area and surface area of a jam have an important effect on the amount of drag related to the jam. *Manners et al.* [2007] found that debris jams are highly porous and treating them as a single non-porous object greatly changes the quantification of drag force around that jam. The reaches with the largest and most complex jams are ESL1, ESL2, ESL5 and FC3. In ESL2, the jam created a reduced water surface slope, causing a reduction in velocity and textural fining (Figure

22). The velocity increases at one of the faster rates in ESL2 ($m = 0.56$) because as discharge increases these finer sediments are quickly submerged, reducing friction and increasing velocity. This is also related to the smaller rate of change of depth ($f = 0.29$). As the roughness elements become more submerged, the water can pass through more quickly and the depth does not change as much with discharge. FC3 is slightly different because a larger portion of the reach is below the large log jam and more steps developed from other log jams. ESL2 has only one step that is related to a log jam and the others are related to boulders. The influence of wood and sediment sorting on the at-a-station exponents may be better understood by differentiating the reaches that are dominated by grain resistance (Figure 24).

Wood, R/D_{84} , bed material size distribution, CVPoolIV, and average roughness area are all variables that represent roughness in each reach from clasts, wood and bedforms. Average roughness area is a variable that integrates grain and form roughness, which is probably why it is the variable significant in the regression with the PCA axis scores.

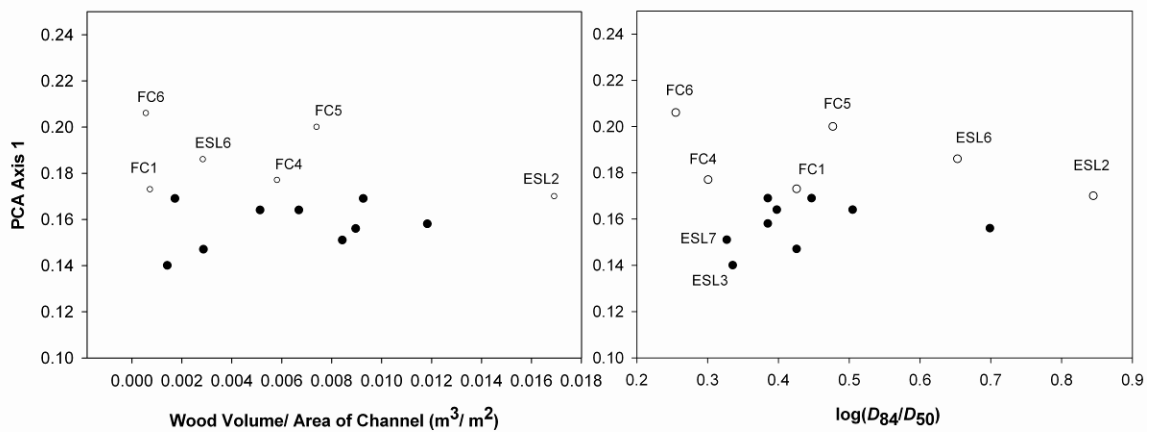


Figure 24: PCA Axis 1 scores versus wood volume per channel area (left) and $\log(D_{84}/D_{50})$ (right). The reaches are divided by those interpreted to be dominated by grain resistance (open circles) and those that are dominated by form and spill resistance (closed circles).

5.5.2 Hydraulic exponents vs. gradient

The second significant variable in the multiple regression with the PCA axis 1 scores is gradient (Table 7). Gradient partly governs the amount of energy available for transporting material or eroding the bed and banks of a channel. Previous studies have shown the importance of gradient in controlling how resistance varies with discharge throughout a channel network [Bathurst, 1993; Comiti *et al.*, 2007; (CHAPTER 4)]. As gradient increases along Axis 1, m and f increase. Gradient increases with each reach for FC1 through FC6 (Figure 21). The bed gradient in this case also represents the average water-surface gradient, which is not significantly different from the average bed gradient. Therefore, as the water surface steepens, the rate of change of velocity with discharge increases, holding constant for roughness area. *Leopold and Maddock* [1953] also found in their original hydraulic geometry study that the rates of change of width, depth and velocity are controlled by the slope of the water surface. *Wohl* [2007] determined that an inflection point in the rate of change of the water-surface gradient with discharge indicated the point between where grain resistance and form resistance dominated. No inflection points were found in the at-a-station graphs, but this may be because of the low sample size for each reach.

5.5.3 Problems with using reach-averaged hydraulic geometry

This study used reach-averaged values of width, depth and velocity to compare at-a-station hydraulic geometry. The use of reach-averaged values meant that the exponents did not always sum to unity for every reach. *Stewardson* [2005] proposed using the coefficient of variation of the width, depth and velocity to characterize the cross-sectional hydraulic geometry of a river reach, but these relations were not found to be significantly

related to discharge. The use of reach-averaged values may reduce the variability in the hydraulic exponents [Jowett, 1998; Lamouroux and Capra, 2002; Stewardson, 2005], but the use of the coefficient of variation of these exponents may not be practicable for these steeper streams. It is also possible that there was a lack of relationship because the study was only done over four flow periods. There is high variability between cross-sections in each of these reaches, but the good fit between width, depth and velocity with discharge is thought to show how well these power relations still characterize these reaches.

5.6 Conclusion

At-a-station hydraulic geometry is an important tool to use to help in our understanding of resistance in steep mountain streams. The hydraulic exponents at the East St. Louis and Fool Creek sites were all within the range of values found by other researchers studying step-pool, cascade and plane-bed reaches. The exponents could not be used to delineate a difference between the three channel types, but may be useful in determining which reaches are dominated by grain resistance versus form resistance. For most study reaches, $m > f > b$, indicating that the rate of change of velocity with discharge is greater than the rate of change of width or depth. This reflects the fact that increasing discharge in these steep, laterally confined streams results mainly in reduced effective hydraulic resistance as sources of grain and form roughness occupy a progressively smaller portion of the flow. Average exponent values for low gradient streams indicate that a larger proportion of the change in discharge is compensated by increasing flow width ($b = 0.4 - 0.5$), with lower rates of change in depth and velocity [Park, 1977]. In contrast, increasing flow in steep mountain streams primarily alters the

effective hydraulic resistance, as reflected in rates of change of velocity and flow depth. These effects increase with gradient, as reflected in higher m and f values at steeper slopes for the East St. Louis and Fool Creek reaches.

These relations are illuminated by PCA analysis. The at-a-station values are significantly related to average roughness area and the bed gradient in each reach. Localized reductions in gradient, sediment size and channel shape explain the connections between cascade and step-pool reaches in two basins with high values of m and x . Further work needs to be done to understand whether reaches with $m > f + b$ are all dominated by grain resistance and whether controls in these reaches should be evaluated separately from controls in reaches that may be dominated by form resistance. However, the results from this study suggest that those reaches are dominated by grain resistance and that those reaches dominated by form resistance create one population with respect to at-a-station hydraulic geometry relations.

CHAPTER 6 COMPARITIVE ANALYSIS OF BED RESISTANCE

PARTITIONING IN HIGH GRADIENT STREAMS

6.1 Abstract

Total flow resistance can be partitioned into its components of grain (ff_{grain}), form (ff_{step}), wood (ff_{wood}), and spill (ff_{spill}) resistance. Methods for partitioning flow resistance are based on methods developed for low gradient streams, including an additive approach that usually leaves the unmeasured component as the largest component. A detailed examination of developed methods for calculating each component of resistance along with the limitations of these methods is undertaken by using data gathered from 15 high gradient ($0.02 < S_0 < 0.195$) step-pool, cascade and plane-bed reaches in Fraser Experimental Forest. Each reach was characterized using a combination of a laser theodolite to gather bed and water-surface elevations, a tripod-mounted LiDAR to obtain channel geometry and wood data, and Rhodamine WT dye tracer to determine reach-average velocity. Grain resistance was calculated using three equations that relate the relative submergence (R/D_m) to ff_{grain} as well as using an additive drag approach. The drag approach was also used for calculating ff_{wood} and ff_{step} . The % ff_{grain} was found to contribute the smallest amount towards all reaches at all flows, although the value varied based on the method used. The *Parker and Peterson* [1980] equation, using D_{90} , was determined to best represent ff_{grain} at high flows, whereas the *Keulegan* [1938] equation, using D_{50} , characterized ff_{grain} at base flows. The results from the analysis of these methods indicated that ff_{grain} may be better represented if two grain sizes are used to calculate this component of resistance. Methods for calculating wood resistance were

found to overestimate the significance of individual logs in the channel. Wood and boulders in steps were considered part of the step form and included in the value of ff_{step} . A method was proposed for evaluating the contribution of ff_{step} , which significantly decreased the contribution of ff_{spill} , particularly at higher discharges. Potential controls and interactions between each component of resistance were also analyzed. Gradient and discharge both were significant controls on each form of resistance except for ff_{step} . Step resistance was only significant at high flows, indicating that ff_{spill} still dominates at lower flows. Grain resistance decreased significantly as wood volume increased, indicating that different forms of resistance interact, thus demonstrating that it is unsuitable to use the additive approach to evaluate component resistance.

6.2 Introduction

Quantifying flow resistance is essential to understanding the hydraulics of streams. Interactions between stream flow and channel boundaries dissipate energy as water moves around and over bed irregularities. Flow resistance is created by viscous skin friction around objects as well as form/pressure drag created from differential pressures around objects [Ferguson, 2007]. The total value of the frictional losses can be represented with the dimensionless Darcy-Weisbach friction factor:

$$ff = \frac{8gR_h S_f}{\bar{v}^2} \quad (6.1)$$

where, ff = Darcy-Weisbach friction factor; g = acceleration due to gravity (m/s^2); R_h = hydraulic radius (m); S_f = friction slope (m/m); \bar{v} = mean velocity (m/s).

There are a number of sources of error in the calculation of ff for steep channels. Each parameter (\bar{v} , S_f , R_h) has error associated with the measurement method. The use of ff , along with Manning's n , nonetheless remains the most common approach to

quantifying resistance in steep streams despite indications that the Manning's equation in particular is poorly suited to steep streams with shallow flows [Ferguson, 2010].

Einstein and Barbarossa [1952] proposed that despite interactions of different components of resistance, the individual components could be quantified and summed. The ff_{total} is most often partitioned into its components of grain, form and spill resistance:

$$ff_{total} = ff_{grain} + ff_{form} + ff_{spill} \quad (6.2)$$

where, ff_{grain} = viscous friction and form drag around grains in the absence of bedforms; ff_{form} = form drag around bedforms, which should not be confused with the individual component of form drag around other objects such as boulders; ff_{spill} = energy dissipation from flow acceleration and deceleration, usually over steps. *Shields and Gippel* [1995] also proposed partitioning ff into the components from wood (ff_{wood}), banks (ff_{banks}) and bends (ff_{bends}). Extensive effort has been devoted to quantifying the relative importance of different components of ff during the past few decades, yet no consensus has been reached regarding the most important components or the most appropriate method to calculate individual components. In this chapter, I evaluate several methods for partitioning ff and identify the limitations of these methods when applied to steep streams.

Additive approaches have been used to investigate the contribution of grains [Einstein and Barbarossa, 1952; Parker and Peterson, 1980, Millar and Quick, 1994; Millar, 1999], wood and spill resistance [Shields and Gippel, 1995; Curran and Wohl, 2003], and bar resistance in gravel-bed rivers [Parker and Peterson, 1980; Prestegard, 1983]. *Wilcox et al.* [2006] demonstrated, however, that the unmeasurable component was always the largest contributor to total resistance, so that an additive approach inflates

the leftover component. Thus, quantifying the relative contribution of different sources of resistance remains a primary challenge to understanding flow resistance in streams.

A second primary challenge is to quantify the total ff in steep streams where the roughness elements are on the same order of magnitude as the flow depth, creating frequent wakes, jets and standing waves, as well as spill resistance where local acceleration and deceleration occur. As discharge increases, elements may be submerged, allowing velocity to increase much faster with discharge than in low-gradient channels [Lee and Ferguson, 2002]. Relative submergence of a characteristic grain size (R_h/D_{84}) is commonly used to predict ff_{total} [Keulegan, 1938; Limerinos, 1970; Hey, 1979; Bathurst, 1985, 1993], although this approach can have high error rates when applied to steep mountain streams [Thorne and Zevenbergen, 1985]. A dimensionless hydraulic geometry approach has been proposed as a more suitable method for predicting velocity in place of using a flow resistance equation in high gradient streams [Rickenmann, 1991; Ferguson, 2007; Zimmerman, 2010], but it remains useful to employ a partitioning method to understand how different objects in the channel affect total flow resistance.

Mountain streams with gradients ≥ 0.02 m/m have distinctive channel morphologies consisting of step-pools, cascades and plane-bed reaches [Montgomery and Buffington, 1997]. Spill resistance contributes a major proportion of flow resistance in step-pool reaches [Abrahams *et al.*, 1995]. As for steep streams in general, understanding the relative contribution of different sources of resistance is challenging for step-pool channels. Most approaches are based on boundary layer theory, which assumes a semi-logarithmic velocity profile, although the profile in steep streams more closely resembles an s-shape [Wiberg and Smith, 1991].

Steps create flow resistance via viscous friction over large particles, but the hydraulics of step-pool reaches indicate that the ff_{total} is a function of more than just the relative submergence of a representative grain size [Lee and Ferguson, 2002; Aberle and Smart, 2003]. Deviations from the relative submergence equations are related to bed material size distribution, shape and orientation [Bathurst, 2002] as well as step geometry [Maxwell and Papanicolaou, 2001].

Step geometry is particularly important because steps create flow resistance by form drag (ff_{step}) from pressure differences around the upstream and downstream sides of the step and spill resistance (ff_{spill}) from flow acceleration and deceleration over the steps [Chartrand and Whiting, 2000]. Form drag varies with step geometry and composition, longitudinal step spacing, and stage [Zimmerman and Church, 2001; Wilcox and Wohl, 2006]. Spill resistance varies with step geometry, wood density and orientation [Comiti et al., 1999; Curran and Wohl, 2003; Wilcox and Wohl, 2006; Comiti et al., 2008].

The contribution of spill versus form resistance depends on the submergence of the step. The flow regime over a step is generally characterized as nappe flow, transition flow, or skimming flow [Chanson, 1994; Church and Zimmerman, 2007; Comiti et al., 2009]. Nappe flow occurs when water free falls over a step and alternates between subcritical and supercritical flow. Nappe flow with a submerged jet is affected by the downstream tailwater [Comiti et al., 2009]. Energy is dissipated by the breakup and mixing of the jet on the step tread and from wake interference flow and turbulence generation in the downstream pools [Wohl and Thompson, 2000]. Skimming flow is characterized by supercritical flow over completely submerged steps and is dominated by form resistance in the cavity recirculation [Chanson and Toombes, 2002]. The flow is

cushioned by a re-circulating fluid trapped between the steps. In a skimming flow regime, early steps do not have air entrainment, but flow becomes rapidly aerated downstream because of turbulence at the boundaries [Chanson, 1994]. Chanson [1994] found that the re-circulating vortices play a major role in dissipating energy in step-pool channels, but Wilcox and Wohl [2006] point out that the smoother water surface and submergence of steps will dramatically decrease flow resistance in comparison with nappe flows. Comiti et al. [2009] concluded that the flow regime must be specified in any attempt to predict total resistance in step-pool channels. Once skimming flow occurs, spill resistance disappears and grain resistance becomes increasingly significant. Skimming flow did not occur over the majority of the steps at the measured high flow during the study summarized here, therefore it is not considered in detail.

Despite the large contribution of ff_{spill} in high gradient streams, the average Froude number (Fr) is consistently measured as subcritical in steep streams, even at bank-filling and flood flows [Jarrett, 1984; Wilcox and Wohl, 2007; Magirl et al., 2009]. Skimming flow is rarely observed in step-pool systems [Comiti et al., 2009]. Grant [1997] hypothesized that the tendency for the flow to accelerate in high gradient streams is counterbalanced by the bedforms, which offset this tendency by dissipating energy. Regardless of local increases in velocities, the drag around boulders, bedforms, and wood maintains a subcritical range across most of a high gradient mountain stream.

Form resistance (ff_{step}) around steps and pools is the form drag created by the adverse pressure gradients around the bedform of the step. Both Wohl and Ikeda [1998] and Canovaro et al. [2007] found that transverse ribs dissipate energy much more effectively than longitudinal ribs. There are three components to a step-pool reach where

velocity and hence form drag and skin friction fluctuate: the step tread, step lip and pool. A fourth component are small runs, or cascading sections, between the steps. The downstream pool has high velocity fluctuations because of a mid-profile shear layer that develops from wake turbulence, creating adverse pressure gradients [Wohl and Thompson, 2000]. Backwater effects and increased turbulence create adverse pressure gradients on step treads as well [Wohl and Thompson, 2000]. Higher velocity over step lips and in runs dampens turbulence, creating favorable pressure gradients and allowing velocity profiles to be dominated by bed-generated turbulence. These results were similar to Wilcox and Wohl [2007], who also found increased turbulence at the base of steps, in pools, and in cascading sections and relatively low turbulence on runs upstream of steps and near step lips. Wilcox and Wohl [2007] established that there is a significant three-dimensional contribution to velocity from vertical and cross-stream components, which increased turbulence in the reach. The adverse pressure gradients mean that form drag dominates on step treads and in pools, whereas skin friction will dominate over the step lip and in longer step treads where runs develop. Larger clasts on the step treads and runs increase turbulence, causing an increase in form drag [Wohl and Thompson, 2000]. Hence, the larger grain size on step treads may increase the contribution of ff_{grain} to total resistance in step-pool reaches, but the adverse pressure gradients in the step treads and pools will lead to an increase in ff_{step} .

Step spacing may also play a role in the effectiveness of ff_{step} and ff_{spill} to dissipate energy. More closely spaced steps significantly increased ff_{total} in a flume study done by Wilcox and Wohl [2006]. They hypothesized that this increase was due solely to an increase in ff_{spill} with a decrease in step spacing. Velocity increases much faster with

discharge than either width or depth [*Rhodes, 1977; Lee and Ferguson, 2002*] as the flow regime changes with submergence of the larger roughness elements. Step-pool streams tend to maximize flow resistance with a spacing of 9 or 10 for the step length (L_s) to step height (H_s) ratio [*Wohl and Ikeda, 1998; Canovaro and Solari, 2006; Canovaro et al., 2007*]. If elements are more closely spaced, then the wake of one element interferes with another, reducing the dissipative abilities of that element.

Wood resistance in step-pool channels is related to the effect of individual pieces (ff_{wood}) and to wood as part of the step form (ff_{step}) [*Curran and Wohl, 2003*]. Parameters such as spatial density of wood, orientation, length, and position significantly affect the drag coefficient [*Young, 1991; Gippel et al., 1992; Wallerstein et al., 2002*] and the contribution of wood to total resistance, which is also influenced by discharge [*Wilcox and Wohl, 2006*]. In-channel wood can change the flow hydraulics, creating localized areas of scour and deposition. Steps that include wood are higher, with larger pools and lower gradient reaches upstream of the step [*McFarlane and Wohl, 2003*]. *Curran and Wohl* [2003] found that steps with wood have a much larger influence on flow resistance than boulder steps, and hypothesized that this was because of an increase in ff_{spill} . *Gippel et al.* [1992] and *Young* [1991] both established that wood orientation, blockage effect, spacing and density all had a significant effect on the drag coefficient. Both also found that the length to diameter ratio and the position above the bed was not significant. On the other hand, *Wallerstein et al.* [2002] determined that wood near the water surface had higher drag coefficients because of the effects on surface wave formation. *Wilcox and Wohl* [2006] also found that ff_{total} will increase with wood density to a point. The amount that wood resistance contributes to total resistance is mediated by discharge. *Wilcox and*

Wohl [2006] showed that higher discharges caused the varying effects of each type of roughness to be reduced. Once density is sufficiently high, the wake interference between pieces of wood will reduce the drag force on each piece, similar to closely spaced boulders [Canovaro *et al.*, 2007].

Wood position and arrangement have a large effect on the influence of wood on total resistance [Wilcox and Wohl, 2006]. Wilcox and Wohl [2006] demonstrated that wood along step lips caused values of ff_{total} to be nearly double compared to when wood was placed on the step treads. Additionally, wood near step lips dammed the flow upstream, causing a larger backwater effect by substantially decreasing the velocity. Wood also interacted with slope, so that there is a decreasing effect of wood density on ff_{total} as slope decreases.

In quantifying grain resistance, most studies use some form of the Keulegan [1938] equation:

$$ff_{grain} = \left[2.03 \log \left(\frac{12.2 \cdot R_h}{k_s} \right) \right]^{-2} \quad (6.3)$$

where k_s = a multiple of a characteristic grain diameter. The values for k_s are typically some multiple of D_{50} , D_{84} or D_{90} [e.g., Parker and Peterson, 1980; Griffiths, 1989; Millar, 1999]. Bray [1982] found no significant difference between using D_{50} , D_{84} , and D_{90} as the characteristic grain diameter. Millar [1999] showed that values of C_{50} (from $k_s = C_{50}D_{50}$) could range between 0.4 and 55.7. Although Wiberg and Smith [1991] showed that the values of k_s and C_{50} increased as the bed became more poorly sorted, no such relationship was found by Millar [1999]. Grain resistance is most often defined as the viscous friction around grains, but in high gradient channels, where boulders are on

the same order of magnitude as flow depth, the grains can contribute significantly to form drag and spill resistance [Zimmerman, 2010]. Grain resistance is defined here as the combined flow resistance (i.e., form drag, skin friction, spill resistance) that results from the presence of the grains in the flow.

In boulder-dominated step-pool reaches, the grain resistance has been found to contribute as much as 20 to 40% of the total flow resistance. On the other hand, in streams with significant amounts of wood, grain resistance was found to be about 10% of total resistance [Curran and Wohl, 2003]. Wilcox and Wohl [2006] found that discharge had the greatest effect on the individual components of resistance, as well as the interaction between components. They determined that grain resistance was minor in comparison to other types of resistance and the effect of grain resistance decreased with discharge.

Baiamonte and Ferro [1997] suggest that total resistance is a function of Fr , the Reynolds number (Re), concentration of coarser elements (Γ), Shields [1936] parameter (τ^*), and measures of longitudinal and transverse distance between roughness elements. The concentration of coarser elements is found using:

$$\Gamma = \frac{N_B \pi D_B^2}{4WL} \quad (6.4)$$

where, N_B = number of boulders on the chute placed over the entire surface of the chute; D_B = median size of boulders. Analogous to step spacing, spatial density of boulders maximizes flow resistance at a concentration between 0.15 and 0.40 [Rouse, 1965; Canovaro et al., 2007] and can be the main factor affecting flow resistance [Pagliara and Chiavaccini, 2006]. Bathurst [1982a] and Judd and Peterson [1969] both suggested

that the ff_{total} is a function of the roughness concentration of the bed elements in boulder-bed streams, which was calculated using the equation:

$$\Lambda = \frac{\sum_1^n A_F}{A_{bed}} \quad (6.5)$$

where, A_F = frontal cross-sectional area of an element; A_{bed} = planimetric bed area; n = number of roughness elements. Once roughness elements are of the same order of magnitude as the flow depth, the flow resistance is dominated by wall effects and can be determined by the combined form drag of each of the roughness elements [Bathurst, 1982a]. Pagliara and Chiavaccini [2006] established that Γ was the main factor affecting flow resistance. The boulders have to be a sufficient distance from each other for the wake from one element not to interfere with the wake from the next element. As long as that holds true, the total drag force is the sum of the individual values. When wakes interact together, then the dissipation from that object decreases. According to Pagliara and Chiavaccini [2006] and Lawrence [2000], a concentration under 50% means that the boulders are sufficiently spaced. Random arrangements of boulders have been shown to produce much smaller increases in ff_{total} than boulders found in rows transverse to the flow direction [Pagliara and Chiavaccini, 2006]. Baiamonte and Ferro [1997] showed dependence between flow resistance and the boulder concentration.

As noted above in the discussion on steps, the relationship between Fr and drag around an object is complex, depending on the relative submergence of the object. Fr is related to the drag coefficient. Fr , combined with the size and spacing of the roughness elements, influences the relative contribution of the free surface drag. Peak drag occurs when Fr is between 0.5 and 0.6 and the relative submergence is greater than 0.8

[Bathurst, 1982a]. The relationship between Fr and total drag on the bed means that the boulder concentration is needed to represent flow resistance from bed elements [Bathurst, 1982a]. ff_{total} is inversely related to Fr [Ferro, 2003].

The Reynolds number (Re) is significantly related to the drag force applied to large bed elements. Bathurst [1982a] demonstrated that in boulder-bed streams a fully turbulent boundary layer may only be attained at $Re > 2 \times 10^5$ and Lawrence [1997] found that the effects of Re are negligible above 10^4 . For flows in the transitional region ($3 \times 10^4 < Re < 2 \times 10^5$), the flow resistance is a function of both the element shape and the structure of the flow. The more concentrated the elements and the rougher the surface, the lower the critical number [Bathurst, 1982a]. Above the critical Re number, an increase in Re will cause a decrease in flow resistance as the drag coefficient decreases.

Understanding the contributions of different sources of roughness in steep streams will improve our ability to calculate ff_{total} in these channels, which is essential for the prediction of velocity and discharge. Velocity and discharge predictions are in turn used by engineers and managers for fish-habitat assessments, stream rehabilitation projects, flood estimation and sediment routing models [Bathurst, 2002; Ferguson, 2007]. Despite some success in using dimensionless hydraulic geometry equations to predict velocity and discharge in high gradient streams [Zimmerman, 2010], we need to improve our understanding of how individual components affect the flow. Consequently, the following analysis focuses on the most commonly used methods for partitioning flow resistance. The primary objectives of this chapter are to:

- 1) Evaluate methods for calculating ff_{grain} , ff_{wood} , and ff_{step} using a dataset from 15 steep stream reaches with step-pool, cascade, and plane-bed morphology.
- 2) Identify limitations in the existing methods of calculating total and component resistance when these methods are applied to steep streams.
- 3) Analyze interrelationships among component resistance and other independent variables such as stage and discharge.

The analyses presented here ignore bank roughness and associated resistance. Although this may be an important source of resistance in steep streams, these analyses follow the precedent of earlier papers in focusing on bed configuration.

6.3 Methods

6.3.1 Field Methods

Fifteen channel reaches on ESL and FC were selected based on visual assessment of morphology; 9 step-pool, 5 cascade, and 1 plane-bed reach. Upper and lower boundaries of each reach were chosen to ensure consistent morphology and gradient within the reach. Reaches are labeled in order from downstream to upstream on each basin (Figure 1). The measurements made in the field and used for calculation are described in detail in CHAPTER 3.

The step-forming material of boulders or wood was identified for each step in the step-pool reaches: a boulder grouping indicates only boulders; Wood1 indicates wood surrounding a keystone boulder; Wood2 indicates only wood with no evident keystone boulder (Figure 25). The majority of wood was found in the steps in almost every reach, except for four of the cascade reaches (ESL3, ESL7, FC5, FC6) and the plane-bed reach

(ESL6). Individual pieces made up a small amount of the wood found in each reach. As the stage went down, many of these logs were no longer within the flow, further reducing the contribution of ff_{wood} to ff_{total} .

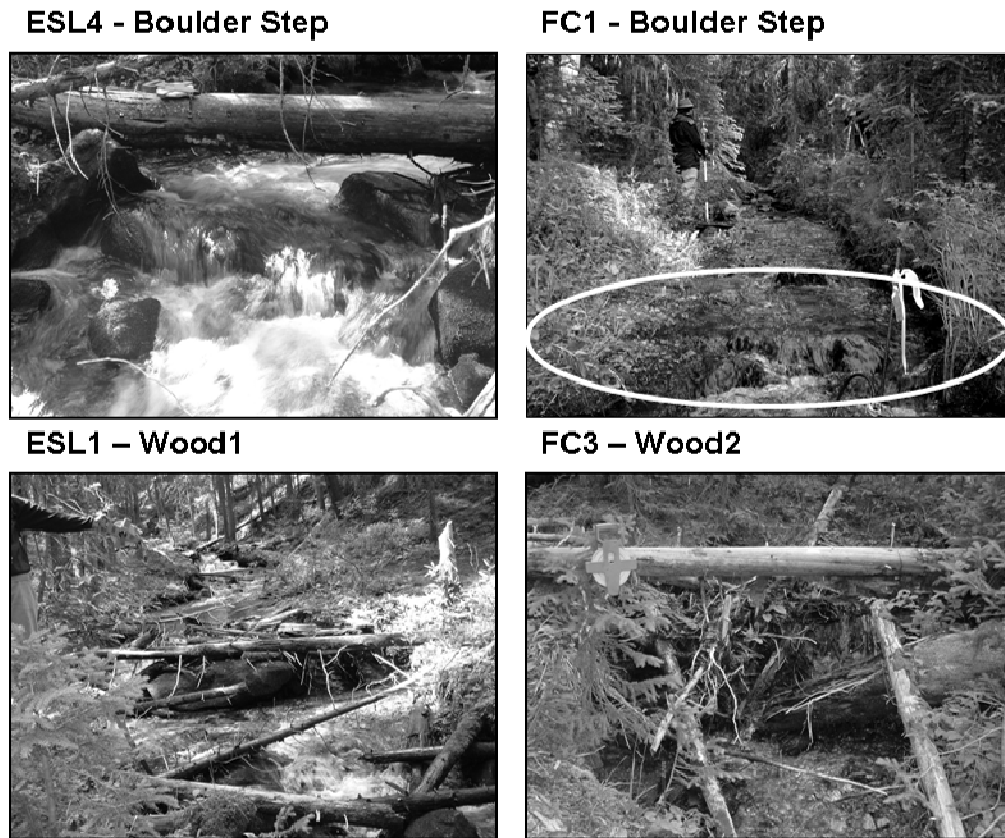


Figure 25: Example of large and small boulder steps in ESL4 and FC1. Example of what is characterized as a Wood1 step in ESL1 and a Wood2 step in FC3.

Cascade reaches were selected based on visual assessment of tumbling flows over irregularly spaced clasts, with no regular sequences of steps and pools. Each cascade reach, except for ESL7, has one or two steps included within the reach. Although there are individual steps and pools, the sequence was not regular enough to categorize the reach as a step-pool. Also, pools were small and under-developed in the majority of the cases. ESL3 has the largest difference from the other cascade reaches because of the large boulder deposit or bar in the middle of the reach. During high flow periods, the

flow is nearly split in half around the boulder bar. At lower flows, the flow is concentrated towards the left bank and on the left side of the boulder bar. ESL8 also has an area where the surface area increases because of flow diverted around wood. Again, at lower flows the majority of the flow remains in the main channel and the diversion contains water moving at very low velocities. FC5 and FC6 are high in the drainage basin and have a smaller wetted width and depth than any of the other reaches.

Wood length and diameter were measured for each flow period using a combination of the LiDAR scans, a tin created of the water surface in Cyclone 5.8.1, and photographs. The wood volume was calculated from these measurements and divided by the plan area of the reach ($L_r * w$). The wood volume includes pieces of wood found as single unattached pieces in the reach as well as in the steps. ESL2 and FC3 have the largest wood load of any of the reaches.

6.3.2 Partitioning Methods

Einstein and Barbarossa [1952] introduced the concept of dividing shear stress into the two components of shear applied to grains in channels without bedforms (τ_0') and shear applied to bedforms (τ_0''):

$$\tau_0 = \tau_0' + \tau_0'' \quad (6.6)$$

where τ_0 = total boundary shear stress. The Darcy-Weisbach friction factor can then be related to the above equation by:

$$ff = 8 \left(\frac{\sqrt{\tau_0 / \rho}}{v} \right)^2 \quad (6.7)$$

where, v = mean flow velocity; ρ = density of water. Each component of shear stress (Equation 6.6) can be substituted into Equation 6.7 to yield the component value of ff . The values of the component friction factor are then substituted back into Equation 6.2. The shear stress applied to each object can be determined by considering the drag force applied to grains, wood or steps in the channel. The total drag force includes both viscous and form effects:

$$F_D = C_D \rho \frac{v^2}{2} A_F \quad (6.8)$$

where, F_D = drag force; C_D = coefficient of drag; A_F = frontal area of object in flow. The shear applied to that object is then found by dividing the drag force by the area the force is applied over:

$$\tau_0 = \frac{F_D}{A_{Channel}} \quad (6.9)$$

where, $A_{channel}$ = surface area force applied over.

$$ff_D = \frac{8\tau_0}{\rho \bar{v}^2} = \frac{4C_D A_F}{W * L} \quad (6.10)$$

where W = width, L = length that force is applied over.

The total friction factor (ff_{total}) is calculated using Equation 6.1 and substituting water surface slope (S_w) for friction slope (S_f). The water surface slope was calculated using the slope of the regression line of the longitudinal survey of the thalweg. The error associated with the method used to calculate the water surface slope is investigated in Section 6.4.4. The following sections review different equations developed for quantifying the resistance created by three specific types of boundary roughness; grain, wood, and form.

6.3.3 Grain Resistance

Of several methods for predicting the portion of resistance related to grains, the most commonly used is the *Millar and Quick* [1994] adaptation of the *Keulegan* [1938] equation, which uses D_{50} as the characteristic grain size:

$$ff_{grain} = 8 * \left[2.5 \ln \left(\frac{12.2 \cdot R_h}{D_{50}} \right) \right]^{-2} \quad (6.11)$$

This equation provides a lower bound for grain resistance [Millar, 1999]. Variants on Equation 6.11 include those developed by *Parker and Peterson* [1980],

$$ff_{grain} = 8 * \left[2.5 \ln \left(\frac{11 R_h}{2 D_{90}} \right) \right]^{-2} \quad (6.12)$$

and a power law relation by *Bathurst* [2002],

$$ff_{grain} = 8 * \left[3.1 \left(\frac{R_h}{D_{84}} \right)^{0.93} \right]^{-2} \quad (6.13)$$

For this dataset, the average D_{50} , as well as the step tread D_{50} , were used to analyze the effect of grain resistance and to evaluate sensitivity of the results to sampling location.

Because the steps are assumed to create their own form of resistance, the step D_{50} was not used to calculate ff_{grain} .

Additive partitioning can only be used if boulders are sufficiently far apart that the wake of one boulder does not interfere with the next boulder [Ferro, 2003]. When depth is on the same order of magnitude as the bed material height ($R/D_{84} < 4$), flow resistance has to be determined from drag forces on boulders rather than from the boundary layer theory [Bathurst, 1993]. Therefore, the drag force approach, described above, was used for individual boulders. Significant clasts were identified as those above

the water surface at low flows, which were thus included in the LiDAR scans. If the boulders were too closely spaced (length to height ratio < 9.0 [Wohl and Ikeda, 1998]), so that wake interference occurred between boulders, the width and representative height of clusters of boulders were used in place of individual boulders. Although the drag coefficient may be closer to 0.9 [Nelson *et al.*, 1993] in streams with large relative roughness, a drag coefficient of 0.4 was used for each boulder as well as clusters of boulders based on the classic Reynolds number drag relationship that represents a sphere in a free stream [Wiberg and Smith, 1991; Lawrence, 2000]. The Reynolds number remained between 10^4 and 10^5 for all flow periods in all streams except for FC3, FC5, and FC6 at low flow. Because the Reynolds number indicates fully turbulent flows in all reaches except the three Fool Creek reaches, the same drag coefficient is used at both low and high flows. FC3, FC5, and FC6 are given a value of 0.6 for the drag coefficient based on the Reynolds number at low flows. The length is the length (L) between boulders, and the width (W) is the wetted width of the cross-section where the boulders were located (Equation 6.10). The frontal area for a fully submerged hemispherical particle is $A_F = 1/2\pi k^2$, where k is the radius of the particle. The frontal area of a partially submerged particle is $A_F = 2kh$, where h is flow depth [Lawrence, 1997]. At low flow the wake effect between particles was not considered to be as large, therefore a value of ff_{grain} based on the drag force approach was calculated for each individual particle rather than for clusters of clasts. This method was used as a means of comparing the additive partitioning of the drag force for individual large bed elements against the other methods of calculating ff_{grain} .

Grain resistance is commonly calculated using a form of the *Keulegan* [1938] equation (Eqs. 6.11 and 6.12), which is based on the assumption that velocity varies with depth in a logarithmic fashion [Wiberg and Smith, 1991; Bathurst, 2002]. The *Bathurst* [2002] equation (Eq. 6.13) is the only equation tested here that is based on a power law relation rather than assuming a logarithmic velocity distribution. The three equations (*Bathurst, Parker and Peterson, Keulegan*) are tested against an additive drag force approach. Errors associated with the calculation of grain resistance involve accurately measuring the hydraulic radius and the grain size. Pebble counts were used to calculate reach average D_{84} , D_{50} , and D_{90} as well as values for the steps, step treads, cascading sections and upstream and downstream pools. Because the objective is to separate grain resistance from ff_{step} , I assume that the grains on the step treads have the greatest influence on grain resistance and best characterize the ff_{grain} in the step-pool reaches. The step grain size may be appropriate for predicting total resistance in a step-pool channel [Lee and Ferguson, 2002], but here the step-forming grains are considered part of ff_{step} and ff_{spill} . The cascade reaches did not have step treads, therefore the D_{84} and D_{50} were split into cascade sections and pool sections. The root-mean-square-error (RMSE) was used to evaluate the goodness of fit between the predicted ff based on the different grain sizes for the reach and the step tread.

Each of the above methods was further evaluated by regressing ff_{grain} against the value of ff_{grain} from the drag approach. The total resistance (ff_{total}) was transformed using the square root to meet regression assumptions of homoscedacity [Kutner et al., 2005].

6.3.4 Wood Resistance (ff_{wood})

Here, ff_{wood} represents individual pieces of wood in the channel that are not part of steps (Figure 26). The majority of wood in step-pool reaches is found within the steps (~90%), but that wood is considered part of the step form and its contribution to ff_{total} is considered a part of ff_{step} and ff_{spill} .

The contribution of individual pieces of wood was calculated using the method outlined by *Wilcox et al.* [2006]. The major assumption is that the drag created by wood is similar to the drag measured around cylinders in a flume [*Gippel et al.*, 1992; *Shields and Gippel*, 1995; *Gippel et al.*, 1996]. The drag force around wood is

$$F_D = \frac{\rho C_D^{app} \bar{v}^2 A_w \sin \theta}{2} \quad (6.14)$$

where, C_D^{app} = apparent drag coefficient (measured for a specific set of geometric and hydraulic conditions and corrected for the blockage effect of LWD); \bar{v} = depth-averaged approach velocity; A_w = submerged cross-sectional area of the wood piece; and θ = angle of the wood piece relative to downstream flow direction. The apparent drag coefficient is then:

$$C_d^{app} = \frac{C_d}{a[1-B]^b} \quad (6.15)$$

where, C_d = drag coefficient in flow without boundary effects; a and b = empirically derived coefficient and exponent; B = blockage ratio. For values of B between 0.03 and 0.4, the values of a and b have been found to equal 1 and 2, respectively.

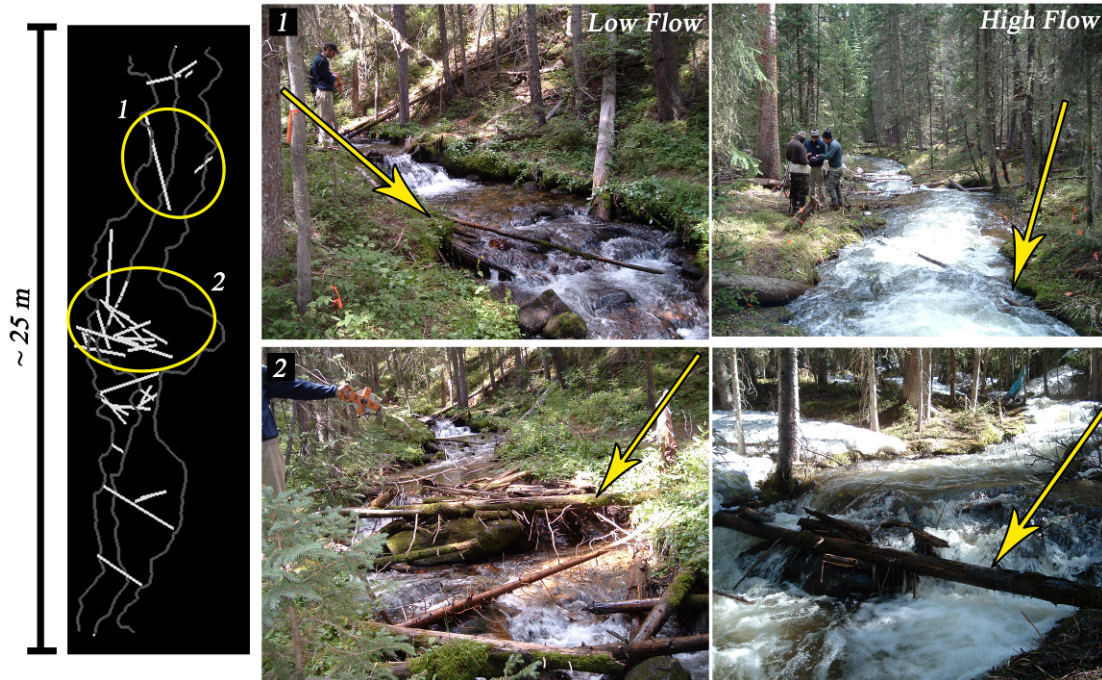


Figure 26: Example of wood as individual piece (1) and wood as part of step (2). Left is a planform view of ESL1 showing individual wood piece (1) and wood jam that is part of a step (2). All pictures are looking upstream except for the top right photo. Yellow arrows are pointing to the same location in photos going from left to right.

The blockage ratio is the ratio of the frontal area of an object to the cross-sectional area of flow and for a cylindrical piece of wood it is defined as:

$$B = \frac{L' d_{wood} \sin \theta + \pi \left(\frac{d_{wood}}{2} \right)^2 \cos \theta}{A_{flow}} \quad (6.16)$$

where, L' = is piece length; d_{wood} = submerged cylinder diameter; A_{flow} = cross-sectional area of the flow. Once the drag force is determined for an individual piece of wood, then the shear stress can be calculated using Equation (6.17):

$$\tau_{wood} = \frac{\rho C_D^{app} \bar{v}^2 d_{wood}}{2X} \quad (6.17)$$

where, X = distance between logs. Equation (6.18) can then be used to calculate the component of ff_{total} related to individual pieces of wood:

$$ff_{wood} = \frac{8\tau_{wood}}{\rho\bar{v}^2} = \frac{4C_D^{app} d_{wood}}{X} \quad (6.18)$$

This method allows the approach velocities to be cancelled out, therefore eliminating the need to measure approach velocities. The minimum and maximum values used in each reach for C_D , C_D^{app} , B , a and b and the resultant ff_{wood} are shown in Table 9. The values of B exceed the range evaluated by *Gippel et al.* [1992] in a few cases. The values of the coefficients a and b in Equation (6.15) were determined based on the range of B measured by *Gippel et al.* [1992], and were generally 0.997 and 2.06, respectively.

Table 9: Minimum and Maximum values used for each log in each reach.

Reach Name		C_D	B	a	b	C_D^{app}	ff_{wood}
ESL1	Min.	0.6	0.01	0.997	2.06	0.63	0.05
	Max.	0.9	0.38	1.02	3.25	2.43	4.43
ESL2	Min.	0.6	0.03	0.997	2.06	0.88	0.05
	Max.	0.9	0.63	0.997	2.06	4.75	2.24
ESL3	Min.	0.6	0.00	0.997	2.06	0.62	0.02
	Max.	0.9	0.14	0.997	2.06	1.24	1.49
ESL4	Min.	0.6	0.00	0.997	2.06	0.61	0.03
	Max.	0.9	0.08	0.997	2.06	1.05	0.74
ESL5	Min.	0.5	0.00	0.997	2.06	0.51	0.03
	Max.	0.9	0.26	0.997	2.06	1.69	1.17
ESL6	Min.	1.0	0.01	0.997	2.06	1.06	0.02
	Max.	1.0	0.11	0.997	2.06	1.27	0.09
ESL7	Min.	0.6	0.00	0.997	2.06	0.60	0.02
	Max.	0.9	0.46	0.997	2.06	3.25	1.74
ESL8	Min.	0.4	0.00	0.997	2.06	0.40	0.01
	Max.	0.9	0.49	0.997	2.06	3.64	1.29
ESL9	Min.	0.9	0.00	0.997	2.06	0.90	0.22
	Max.	0.9	0.38	0.997	2.06	2.42	0.91
FC1	Min.	0.8	0.27	0.997	2.06	1.51	0.37
	Max.	0.8	0.27	0.997	2.06	1.51	0.37
FC2	Min.	0.2	0.01	0.997	2.06	0.20	0.01
	Max.	0.6	0.18	0.997	2.06	0.91	1.14
FC3	Min.	0.6	0.01	0.997	2.06	0.63	0.07
	Max.	0.9	0.07	0.997	2.06	1.04	0.48
FC4	Min.	0.3	0.01	0.997	2.06	0.31	0.09
	Max.	0.9	0.18	0.997	2.06	1.36	0.50
FC5	Min.	0.9	0.05	0.99	2.06	1.01	0.03
	Max.	0.9	0.11	0.997	2.80	1.28	0.14
FC6	Min.	0.9	0.03	0.997	2.06	0.95	0.04
	Max.	0.9	0.18	0.997	2.06	1.34	1.13

6.3.5 Form Resistance (ff_{step})

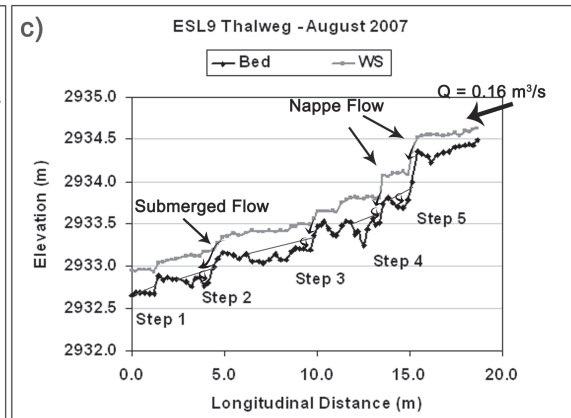
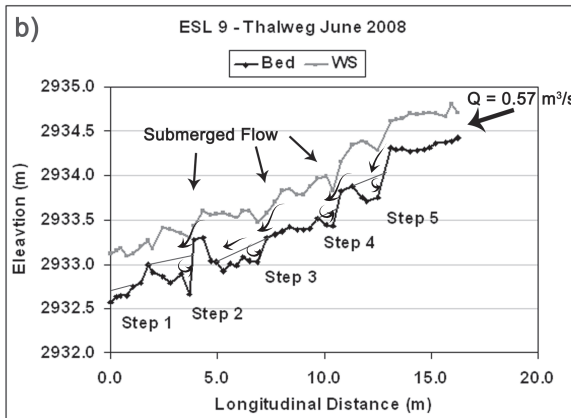
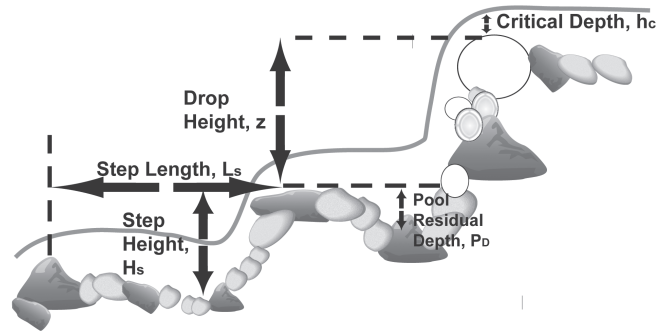
Because the main bedforms in the steep stream reaches examined here are steps and pools, the form resistance is denoted as ff_{step} rather than ff_{form} . Other sources of form resistance are considered separately as ff_{wood} and ff_{spill} . Form resistance related to banks, bends, and sinuosity is important, but is not calculated here since the primary focus is the contribution from bed roughness towards total flow resistance. Other components of resistance are folded into spill resistance (ff_{spill}).

Much of the energy loss associated with steps and pools is related to the flow acceleration and deceleration as water spills over the step lip into the pool (Figure 27). During nappe flow, the majority of the energy loss is from flow re-circulation in the pool. If the drop is not shear, a hydraulic jump dissipates the energy. As a step becomes submerged during higher flows, the step shape itself may also create losses from form resistance. The step submergence can be evaluated using the ratio of critical depth (h_c) to drop height (z). *Comiti et al.* [2009] found a transition in the significance of grain resistance versus spill resistance at a value of h_c/z of 1.2. Consequently, I hypothesize that steps with a value of $h_c/z > 1.2$ should also have a form resistance component (ff_{step}) related to the step shape. I evaluated step submergence based on longitudinal profiles and photographs. The portion of ff related to steps can be calculated using a methodology similar to calculating drag around in-channel wood:

$$ff_{step} = \frac{4C_D A_{step}}{A_{channel}} \quad (6.19)$$

where, C_D = drag coefficient of steps; A_{step} = frontal area of step; $A_{channel}$ = surface area of step. The frontal area of the step was the product of the upstream pool depth (P_D) and width (P_w). A schematic of a step-pool channel is shown in Figure 27.

a) Idealized schematic of a step-pool reach



June 2008



July 2008



August 2007

Figure 27: Schematic of a wood and boulder step-pool reach.

Drag coefficients of steps were estimated based on the step composition; i.e., boulder, wood1 or wood2. Values were based on results from flumes [Gippel *et al.*, 1992; Hygelund and Manga, 2003] for individual cylinders (between 0.4 to 4.5) and results for a wood jam (between 2.6 to 9.0) [Manners *et al.*, 2007]. Because drag

coefficients increase with dimensionless wood surface area [Manners et al., 2007], initial values for the drag coefficient were assigned based on values of wood surface area/channel surface area (Figure 28). Boulder steps were given an initial value of 1.0 for C_D ; wood1 and wood2 steps were given initial values between 2.8 and 1.4. A limitation of this method is the lack of measured drag coefficients around wood and boulder steps. Because the drag coefficients were unknown, a sensitivity analysis was performed. The initial value of C_D was assigned for each step as described above, and then each drag coefficient was increased by 0.2 in five increments to calculate six different values of ff_{step} , starting with a conservative estimate for the drag coefficients. The value of ff_{step} was calculated for each individual step that is submerged according to the value of h_c/z using the drag force approach described above (Equation 6.6 – 6.10) and then summed to give the total value of ff_{step} for each reach. The cascade reaches typically included one or two steps within the reach, but only a few of these steps were sufficiently submerged to have values for ff_{step} as well.

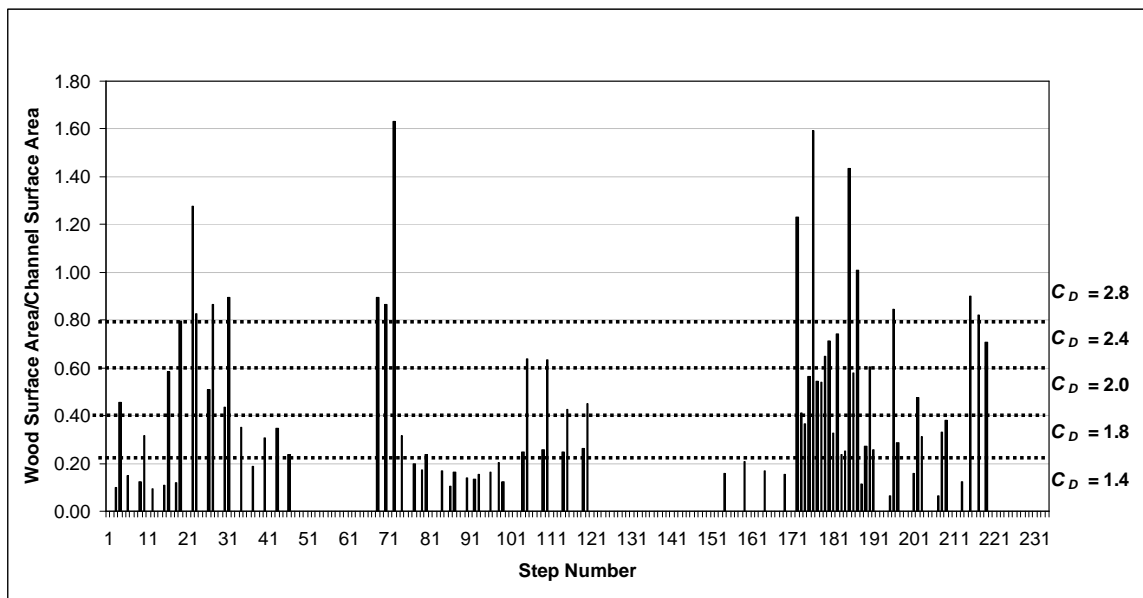


Figure 28: Dimensionless surface area for each step showing divisions of the drag coefficient for steps.

6.4 Results

6.4.1 Grain Resistance, ff_{grain}

The variety and distribution of grain sizes can have a large effect on grain resistance, particularly in step-pool reaches, depending on where grains are measured within a reach. The step-pool reaches tend to have much larger variability in grain size than the cascade reaches (Figure 29), probably because of the larger range in gradient and morphology. The variability in D_{50} between sections of a reach was much larger than the variability in D_{84} , indicating that D_{84} may better represent average grains protruding above the bed for the entire reach. The grain size in the downstream pools and on the steps varied the most from the reach D_{84} (Figure 29). The variety and distribution of grain sizes can have a large effect on the value of the grain resistance, particularly in the step-pool reaches, depending on what portion of the reach grains were measured. The downstream pools are commonly assumed to have the smallest grains, but the pools just downstream of a plunging step often contained some large boulders in the middle. Figure 30 shows a sensitivity analysis of each of the three grain resistance equations using D_{50} , D_{84} , and D_{90} for the characteristic grain size.

Because in this case the objective is to separate the grain resistance from ff_{step} , I assume that the grains on the step treads have the biggest influence on grain resistance and best characterize the ff_{grain} in the step-pool reaches. The values of ff_{grain} using a reach grain size are compared against the values using a characteristic grain size for the step tread. The cascade reaches did not have step treads, therefore the D_{84} and D_{50} were split up into cascade sections and pool sections, where necessary. The values for FC5 and FC6 could not be split up this way because the smaller channel size made cross-section

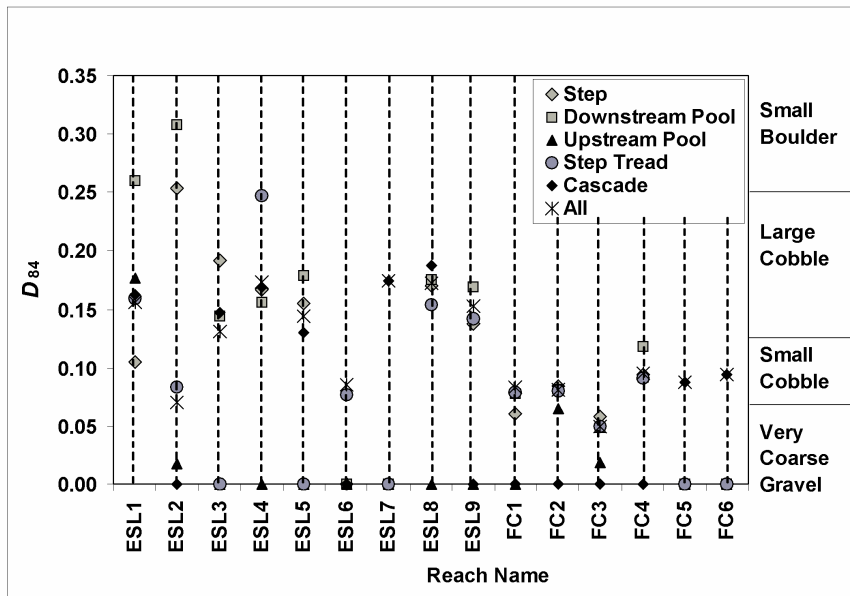
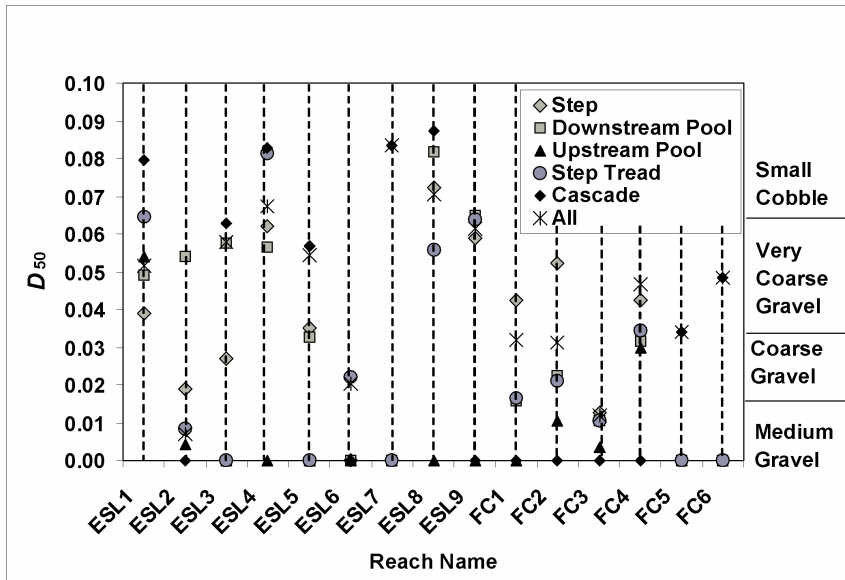


Figure 29: Separated D_{50} and D_{84} for each reach, illustrating the range in values, depending on the portion of the bed measured. Step D_{84} RMSE = 0.061; Downstream Pool D_{84} RMSE = 0.079; Upstream Pool D_{84} RMSE = 0.045; Step Tread D_{84} RMSE = 0.025. Step D_{50} RMSE = 0.014; Downstream Pool D_{50} RMSE = 0.018; Upstream Pool D_{50} RMSE = 0.018; Step Tread D_{50} RMSE = 0.010

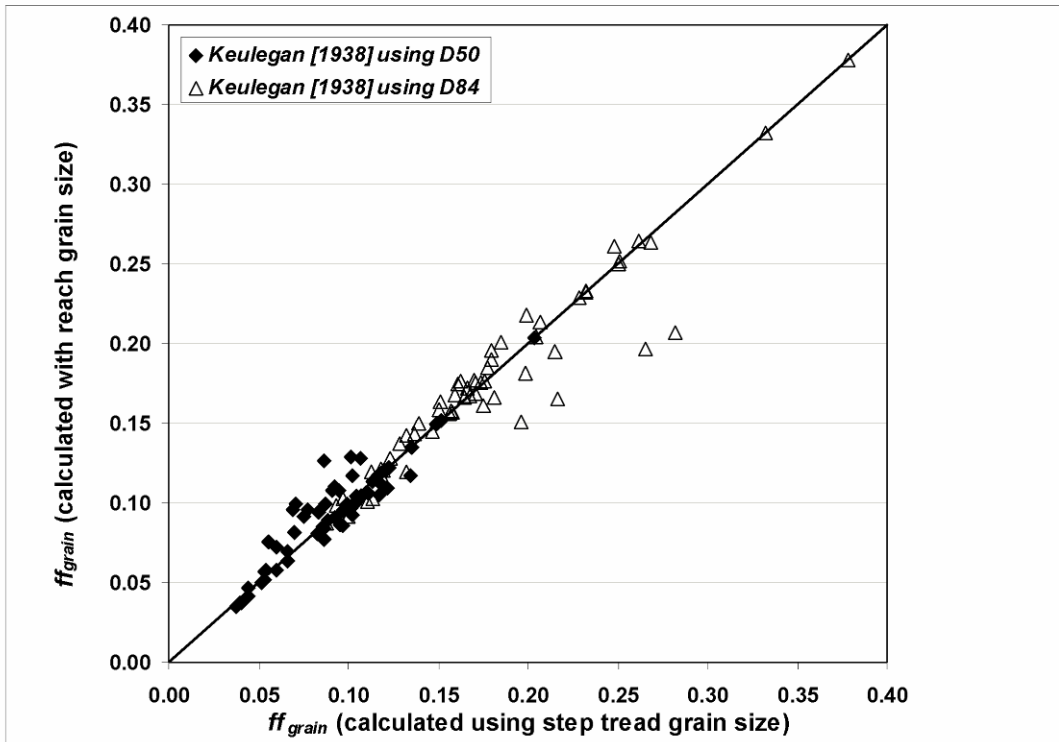
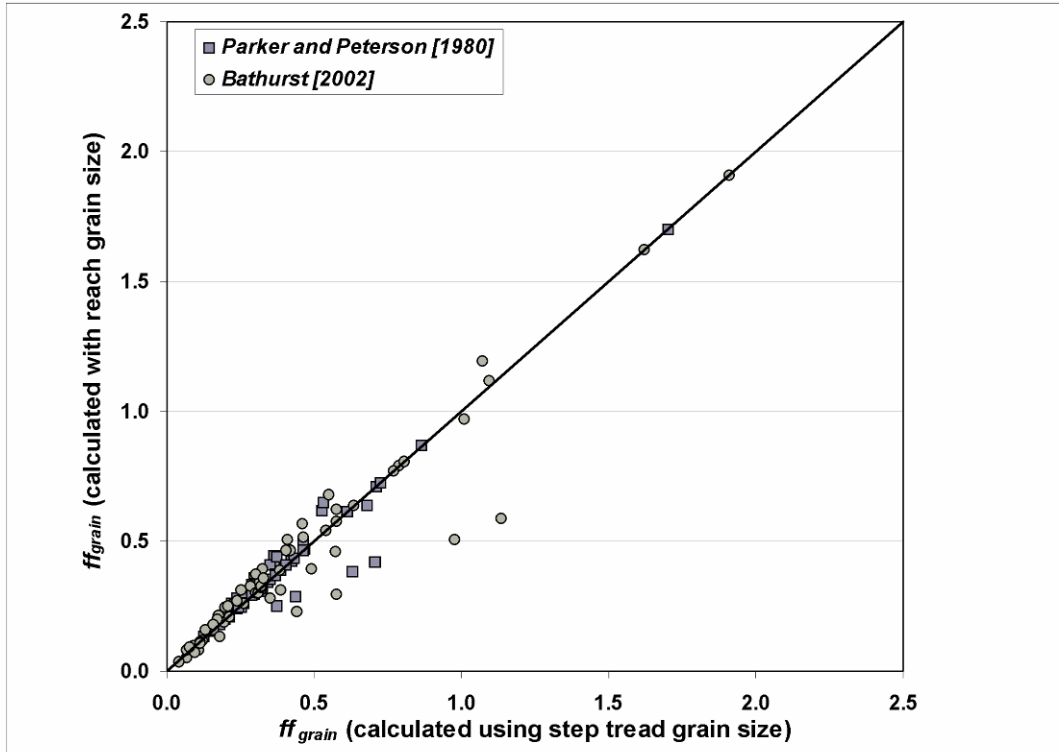


Figure 30: Sensitivity analysis using reach D_{50} and D_{84} vs. step tread D_{50} and D_{84} . Keulegan (D_{50}) RMSE = 0.012; Keulegan (D_{84}) RMSE = 0.018; Parker and Peterson (D_{84}) RMSE = 0.06; Bathurst (D_{84}) RMSE = 0.115. ESL4 is the largest source of error in each equation.

surveys impractical. The root-mean-square-error (RMSE) was used to evaluate the goodness of fit. The *Parker and Peterson* [1980] equation varies the least (RMSE = 0.06), whereas the *Bathurst* [2002] equation varies the most (RMSE = 0.115) (Figure 30). Results from the *Keulegan* [1938] equation using both D_{50} and D_{84} are fairly similar (RMSE = 0.012 and 0.018, respectively).

Figure 31 illustrates the percent contribution of ff_{grain} to ff_{total} for each equation at low and high flows. The June 2008 mean value for ff_{grain} calculated with any of the equations and using either the step tread or reach average grain size was always significantly less than the August 2007 mean value of ff_{grain} (Figure 32). Therefore, in the following analysis, comparisons focus on differences between June 2008 and August 2007 flows. ff_{grain} calculated from the *Keulegan* equation contributes the smallest amount towards ff_{total} at both low and high flows, indicating that it gives a lower bound of grain resistance. The percent contribution of ff_{grain} is largest when calculated using the *Parker and Peterson* equation at high flows and the *Bathurst* equation at low flows. These equations are similar, since each uses a larger representative grain size and calculates an average value of ff_{grain} . The *Keulegan* equation calculates slightly larger values of ff_{grain} based on D_{84} instead of D_{50} (Figure 30), but not as large as the *Parker and Peterson* or *Bathurst* relations.

ff_{grain} calculated with the *Parker and Peterson* equation occasionally contributes up to 100% of total resistance at high flows in the plane-bed reach (ESL6; Figure 31). Since the ff_{wood} also increases at high flow in this reach and contributes to ff_{total} , the *Parker and Peterson* equation is likely inflating the value of ff_{grain} . Therefore, the *Parker and Peterson* equation may be an overestimate of ff_{grain} at high flows.

As grains become submerged, it is expected that the contribution of ff_{grain} to total resistance will decrease. Although the values of ff_{grain} do increase at lower flows (Figure 32), the contribution of ff_{grain} to ff_{total} is much smaller at low flows for each of the three equations except for the drag force approach (Figure 31). The means vary between 0.11 and 0.08 from low to high, respectively, for the *Keulegan* equation and from 0.58 to 0.24 for the *Parker and Peterson* equation. In no case do the values ff_{grain} go above 2.0 when using any of the three equations, despite drastic increases in ff_{total} up to 42.0 during low flows. Therefore, many of these equations may be underestimating ff_{grain} at all flows, but more specifically at low flows.

Figure 31 also displays the results of the additive drag approach for individual boulders. The percent contribution of ff_{grain} to ff_{total} is much larger when ff_{grain} is calculated in this manner for both the June 2008 flows and the August 2007 flows. ESL7 has a percent of ff_{total} greater than 100 for the drag approach, indicating that this value is unrealistic. The high values in ESL7, ESL8 and ESL9 reveal problems with using the drag approach during lower flows. Each of these three reaches has the largest number of boulders (23 to 28) compared to other reaches that only had 5 or 6. The additive approach causes the significance of ff_{grain} to be inflated because of the number of boulders. Both ESL8 and ESL9 are step-pool reaches that will have a large contribution from ff_{step} , ff_{wood} , and ff_{banks} . Therefore, the percent contribution of ff_{grain} is too high for these reaches once other sources of resistance are considered from field observations and the analysis below. Alternatively, the high values of ff_{grain} calculated around individual grains that are not step-forming grains reveal that ff_{grain} may be greatly underestimated in these reaches by using one of the *Keulegan*, *Bathurst*, or *Parker and Peterson* equations.

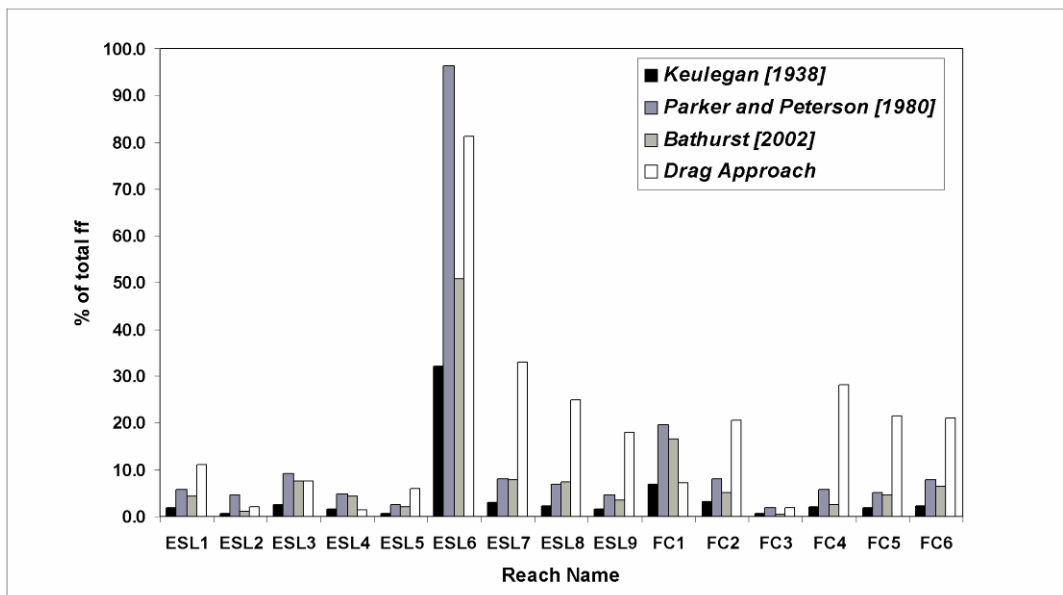
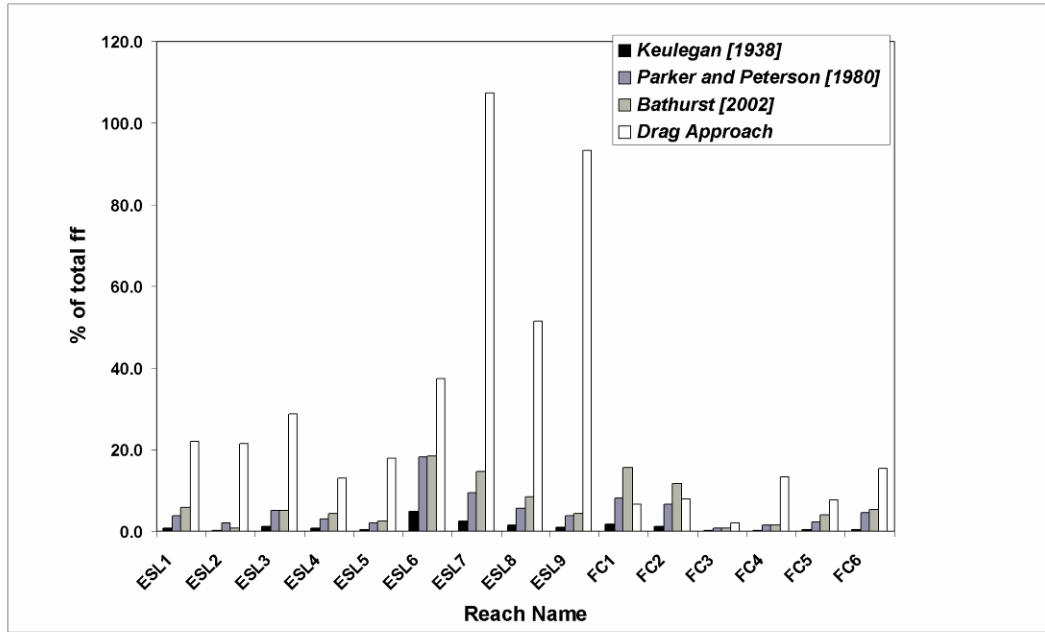


Figure 31: Percent contribution of each grain resistance equation of total resistance. Top shows August 2007 (low) flows and bottom shows June 2008 (high) flows.

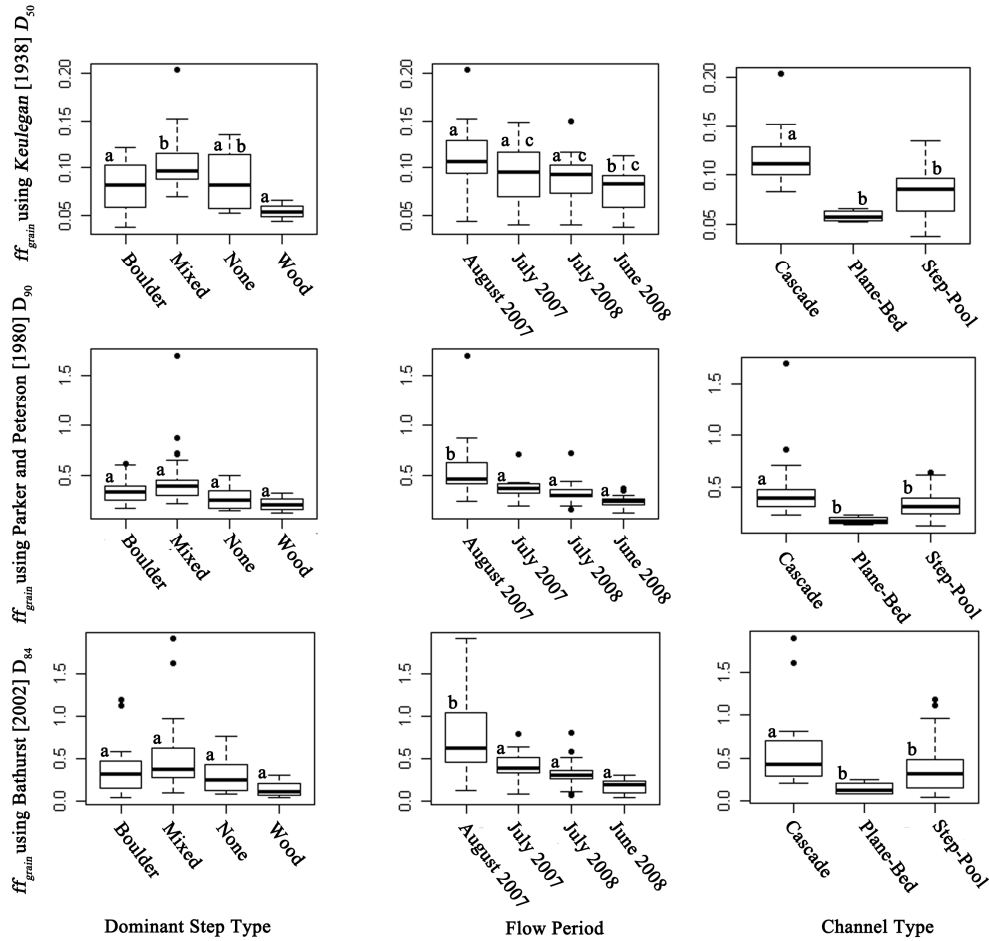


Figure 32: Boxplot of grain resistance equations against step type, flow period and channel type. Step categories: Boulder = reaches with only boulder steps, Mixed = reaches with both wood and boulder steps, None = reaches with no steps (only ESL6 and ESL7), Wood = reaches with only wood steps. Lower case letters, a, b, and c show which means are significantly different from each other based on Tukey HSD test in an ANOVA.

Each of the above methods was further evaluated by regressing ff_{grain} against ff_{total} and the value of ff_{grain} from the drag approach (Table 10 and Table 11). The total resistance was transformed using the square root to meet normality assumptions. The *Parker and Peterson* and *Keulegan* equations using D_{90} and step tread D_{50} , respectively, explained the most variability in the data set. All iterations except two showed a significant difference in ff_{grain} between June 2008 and August 2007 flows. Although a regression analysis reveals which equation explains a larger percentage of the variability in ff_{total} , it does not necessarily reveal which equation best calculates ff_{grain} .

Each method was evaluated against the drag approach, assuming that the drag approach can show precise trends in the data without the values necessarily being accurate. The trends may be more precise with the drag approach because every large bed element above the surface during the August 2007 flows was accounted for.

Table 10: Regression for ff_{total} vs. ff_{grain} . Regressed against $\sqrt{ff_{total}}$ to meet normality assumptions (df = 53). FC3 July 2008 was an outlier and removed from regression. Additionally FC3 August 2007 and FC6 August 2007 were found to be outliers for Parker and Peterson equation and removed from those regressions. Parker and Peterson = 51 df. $\alpha = 0.05$ **; $\alpha = 0.10$ *

	Keulegan (D_{50})	Keulegan (tread D_{50})	Keulegan (D_{84})	Keulegan (tread D_{84})	Parker and Peterson (D_{90})	Parker and Peterson (tread D_{90})	Bathurst (D_{84})	Bathurst (tread D_{84})
Intercept	1.92**	1.69**	1.24*	1.88**	0.94*	1.66**	2.49**	2.59**
ff_{grain}	16.25**	18.80**	11.25**	9.35**	5.28**	3.92**	1.65**	1.50**
August 2007	0.00	0.00	0.00	0.00	0.00	0.00	0.00	0.00
July 2007	-0.63	-0.58	-0.37	-0.70*	-0.04	-0.26	-0.30	-0.37
July 2008	-0.43	-0.59	-0.13	-0.66	0.06	-0.18	-0.07	-0.13
June 2008	-1.21**	-1.16**	-0.79*	-1.19**	-0.24*	-0.64	-0.81	-0.90*
R²	0.39	0.46	0.42	0.42	0.53	0.43	0.39	0.38
adj-R²	0.34	0.42	0.37	0.37	0.49	0.39	0.34	0.33
p-value	< 0.001	< 0.001	< 0.001	< 0.001	< 0.001	< 0.001	< 0.001	< 0.001

Table 11: Each grain resistance equation vs. f_{drag} . ESL3 and ESL4 outliers for Bathurst (tread). ESL4 removed as outlier in Keulegan (ST). In every regression ESL3, ESL4 and FC4 seem to have higher leverage than other reaches. For August 2007 regressions ESL9 and FC6 were outliers.

June 2008	Keulegan (D_{50}) sqrt(fd rag)	Keulegan (tread D_{50}) sqrt(fdrag)	Keulegan (D_{84})	Keulegan (tread D_{84})	Parker and Peterson (D_{90})	Parker and Peterson (tread D_{90})	Bathurst (D_{84})	Bathurst (tread D_{84})
Intercept	-0.05	0.08	-0.55	-0.46	-0.40	0.36	0.19	0.10
ff_{grain}	9.34*	7.82**	8.15**	7.88**	4.13**	1.69	1.99	3.15**
R²	0.42	0.34	0.30	0.31	0.37	0.20	0.19	0.40
adj-R²	0.37	0.29	0.25	0.26	0.31	0.14	0.13	0.35
p-value	0.009	0.02	0.03	0.04	0.02	0.11	0.11	0.02
August 2007								
Intercept	0.92*	0.75	-0.55	2.64	1.56	2.42	2.90*	3.09**
ff_{grain}	6.17	7.92**	8.15**	0.75	2.47	0.76	-0.14	-0.38
R²	0.16	0.27	0.30	0.0006	0.05	0.006	0.001	0.008
adj-R²	0.09	0.21	0.25	-0.09	-0.03	-0.08	-0.09	-0.08
p-value	0.16	0.06	0.03	0.94	0.45	0.81	0.92	0.77

The regression analysis shows that the ff_{grain} values from the *Keulegan* relations using the D_{50} , step tread D_{50} , and D_{84} were all significantly related to the ff_{grain} values from the drag approach during the June 2008 flows. None of the intercepts were significant in any of the regressions. Only the *Keulegan* step tread D_{50} and *Keulegan* D_{84} were significantly related to ff_{drag} at low flows.

Despite these differences in values, the *Keulegan*, *Bathurst* and *Parker and Peterson* relations show similar trends (Figure 32). Each equation was evaluated looking for significant differences in the value of ff_{grain} among channel types, flow period and dominant step type in the reach. Figure 32 shows boxplots using the ff_{grain} equation with the minimum values (*Keulegan* [1938]) and the ff_{grain} equation with the maximum values (*Parker and Peterson* [1980]). The *Keulegan* equations (using both reach average and step tread values for D_{50} and D_{84}) indicate that reaches with mixed boulder and wood steps have a higher grain resistance than reaches with only boulder, only wood, or no steps. Both the *Bathurst* [2002] and *Parker and Peterson* [1980] equations show no significant difference based on step type. The difference in ff_{grain} based on the dominant step type may be related to differences in step dimensions based on step composition (Figure 33). Steps that are a mixture of wood and boulders tend to have a larger drop height, step height, pool depth and step width.

The value of ff_{grain} was evaluated against flow period and channel type as well (Figure 32). All the equations, including using the drag force approach, showed significantly higher values of ff_{grain} in August 2007 versus June 2008. The drag force approach also indicated significantly higher values of ff_{grain} for reaches with mixed step types versus boulder step types in both August 2007 and June 2008. All equations,

except for the drag force approach, indicated that the values of ff_{grain} are significantly higher in cascade reaches versus step-pool and plane-bed reaches, probably because cascade reaches tend to be on steeper slopes with smaller values of R/D_{84} (between 0.5 and 1.7).

In summary, estimates of percent contribution of grain resistance to ff_{total} are quite sensitive to the equation used for this purpose, ranging in some channel reaches from 32% to 96% at high flows and 3% to 15% at low flows. At high flows, the *Parker and Peterson* equation consistently produces the highest estimates and the *Keulegan* equation consistently produces the lowest estimates of ff_{grain} . At low flows, the *Bathurst* equation or drag approach produce the highest estimates and the *Keulegan* equation produces the lowest estimates of ff_{grain} , indicating, as has been previously suggested by *Millar* [1999], that the *Keulegan* serves as a lower bound for grain resistance.

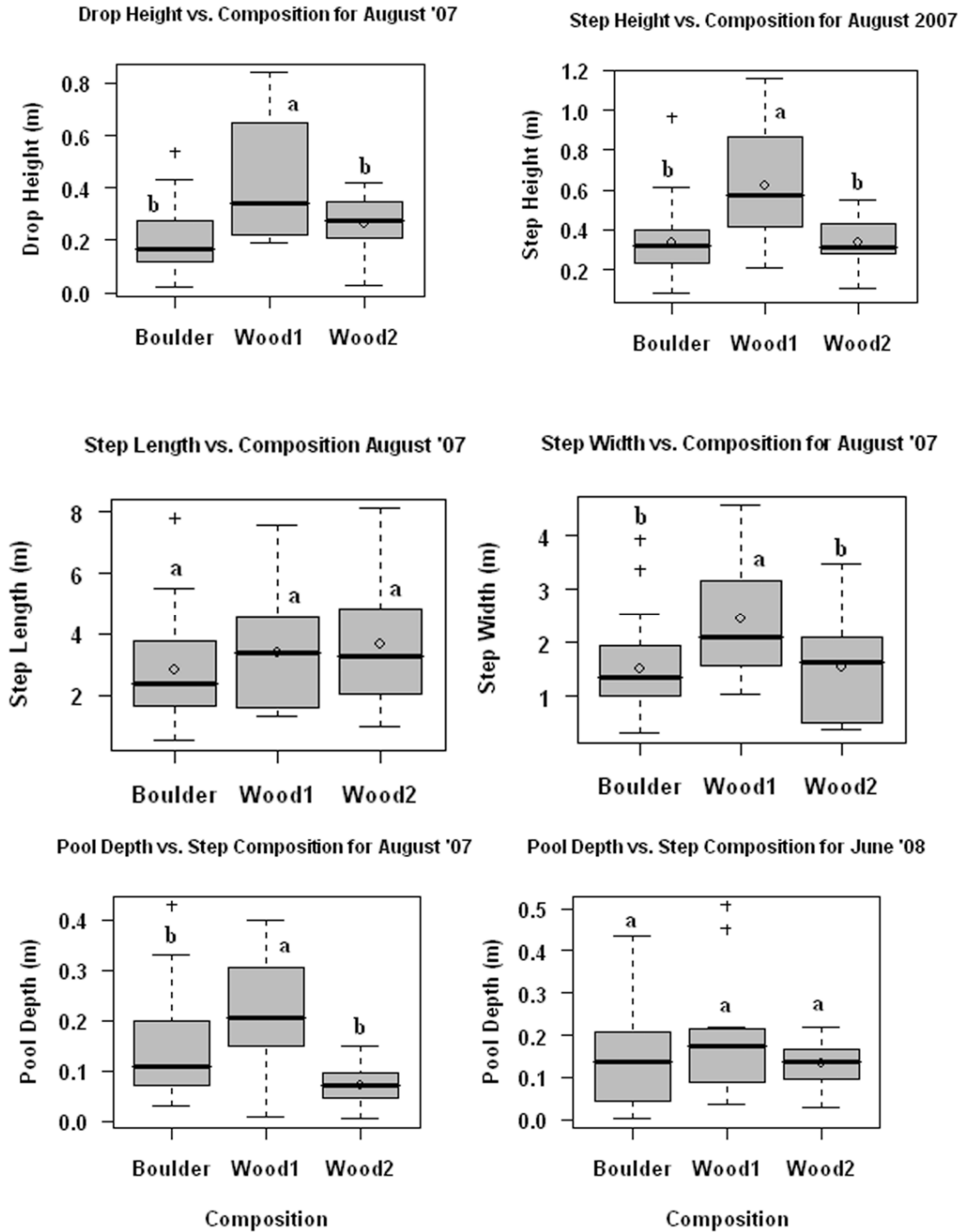


Figure 33: Boxplot of step dimensions for every individual step in every reach based on step composition. Boulder = steps only made up of large grains, Wood1 = steps made up of a keystone boulder and wood, Wood2 = steps only made up of wood. Lower case letters a and b indicate which means are significantly different from each other using a Tukey HSD test in an ANOVA.

6.4.2 Wood Resistance, ff_{wood}

Wood resistance was calculated using the *Shields and Gippel* [1995] approach. There are many potential sources of error in this approach, including the measurement of X (distance between logs), calculation of C_D^{app} , and determination of which pieces constitute significant in-channel wood. The problems with determining values for each of these variables are discussed in more detail in Section 6.4.4.3. The values of ff_{wood} ranged between 0.01 and 4.43 (Table 9), making up anywhere from 0 to 87% of the ff_{total} in individual reaches. Although the results in CHAPTER 4 indicate that the wood density using individual logs ($(\sum \text{Surface Area of Individual Logs})/\text{Reach Surface Area}$) was not significantly related to ff_{total} , wood is significantly related to ff_{total} once the wood in steps is included as part of the wood density. Therefore, an additive drag approach may be overestimating the influence of individual logs that are not part of steps on total flow resistance. In some cases, inclusion of all pieces of wood caused the value of ff_{wood} to be more than double the measured value of ff_{total} .

Complexly shaped wood pieces also created uncertainty. ESL5 had a log that was primarily a bridge with branches hanging down into the flow (Figure 34). Branches increase the surface area of a log, but also create more flow separation and turbulence [*Hygelund and Manga*, 2003]. Hence, the area increases but the drag force does not, so that the apparent drag coefficient decreases. Field observations reveal that the log in ESL5 affects the velocity and depth near the bank, but the *Shields and Gippel* [1995] equation does not provide a way of accurately quantifying that effect. Similarly, a log along the left bank of ESL6 helped to create flow separation and a backwater area, but this area was no longer in the major portion of the flow (Figure 34). The values of ff_{wood}

calculated for these individual pieces inflated the actual effect these logs were having on the majority of the flow. Therefore, the only piece included in ESL6 was an individual log that lay across the reach (Figure 34). The value of ff_{wood} was still calculated to contribute 50% to ff_{total} . During high flows this log helped create a small hydraulic jump and caused the flow depth to increase behind the log, but the value of ff_{wood} seems overly large. This problem was observed in many reaches, particularly when logs contained branches and were not necessarily in the thalweg, but were obviously responsible for creating flow separation and backwaters.

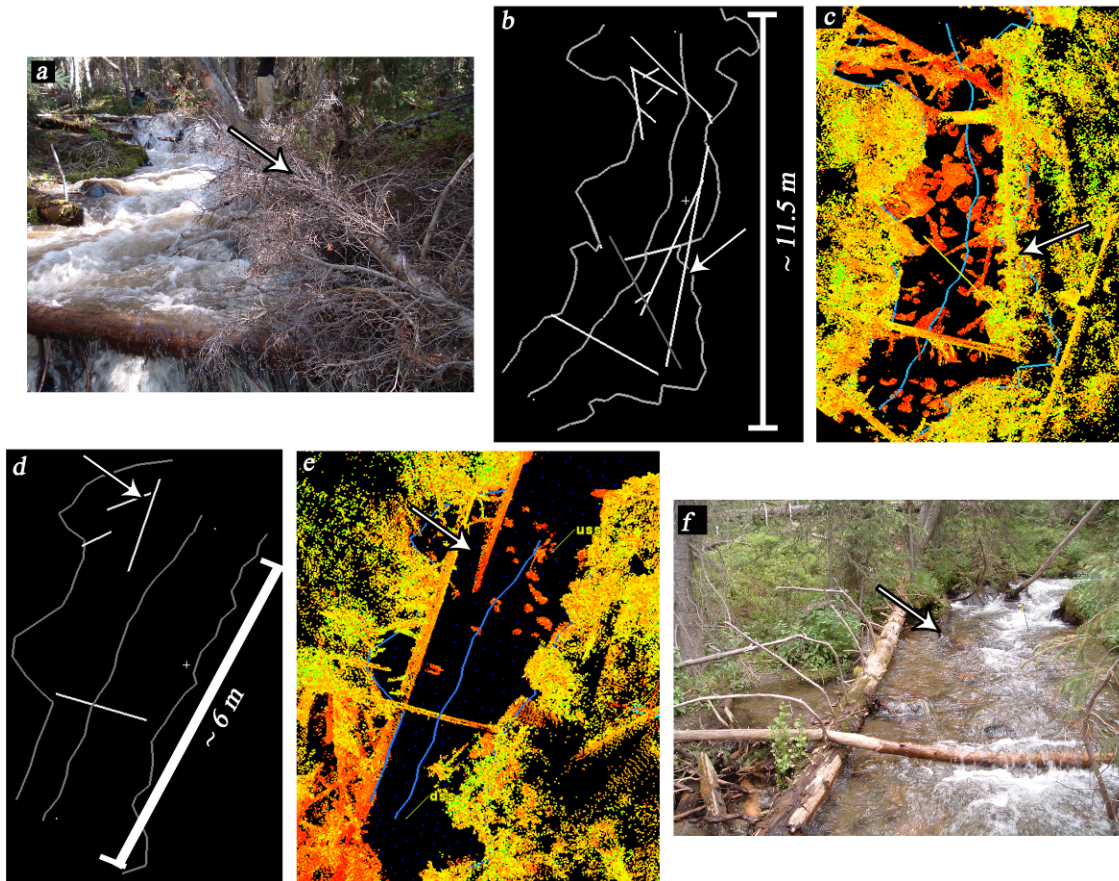


Figure 34: Example of wood in ESL 5 (a - c) and ESL6 (d - f). a) Picture of log in ESL5 during high flow. b and c) Plan view of ESL5 showing location of logs and LiDAR scan of ESL5. d and e) Plan view of ESL6 showing logs and LiDAR scan with measured thalweg in the center. f) Photograph of ESL6 in July 2008.

Wood resistance was found to contribute anywhere between 0 to 87% of ff_{total} using the *Shields and Gippel* [1995] drag approach. The contribution of ff_{wood} was not found to vary in any significant fashion with ff_{total} . More likely the relationship between the two variables is much more complex, because of branches and interactions between in-channel wood and other large roughness elements such as steps and boulders.

6.4.3 Step Resistance, ff_{step} and ff_{spill}

Steps likely contribute the greatest proportion of resistance in step-pool channels from both spill and form resistance [*Curran and Wohl*, 2003; *Wilcox et al.*, 2006]. Form resistance relates to energy losses from circulation in the pools, but as steps become submerged, the step shape can also contribute to form losses. We calculated form resistance around steps using a drag force approach. Because C_D is unknown, we performed a sensitivity analysis for one cascade and two step-pool reaches (Figure 35). The percent contribution of ff_{step} to ff_{total} can vary from 1 to 63% within a reach, depending on the values of the drag coefficient. The more conservative lower values of ff_{step} , using the smallest values of C_D , were compared to the other components because the larger values sometimes exceeded ff_{total} when added together with the other components of resistance. The contribution of ff_{step} to ff_{total} tended to be highest during the high flows, since these were the times that the steps had either submerged or skimming flow over the step. *Smart et al.* [2002] argued that bedforms are not significant in streams where other bed elements are on the same order of magnitude as the flow depth, but my results suggest that the adverse pressure gradient around bedforms may become increasingly important as flow increases despite the presence of other bed elements on the same order

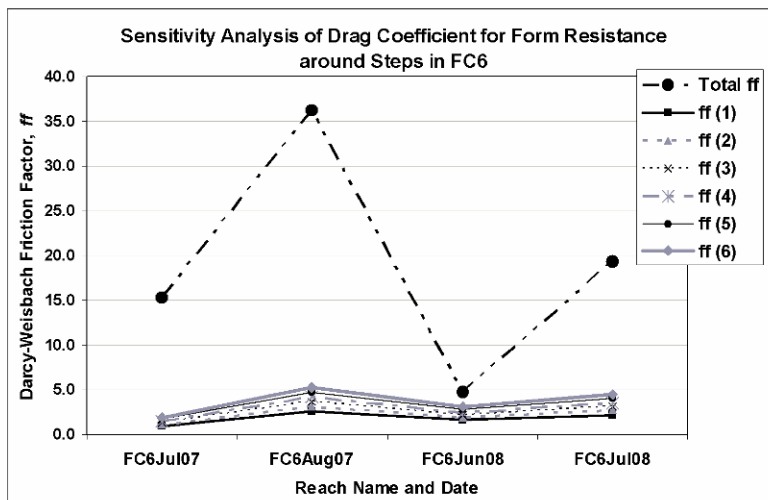
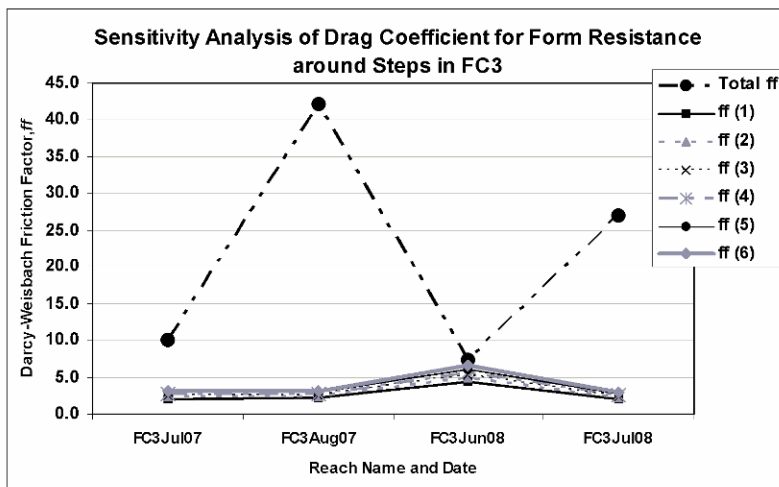
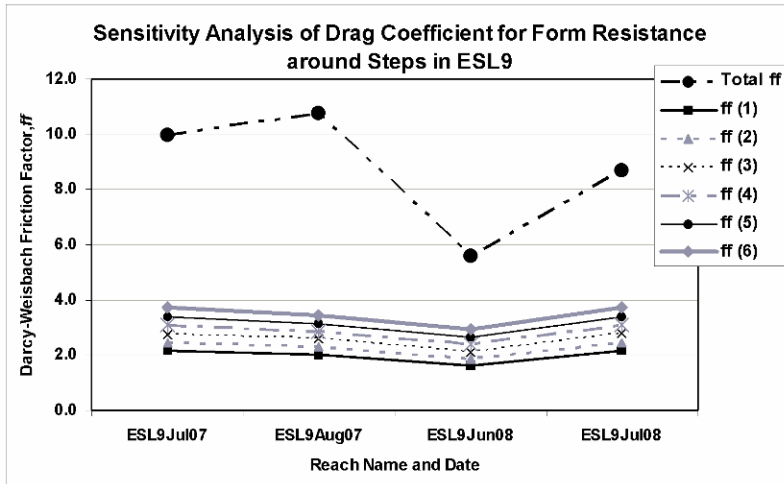


Figure 35: Example of sensitivity analysis for ff_{step} . Each number in the key (1 – 6) indicates that a different drag coefficient was used for each iteration. One is related to the smallest values of C_D used and six are the max values. Depending on the reach, the larger drag coefficients could double the percent contribution of ff_{step} : ESL9 ranged from 28 to 52% at high flows and 18 to 32% at low flows. FC3 went from 61 to 89% at high flows to 5 to 7% at low flows, FC6 goes from 33 to 66% at high and 7 to 14% at low flows.

of magnitude as flow depth. At lower discharges, ff_{spill} may dominate with higher drop heights and smaller pools. Table 12 shows that at high flows ff_{step} is significantly related to ff_{total} as a power function.

Table 12: Linear regression of ff_{total} vs. ff_{step1} for June 2008 flows. The relationship is a power function with 10 degrees of freedom.

	Estimate	p-value	R ²	p-value
Intercept, β_0	3.63	< 0.001	0.33	0.05
ff_{step1}	0.52	0.05		

6.4.4 Limitations in calculating total and component resistance in steep streams

6.4.4.1 Limitations in calculating ff_{total}

There are a number of sources of error in the calculation of ff_{total} . Each parameter (v , S_f , R_h) has error associated with the method used for measuring it. The friction slope is not directly measured and is not steady or uniform in mountain channels. The water surface slope is used as an approximation of S_f for calculating ff_{total} . The water surface slope (S_w) was approximated using a linear regression of the survey points (Figure 36). Typically the water surface slope is not directly measured, in which case the bed slope (S_0) is used to approximate S_f . Figure 36 shows that at high flows (June 2008) the S_w and S_0 are close approximations of each other. At high flows the water surface tends to submerge many of the roughness elements, causing it to be much smoother than at low flows. During the August 2007 flows, there is a larger difference between S_w and S_0 . The changes in the gradient throughout the reach are much sharper. The RMSE for the difference in ff_{total} based on using S_w and S_0 during the June 2008 flows is 0.207 and this can go up to 0.635 for the August 2007 flows. This results in over- or under-estimation of point-specific S_f by as much as 2.0%, which can in turn introduce errors as great as 2.0% in ff_{total} . Many reaches followed this trend, where the regression line had a better fit at high flow versus low flows.

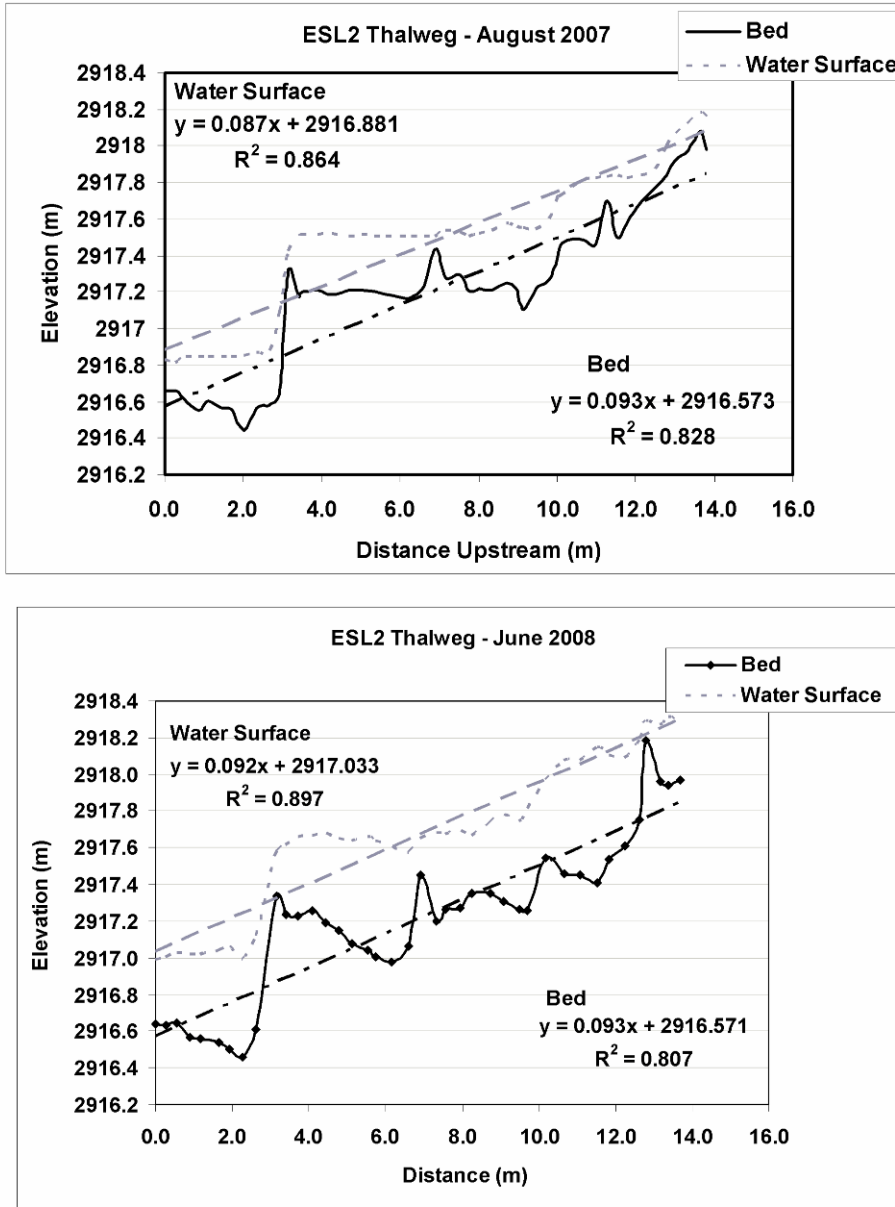


Figure 36: Example of water surface and bed slope regression lines for ESL2.

Seven methods of calculating slope were analyzed and the effects on calculating ff_{total} are evaluated in Figure 37: (1 and 2) S_w was calculated simply by taking the difference between the upstream and downstream water surface elevation, as was S_0 . (3) S_f was approximated by calculating the change in the total head (dH) over the reach length (dx). The total head is equivalent to:

$$H = z + d + \frac{v^2}{2g} \quad (6.20)$$

where, z = bed elevation; d = local flow depth (m); v = local velocity (m/s); g = acceleration due to gravity (m/s^2). The local velocity was calculated using the continuity equation. This calculation of S_f was not used in the final version of the equation for ff_{total} because of problems with estimating the local velocity. (4) The regression line was calculated for S_0 . (5) A step gradient was calculated. (6) An effective hydraulic radius was calculated. (7) The thalweg water surface slope was averaged with the right and left bank water surface slopes.

Another major source of error relates to the calculation of the hydraulic radius using the average cross-sectional area and wetted perimeter. The reach-average velocity was measured in each reach using tracers. The continuity equation was then used to calculate discharge by using the average cross-sectional area and the reach-average velocity. Discharge was also measured using the Forest Service gages that were located just below ESL1, FC1, and FC5. There are no major inputs or outputs between each reach and the nearest gage. Therefore, the gage discharge should measure the reach discharge. Velocities for each reach were estimated from the gage discharge by using the reach-average cross-sectional area. Figure 38 shows that the tracer velocities are systematically higher than the gage velocities. This is particularly true at the higher flows, which correlate with the higher velocities. The discrepancy between the two may reflect error in the calculation of reach-average cross-sectional area. Field observations revealed that there were areas of significant flow separation in each reach and backwater areas, particularly at high flow. Therefore, the cross-sectional area may be overestimated in each reach and an effective cross-sectional area and effective hydraulic radius should

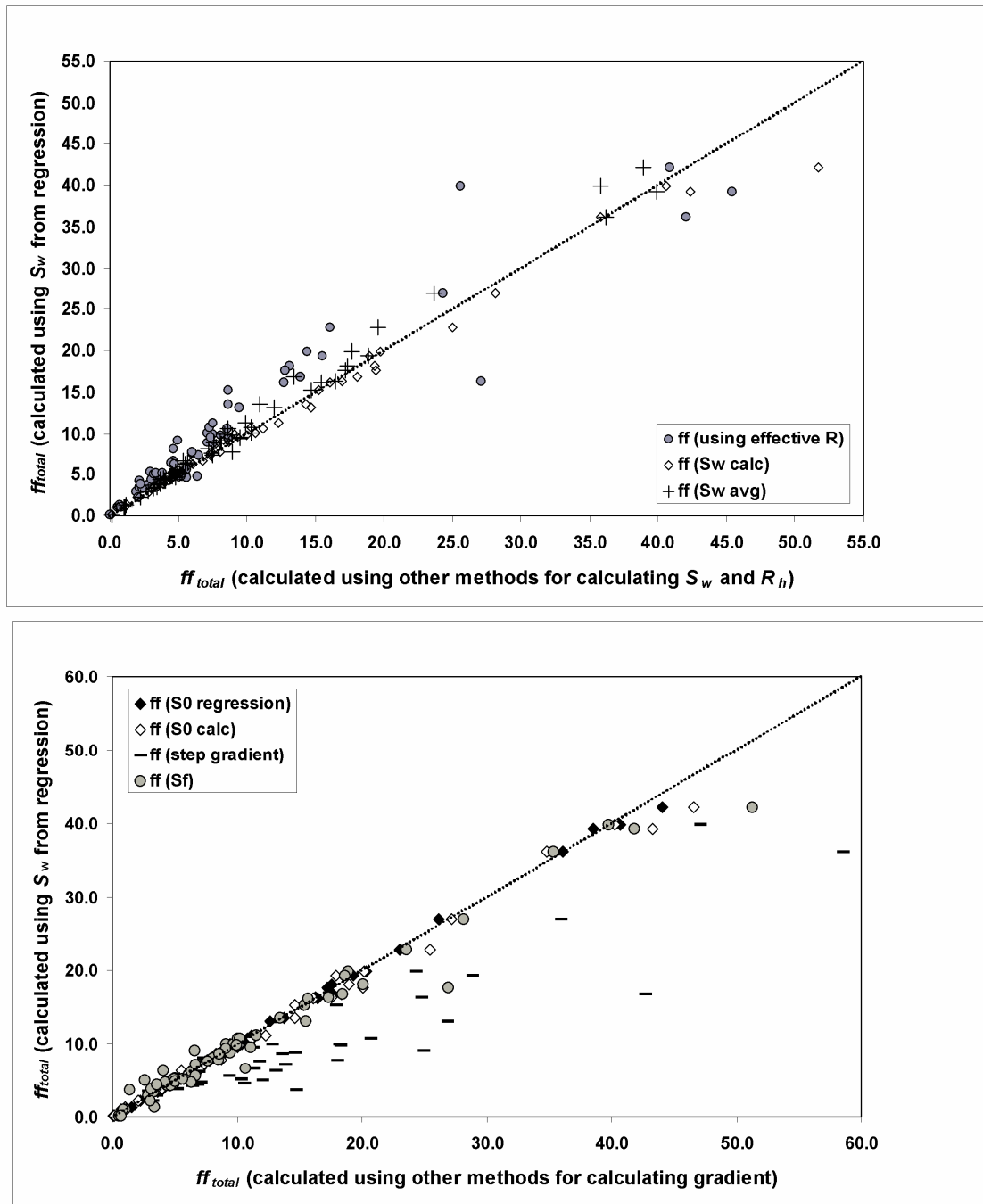


Figure 37: Sensitivity analysis for calculating ff_{total} . The y-axis shows the values of ff_{total} used all other analyses, the x-axis shows values of ff_{total} calculated using other methods. RMSE for S_0 regression = 0.406; RMSE S_0 calc = 1.103; RMSE for S_w calc = 1.451; RMSE step gradient = 8.513; RMSE for R_{eff} = 3.642; RMSE for S_f = 2.061; RMSE for S_w avg = 1.263.

be used for the calculation of ff_{total} . These effective areas represent the cross-sectional area and hydraulic radius that the majority of the flow moves through and ignores the

backwater areas along the banks with a large secondary circulation component. Using the gage discharge and tracer velocity, a new average cross-sectional area was calculated for each reach. The new cross-sectional areas were on average 32% smaller for the June 2008 high flows, 23% smaller for the July flows and 25% smaller for the August 2007 flows. The percent difference between the measured cross-sectional area and the effective cross-sectional area was used to calculate a new hydraulic radius (R_{eff}) for each reach. The effective R was then used to calculate a new ff_{total} (Figure 37). Using the R_{eff} causes the ff_{total} to be smaller than the values with the total R . The error between ff_{total} calculated using R vs. R_{eff} was one of the highest at 3.642. The lowest error was related to using the regression lines for S_w versus S_o (RMSE = 0.406).

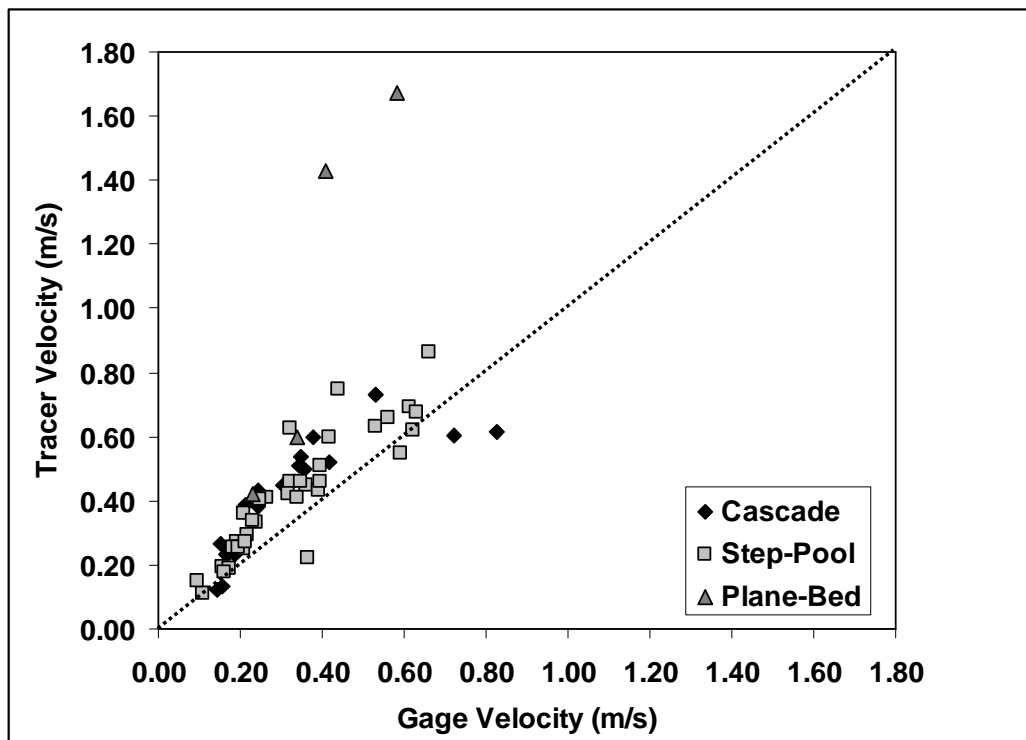


Figure 38: Comparison of velocities measured using tracer and velocities calculated from gage discharge. Gray dotted line is 1:1 line. RMSE for all data = 0.235; RMSE for Step-pool = 0.120; RMSE for Cascade = 0.149; RMSE for Plane-bed = 0.764.

6.4.4.2 Limitations in calculating ff_{grain}

The major limitation for calculating grain resistance is that, because there is no absolute or widely accepted measure against which to compare varying methods of estimation, it is difficult to find a way to evaluate which equation is capturing the actual value of ff_{grain} . Many studies have assumed that the value is small and the remaining resistance is related to the unaccounted sources of resistance, but *Wilcox et al.* [2006] showed in their flume study that both the *Bathurst* and *Parker and Peterson* equations commonly underestimate ff_{grain} . In a natural setting, it is difficult to find an appropriate measure to compare each equation against, to determine which method accurately characterizes grain resistance. *Pagliara and Chiavaccini* [2006] found that an increase in flow resistance due to the presence of boulders is significantly related to the boulder concentration (Γ). Each of these methods should represent the energy dissipated as flow moves around and over the larger bed elements, therefore the boulder concentration (Γ) was used to evaluate how well each equation represents the grain resistance at both low and high flows (Figure 39). Table 13 indicates that while holding Q constant, ff_{total} is significantly related to Γ . Therefore, I assumed that this is an appropriate variable to use for comparing each ff_{grain} equation and assessing the ability of each equation to accurately predict ff_{grain} .

Table 13: Multiple regression for $\log(ff)$, 52 df.

	Estimate	p-value	R ²	p-value
Intercept, β_0	2.40	<0.001	0.56	< 0.001
$\log(Q)$	-0.44	< 0.001		
$\log(\Gamma)$	0.36	< 0.001		

Each equation was evaluated using the reach characteristic grain size as well as the step tread grain size, which represent both the 50th (D_{50}) and 84th (D_{84}) percentile of a

cumulative grain distribution. The results in Figure 39 indicate that all four equations are significantly related to boulder concentration at high flows, but only the *Keulegan* equation using both D_{50} and D_{84} is significantly related at low flows. The boulder concentration only changes slightly with flow, but the submergence of the boulders changes. The significant relationship between boulder concentration and each equation at high flow exists because the boulders are almost completely submerged. As flow decreases the water begins to flow around the boulders, rather than over, and the characteristics of the flow change. Therefore, the boulder concentration may not be an appropriate measure of evaluating the ff_{grain} equations at low flows, or each of the equations do not capture values of ff_{grain} at low flows.

The value of ff_{grain} found by using the drag force approach was also significantly related to the boulder concentration (Figure 40), which is expected since a drag force is calculated around each boulder. The drag around a cluster of boulders was calculated as a single object when the boulder length to height ratio was greater than 9.0 [Wohl and Ikeda, 1998] because such closely spaced boulders have wake interference between them, which makes an additive method unrealistic. Figure 41 shows a schematic of water moving over boulders at high flow and around boulders at low flow. Although the wake is probably reduced at low flow, there is still a large amount of error because of the disruption of the surface flow and constant divergence and convergence of flow lines. Also, the values of C_D are usually calculated for submerged objects, not partially submerged grains.

Therefore, the lack of any relationship between boulder concentration and either the *Bathurst* or *Parker and Peterson* equation during the August 2007 flows indicates

that neither of these equations represents ff_{grain} at these flows. The *Keulegan* relation using the step tread D_{50} was the most significant regression with boulder concentration, indicating that this equation may provide a lower bound to ff_{grain} at low flows despite problems with the mathematical validity of the equation at low flows.

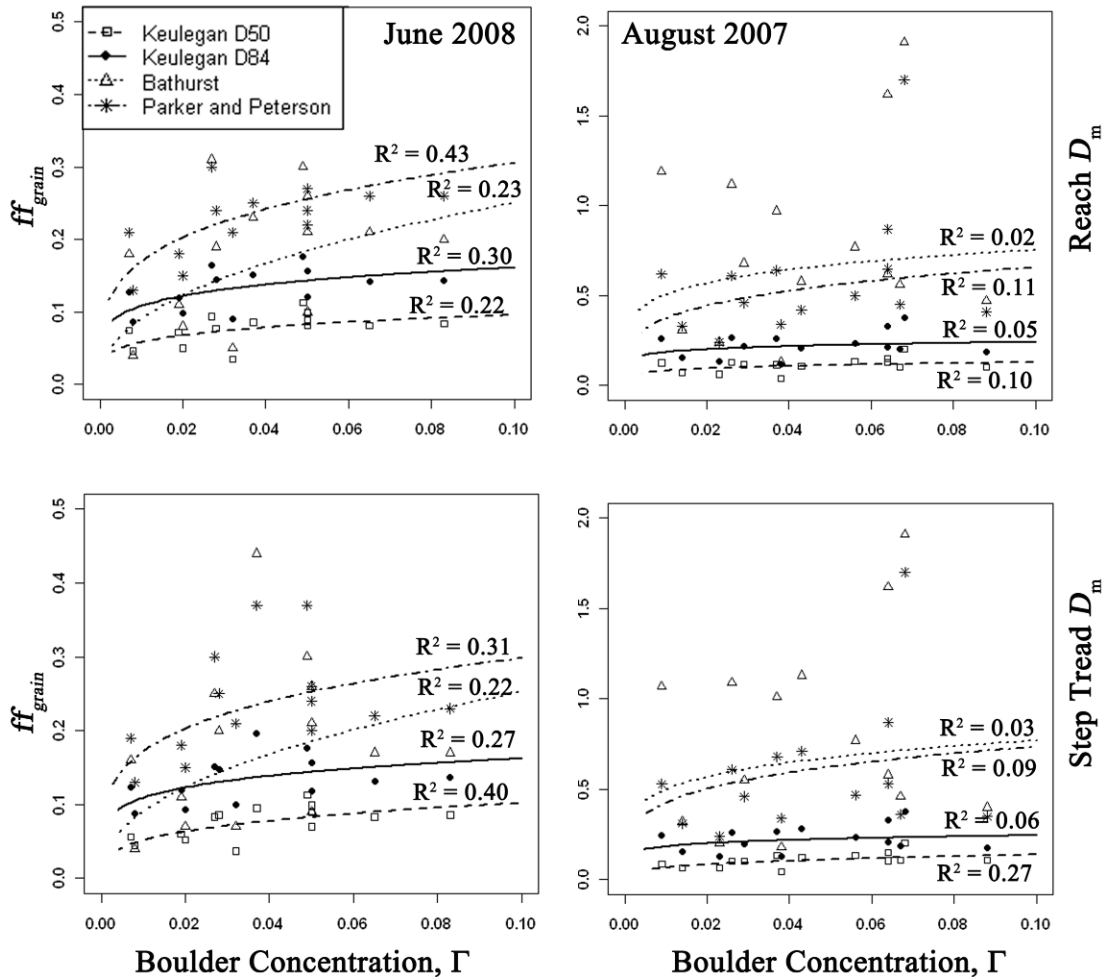


Figure 39: ff_{grain} regressed against boulder concentration for high (June 2008) and low (August 2007) flows as a measure of evaluating applicability of each grain resistance method. Bottom two regression lines are for *Keulegan D_{50}* , and *Keulegan D_{84}* , respectively, in each plot. Top two lines are for *Bathurst* and *Parker and Peterson*, respectively, for the June 2008 flows and the opposite for the August 2007 flows. Neither the Parker and Peterson equation nor the Bathurst equation is significant at the lower flows at $\alpha = 0.05$. ESL3 is excluded because it is an outlier with a much larger boulder concentration than any other reach (~ 0.20).

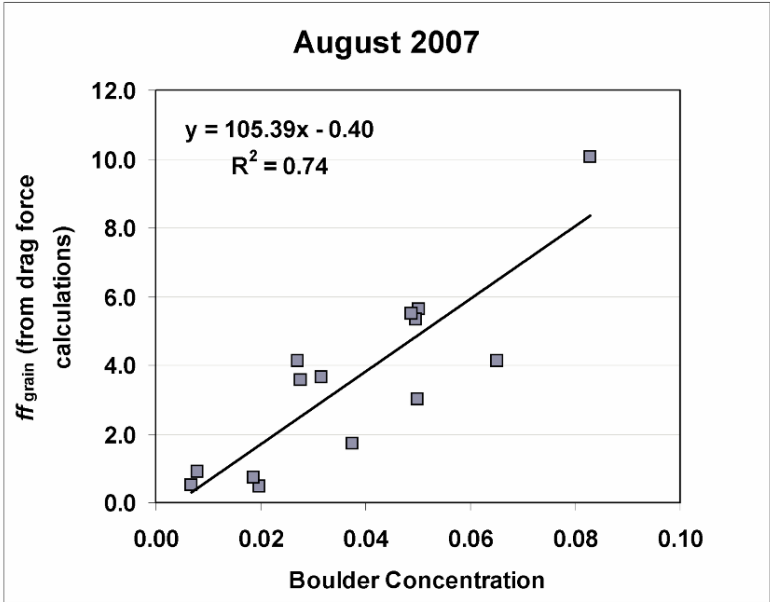
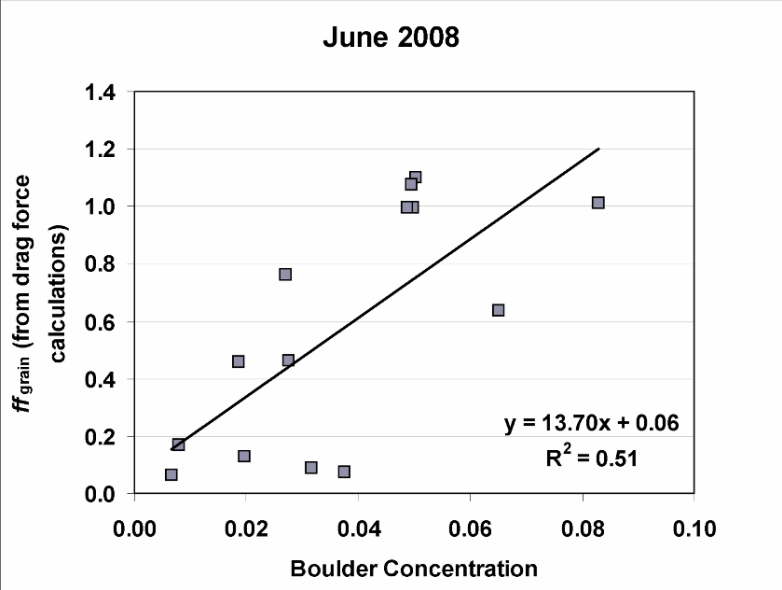


Figure 40: ff_{grain} from drag approach vs. boulder concentration at August 2007 and June 2008 flows (R^2 significant at the $\alpha = 0.05$ level).

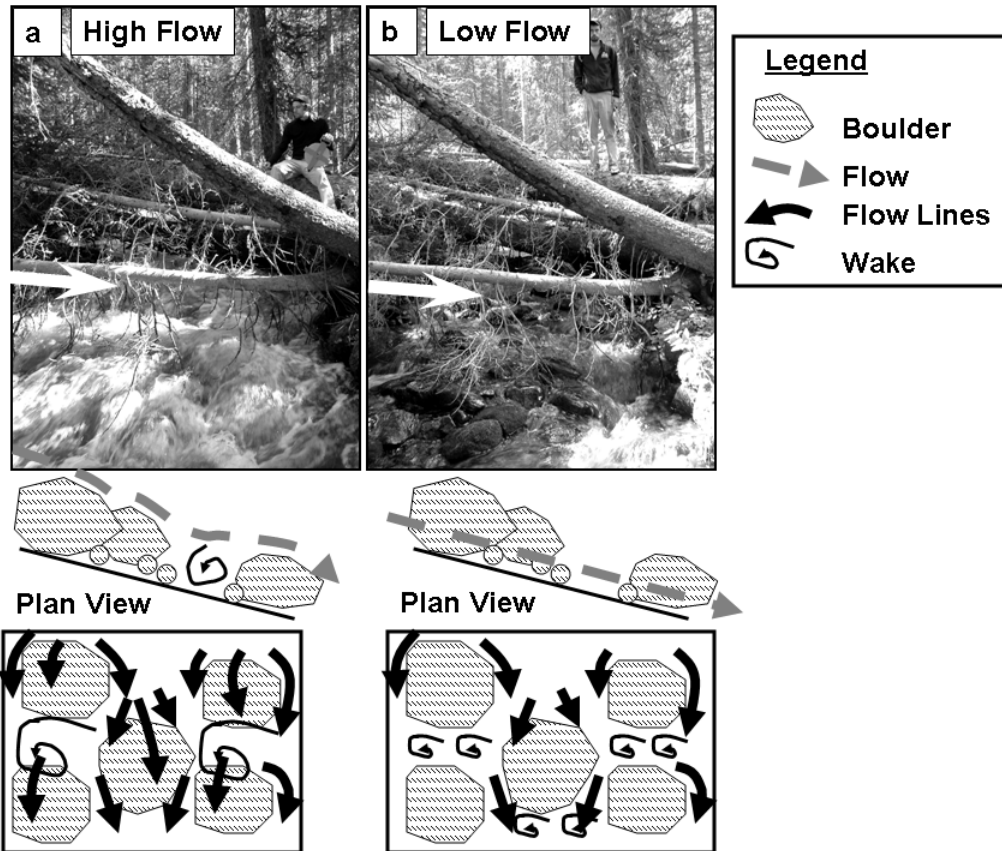


Figure 41: Flow moving over boulders in a cascade reach (ESL7) at high (a) and low (b) flows. The side and plan view are idealized versions of how flow is moving around boulders in the photograph above and does not actually represent the location of boulders in ESL7.

6.4.4.3 Limitations in calculating ff_{wood}

There are many potential sources of error when using the drag force approach for calculating ff_{wood} . First, wood in steps were considered part of the step form and thus were not considered as part of ff_{wood} . Each parameter in Equations 6.14 through 6.18 has potential error associated with it based on measurement errors as well as estimating unknowns such as the drag coefficient (C_D). The diameter and length of each log were measured using the LiDAR scans of each reach. The LiDAR scans were done during the lowest flows (August 2007) so that a larger proportion of the bed was exposed, but anything under the August water surface was not captured by the scans. Some of the log diameters may be smaller than the actual diameters if the bottom of the log was below the

August water surface. Therefore, the frontal area of the log may be underestimated for all flows. The piece length may also be underestimated if part of the log was completely submerged beneath the water surface during August flows. Most of the log diameters were larger than the water depth during the lowest flows, therefore it is unlikely that the entire length of the log was not captured. Consequently, the largest error in measuring the log size is probably related to the diameter.

The drag coefficient and empirically derived values for a and b are most likely the largest source of error in the calculation of ff_{wood} . The C_D was estimated using flume-derived values from *Gippel et al.* [1992]. *Gippel et al.* [1992] showed that the drag coefficient changed based on the angle of flow, the distance between cylinders, the Froude number, and the blockage ratio. They also showed that cylinders that included branches had relatively lower drag coefficients than cylinders without branches as well as varying less with rotation relative to the flow. *Hygelund and Manga* [2003] determined that if a log's diameter is greater than one-third the channel depth, then the drag on the log does not vary with depth. They propose that the depth-averaged velocity is most important for determining drag around large logs, whereas the local velocity is most important for determining drag around smaller logs. *Hygelund and Manga* [2003] also showed that branches cause flow separation and turbulence, reducing the apparent drag because the area increases, but the drag force does not. The drag coefficients in the current study were determined based on all the above criteria. Mainly, the graphs in *Gippel et al.* [1992] were used to pick appropriate values of C_D . Figure 42 shows the range of C_D values versus the range of orientation of the logs to the flow and the blockage ratio. There is no apparent correlation between these variables, because of the

combination of factors that was considered when determining an appropriate value for C_D . The blockage ratio is above the maximum value (0.4) investigated by *Gippel et al.* [1992], but the main determination of the drag coefficient was angle, distance between logs (X), blockage ratio, and depth of log in relation to the flow depth. The reaches with high blockage ratios > 0.4 are ESL2, one log in ESL8, and one log in ESL7. The logs that were bridges over the reach with branches hanging down into the flow were given very low values of C_D , since the frontal area used was probably larger than the actual frontal area of each individual branch.

The values of the C_D were kept under 1.0 because any higher values led to values of ff_{wood} that exceeded calculated values of ff_{total} . Figure 43 shows a sensitivity analysis for calculating ff_{wood} for two step-pool reaches (ESL1 and ESL4). The ff_{wood} calculated using different drag coefficients for each log based on the parameters described above is compared against using a minimum C_D of 0.6 for all logs and a maximum C_D of 2.0. This range of values agrees with the values used by *Wilcox et al.* [2006] and *Gippel et al.* [1992]. Any value of C_D greater than 2.0 was found to cause the value of ff_{wood} to exceed the value of ff_{total} . Figure 43 indicates that the larger the value of ff_{wood} , the greater the error associated with choosing a value of C_D . In the case of ESL1, a C_D of 2.0 causes ff_{wood} to exceed values of ff_{total} over all flows.

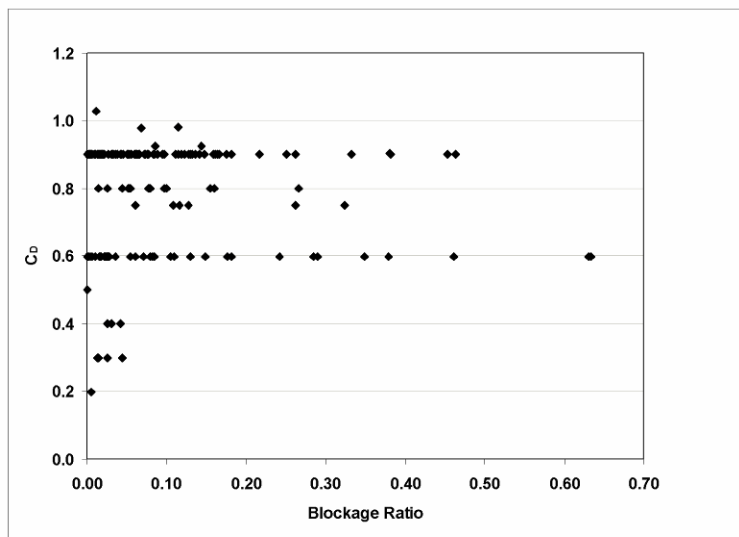
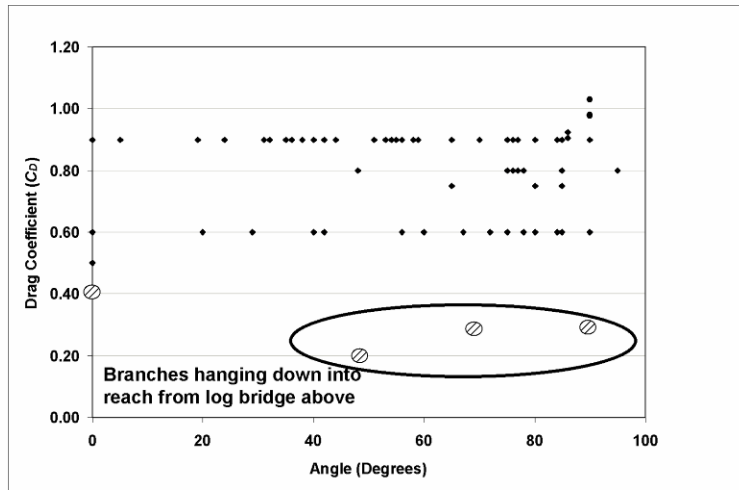


Figure 42: Drag coefficient versus the log orientation and the blockage ratio. These plots indicate that drag coefficient, as calculated here, is not sensitive to angle or blockage ratio.

Figure 43 also shows that the value of ff_{wood} can in some cases be smaller during the high flow period. Most commonly, ff_{wood} increased as flow increased because more logs were being submerged as the stage rose. In ESL4, the value of ff_{wood} decreased for one log, because the spacing between the log and the next object upstream increased as flow increased. The distance between objects is the next variable that was a large source of error. The value X in Equation (15) is most often the distance between logs, but in the case of these high gradient mountain streams, logs were not the only objects significantly

affecting the flow and creating wakes that affect the drag around individual logs. Therefore, X was determined to be the distance between these objects, which included steps and large boulders that were observed to help in the formation of wave drag. Boulders were considered significant as long as they were considered large-scale roughness with $d/D_b < 1$ (D_b = boulder diameter). In some cases X would be the distance between a piece of wood and a step, in other cases the distance between the log and a large boulder. Occasionally, smaller values of X caused ff_{wood} to be too large and exceed the value of ff_{total} . Figure 44 shows how the value of X changes in ESL4 based on the flow. As flow increased in this reach, the area where the majority of the water passes over and around the log changed. In August 2007, the water flows around a large boulder before approaching a small portion of the log. During high flow, the momentum of the water pushes the flow between two boulders before approaching a larger portion of the log that is submerged at higher flow depths, therefore the upstream distance to the next object was increased to be the distance between the log and a boulder step upstream.

The value of C_D^{app} was calculated using Equation (6.14), with values ranging between 0.20 and 4.75. This range is wider than that found by *Hygelund and Manga* [2003] and *Manga and Kirchner* [2000]. Equation (6.14) assumes that C_D^{app} is dependent on the blockage effect, although *Hygelund and Manga* [2003] showed no such relationship existed between C_D^{app} and B . They propose that the pressure on the upstream side of the log is proportional to the incoming velocity, therefore the value of C_D^{app} is dominated by the upstream velocity. Since the local velocities were not measured in the field and it was determined that the continuity equation did not give appropriate velocities at each cross-section, the procedure outlined by *Gippel et al.*

[1996] and *Shields and Gippel* [1995] was followed. The values for the coefficient a and the exponent b are also unknowns and were experimentally derived by *Gippel et al.* [1992]. Mainly, values of 0.997 and 2.06 were used, respectively, unless the logs were stacked, in which case 1.02 and 3.25 were used. These values are another potential source of error in the calculation of C_D^{app} .

Wood resistance from individual logs in the reach was found to contribute a significant amount to ff_{total} at high flows, but the importance of wood actually decreases as flow decreases because most of the wood is no longer in the flow during the August 2007 flows. The major contribution from wood during these flows is probably from the wood steps. There are a number of sources of error in calculating values of ff_{wood} , including determining a suitable value of C_D and C_D^{app} . Further work needs to be conducted in a flume, as well as making specific velocity measurements around wood in a natural setting, to determine realistic values of these drag coefficients. Large roughness elements, such as steps and large boulders, complicate the equation for calculating the drag force around these logs since these elements can create a wake that reduces drag around the in-channel wood. Branches are another factor that is difficult to account for with the current formulae, particularly branches that reach down into the channel and create more flow separation and wave drag at high flow. Most likely there are not enough individual logs in these reaches to be a significant source of resistance, as is indicated in the regression analysis done in CHAPTER 4. Therefore, it would also be interesting to examine how much wood is needed in a reach as individual pieces before it becomes a significant source of roughness, in comparison to the wood found in the steps.

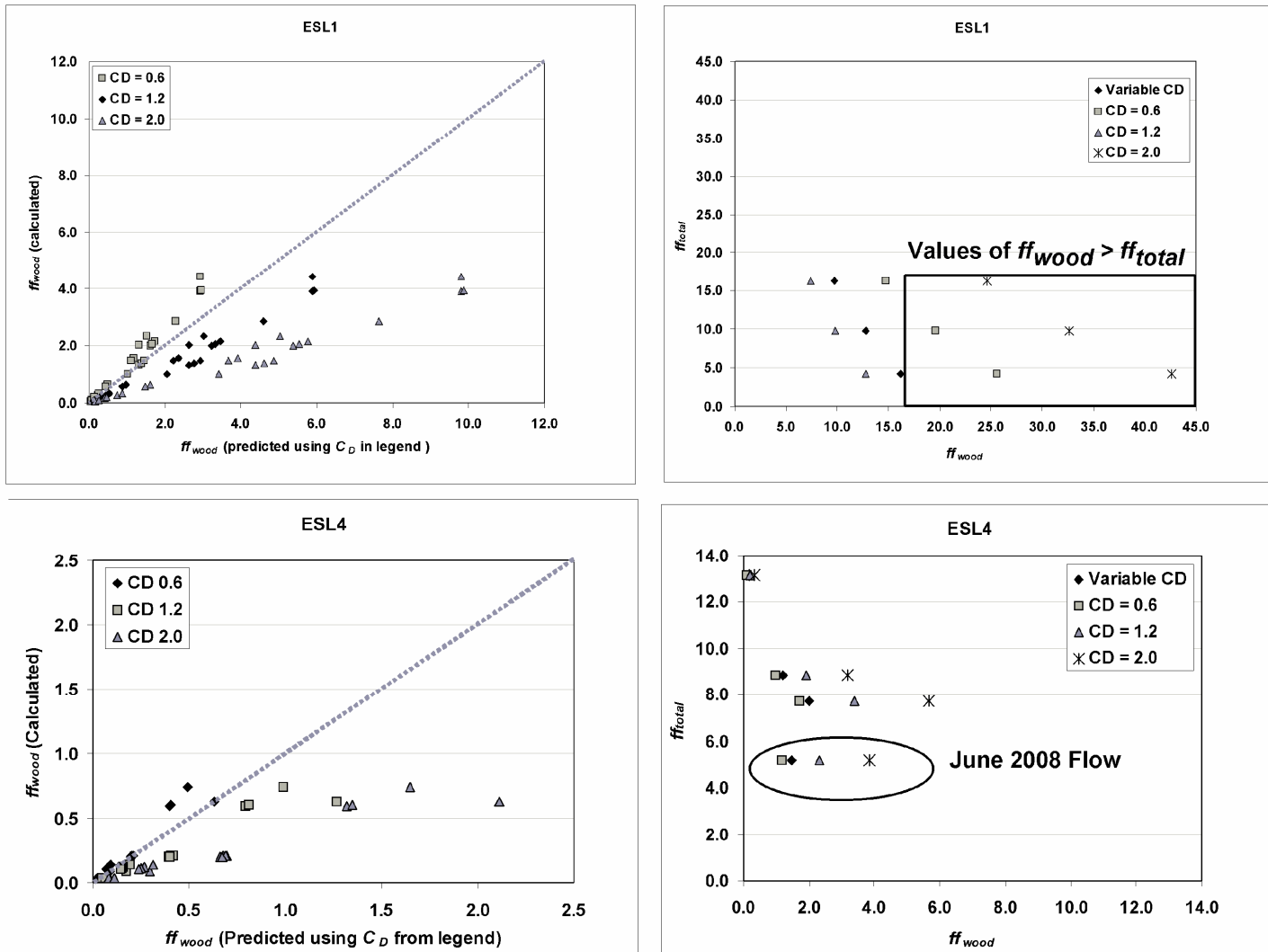


Figure 43: Sensitivity analysis of drag coefficient for calculating ff_{wood} .

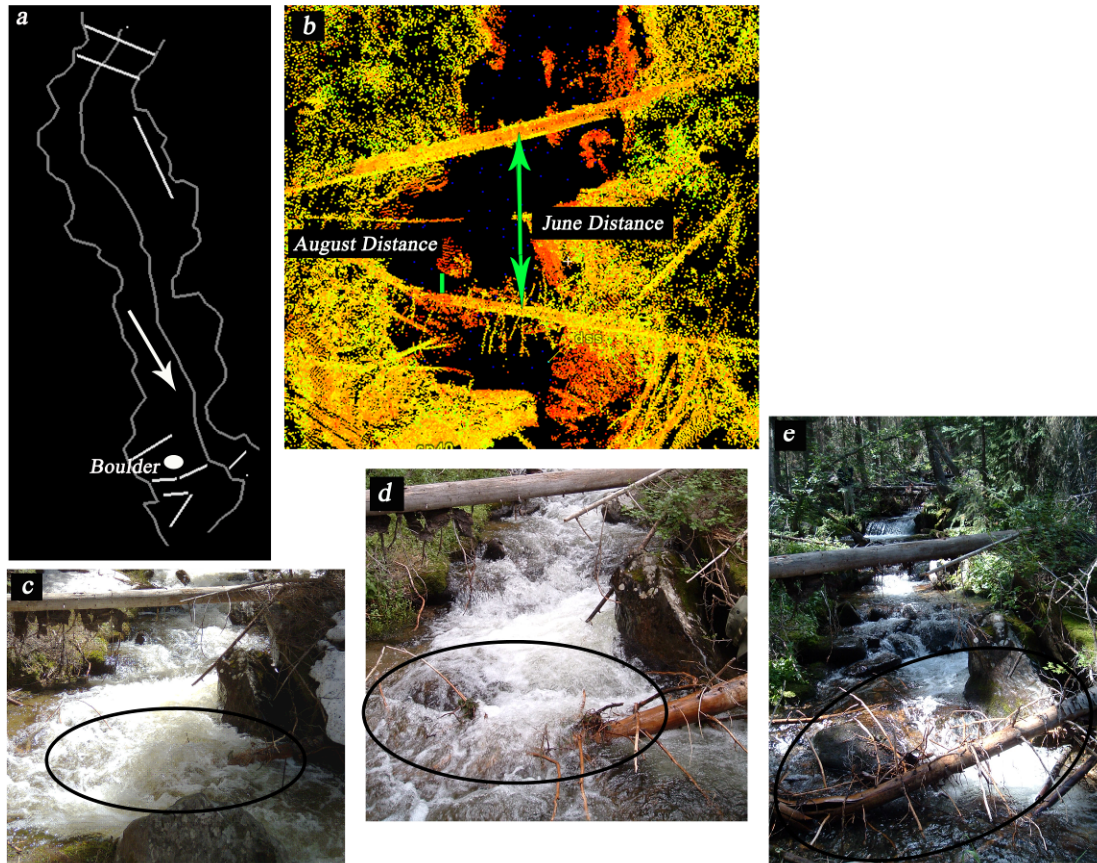


Figure 44: Measuring distance, X , between logs and other objects in ESL4. a) Plan view of ESL4 showing June 2008 bank outline and thalweg. The arrow points in the direction of flow and the white bars indicate the location of in-channel wood. b) LiDAR scan of ESL4 showing the June distance (X) between the log and the next log object upstream and the August distance (between the log and the boulder). c) Photograph of June 2008 flow in ESL4. Black circle shows where log in question is submerged in water. d) Photograph of July 2008 flow; circled area shows boulder and log. e) August 2007 flow in ESL4; circled area shows boulder and log.

6.4.5 Overview of total and component resistance

The results of the additive partitioning of ff_{grain} , ff_{wood} , ff_{step} , and ff_{spill} are shown in Figure 45a for the step-pool reaches and Figure 45b for the cascade and plane-bed reach. The *Keulegan* equation was used to calculate grain resistance using D_{50} since this equation seemed to better represent values at lower flows than the other equations. The same equation was used for both low and high flows so that another source of variability is not introduced at this stage by including more than one grain-resistance equation. The wood and step components were calculated using the drag approach outlined above.

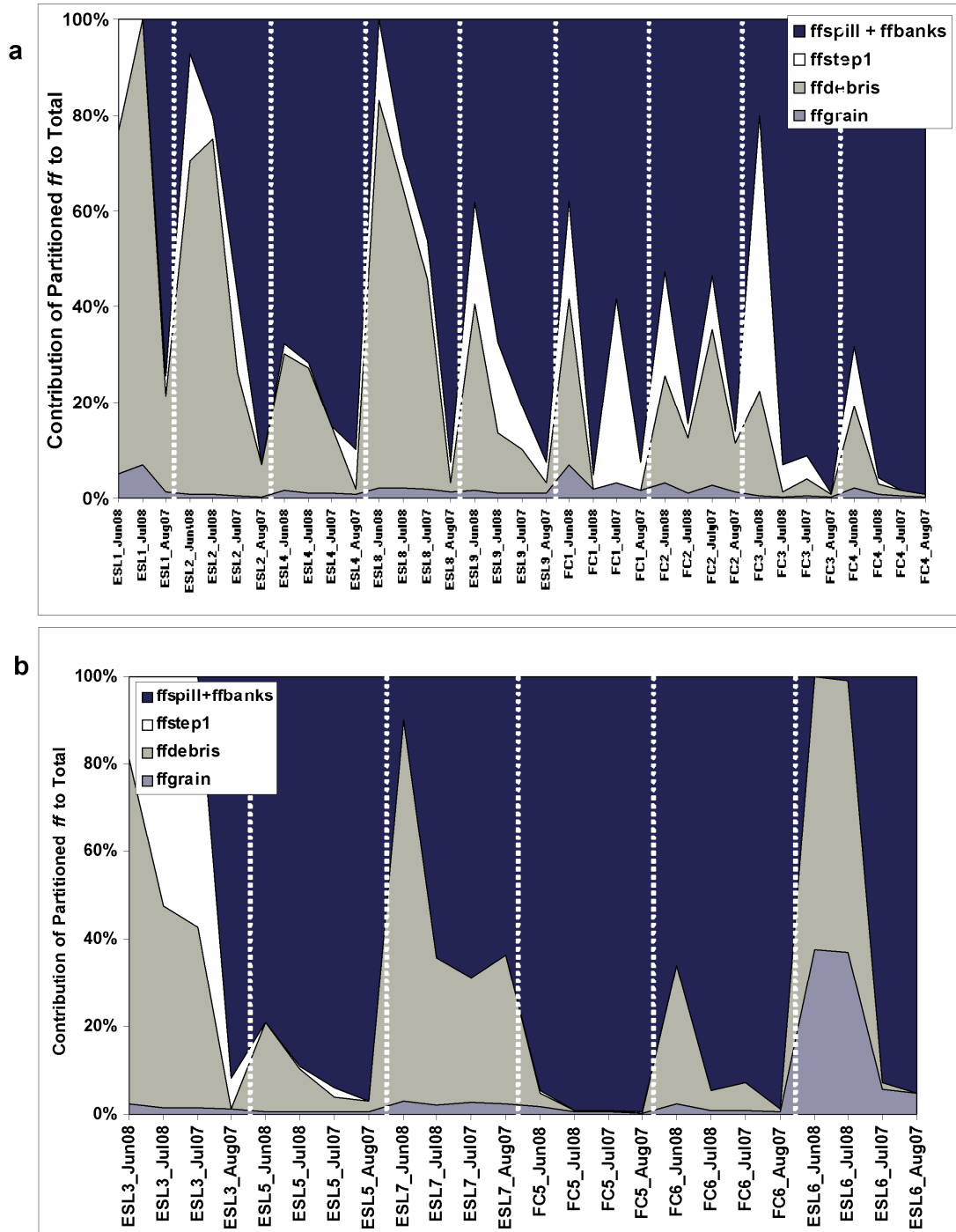


Figure 45: Contribution of partitioned friction factor to total. Dotted white lines indicate division between reaches. The ff_{spill} were made to be zero where negative values existed, because additive components exceeded the value of ff_{total} . Figure shows partitioned values for each reach over each flow period. a) Step-pool reaches b) Cascade reaches and plane bed reach

Spill resistance was estimated as the component remaining after all other components were subtracted from ff_{total} , although the term spill also incorporates any other unmeasured form of resistance such as bank resistance. Each component of resistance most likely interacts with other components, so bank effects may also be included in the step, wood, or grain component. In the additive approach, some of the added values of total resistance from $ff_{grain} + ff_{wood} + ff_{step}$ exceeded ff_{total} , therefore these reaches are not shown to contain any ff_{spill} because of the overestimate of one or all of the other components. Grain resistance contributed the smallest amount for all the reaches, including the plane-bed reach. Wood resistance contributed a large proportion of the total resistance at high flows and progressively smaller amounts as discharge decreased and logs were no longer submerged. Conversely, the contributions of ff_{spill} increased progressively as discharge decreased (Figure 46). Step resistance is related to discharge in that it was calculated only for steps that met a specific submergence criterion. Spill and ff_{step} contributed the greatest amount to total resistance at all flows for a majority of the reaches, except for four reaches during high flows. Two of these reaches do not include any steps and all four have a large wood component at high flows.

The cascade reaches had a smaller contribution from ff_{step} to ff_{total} , therefore the unmeasured component (ff_{spill}) contributed the most in these reaches. However, the unmeasured component of spill resistance was not always the largest proportion of the total resistance in every reach (Figure 45). Boxplots of the percent contribution of each component of resistance for cascade versus step-pool reaches (Figure 47) indicate that the only significant difference in the percent contribution is from ff_{step} during high flows. There are significantly higher values of ff_{grain} in the cascade reaches (Figure 32), but

overall the $\%ff_{grain}$ is not different for these reaches versus the step-pool reaches. There is more variability in $\%ff_{grain}$ in the step-pool reaches during low flows and greater variability in the $\%ff_{wood}$ for cascade reaches during high flows, despite a lack of significant differences between the means (Figure 47). The contribution from each component of resistance also varied with the step composition (Figure 48). The percent contribution of ff_{grain} and ff_{wood} was significantly higher for reaches without any steps than for the reaches with steps. The reaches dominated by boulder steps had a higher $\%ff_{grain}$ than reaches with only wood steps.

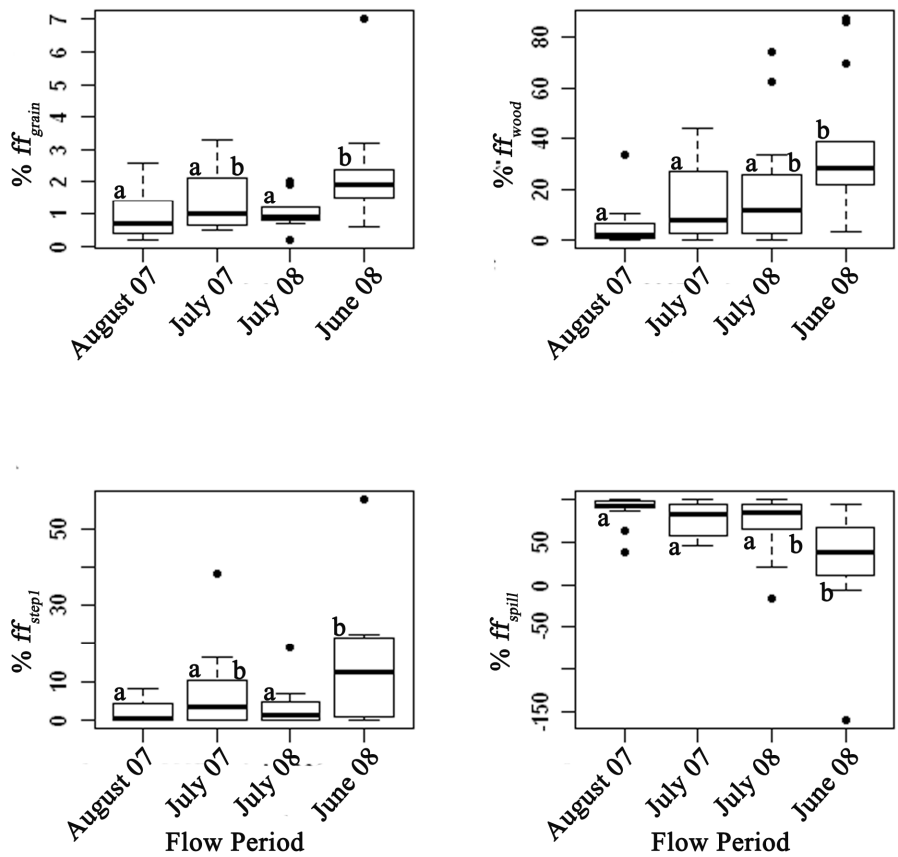


Figure 46: Boxplots of percentage contribution of each component of resistance for each flow period. ESL3 is excluded from the boxplots. Boxes with the same letter (a, b, c) have means similar at $\alpha = 0.05$.

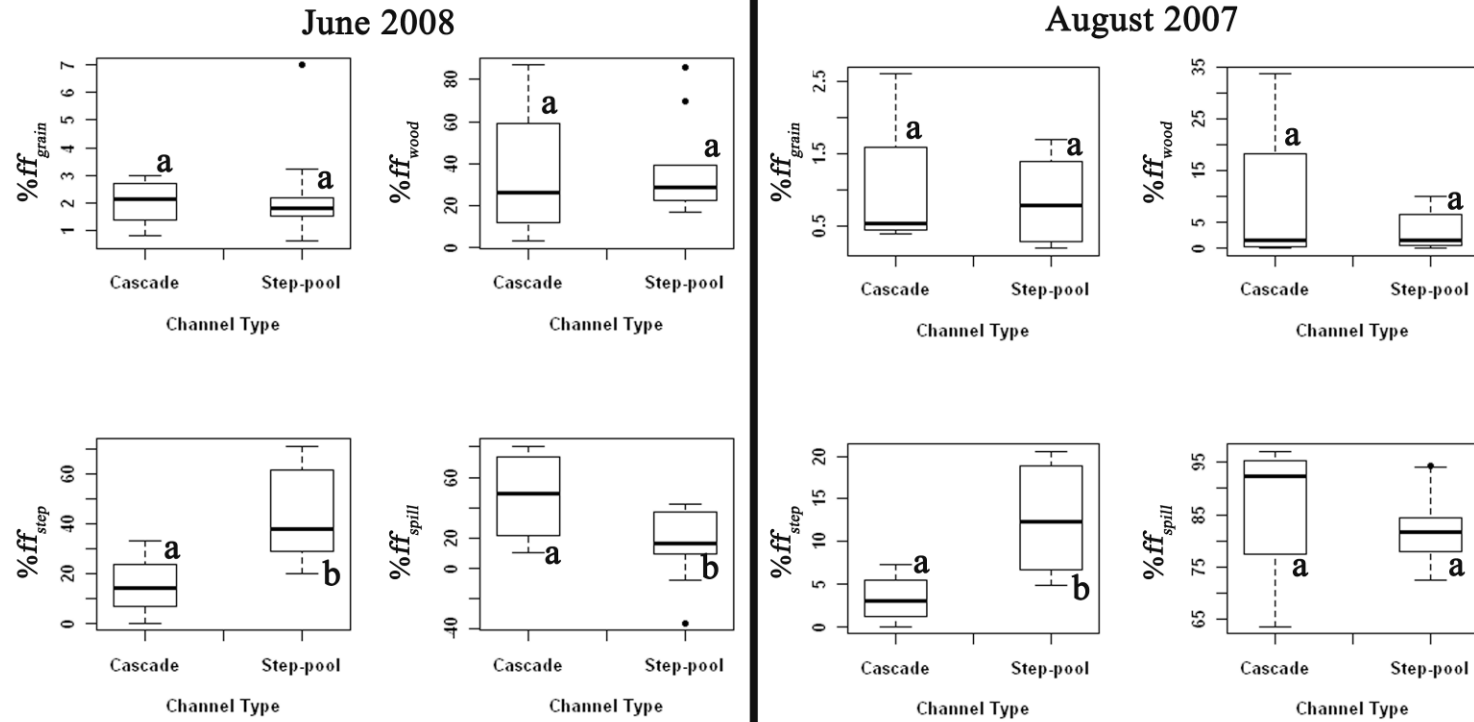


Figure 47: Boxplots showing the % of total resistance dominated by grain, wood, step and spill for each channel type. $\%ff_{step}$ has significantly different means for cascade versus step-pool reaches. Letters *a* and *b* indicate significantly different means using Tukey HSD test in an ANOVA.

On average, the major contributions towards ff_{total} are from ff_{wood} and ff_{spill} . As noted in the flume by Wilcox *et al.* [2006], the contribution from ff_{spill} is reduced during high flows (Figure 46). Otherwise, the contribution of each component (ff_{wood} , ff_{step} , ff_{grain}) is significantly larger during high flows.

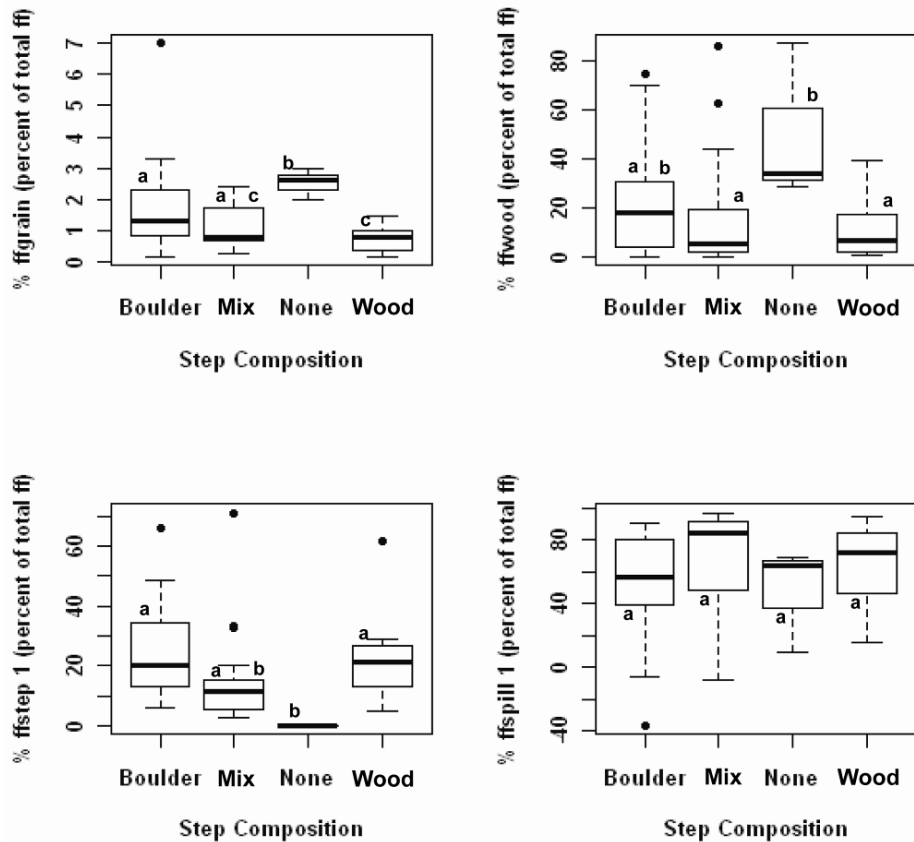


Figure 48: Boxplot of % contribution of each partitioned component divided by dominant step composition within the reach. Boulder = reach dominated by boulder steps; Mix = reach has a combination of wood and boulder steps; None = reach has no steps (only ESL7); Wood = Reach only has wood steps. ESL6 excluded from these groupings, but inclusion only increases difference between None and other categories. ESL3 is excluded because of the large deviation from ff_{total} due to the large number calculated for ff_{step} . Boxes with the same letter (a, b, c) have means similar at $\alpha = 0.05$.

6.4.6 Relationship of ff_{grain} , ff_{spill} , and ff_{step} to Q , and S_0 , and wood as well as interrelationship between components

Multiple regressions were used to evaluate the relationship between ff_{grain} and other control variables such as S_0 and Q . ff_{grain} was found to be significantly related to Q , S_0 and wood volume as well as wood surface area per channel surface area (Table 14). The value of ff_{grain} decreases with increasing Q and increases with increasing S_0 . The grain resistance decreases with the amount of wood in the reach. Wood increases the backwater in a reach, probably increasing the submergence of grains and thus decreasing grain resistance. The combined wood and boulder steps are larger and increase the backwater and storage of finer sediments. Another possibility is that the inclusion of wood in a reach causes finer sediment to be deposited, leading to increased ff_{wood} and causing a smaller amount of ff_{grain} because of the increased fines. This interaction can also be seen in Figure 48, where the $\%ff_{grain}$ is much smaller in reaches that contain only wood steps.

Table 14: Multiple Regression for ff_{grain} , n=59, df = 55, discharge log transformed to meet normality assumptions.

	Estimate	p-value	R ²	p-value
Intercept, β_0	0.056	< 0.001	0.58	< 0.001
$\log(Q)$	-0.008	< 0.001		
S_0	0.327	< 0.001		
Total Wood Volume	-0.051	< 0.001		

	Estimate	p-value	R ²	p-value
Intercept, β_0	0.057	< 0.001	0.67	< 0.001
$\log(Q)$	-0.011	< 0.001		
S_0	0.300	< 0.001		
Wood Surface Area/Reach Surface Area	-0.130	< 0.001		

ff_{step} was found to be significantly related to wood density (Table 15) and to slope while holding wood density and discharge constant (Table 16). It was not significantly related to discharge or grain size.

Spill resistance is the unmeasured component. The value of spill resistance may also contain other unmeasured components such as bank resistance and bends. The multiple regression in

Table 17 indicates that ff_{spill} is significantly related to Q and total wood volume at the $\alpha = 0.10$ level. The ff_{spill} was not found to be significantly related to the step grain size. Since ff_{spill} is the unmeasured component and is arrived at by subtracting the other components, it tends to mirror ff_{total} and the significant relationships found when evaluating ff_{total} .

Table 15: Linear regression for ff_{step1} vs. wood density (wood surface area/reach surface area).

	Estimate	p-value	R ²	p-value
Intercept, β_0	1.12	< 0.001	0.28	0.001
Wood Density	3.23	0.001		

Table 16: Multiple regression of ff_{step1} . Reaches without steps are excluded (ESL6, ESL7) and ESL3

	Estimate	p-value	R ²	p-value
Intercept, β_0	-0.14	0.78	0.42	0.001
Wood Density	2.83	0.003		
S_0	14.4	0.009		
Q	-0.25	0.66		

Table 17: Multiple regression for ff_{spill} (all reaches included, n=59)

	Estimate	p-value	R ²	p-value
Intercept, β_0	-6.75	0.02	0.60	< 0.001
$\log(Q)$	-5.53	< 0.001		
S_0	34.61	0.14		
Total Wood Volume	8.07	0.10		
Step D_{84}	-10.99	0.48		

The multiple regression of ff_{wood} indicates that the values are related to Q and S_0 (Table 18). As both increase, the value of ff_{wood} increases. The value of ff_{wood} increases with Q because as discharge increases more logs become submerged.

Wood resistance also seems to have a complex relationship with the grain size. Just as the submergence of grains may be increased by the presence of wood, the reverse can hold true as well. Larger boulders may cause pieces of wood to become submerged at lower flows by increasing roughness, decreasing velocity and thus increasing depth, causing higher values of ff_{wood} . Also, large boulders can create backwater areas where depth is increased and wood becomes submerged. Figure 49 shows that this may be true at higher flows, but at low flows there does not seem to be any relationship between grain size and ff_{wood} , most likely because the lower flows have depths too shallow to cause sufficient backwaters to submerge logs.

Table 18: Multiple regression with ff_{wood} (all reaches included, n=59)

	Estimate	p-value	R²	p-value
Intercept, β_0	1.20	< 0.001	0.32	< 0.001
$\log(Q)$	0.45	< 0.001		
S_0	7.14	< 0.001		

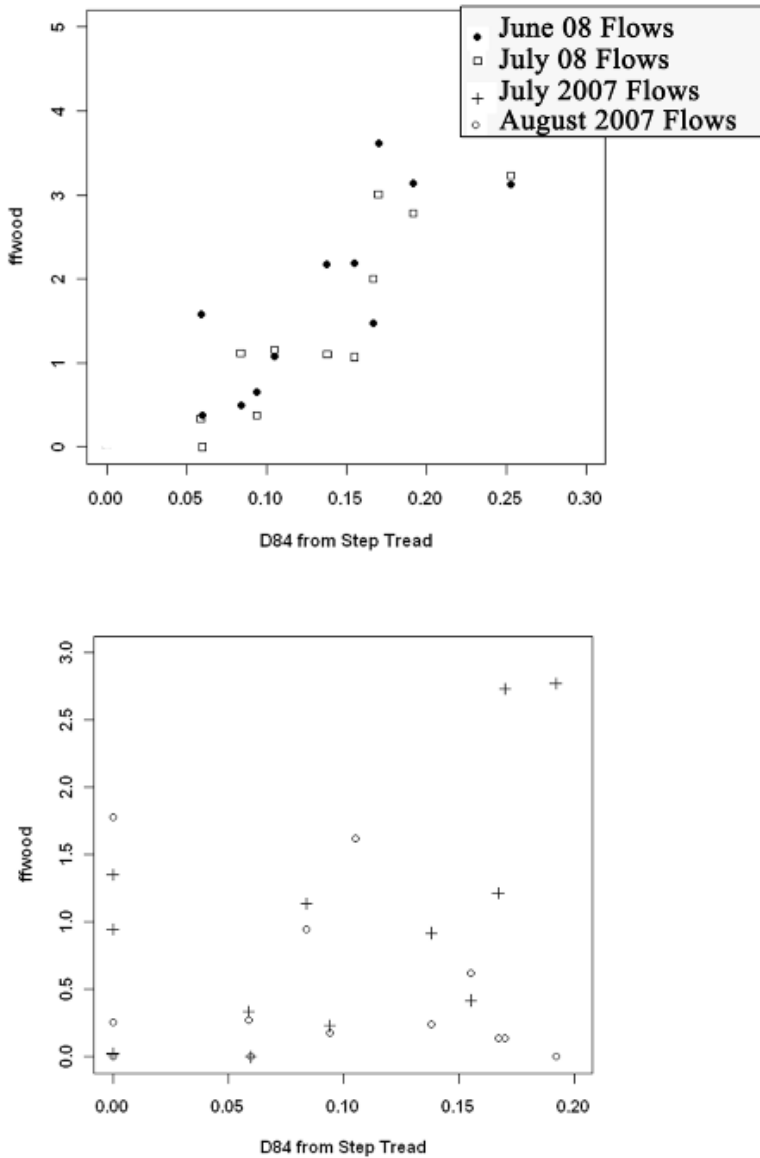


Figure 49: ff_{wood} vs. D_{84} from the step tread for each flow period, June and July 08 (top); July and August 07 (bottom).

6.5 Discussion

Ability to quantify the effects of each component of total resistance remains limited by the available methods. The methods discussed here assume that each component of resistance affects the total in isolation and that the individual components can be added to calculate ff_{total} [Wilcox *et al.*, 2006]. The unmeasured component remained the largest in most of our study reaches, particularly at lower flows. The

unmeasured component is assumed to be related to ff_{spill} , although it could also be related to bank resistance, which was neglected in this study. The results suggest that the current additive approach is not appropriate and that the unmeasured component tends to be large because individual sources of resistance interact in complex fashions that effectively alter the resistance associated with any individual component relative to the resistance of that component in isolation. Yet, the additive approach could be greatly improved if the error associated with many of the variables (e.g., C_D^{app}) used to calculate ff_{grain} , ff_{wood} , or ff_{step} was reduced.

6.5.1 Methods for calculating ff_{grain} and associated limitations

Each of the current methods used for calculating ff_{grain} may be appropriate for high flows, where the majority of the grains are submerged, but appear to completely underestimate the contribution of ff_{grain} during low flows. Low flows are distinct from other stages by having a majority of the larger bed material only partially inundated and a relative roughness $R/D_{84} \leq 1$. Although researchers have defined shallow flows as $R/D_{84} \leq 4$ [Ferguson, 2007], the reaches in this study are all below 4 at both high and low flows. Divisions for R/D_{84} should also vary based on gradient (CHAPTER 4) such that, for gradients closer to 0.10, the limit for shallow flows might lie closer to 1.5-2.0.

During low flows, the values of grain resistance increase, but the contributions towards ff_{total} decrease. Each of these equations is possibly underestimating ff_{grain} at low flows because of the inherent unsuitability of using an approach that assumes a logarithmic velocity profile [Wiberg and Smith, 1991; Katul et al., 2002]. Near-bed velocities remain low up to a grain size of D_{16} and increase rapidly when flow is above the range of D_{50} and D_{84} [Wiberg and Smith, 1991].

Despite these differences, I still found D_{84} to be a representative length scale and the relative roughness can be related to the nondimensionalized velocity (\bar{v}/u^*) by a log linear curve. Summing the contribution of each large grain over the entire reach using the drag force approach indicates that the contribution from ff_{grain} could be much larger than calculated by these equations (Figure 31). *Wilcox et al.* [2006] also found that both the *Bathurst* and *Parker and Peterson* equations consistently underestimated grain resistance.

The *Keulegan* equation, using both D_{50} and D_{84} , consistently underestimated ff_{grain} , which was determined by evaluating the contribution of $\%ff_{grain}$ to ff_{total} in the plane-bed reach. At the lowest flow, when the other sources of resistance are reduced by the lack of in-channel wood and reduced bank resistance, the $\%ff_{grain}$ was 4.9% (Figure 31). In contrast, the drag approach indicates that ff_{grain} makes up 33% of ff_{total} . The drag approach is probably also underestimating ff_{grain} since only a few larger grains were exposed at low enough flows to be surveyed in this reach using the LiDAR pointclouds. Smaller grain sizes probably start to affect the flow as stage decreases, so these should be accounted for in a drag approach. On the other hand, the *Keulegan* equation had a more precise relationship with ff_{total} and ff_{drag} at all flows, particularly when using the step tread D_{50} , despite the assumed lack of a logarithmic velocity profile (Table 10 and Table 11). The relationship between the *Keulegan* and ff_{drag} indicates that even with the use of a smaller grain size such as D_{50} , the *Keulegan* still captures a portion of the form drag component around the grains.

Flow accelerates on the step tread as it approaches the step lip [*Wohl and Thompson, 2000; Wilcox and Wohl, 2007*]. An interaction of processes is evident here; a

larger step causes a larger backwater area, allowing deposition of finer material and greater difference in flow acceleration between low and high flows. Reaches with large wood steps have finer material and larger rates of change of velocity with discharge (CHAPTER 5). Both grain resistance and ponding are significant at low flows and can drastically reduce velocity. The effect of grain resistance at those lower stages is not easily quantified by equations based on the law of the wall and a large characteristic grain diameter. There are two levels of resistance related to the presence of grains in the flow: 1) water flowing around large boulders creating areas of flow separation and reattachment; and 2) water flowing over smaller grains creating small surface waves and hydraulic jumps, which can also be defined as spill resistance over the grains. Since the spill resistance is caused by the presence of grains, we still define it here as grain resistance. Additionally, both levels include viscous skin friction around the grain. The first type of grain resistance may be best represented by a large characteristic grain size, D_{90} . *Parker and Peterson's* equation was significantly related to boulder concentration at high flows, indicating that a larger representative grain size captures the combined form drag and skin friction around individual boulders. The second grain resistance may be best characterized by D_{50} , since the *Keulegan* equation was significantly related to both the values determined from the drag force equation and the boulder concentration. The median grain size is more likely to remain submerged at lower flows.

Although sorting was not significantly related to ff_{total} (CHAPTER 4), the sorting may have a significant effect on the values of ff_{grain} at low flow. The larger boulders and smaller grains influence the overall hydraulics in a very different way at low flows. The flow around the boulders is retarded by drag and other resistance effects, whereas the

flow above the boulders can be unimpeded by these effects depending on submergence [Bathurst, 1993]. The flow structure in streams with large roughness elements is considered to be multilayered [Canovaro et al., 2007]. The lower layer of flow includes constant interaction between flow and roughness elements, thus causing the flow to slow from loss of momentum from the drag force around each element. In the upper layer, velocity increases at a higher rate with depth because of the reduction in shear stress where particles are submerged (Figure 41). In some reaches, or particular sections of the reach, the flow is constantly distorted by the protrusion of boulders at low values of relative submergence, meaning that the majority of the flow is in the lower layer (Figure 50). In both low and bank-filling flows in these reaches, the roughness elements affect the entire depth of flow in some form, either by the loss of momentum around the element or in the creation of surface wave drag and wake interference with other elements. Most studies focus on finding one representative grain size and determining a multiplier for that grain size to fit it into some type of Keulegan [1938] relation [Hey, 1979; Reid and Hickin, 2008]. In mountain streams, it is possible that two values of ff_{grain} should be estimated from two different representative grain sizes (e.g., D_{50} and D_{90}), as suggested by Ferguson [2007].

The spatial density and planform arrangement of boulders were found to be significantly related to flow resistance in a flume study [Ferro, 2003; Pagliara and Chiavaccini, 2006; Canovaro et al., 2007]. Canovaro et al. [2007] found that the flow resistance was maximized when the spatial density (Γ) was between 0.20 and 0.40. All the reaches, except ESL3, had a boulder concentration < 0.10 . This may be because in some reaches the boulders were concentrated in patches and the spatial density of each of

these patches needed to be calculated separately (Figure 51). ESL9 and FC3 in Figure 51 show examples of one step-pool reach that has fairly evenly distributed boulders and another reach (FC3) that really only has one large patch of boulders. Therefore, the value of boulder concentration may represent ESL9 fairly well, but not FC3. More boulders could be found in FC3 in the pools, but these were not exposed at low flows for the LiDAR scanner to pick them up. Also, the boulders in pools may increase turbulence by causing more flow separation and secondary circulation, but this does not necessarily contribute to grain resistance. *Pagliara and Chiavaccini [2006]* showed that the increase

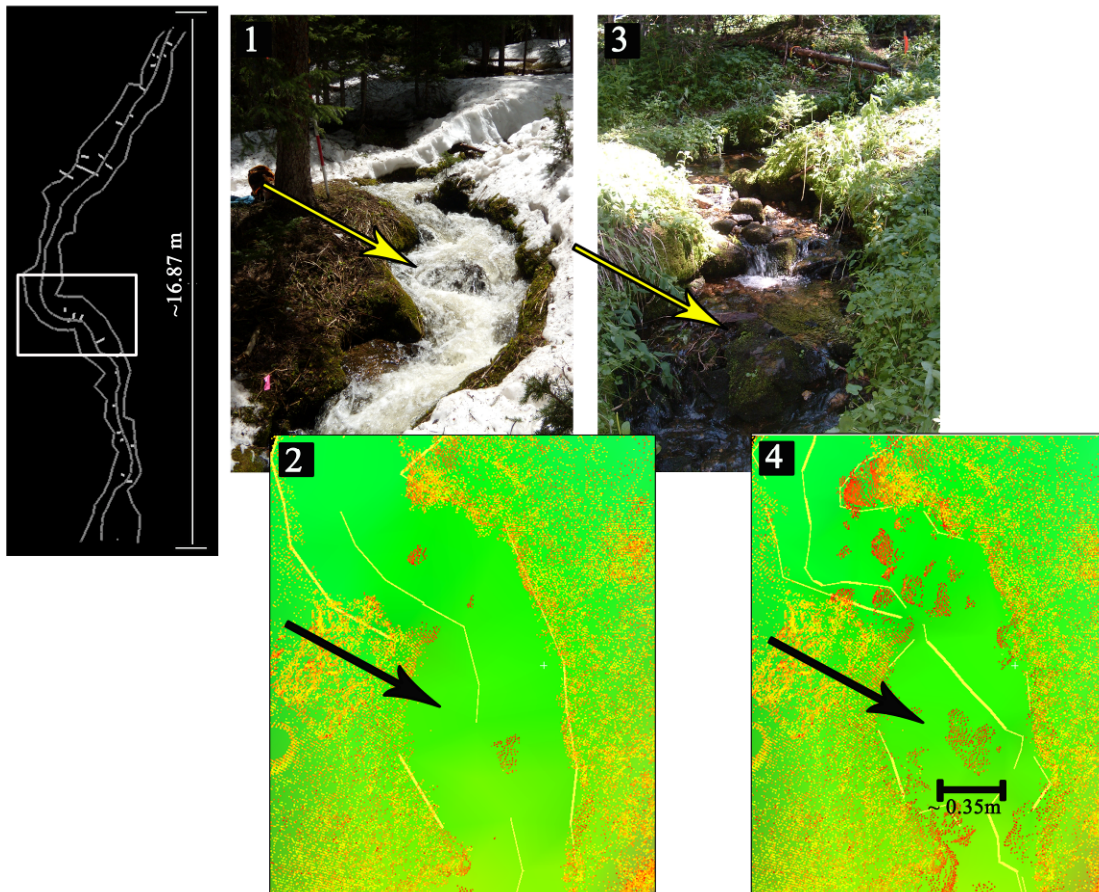


Figure 50: FC6 at low (1 - 2) and high (3 -4) flows. Picture at top left shows reach outline with small lines to indicate location of boulders. Arrows indicate same location on each image. Photograph and LiDAR image show exposure of more grains at low flows, as well as increased sinuosity of thalweg (light yellow line in center of channel).

in resistance because of boulders is related to a number of variables including boulder concentration (Γ), spatial arrangement, and surface roughness of boulders. *Ferro* [1999] and *Lawrence* [2000] found that $\Gamma < 50\%$ meant that the boulders were sufficiently spaced so that the wake of one boulder did not interfere with the wake of another. Since the reach length and width were used to find Γ , in some cases the value may be smaller than the actual spatial concentration of boulders (Figure 51). All the macro-roughness elements in FC3 are clustered together, indicating that these elements will probably interact with each other at both low and high flows. In the case of FC6 (Figure 50), the roughness elements are spaced so closely together and are so small in comparison to flow depth that skimming flow probably occurs at high flows. Also, resistance is increased at lower flows as the thalweg becomes more sinuous. The effect of sinuosity was not accounted for in this study, but could be significant, particularly in small channels with large macro-roughness elements that the flow has to circumvent. Therefore, the spacing between boulders significantly effects the relative contribution of each boulder towards total resistance and that spacing can be determined by the boulder concentration. In the case of a natural channel, where boulders tend to cluster together and are not evenly spaced, the boulder concentration may need to be calculated for individual sections of the reach and then averaged.

Considering the drastic reduction in ff_{total} in the plane-bed reach at high flows (13 times lower than August 2007 value), it is evident that grain resistance plays a much larger role at low flows than is calculated by any of the three relations (*Keulegan*, *Bathurst*, *Parker and Peterson*). *Lawrence* [2000] noted that the value of the C_D increased substantially when elements were only partially submerged. The values of C_D

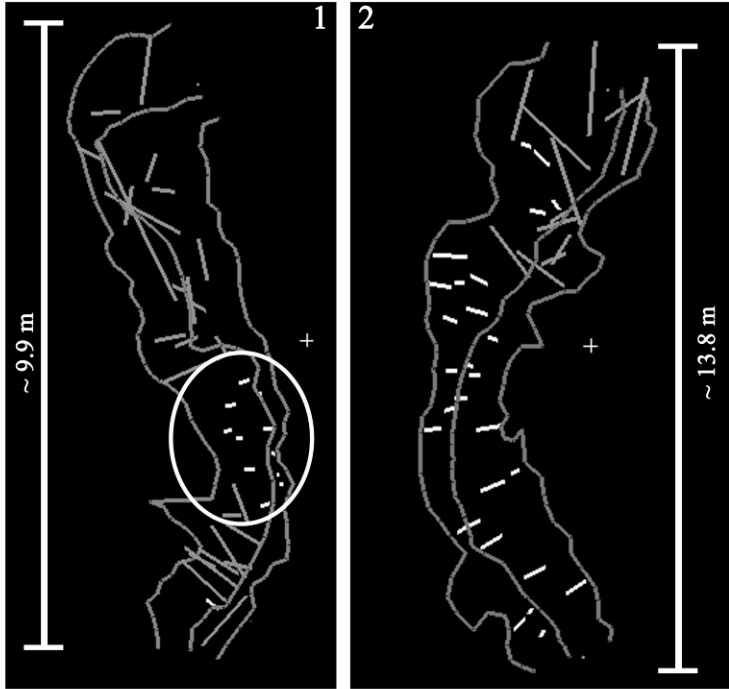


Figure 51: Boulders and wood on FC3 (1) and ESL9 (2). Boulders are shown in white and wood in grey. Banks and thalweg also shown in grey. The $\Gamma = 0.008$ for FC3 and 0.083 for ESL9.

ranged between 4.5 and 0.19. With higher values of percent cover, and essentially higher values of Γ , the drag coefficients were significantly smaller. *Lawrence* [2000] concluded that form drag alone could not account for the reduction in C_D when objects were partially inundated. *Lawrence* [2000] showed that greater boulder concentration led to more disturbance of the surface, with higher wave drag leading to increased energy dissipation in overland flow. The C_D is also related to other parameters such as the shape of the object, the Fr , and Re particle number. *Thorne and Zevenbergen* [1985] showed that although there is a significant difference in resistance around blocks versus hemispheres, the bed material is much more similar in shape in a channel, therefore the differences between objects in a reach would not be large based on shape.

Based on the analyses presented above, I recommend using the *Parker and Peterson* [1980] approach to calculate ff_{grain} in steep streams during bank-filling flows.

This approach is the least sensitive to morphological location of the pebble count because it uses such a large characteristic grain size, but it takes a much larger sample size pebble count to estimate D_{90} with the same accuracy as D_{50} . Also, the values of ff_{grain} for the *Parker and Peterson* equation were most significantly related to the boulder concentration at high discharges. At low flows *Keulegan* might be the better approach, despite being dependent on a logarithmic velocity profile. At low flows, the values of relative submergence (R/D_{84}) approach zero, with values ranging between 0.52 and 2.18. Using a smaller characteristic grain size at low flows will improve the validity of these equations. Also, the predictions at low flow may be improved by developing an equation that uses two characteristic grain sizes. One grain size should represent the larger bed elements that are only partially inundated and cause the flow to move around rather than over the objects. The second should represent the grains that are submerged but still cause distortions in the flow field. The difference between high and low flows is related to the relative submergence, Fr , and Re . The combined approach may be best utilized by adding the drag force component around boulders as large as the D_{90} . The *Keulegan* equation can be used for calculating the grain resistance related to skin friction and form drag along smaller, submerged grains. In step-pool reaches, the step tread grain size should be used to account only for grain resistance. Grains that are part of the actual step should be included as the ff_{spill} and ff_{step} components.

6.5.2 Methods for calculating ff_{wood} and associated limitations

The *Shields and Gippel* [1995] approach of calculating ff_{wood} was found to commonly overestimate the total value of ff_{wood} . Although the values of the C_D were well within the range found by *Gippel et al.* [1992], there is still some question as to what

appropriate values are in the field. The blockage ratio exceeded the range tested by *Gippel et al.* [1992], meaning that the empirically derived values of the coefficient, a , and exponent, b , used in Equation (6.14) may not be correct for these streams. In other studies the C_D has ranged from 1.2 [*Manga and Kirchner, 2000; Hygelund and Manga, 2003*] to 6.0 [*Curran and Wohl, 2003*], but Figure 43 shows that values over 1.0 often led to values of ff_{wood} that exceeded ff_{total} .

There are a number of problems with this approach revealed in this analysis. First, the *Shields and Gippel* [1995] approach assumes that ff_{wood} can be calculated for each individual log and then added to estimate total ff_{wood} . Second, the drag force approach does not account well for logs with branches or for the position of the log in the water column. Third, *Hygelund and Manga* [2003] found that C_D^{app} scaled with depth ratio (a measure of the relative depth of the log) more than with blockage ratio. Field observations indicate that logs near the surface contributed to surface wave drag. Also, logs on the channel bed and with diameters on a scale with the water depth locally increased water depth and created a significant backwater effect. Conversely, logs that were near the water surface and only in the flow during high flow conditions may create a large increase in velocity beneath the log and a hydraulic jump above the log, causing localized supercritical flow (Figure 52). Fourth, the drag force approach did not do well in capturing the wake effect from upstream objects, which may reduce the effect of the log downstream. Fifth, the distance between objects, X , is difficult to determine since there is no standardized approach for evaluating X . Also, the more closely spaced objects were, the higher the value of ff_{wood} . This approach assumes that the drag force is applied

over a short distance, but does not account for the effect of the wake interference from the upstream object, which could cause reduced drag on the downstream object (Figure 44).

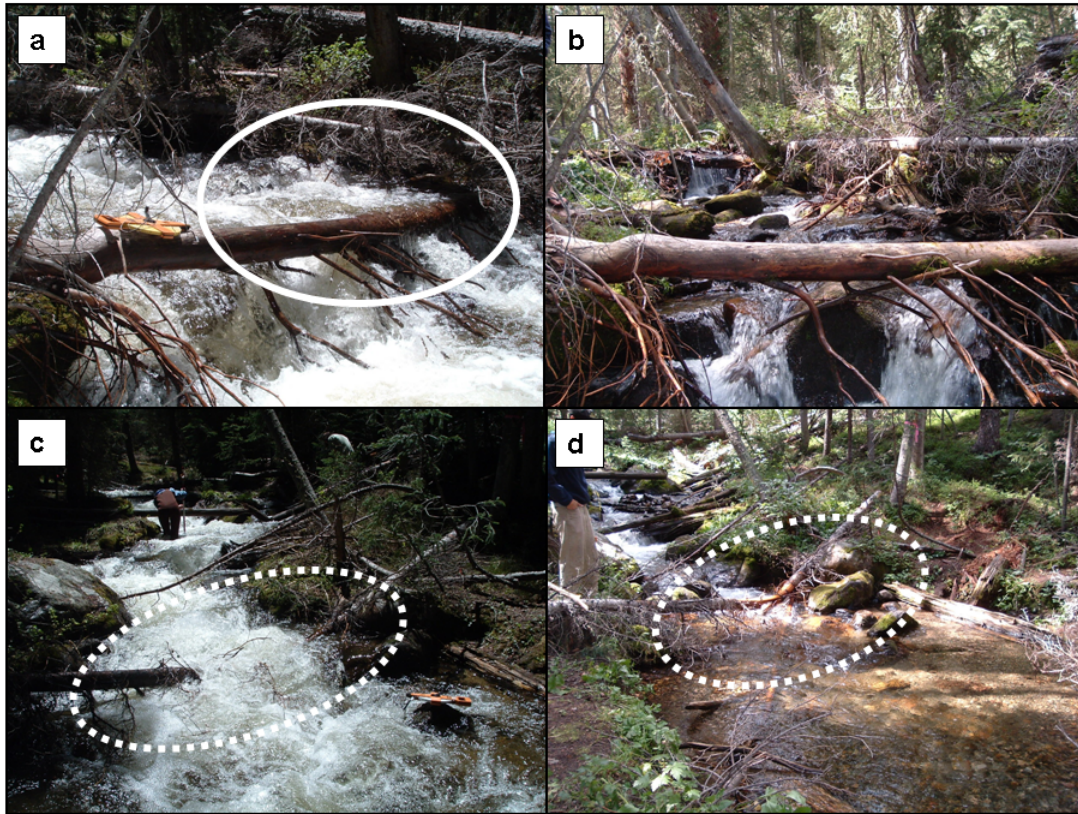


Figure 52: Examples of individual pieces of wood in the study reaches. Note that these pieces are only in the flow during high flow. a) ESL5 June 2008 – log that crosses over stream and creates a slight backwater on left bank side of log. b) ESL5 August 2007 – same log, but now water goes completely underneath the wood. c) ESL2 June 2008 – broken log with water cascading over the top. d) ESL2 August 2007 – same log, but water now flows completely underneath.

6.5.3 Methods for calculating ff_{step} and associated limitations

Many researchers have found that step height and length are both significantly related to the ff_{total} in step-pool channels [Abrahams *et al.*, 1995; Maxwell and Papanicolaou, 2001], but both H_s and L_s are assumed to only be related to ff_{spill} . Smart *et al.* [2002] argue that the form drag around bedforms is not as significant as form drag around individual particles, since the individual particles are of the same size as the flow

depth. This may be true, depending on the size of the bed elements relative to the flow depth, but does not explain the paucity of data on evaluating the form drag around the step and pool bedforms, rather than just the spill resistance. Random arrangements of boulders dissipate much less energy than boulders arranged in rows [Pagliara and Chiavaccini, 2006]. The results of an analysis of the drag force around the step bedforms indicate that as the bedform becomes increasingly submerged and the flow approaches a skimming flow, a wake can develop around the bedform, increasing the form resistance at higher flows (Figure 27 and Table 12). As grains on step treads and even in the pools protrude further into the flow with decreasing stage, the effect of the bedforms may disappear relative to the effect of the grains and from nappe flow increasing spill resistance over the step. The conflicting interpretations from previous studies suggest that systematic evaluations of form drag around bedforms in relation to varying stage are needed, particularly when steps are more closely spaced together.

The wood jams that make up a number of steps create added drag depending on the porosity of the jam. Increased porosity leads to increased flow through the jam and increased shear stress applied to the bed downstream from the jam [Manners *et al.*, 2007]. The jam that Manners *et al.* [2007] studied did not create a step, as jams tend to in high gradient channels, but further work is needed on how flow through and over steps varies the drag force and contribution of the step to ff_{total} . Manners *et al.* [2007] also suggested that the jam geometry is inextricably linked with the drag coefficient, meaning that a combined value needs to be calculated for each jam. Since local velocities were not measured, this was not attempted in these reaches, but may be important to consider in future work.

6.5.4 Methods for calculating ff_{total} and associated limitations

The major sources of error in calculating ff_{total} are in the measurement of R_h , V , and S_f . Surveys become less precise with higher gradient channels, although the LiDAR together with a detailed bed survey were used to reduce the error as much as possible [Ferguson, 2007]. Reach-average velocity measurements were made to reduce error in measuring velocity. *Wiberg and Smith* [1991] showed that, despite an s-shaped profile, mean velocities could still be calculated with measurements taken from 0.6 of the flow depth. *Comiti et al.* [2007] also noted a large discrepancy (0.3 to 2 times) between the measured flow depth and the back-calculated flow depth from continuity in steep streams. The values for calculating ff_{total} were 20% larger when using reach-average depths versus cross-section surveys. Grain size measurements have high errors in boulder bed streams where it is difficult to see the whole grain. *Ferguson* [2007] reported that errors could be anywhere from $\pm 10\%$ to $\pm 20\%$.

6.5.5 Relationships between ff_{grain} , ff_{wood} , ff_{step} , and ff_{spill} and potential control variables

The interrelationships between each component of resistance can be complex. Wood in channels creates backwaters, particularly during high flows, increasing depth and further reducing the influence of grain resistance. On the other hand, larger grains may cause a backwater effect that causes wood to be submerged and the effect of ff_{wood} to be reduced. Grain, step and spill resistance were all found to be significantly related to wood density. Grain and wood resistance were both significantly related to discharge and bed gradient, but ff_{step} was only significantly related to bed gradient. Each component of resistance increases with bed gradient while holding discharge or wood density constant.

Step resistance is larger when there is a greater density of wood in the channel. Figure 33 shows that steps that include a combination of wood and boulders have significantly higher drops and are significantly wider. The step dimensions are then directly related to any drag force that is created by the bedform. In terms of ff_{spill} , the drop height over the step is highest at low flows, maximizing the effectiveness of the steps [Chin, 2003]. Therefore, the same steps with the highest ff_{step} values at high flows should also have the highest values of ff_{spill} at low flows. At lower flows it is expected that the step bedform will become less significant relative to macro-roughness elements on the step tread and in the pools, as well as increased thalweg sinuosity, ponding and increased ff_{spill} [Bathurst, 1982b].

The August 2007 data for FC3, FC4, FC5, and FC6 were commonly found to be outliers. Although Re and Fr cannot be directly related to ff_{total} , because of inherent interrelationships, these reaches stand out in that they all have the lowest values of both Re and Fr (Figure 53). The relationship between C_D and flow changes at lower values of Re and Fr . The Fr is used to account for energy losses from the distortion of the free surface when boulders protrude through the surface [Bathurst, 1993]. Flammer *et al.* [1970] found that for a relative submergence < 4 , the C_D generally decreased with increasing Fr . Above relative submergence values of 4 the C_D does not vary with the Fr . Drag coefficient has also been found to significantly vary with Re below 10^4 for both grains and wood [Shields and Gippel, 1995]. Above 10^4 , drag coefficient remains fairly constant. The relationship between ff_{total} and the Re and Fr could not be tested because of the inherent interrelationship between these variables, but for FC4, FC5 and FC6 the low

calculated values of Re and Fr may indicate that the error is much higher for the calculation of drag force around objects and steps at the lowest flows.

Largely ignored in this analysis are resistance related to flow sinuosity and banks. Each of these roughness elements are subsumed in the ff_{spill} term. At lower flows, the thalweg becomes increasingly sinuous, which can also cause an increase in ff_{total} .

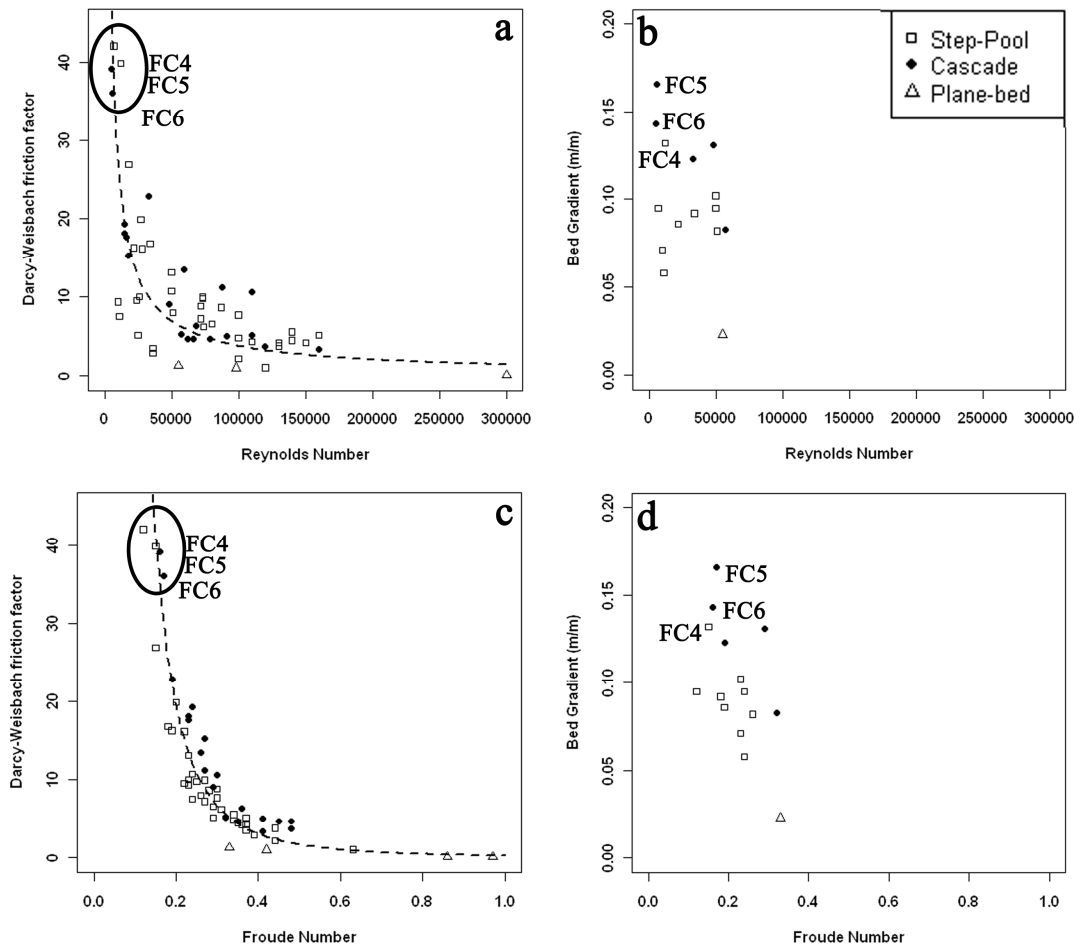


Figure 53: Reynolds number and Froude number versus Darcy-Weisbach friction factor (a and c) and S_0 (b and d); a and c show all the reaches during all measured flows. The circled reaches have the lowest value of both Fr and Re during August 2007 flow period. Portions c and d show reaches only during August 2007 flows. The R^2 for the best-fit line in a is 0.54 and in b is 0.85.

6.6 Conclusion

The method of additive partitioning does not work for high gradient step-pool and cascading streams. Problems were identified even in the calculation of ff_{wood} in the smaller and less complicated plane-bed reach. Each method for calculating each component had many problems and limitations once applied to these steep streams with large wood contributions. It was difficult to evaluate which method of calculating ff_{grain} worked the best, since there is no standard to compare the values against. The *Parker and Peterson* equation seemed to better represent ff_{grain} at high flows based on its relationship to boulder concentration at higher flows and the insensitivity of the equation to the morphologic position of the grains. On the other hand, the *Bathurst* equation is more often preferred because it is based on a power relationship and not a logarithmic relationship. No correlation was found between the *Parker and Peterson* equation and boulder concentration for ff_{grain} from form drag at low flows. The *Keulegan* equation using both D_{84} and D_{50} had the closest relationship with some of the physical descriptors related to grain resistance, but could still be underestimating the actual values of ff_{grain} . The values were always the smallest at both low and high flows, but at low flows the *Keulegan* equation was significantly related to both boulder concentration and ff_{grain} from the drag approach. The *Keulegan* equation would therefore be a conservative lower estimate of ff_{grain} at low flows, but more work needs to be done to determine how best to calculate grain resistance when $R/D_{84} \ll 1$.

The lower flow regime may create problems in calculating drag around objects because of the variation in the drag coefficient with $Re < 10^4$. Low flows are identified as those with $R/D_{84} < 1$, $Fr < 0.3$, and $Re < 10^4$. The relative submergence of the step, in

relation to nappe, submerged nappe, and skimming flows, may be significant when determining separate contribution from ff_{step} and ff_{spill} . During low flows the effect of ff_{spill} just downstream of steps and ff_{grain} on step treads may begin to dominate ff_{total} . Also, at lower flows the drag coefficient can vary drastically with small changes in both the Fr and Re , meaning that the use of a constant drag coefficient in the above calculations may mean a higher error in values of ff_{grain} (from drag approach), ff_{step} and ff_{wood} . More work needs to be done to understand how form drag around step bedforms contributes to flow resistance.

The drag method for calculating ff_{wood} was applied to individual logs in the channel, but the large number of variables in which there is uncertainty allows large sources of error. The distance between logs, X , should be better defined for natural channels where there are other large sources of resistance. Nonetheless, the contribution of ff_{wood} towards ff_{total} was higher than expected for many of the reaches based on field observations. The value of ff_{wood} was highly dependent on discharge, since at lower flows very few logs were effectively within the flow. Also, values of C_d from low-gradient flumes do not necessarily apply well to wood in high-gradient channels. More work is needed to measure values of C_d in the field. Physically-based methods for estimating spill resistance and partitioning of resistance that include the interactions among components are also needed. Flume experiments may be particularly helpful in developing new methods and numerical simulations applicable to high-gradient channels.

In quantifying ff_{total} , there are large potential sources of error in the measurement of R_h , S_f and V . The tracer method is considered to be an appropriate method of obtaining mean velocity with a low source of error, therefore this is not considered the largest

source of error. There are a number of ways that the slope could be calculated and surprisingly the RMSE was fairly low between the methods (from 0.46 to 2.061). The highest RMSE was when an average step gradient was used. The step gradient was only used to demonstrate how large the error can be depending on the section of reach where measurements are made. The second highest error was related to the use of the effective R_h . The discharge measured in the gage just downstream of each of these reaches was often smaller than the discharge calculated using the continuity equation and the mean reach velocity and cross-sectional area. Assuming that the error for the mean velocity measurement is small, the error would then have to be in the reach average cross-sectional area. Field observations showed a significant amount of flow separation and backwater in these reaches, indicating that perhaps an effective R_h should be used rather than the measured average R_h . More work should be done in a step-pool reach with banks that regularly expand and contract downstream, to determine if there is an effective flow area for which ff_{total} should be calculated rather than the whole flow area. Also, for the sake of comparison between research projects, a standard approach should be determined for calculating S_f based on field measurements. The water surface slope found from a reach regression line seemed to work fairly well and maintain a low error.

CHAPTER 7 CONCLUSIONS

Gradient (S_0) is a dominant channel characteristic that influences variations in ff among all the reaches. Gradient was found to be a significant control in each component of my study, controlling variations in ff_{total} throughout the channel network, variations in the rates of change of velocity with discharge at-a-station, and variations in the values of ff_{grain} , ff_{step} and ff_{wood} . Gradient is related to all other potential control variables such as grain size and channel type, but these other variables were not necessarily significantly related to ff . It is important to understand how S_0 is related to ff and other stream characteristics, since this is a metric that can be used to remotely predict these characteristics as the resolution of remote data improves with time [Wohl *et al.*, 2007]. The values of ff_{total} were found not to vary significantly between step-pool and cascade channels, but were significantly different in plane-bed reaches. Therefore, even though the components of resistance may vary based on channel type, the overall values of the combined flow resistance were not significantly different based on channel type.

Similar to Comiti *et al.* [2005] and Ferguson [2007], q^* was found to be an appropriate measure for evaluating variations in flow resistance with discharge. Each relative submergence variable (R/D_{84} , R_r/H , R/s_{bed}) was found to explain a significant amount of variation in ff_{total} . The significant relationship between each type of relative submergence variable differed based on channel type, mirroring the significance of the calculated components of resistance. The relative submergence of the characteristic grain size (R/D_{84}) was found to be significantly related to ff_{total} in cascade reaches, but not in step-pool reaches. Alternatively, the relative submergence of the step height was

significant in step-pool reaches. These results mirror the larger values of ff_{grain} found in cascade reaches and larger values of ff_{step} in step-pool reaches, although the percent contribution of ff_{grain} towards ff_{total} was not significantly different in cascade versus step-pool reaches.

Methods for partitioning flow resistance into components of ff_{grain} , ff_{wood} , ff_{step} and ff_{spill} were found to have high sources of error and to be in need of more detailed flume and field studies to specify drag coefficients for partially submerged bed elements. The significance of different forms of resistance varied based on step type and discharge. Values for the lowest measured flows, in August 2007, were most often significantly different from the highest, bank-filling flows (June 2008). The intermediate flows (July 2007 and July 2008) were often significantly similar to June or August flows, depending on the variable being analyzed. The percent contribution for each source of resistance was determined to be significantly different for reaches with boulder steps versus wood steps.

The statistical analysis from CHAPTER 4 and the partitioning in CHAPTER 6 both showed how the different sources of resistance interacted. The inclusion of wood commonly caused variations in the contribution of other sources of resistance. Inclusion of wood in a reach could increase roughness, causing a decrease in velocity and a corresponding increase in depth. This could then lead to a decrease in grain resistance as grains become submerged from the increase in depth (CHAPTER 6, Table 14). Also, wood in steps causes higher and wider steps, creating larger dam pools as well as plunge pools. In both cases, total flow resistance increases, decreasing the ability of the reach to transport sediment and causing finer sediment to be deposited, as well as causing overall

values of ff_{grain} to be smaller in these reaches. The total wood load explained more of the variability in ff_{total} in cascade reaches (Chapter 4), most likely because there is much larger variation in wood load in these reaches versus step-pool reaches.

Channel type is a significant explanatory variable only if flow period, q^* , and S_0 are held constant in the regression (CHAPTER 4). Therefore, at particular flows and S_0 there are significant differences between step-pool and cascade reaches. The overall values of total ff in step-pool reaches were higher than in cascade reaches for a given S_0 and flow period. The plane-bed reach was consistently different from all other channel types. These differences suggest that each channel type may need to be accounted for separately when developing equations to predict ff . The interrelationship between S_0 , D_{84} , H_s/L_s , wood load, and channel type means that S_0 may be able to be used to remotely determine channel features. Further work should be done to consider whether separate resistance equations could then be applied to those channel types determined from remote data.

At-a-station hydraulic geometry is an important tool to use to help in our understanding of resistance in steep mountain streams. The hydraulic exponents at the East St. Louis and Fool Creek sites were all within the range of values found by other researchers studying step-pool, cascade and plane-bed reaches. The exponents could not be used to delineate a difference between the three channel types, but may be useful in determining which reaches are dominated by grain resistance versus form resistance. For most study reaches, $m > f > b$, indicating that the rate of change of velocity with discharge is greater than the rate of change of width or depth. This reflects the fact that increasing discharge in these steep, laterally confined streams results mainly in reduced

effective hydraulic resistance as sources of grain and form roughness occupy a progressively smaller portion of the flow. The at-a-station results show that there are 6 reaches with $m > f + b$ (ESL2, ESL6, FC1, FC4, FC5, FC6). I hypothesized that these reaches had similar values because they were all dominated by grain resistance, although further analysis indicates that the relationship may be more complex. The lower gradients of ESL2, ESL6, FC1 and the smaller surface area of FC5 and FC6 may mean that skimming flows develop over the grains found in these reaches, changing the characteristic of flow resistance in these reaches. Also, FC4, FC5 and FC6 were found to have much lower values of Re and Fr at low flows than any other reaches, causing the drag coefficient to vary with both Re and Fr , rather than remaining constant. The percent contribution of ff_{grain} and overall values of ff_{grain} were not found to be significantly larger in all of these reaches combined than in any other reach, therefore I hypothesize that the similarities are related to how the flow interacts with bed elements.

On the other hand, it was difficult to evaluate which method of calculating ff_{grain} worked best, since there is no standard against which to compare the values. The *Parker and Peterson* equation seemed to better represent ff_{grain} at high flows, but no correlation was found between this equation and boulder concentration for ff_{grain} from form drag at low flows. The *Keulegan* equation using both D_{84} and D_{50} seems to be a conservative way to evaluate grain resistance in these types of channels. The values were always the smallest at both low and high flows, but at low flows the *Keulegan* equation was significantly related to both boulder concentration and ff_{grain} from the drag approach, indicating that this equation may provide a lower bound of grain resistance at all flows.

Low flows are identified as those with $R/D_{84} < 1$, $Fr < 0.3$, and $Re < 10^4$. The low flow regime also has distinct nappe flow with an unsubmerged jet over every step in the reach. Each of these characteristics affects some characteristic of flow resistance. The nappe flow over a large step causes increased ff_{spill} . Both the Fr and Re are related to the drag coefficient. At low values of Re the drag coefficient changes with Re , meaning that the use of a constant drag coefficient in the above calculations may result in a higher error in values of ff_{grain} (from drag approach), ff_{step} and ff_{wood} . The effect of adverse pressure gradients around the step bedform is most likely more significant at higher flows when the bedform is submerged. During low flows, the effect of ff_{spill} just downstream of steps and ff_{grain} on step treads may begin to dominate ff_{total} . More work needs to be done to understand how form drag around the bedform of the step contributes to flow resistance. A flume study would probably be the best route, since other forms of resistance can be controlled.

Therefore, gradient is the dominant controlling variable influencing total resistance over all channel types and components of resistance. Discharge is also significant in varying how different components of resistance interact and controlling the submergence of large bed elements by changing flow patterns over boulders and logs from flow lines forced to separate around the object to skimming flows over the object. Changes in the submergence of larger elements also cause the relationship between the drag force and each of these elements to change. Further work needs to be done to understand and quantify individual components of resistance as well as understanding how these components interact. Understanding of the components will help in further developing predictive equations for calculating ff_{total} in steeper channels. Suggestions for

future research are below.

7.1 Suggestions for Future Research

More flume studies are needed on both step-pool and cascade channel types. Much work seems to focus on averaging variables over reaches, whereas the spatial variability may be the most significant characteristic of these reaches. When considering larger bed elements such as logs and boulders, I noted that in some reaches these elements seemed somewhat evenly spaced, whereas in other reaches these elements were clumped together in specific sections of the reach. Existing work on the effects of individual logs more commonly spaces the logs evenly, making it easy to calculate X in a flume, but difficult in the field. Therefore, flume work that specifically investigates the effect of the heterogeneity of wood and boulder location would be useful in further understanding how ff changes in a natural setting based on the spatial distribution of large roughness elements.

The concentration of boulders was also averaged over the reach, but further evaluation showed that a large boulder by itself would have a very different effect on the flow than a cluster of boulders. A reach average of this value tended to lead to small numbers for the concentration (Appendix E). Further work should be done in the flume, coupled with field work, to measure velocity and drag force at different flows. Particularly, more work needs to be done to understand how to calculate drag around a partially submerged boulder.

Steps in a reach contribute a significant proportion to the total resistance from both ff_{spill} and ff_{step} . The pressure differential around the bedform of the step is typically

ignored in favor of lumping the unmeasurable component into ff_{spill} . Although the importance of this may vary based on the step type, step spacing, and size of bed material on the step tread, more work should be done to evaluate this. Further work should be done in a flume, using a smaller model of a field measured step-pool reach, to evaluate whether the bedform without the grains contributes to total resistance. There is still no accepted method of calculating ff_{spill} , so even in this setting it may be hard to separate ff_{step} from ff_{spill} . However, a step-pool reach without an upstream pool (with an adverse bed gradient) can be compared to a step-pool reach that has an upstream pool. The channels should be compared at both low and high flows to determine whether the value of ff_{step} becomes less significant as ff_{spill} dominates at lower flows. Once these values are measured in the flume, then grains should be added to the step treads to evaluate the effects of both large and small grains on ff_{total} . In this way the interaction between ff_{grain} and ff_{step} can be assessed.

Another question to investigate in the flumes is to assess the effect of large boulders in the downstream plunge pools on turbulence, ff_{spill} and ff_{total} . The presence of these boulders was noted in a number of plunge pools, but the overall effect on turbulence has not been previously reported.

The effect of porosity of wood steps, versus reaches with only boulder steps, is another component that can be investigated more easily in a flume. Wood steps were found to create more diverse flow paths and, particularly at low flows, cause water to flow through sections of the step rather than directly over the step. At higher flows this may not be as significant; where the water takes a straighter path through the channel. The intricate pathways during lower flows over these steps may be part of the reason

values of ff_{total} were much higher in particular reaches with wood steps (e.g., FC3). When a reach contained a boulder step, flow generally moved over the step in a similar manner between low and high flows, although sometimes flow lines diverged to move around individual boulders rather than over them all. Therefore, more work needs to be done to investigate how the divergence of pathways over steps affects the total resistance. This can be most easily done in a flume where different step forms are created and discharge can be held constant.

More work could also be completed with regard to different methods of calculating ff_{total} . Typically, methods of determining S_f and R_h are not reported in the literature, but there can be large sources of error depending on the method used, particularly in determining hydraulic radius. Therefore, I suggest flume work combined with modeling work to further investigate the individual methods used to calculate the variables in the Darcy-Weisbach equation.

Much work so far has focused on predicting ff_{total} at high flows, but understanding variations in ff_{total} at base flows may be extremely important for stream rehabilitation applications that are interested in maintaining healthy aquatic ecosystems. Therefore, even though the system appears to be much more complex at low flows and difficult to characterize, much more work needs to be done in the range where the relative submergence is much smaller than one and flow is more commonly going around objects than over them.

Additionally, the effect of banks, bends, and channel sinuosity on roughness was ignored in this investigation. Further field work should be conducted to investigate how each of these components affects ff_{total} . The interaction between the bed and banks may

also be significant. A rougher bed may divert flow towards the banks, causing the banks to become rougher, subsequently further decreasing velocity in these channels.

Generally, high gradient channels have a much lower sinuosity than low gradient systems, but channel bends may still cause dissipation of energy and a decrease in velocity. Appendix F shows some preliminary data indicating that some of the reaches were located along significantly larger bends in the overall channel than others. Further work needs to be done to understand the effects of these larger bends.

CHAPTER 8 REFERENCES

- Abbe, T. B. and D. R. Montgomery (1996), Large woody debris jams, channel hydraulics and habitat formation in large rivers, *Reg. Riv. Res. Man.*, 12, 201 – 221.
- Aberle, J., and G. M. Smart (2003), The influence of roughness structure on flow resistance on steep slopes, *J. Hydraul. Res.*, 41, 259 – 269.
- Abrahams, A. D., G. Li, and J. F. Atkinson (1995), Step-pool streams: adjustment to maximum flow resistance, *Water Resources Research*, 31, 2593 – 2602.
- Baiamonte, G. and V. Ferro (1997), The influence of roughness geometry and Shields parameter on flow resistance in gravel-bed channels, *Earth Surface Processes and Landforms*, 22, 759 – 772.
- Bates, B.C. (1990), A statistical log piecewise linear model of at-a-station hydraulic geometry, *Water Resources Research* 26, 109 – 118.
- Bathurst, J.C. (1982a) Flow resistance in boulder-bed streams, in *Gravel-bed Rivers*, edited by R. D. Hey, J. C. Bathurst and C. R. Thorne, pp. 443 – 465, John Wiley, Hoboken, N. J.
- Bathurst, J. C. (1982b), Theoretical aspects of flow resistance, in *Gravel-bed Rivers*, edited by R. D. Hey, J. C. Bathurst and C. R. Thorne, pp. 83 – 108, John Wiley, Hoboken, N. J.
- Bathurst, J. C. (1985), Flow resistance estimation in mountain rivers, *J. Hydr. Eng.*, 111, 625 – 643.
- Bathurst, J. C. (1986), Slope-area discharge gaging in mountain rivers, *J. Hydr. Eng.*, 112, 376 – 391.
- Bathurst, J. C. (1993), Flow resistance through the channel network, in *Channel Network Hydrology*, edited by K. Beven and M. J. Kikby, pp. 69 – 98, John Wiley, Hoboken, N. J.
- Bathurst, J. C. (2002), At-a-site variation and minimum flow resistance for mountain rivers, *J. Hydrol.*, 269, 11 – 26.
- Bjerklie, D.M., S.L. Dingman, and C.H. Bolster (2005), Comparison of constitutive flow resistance equations based on the Manning and Chezy equations applied to natural rivers, *Water Resources Research*, 41, W11502.

- Bray, D.I. (1982), Flow resistance in gravel-bed rivers, in *Gravel-bed Rivers*, edited by J. C. Bathurst, and C. R. Thorne, 517 – 542 pp., John Wiley, Chichester.
- Buffington J.M. and D.R. Montgomery (1999), Effects of hydraulic roughness on surface textures of gravel-bed rivers, *Water Resources Research*, 35, 3507 – 3521.
- Calkins, D. and T. Dunne (1970), A salt tracing method for measuring channel velocities in small mountain streams, *Journal of Hydrology*, 11, 379 – 392.
- Canovaro, F. and L. Solari (2006), Flow resistance associated to a schematic step-pool pattern, in *River Flow* edited by L. Ferreira, Alves and Cardoso, volume 1, pp. 1005–1011.
- Canovaro, F., E. Paris, and L. Solari (2007), Effects of macro-scale bed roughness geometry on flow resistance, *Water Resources Research*, 43, W10414, doi:10.1029/2006WR005727.
- Chang, H.H. (1980) Geometry of gravel streams, *Journal of Hydraulics Division American Society of Civil Engineers*, 106, HY9, 1143 – 1156.
- Chanson, H. (1994), *Hydraulic Design of Stepped Cascades, Channels, Weirs and Spillways*, 261 pp., Elsevier, New York.
- Chanson, H. and L. Toombes (2002), Experimental investigations of air entrainment in transition and skimming flows down a stepped chute, *Canadian Journal of Civil Engineering*, 29(1), 145 – 156.
- Chartrand, S. M. and P. J. Whiting (2000), Alluvial architecture in headwater streams with special emphasis on step-pool topography, *Earth Surf. Processes and Landforms*, 25, 583 – 600.
- Cherry, J. and R. L. Bescheta (1989), Coarse woody debris and channel morphology: a flume study, *Water Resour. Res.*, 25, 1031 – 1036.
- Chin, A. (2003), The geomorphic significance of step-pools in mountain streams, *Geomorphology*, 55, 125 – 137.
- Church, M., and A. Zimmerman (2007), Form and stability of step-pool channels: research progress, *Water Resour. Res.*, 43, W03415, doi:10.1029/2006WR005037.
- Comiti, F., D. Cadol, and E. Wohl (2009), Flow regimes, bed morphology, and flow resistance in self-formed step-pool channels, *Water Resources Research*, 45, W04424.
- Comiti, F., A. Andreoli, L. Mao, and M. A. Lenzi (2005), Morphological effects of local scouring in step-pool streams, *Earth Surf. Processes and Landforms*, 30(12), 1567 – 1581, doi:10.1002/esp.1217.

- Comiti, F., A. Andreoli, L. Mao, and M. A. Lenzi (2008), Wood storage in three mountain streams of the Southern Andes and its hydro-morphological effects, *Earth Surf. Proc. and Landforms*, 33, 244 – 262, doi:10.1002/esp.1541.
- Comiti, F., D. Cadol, and E. Wohl (2009), Flow regimes, bed morphology and flow resistance in self-formed step-pool channels, *Water Resources Research*, 45, W04424, doi:10.1029/2008WR007259.
- Comiti, F., L. Mao, A. Wilcox, E. E. Wohl, and M. A. Lenzi (2007), Field-derived relationships for flow velocity and resistance in high-gradient streams, *J. Hydrol.*, 340, 48 – 62, doi:10.1016/j.jhydrol.2007.03.021.
- Curran, J. C., and P. R. Wilcock (2005), Characteristic dimensions of the step-pool bed configuration: An experimental study, *Water Resources Research*, 41.
- Curran, J. H., and E. E. Wohl (2003), Large woody debris and flow resistance in step-pool channels, Cascade Range, Washington, *Geomorphology*, 51, 141 – 157.
- Daniels, M. D., and B. L. Rhoads (2004), Effect of large woody debris configuration on three-dimensional flow structure in two low-energy meander bends at varying stages, *Water Resources Research*, 40, W11302, doi:10.1029/2004WR003181.
- Dudley, S. J., Fischenich, J. C., and S. R. Abt (1998), Effect of woody debris entrapment on flow resistance, *Journal of the American Water Resources Association*, 34(5), 1189 – 1197.
- Einstein, H. A., and N. L. Barbarossa (1952), River channel roughness, *Trans. Am. Soc. Civ. Eng.*, 117, 1121 – 1146.
- Ferguson, R.I. (1986), Hydraulics and hydraulic geometry. *Progress in Physical Geography*, 10, 1 – 31.
- Ferguson, R.I. (2007), Flow resistance equations for gravel- and boulder-bed streams, *Water Resources Research*, 43, W05427, doi: 10.1029/2006WR005422.
- Ferguson, R.I. (2010), Time to abandon the Manning equation?, *Earth Surf. Processes Landforms*, 35, 1873-1876.
- Ferro, V. (1999), Friction factor for gravel bed channel with high boulder concentration, *J. Hydraul. Eng.*, 125(7), 771 – 778.
- Ferro, V. (2003), Flow resistance in gravel-bed channels with large-scale roughness, *Earth Surf. Processes and Landforms*, 28, 1325 – 1339, doi:10.1002/esp.589.
- Flammer, G. H., J. P. Tullis, and E. S. Mason (1970), Free surface, velocity gradient flow past hemisphere, *Journal of the Hydraulics Division*, ASCE, 96, No. HY7, Proc Paper 7418, 1485 – 1502.

- Gippel C. J., B. L. Finlayson, I. C. O'Neill (1996), Distribution and hydraulic significance of large woody debris in lowland Australian river, *Hydrobiologia*, 318, 179 – 194.
- Grant, G. E. (1997), Critical flow constrains flow hydraulics in mobile-bed streams: a new hypothesis, *Water Resources Research*, 33, 349 – 358.
- Grant, G. E., F. J. Swanson, and M. G. Wolman (1990), Pattern and origin of stepped-bed morphology in high-gradient streams, Western Cascades, Oregon, *Geol. Soc. Am. Bull.*, 102, 340 – 352.
- Griffiths, G. A. (1989), Form resistance in gravel channels with mobile beds, *J. Hydraul. Eng.*, 115, 340 – 355.
- Hey, R. D. (1979), Flow resistance in gravel-bed rivers. *J. Hyraul. Eng.*, 110(11), 1519 – 1539.
- Hickin E. J. (1995), Hydraulic geometry and channel scour, Fraser River, British Columbia, Canada, in *River Geomorphology* edited by E. J. Hickin, John Wiley and Sons, Ltd, pp. 155 – 167, Chichester.
- Hogan D. L., and M. Church (1989), Hydraulic geometry in small, coastal streams-progress toward quantification of salmonid habitat, *Canadian Journal of Fisheries and Aquatic Sciences*, 46, 844 – 852.
- Huang H. Q., and G. C. Nanson (2000), Hydraulic geometry and maximum flow efficiency as products of the principle of least action, *Earth Surf. Process. Landforms*, 25, 1 – 16.
- Hygelund, B., and M. Manga (2003), Field measurements of drag coefficients for model large woody debris, *Geomorphology*, 51, 175 – 185.
- Jarrett, R.D. (1984), Hydraulics of high-gradient rivers, *Journal of Hydraulic Engineering*, 110, 1519-1539.
- Jongman, R. H., C. F. J. ter Braak, O. F. R. Van Tongeren, (1995), *Data analysis in community and landscape ecology*, 279 pp., Cambridge University Press, Cambridge.
- Jowett I. G. (1998), Hydraulic geometry of New Zealand rivers and its use as a preliminary method of habitat assessment, *Regulated Rivers: Research and Management*, 14, 451 – 466.
- Judd, H.E. and D. F. Peterson (1969) Hydraulics of large bed element channels. Utah State Univ., *Water Resources Laboratory Report*, 112 pp.
- Julien, P. Y. (1998), *Erosion and Sedimentation*, Cambridge University Press, 280 pp., Cambridge.

- Katul, G., P. Wiberg, J. Albertson, and G. Hornberger (2002), A mixing layer theory for flow resistance in shallow streams, *Water Resources Research*, 38(11), 1250, doi:10.1029/2001WR000817.
- Kean, J. W. and J. D. Smith (2006), Form drag in rivers due to small-scale natural topographic features: 2. irregular sequences, *Journal of Geophysical Research*, 111, F04010, doi:10.1029/2006JF000490.
- Keller, E. A. and F. J. Swanson (1979), Effects of large organic material on channel form and fluvial processes, *Earth Surf. Process. Landforms*, 4(4), 361 – 380.
- Keulegan, G.H. (1938), Laws of turbulent flow in open channels. *J. Res. Natl. Bur. Stand.*, 21, 707– 741.
- Kirkby M. J. (1977), Maximum sediment efficiency as a criterion for alluvial channels. In *River channel changes*, edited by K. J. Gregory, pp. 429 – 442, Chichester: Wiley-Interscience.
- Knighton, A. D. (1974), Variation in width-discharge relation and some implications for hydraulic geometry, *Geological Society of America Bulletin*, 85, 1069 – 1076.
- Knighton, A. D. (1975), Variations in at-a-station hydraulic geometry, *American Journal of Science*, 275, 186 – 218.
- Knighton, A. D. (1998), *Fluvial Forms and Processes*, pp., Oxford University Press Inc., New York.
- Kovach Computing System. 2002. Multivariate Statistical Package (MVSP). Anglesey, Wales.
- Kutner, M.H., C. J. Nachtsheim, J. Neter, W. Li (2005) *Applied Linear Statistical Models*, 1396 pp., McGraw-Hill/Irwin, New York.
- Lamb, M. J., W. E. Dietrich, and J. G. Vinditti (2008), Is the critical Shields stress for incipient sediment motion dependent on channel bed-slope?, *Journal of Geophysical Research*, 113, F02008, doi:10.1029/2007JF000831.
- Lamouroux, N., and H. Capra, (2002), Simple predictions of instream habitat model outputs for target fish populations, *Freshwater Biology*, 47, 1543 – 1556.
- Langbein, W. B. (1964), Geometry of river channels, *Journal of Hydraulic Division, Proceedings of the American Society of Civil Engineers*, 90, 301 – 312.
- Lawrence, D. S. L. (1997), Macroscale surface roughness and frictional resistance in overland flow, *Earth Surf. Processes Landforms*, 22, 365 – 382.

- Lawrence, D. S. L. (2000), Hydraulic resistance in overland flow during partial and marginal surface inundation: Experimental observations and modeling, *Water Resour. Res.*, 36, 2381 – 2393.
- Lawrence, D. S. L. (2007), Analytical derivation of at-a-station hydraulic geometry relations, *Journal of Hydrology*, 334, 17 – 27.
- Lee, A. J., and R. I. Ferguson (2002), Velocity and flow resistance in step-pool streams, *Geomorphology*, 46, 59 – 71.
- Leica Geosystems (2008), *Cyclone 5.8.1.: Comprehensive software for working with laser scan data*, Leica Geosystems HDS LLC, San Ramon, CA.
- Legleiter, C. J., T. L. Phelps, and E. E. Wohl (2007), Geostatistical analysis of the effects of stage and roughness on reach-scale spatial patterns of velocity and turbulence intensity, *Geomorphology*, 83, 322 – 345.
- Leopold, L. B., and T. Maddock, (1953), The hydraulic geometry of stream channels and some physiographic implications, *U.S. Geological Survey Professional Paper*, 252, 57 pp.
- Leopold, L. B., R. A. Bagnold, M. G. Wolman, and L. M. Brush, (1960), Flow resistance in sinuous or irregular channels, *United States Geological Survey Professional Papers*, 282D, 111 – 134.
- Leopold, L.B., M. G. Wolman, and J. P. Miller (1964), *Fluvial Processes in Geomorphology*, 522 pp., Dover, Mineola, N.Y.
- Limerinos, J. T. (1970), Determination of the Manning coefficient for measured bed roughness in natural channels, *Water Supply Paper 1898-B.*, U.S. Geological Survey, Washington D. C.
- Magirl, C. S., J. W. Gartner, G. M. Smart, and R. H. Webb (2009), Water velocity and the nature of critical in large rapids on the Colorado River, Utah, *Water Resour. Res.*, 45, W05427, doi:10.1029/2009WR007731.
- Manga, M., and J. W. Kirchner (2000), Stress partitioning in streams by large woody debris, *Water Resour. Res.*, 36, 2373 – 2379.
- Manners, R. B., M. W. Doyle, and M. J. Small (2007), Structure and hydraulics of natural woody debris jams, *Water Resour. Res.*, 43, W06432, doi:10.1029/2006WR004910.
- Maxwell, A. R. and A. N. Papanicolaou (2001), Step-pool morphology in high-gradient streams, *International Journal of Sediment Research*, 72, 99 – 108.
- McCune B., and J. B. Grace, (2002), *Analysis of Ecological Communities*, Glenden Beach, OR, MjM Software Design, 300 pp.

- McFarlane, W. A., and E. Wohl (2003), Influence of step composition on step geometry and flow resistance in step-pool streams of the Washington Cascades, *Water Resour. Res.* 39(2), 1037, doi:10.1029/2001WR001238.
- Millar, R.G. (1999), Grain and form resistance in gravel-bed rivers, *Journal of Hydraulic Research*, 37, 303 – 312.
- Millar, R. G. and Quick, M. C. (1994), Flow resistance of high-gradient gravel channels, in *Hydraulic Engineering '94 ASCE*, edited by G. V. Cotroneo and R. R. Rumer, pp. 717 – 721, Buffalo, N.Y.
- Montgomery, D. R., and J. M. Buffington (1997), Channel-reach morphology in mountain drainage basins, *Geol. Soc. Am. Bull.*, 109, 596 – 611.
- Montgomery, D. R., T. B. Abbe, J. M. Buffington, N. P. Peterson, K. M. Schmidt, and J. D. Stock (1996), Distribution of bedrock and alluvial channels in forested mountain drainage basins, *Nature*, 381, 587 – 589.
- Mussetter, R. A. (1989), Dynamics of mountain streams. Ph.D. Thesis, Colorado State University, Fort Collins.
- Nelson, J., W. W. Emmett, and J. D. Smith (1991), Flow and sediment transport in rough channels, in *Proceedings of the 5th interagency sedimentation conference*, pp. 55–62, Dept. of Energy.
- Olsen, N. R. B., and M. C. Melaaen (1993), Three-dimensional calculations of scour around cylinders, *Journal of Hydraulic Engineering*, 119, 1048 – 1054.
- Pagilara, S. and P. Chiavaccini (2006), Flow resistance of rock chutes with protruding boulders, *Journal of Hydraulic Engineering*, 132, 545 – 552.
- Park, C. C. (1977), World-wide variations in hydraulic geometry exponents of stream channels: An analysis and some observations, *Journal of Hydrology*, 33, 133 – 146.
- Parker, G., and A. W. Peterson (1980), Bar resistance of gravel-bed streams, *J. Hydraul. Eng. Div. Am. Soc. Civ. Eng.*, 106, 1559 – 1573.
- Prestegard, K. L. (1983), Bar resistance in gravel bed streams at bankfull discharge, *Water Resources Research*, 19, 472 – 476.
- Ranga Raju, K. G., O. P. S. Rana, G. L. Asawa, and A. S. N. Pillai (1983), Rational assessment of blockage effect in channel flow past smooth circular cylinders, *J. Hydr. Res.*, 21, 289 – 302.
- R Core Development Team (2007), *R: A Language and Environment for Statistical Computing*, R Found. for Stat. Comput., Vienna.

- Reid, D. E. (2005), Low-Flow Hydraulic Geometry of Small, Steep Streams in Southwest British Columbia, M.Sc. thesis, Simon Fraser University.
- Reid, D. E., and E. J. Hickin (2008), Flow resistance in steep mountain streams, *Earth Surf. Processes Landforms*, 33, 2211 – 2240, doi:10.1002/esp.1682.
- Rhoads, B. L. (1992), Statistical models of fluvial systems, *Geomorphology*, 5, 433 – 455.
- Rhodes, D. D. (1977), The b-f-m diagram: graphical representation and interpretation of at-a-station hydraulic geometry, *American Journal of Science*, 277, 73 – 96.
- Richards, K. S. (1973), Hydraulic geometry and channel roughness – a non-linear system, *American Journal of Science*, 273, 877 – 896.
- Richards, K. S. (1976), Complex width-discharge relations in natural river sections, *Geological Society of America Bulletin*, 87, 199 – 206.
- Rickenmann, D. (1991) Hyperconcentrated flow and sediment transport at steep slopes, *J. Hydr. Eng.*, 117, ASCE, 1419-1439.
- Ridenour, G. S., and J. R. Giardino, (1991), The statistical study of hydraulic geometry: A new direction for compositional data analysis, *Mathematical Geology*, 23, 349 – 366.
- Ridenour, G. S., and J. R. Giardino, (1995), Logratio linear modeling of hydraulic geometry using indices of flow resistance as covariates, *Geomorphology*, 14, 65 – 72.
- Rouse, H. (1965), Critical Analysis of Open-Channel Resistance, *Journal of the Hydraulics*, ASCE, 91, Paper No. 4387, HY4,1-25.
- Shields, F. D. Jr, and C. J. Gippel (1995), Prediction of effects of woody debris removal on flow resistance, *J. Hydr. Engin.*, 121, 341 – 354.
- Singh, V. P., and L. Zhang, (2008a), At-a-station hydraulic geometry relations, 1: theoretical development, *Hydrological Processes*, 22, 189 – 215, doi: 10.1002/hyp.6411.
- Singh, V. P., and L. Zhang, (2008b), At-a-station hydraulic geometry relations, 2: calibration and testing, *Hydrological Processes*, 22, 216 – 228, doi: 10.1002/hyp.6412.
- Smart, D.M., M. J. Duncan, and J. M. Walsh (2002), Relatively rough flow resistance equations, *J. of Hydr. Eng.*, 128, 568 – 578, doi: 10.1061/(ASCE)0733-9429(2002)128:6(568).
- Stewardson M. (2005), Hydraulic geometry of stream reaches, *Journal of Hydrology*, 206, 97 – 111, doi: 10.1016/j.jydrol.2004.09.004.

- Taylor, R. B. (1975), Geologic map of the Bottle Pass quadrangle, Grand County, Colorado. *Cr.S. Geological Survey map* GQ-1244. Scale 1:24,000.
- Thompson, S. M., and P. L. Campbell (1979), Hydraulics of a large channel paved with boulders, *J. Hydraul. Res.*, 17, 341 – 355.
- Thorne, C. R., and L. W. Zevenbergen (1985), Estimating mean velocity in mountain rivers, *J. Hydr. Engineer.*, 111, 612 – 624.
- Trayler, C. R., and E. E. Wohl (2000), Seasonal changes in bed elevation in a step-pool channel, Rocky Mountains, Colorado, U.S.A., *Arct. Antarc. and Alp. Res.*, 32, 95 – 103.
- USDA Forest Service (2009), About Fraser Experimental Forest, <http://www.fs.fed.us/rm/fraser/about/index.shtml>.
- Vallé, B. L. and G. B. Pasternack (2006), Submerged and unsubmerged natural hydraulic jumps in a bedrock step-pool mountain channel, *Geomorphology*, 82, 146 – 159.
- Wallerstein, N. P., C. V. Alonso, S. J. Bennett, and C. R. Thorne (2002), Surface wave forces acting on submerged logs. *J. of Hydraulic Engineering*, 128(3), 349-353.
- Wallerstein, N. P., and C. R. Thorne (2004), Influence of large woody debris on morphological evolution of incised, sand-bed channels, *Geomorphology*, 57, 53 – 73.
- White, W. R., R. Bettess, and E. Paris (1982), Analytical approach to river regime, *Journal of the Hydraulics Division American Society of Civil Engineers*, 108, 1179 – 1193.
- Whiting, P. J., and W. E. Dietrich (1990), Boundary shear stress and roughness over mobile alluvial beds, *Journal of Hydraulic Engineering*, 116, 1495 – 1511.
- Wiberg, P. L., and J. D., Smith (1991), Velocity distribution and bed roughness in high-gradient streams, *Water Resour. Res.*, 23, 1471 – 1480.
- Wilcox, A. C., and E. E. Wohl, (2006), Flow Resistance dynamics in step-pool stream channels: 1. Large woody debris and controls on total resistance, *Water Resources Research*, 42, W05418, DOI:10.1029/2005WR004277.
- Wilcox, A. C., and E. E. Wohl (2007), Field measurements of three-dimensional hydraulics in step-pool channel, *Geomorphology*, 83, 215 – 231, doi:10.1016/j.geomorph.2006.02.017.
- Wilcox, A. C., J. M. Nelson, and E. E. Wohl (2006), Flow resistance dynamics in step-pool channels: 2. Partitioning between grain, spill, and woody debris resistance, *Water Resour. Res.*, 42, W05419, doi:10.1029/2005WR004278.

- Wohl, E. (2000), *Mountain Rivers*, 320 pp., Am. Geophys. Union Press, Washington, D.C.
- Wohl, E. (2007), Channel-unit hydraulics on a pool-riffle channel, *Physical Geography*, 28, 233 – 248.
- Wohl, E. D. Cooper, L. Poff , F. Rahel, D. Staley, and D. Winters (2007), Assessment of Stream Ecosystem Function and Sensitivity in the Bighorn National Forest, Wyoming, *Environmental Management*, 40, 284–302, doi:10.1007/s00267-006-0168-z.
- Wohl, E. E., and T. Grodek (1994), Channel bed-steps along Nahal Yael, Negev desert, Israel, *Geomorphology*, 9, 117 – 126.
- Wohl, E. E., and H. Ikeda (1998), The effect of roughness configuration on velocity profiles in an artificial channel, *Earth Surf. Processes Landforms*, 23, 159 – 169.
- Wohl, E., J.N. Kuzma and N.E. Brown (2004), Reach-scale channel geometry of a mountain river, *Earth Surface Processes and Landforms*, 29, 969-981.
- Wohl, E. E., and D. M. Thompson (2000), Velocity characteristics along a small step-pool channel, *Earth Surf. Processes Landforms*, 25, 353 – 367.
- Wohl, E. E. and D. Merritt (2005), Prediction of mountain stream morphology, *Water Resour. Res.*, 41, W08419, doi:10.1029/2004WR003779.
- Wohl, E. and D. Merritt (2008), Reach-scale channel geometry of mountain streams, *Geomorphology*, 93, 168 – 185.
- Wolman, M. G. (1954), A method for sampling coarse river-bed material, *Transactions-American Geophysical Union*, 35, 951 – 956.
- Yang, C. T. (1976), Minimum unit stream power and fluvial hydraulics, *Journal of the Hydraulics Division American Civil Engineers*, 102, HY7, 919 – 934.
- Young, W. J. (1991), Flume study of the hydraulic effects of large woody debris in lowland rivers, *Regul. Riv.*, 6, 203 – 211.
- Zimmerman, A. (2010), Flow resistance in steep streams: an experimental study, *Water Resources Research*, 46, W09536, doi:10.1029/2009WR007913.
- Zimmerman, A., and M. Church (2001), Channel morphology, gradient profiles and bed stresses during flood in a step-pool channel, *Geomorphology*, 40, 311 – 327.

CHAPTER 9 APPENDICES

9.1 Appendix A: Reach-average values of channel and hydraulic variable for each reach at each flow

Table 19: Summary of channel and hydraulic variables used for each reach, where L_r = reach length; S_0 = bed gradient; A = cross-sectional area; R = hydraulic radius; L_s = step length; D_{50} = grain size in which 50% is smaller; D_{84} = grain size in which 84% are smaller; V = reach-average velocity; Q = discharge; u^* = shear velocity; Fr = Froude number; Re = Reynolds number; ff = Darcy-Weisbach friction factor

Reach	Channel Type	Flow Period	L_r (m)	S_0 (m/m)	A (m ²)	R (m)	W (m)	H (m)	L_s (m)	D_{50} (m)	D_{84} (m)	V (m/s)	Q (m ³ /s)	u^* (m/s)	Fr	Re	ff
ESL1	Step-Pool	June2008	29.37	0.093	0.99	0.25	2.92	0.63	4.64	0.05	0.16	0.66	0.66	0.49	0.36	1.5E+05	4.23
		July2008	27.30	0.104	0.70	0.20	2.60	0.76	4.31	0.05	0.16	0.41	0.29	0.46	0.25	7.3E+04	9.81
		Aug2007	31.57	0.086	0.29	0.12	2.01	0.62	4.97	0.05	0.16	0.22	0.06	0.32	0.19	2.2E+04	16.32
ESL2	Step-Pool	June2008	13.70	0.093	1.00	0.25	3.21	0.52	2.56	0.01	0.07	0.63	0.63	0.48	0.35	1.4E+05	4.51
		July2008	13.99	0.089	0.74	0.21	2.97	0.44	2.75	0.01	0.07	0.60	0.44	0.45	0.37	1.1E+05	4.35
		July2007	13.95	0.095	0.68	0.20	2.86	0.35	2.58	0.01	0.07	0.46	0.31	0.42	0.29	8.0E+04	6.60
		Aug2007	14.04	0.092	0.45	0.15	2.57	0.46	2.78	0.01	0.07	0.25	0.11	0.38	0.18	3.4E+04	16.84
ESL3	Cascade	June2008	10.24	0.140	0.87	0.18	3.63	0.51	0.77	0.06	0.13	0.73	0.64	0.48	0.48	1.2E+05	3.75
		July2008	10.69	0.124	0.80	0.17	3.54	0.48	1.30	0.06	0.13	0.60	0.48	0.45	0.41	9.1E+04	5.02
		July2007	10.69	0.131	0.61	0.15	3.03	0.48	1.57	0.06	0.13	0.50	0.30	0.43	0.36	6.8E+04	6.34
		Aug2007	11.32	0.131	0.42	0.14	2.41	0.48	1.03	0.06	0.13	0.39	0.16	0.40	0.29	4.8E+04	9.15
ESL4	Step-Pool	June2008	15.57	0.128	0.99	0.26	2.86	0.53	2.22	0.07	0.17	0.69	0.68	0.56	0.37	1.6E+05	5.17
		July2008	16.31	0.110	0.78	0.23	2.69	0.60	2.64	0.07	0.17	0.51	0.40	0.51	0.30	1.0E+05	7.56
		July2007	15.75	0.121	0.57	0.18	2.48	0.55	2.87	0.07	0.17	0.45	0.26	0.47	0.30	7.2E+04	8.85
		Aug2007	16.54	0.102	0.50	0.17	2.32	0.47	2.49	0.07	0.17	0.33	0.16	0.45	0.23	5.0E+04	13.15
ESL5	Cascade	June2008	12.50	0.155	1.20	0.24	4.04	1.03	1.00	0.05	0.14	0.52	0.63	0.61	0.30	1.1E+05	10.66
		July2008	13.89	0.130	1.09	0.22	3.95	0.70	3.40	0.05	0.14	0.45	0.49	0.56	0.27	8.8E+04	11.22
		July2007	13.51	0.143	0.78	0.18	3.58	0.87	1.04	0.05	0.14	0.38	0.29	0.51	0.26	5.9E+04	13.46
		Aug2007	15.11	0.123	0.59	0.15	3.25	0.88	1.18	0.05	0.14	0.25	0.15	0.44	0.19	3.3E+04	22.85

ESL6	Plane-Bed	June2008	6.40	0.018	0.89	0.26	2.98	N/A	N/A	0.02	0.09	1.67	1.85	0.25	0.97	3.8E+05	0.16
		July2008	6.42	0.020	0.79	0.24	2.85	N/A	N/A	0.02	0.09	1.43	1.13	0.19	0.86	3.0E+05	0.14
		July2007	6.54	0.017	0.56	0.19	2.69	N/A	N/A	0.02	0.09	0.60	0.34	0.17	0.42	9.8E+04	1.02
		Aug2007	6.22	0.023	0.44	0.15	2.65	N/A	N/A	0.02	0.09	0.42	0.18	0.17	0.33	5.5E+04	1.31
ESL7	Cascade	June2008	22.10	0.099	0.97	0.25	3.02	N/A	N/A	0.08	0.17	0.73	0.71	0.46	0.41	1.6E+05	3.34
		July2008	23.99	0.093	0.86	0.23	2.93	N/A	N/A	0.08	0.17	0.54	0.46	0.42	0.32	1.1E+05	5.18
		July2007	22.86	0.094	0.57	0.18	2.71	N/A	N/A	0.08	0.17	0.51	0.29	0.39	0.35	7.9E+04	4.74
		Aug2007	24.31	0.083	0.42	0.15	2.46	N/A	N/A	0.08	0.17	0.43	0.18	0.35	0.32	5.7E+04	5.26
ESL8	Step-Pool	June2008	30.68	0.099	0.91	0.23	3.16	0.39	4.50	0.07	0.17	0.62	0.57	0.44	0.37	1.3E+05	4.22
		July2008	32.65	0.086	0.78	0.21	3.03	0.42	4.58	0.07	0.17	0.55	0.43	0.43	0.34	1.0E+05	4.82
		July2007	31.38	0.091	0.59	0.18	2.73	0.41	4.48	0.07	0.17	0.46	0.27	0.40	0.31	7.4E+04	6.22
		Aug2007	35.48	0.082	0.48	0.16	2.58	0.43	5.87	0.07	0.17	0.36	0.17	0.36	0.26	5.1E+04	8.05
ESL9	Step-Pool	June2008	16.26	0.115	0.92	0.25	2.79	0.44	2.62	0.06	0.15	0.62	0.57	0.49	0.34	1.4E+05	5.60
		July2008	16.51	0.111	0.72	0.22	2.62	0.43	2.69	0.06	0.15	0.46	0.33	0.45	0.28	8.7E+04	8.68
		July2007	16.22	0.117	0.64	0.20	2.53	0.46	2.59	0.06	0.15	0.42	0.27	0.45	0.27	7.3E+04	10.00
		Aug2007	18.64	0.095	0.47	0.17	2.28	0.44	3.08	0.06	0.15	0.34	0.16	0.39	0.24	5.0E+04	10.78
FC1	Step-Pool	June2008	23.12	0.062	0.38	0.16	1.97	0.20	2.78	0.03	0.08	0.86	0.33	0.32	0.63	1.2E+05	1.07
		July2008	23.20	0.060	0.17	0.10	1.57	0.20	3.22	0.03	0.08	0.29	0.05	0.24	0.29	2.5E+04	5.18
		July2007	23.74	0.060	0.18	0.10	1.63	0.19	2.83	0.03	0.08	0.41	0.08	0.25	0.39	3.6E+04	2.90
		Aug2007	25.12	0.058	0.09	0.06	1.28	0.19	2.42	0.03	0.08	0.20	0.02	0.19	0.24	1.1E+04	7.58
FC2	Step-Pool	June2008	14.38	0.074	0.39	0.18	1.63	0.25	2.30	0.03	0.08	0.68	0.26	0.35	0.44	1.0E+05	2.23
		July2008	14.18	0.077	0.20	0.11	1.41	0.22	2.44	0.03	0.08	0.25	0.05	0.28	0.22	2.4E+04	9.59
		July2007	15.05	0.073	0.17	0.10	1.41	0.19	3.01	0.03	0.08	0.41	0.07	0.27	0.37	3.6E+04	3.49
		Aug2007	14.93	0.071	0.08	0.06	1.13	0.20	2.72	0.03	0.08	0.19	0.01	0.20	0.23	1.0E+04	9.39

FC3	Step-Pool	June2008	13.48	0.093	0.55	0.19	2.12	0.36	2.51	0.01	0.05	0.43	0.24	0.42	0.27	7.2E+04	7.24
		July2008	12.22	0.092	0.24	0.11	1.66	0.29	2.44	0.01	0.05	0.18	0.04	0.33	0.15	1.8E+04	26.92
		July2007	14.87	0.079	0.23	0.11	1.64	0.33	3.55	0.01	0.05	0.27	0.06	0.31	0.23	2.6E+04	10.04
		Aug2007	11.90	0.095	0.12	0.07	1.36	0.32	2.92	0.01	0.05	0.11	0.01	0.28	0.12	6.9E+03	42.13
FC4	Step-Pool	June2008	18.86	0.141	0.49	0.20	1.65	0.49	2.87	0.05	0.10	0.75	0.37	0.52	0.44	1.3E+05	3.82
		July2008	19.82	0.130	0.21	0.12	1.39	0.42	3.63	0.05	0.10	0.27	0.06	0.38	0.22	2.8E+04	16.20
		July2007	19.01	0.136	0.23	0.12	1.45	0.49	2.97	0.05	0.10	0.25	0.06	0.40	0.20	2.7E+04	19.90
		Aug2007	19.23	0.132	0.14	0.09	1.25	0.38	3.01	0.05	0.10	0.15	0.02	0.34	0.15	1.2E+04	39.89
FC5	Cascade	June2008	11.87	0.163	0.20	0.13	1.15	0.50	0.83	0.03	0.09	0.60	0.12	0.48	0.45	6.6E+04	4.64
		July2008	11.89	0.163	0.10	0.08	0.94	0.62	0.98	0.03	0.09	0.24	0.02	0.37	0.23	1.6E+04	17.64
		July2007	12.80	0.159	0.09	0.08	0.91	0.59	0.69	0.03	0.09	0.23	0.02	0.36	0.23	1.5E+04	18.12
		Aug2007	14.24	0.143	0.05	0.05	0.74	0.24	0.74	0.03	0.09	0.12	0.01	0.28	0.16	5.5E+03	39.22
FC6	Cascade	June2008	19.06	0.195	0.17	0.12	1.07	0.39	1.33	0.05	0.09	0.61	0.10	0.48	0.48	6.2E+04	4.73
		July2008	20.61	0.181	0.09	0.07	0.92	0.38	1.59	0.05	0.09	0.23	0.02	0.36	0.24	1.5E+04	19.33
		July2007	19.38	0.185	0.09	0.07	0.91	0.49	2.33	0.05	0.09	0.27	0.02	0.37	0.27	1.8E+04	15.29
		Aug2007	22.11	0.166	0.04	0.05	0.67	0.36	1.71	0.05	0.09	0.13	0.01	0.28	0.17	5.7E+03	36.16

9.2 Appendix B: Gage Flow Data

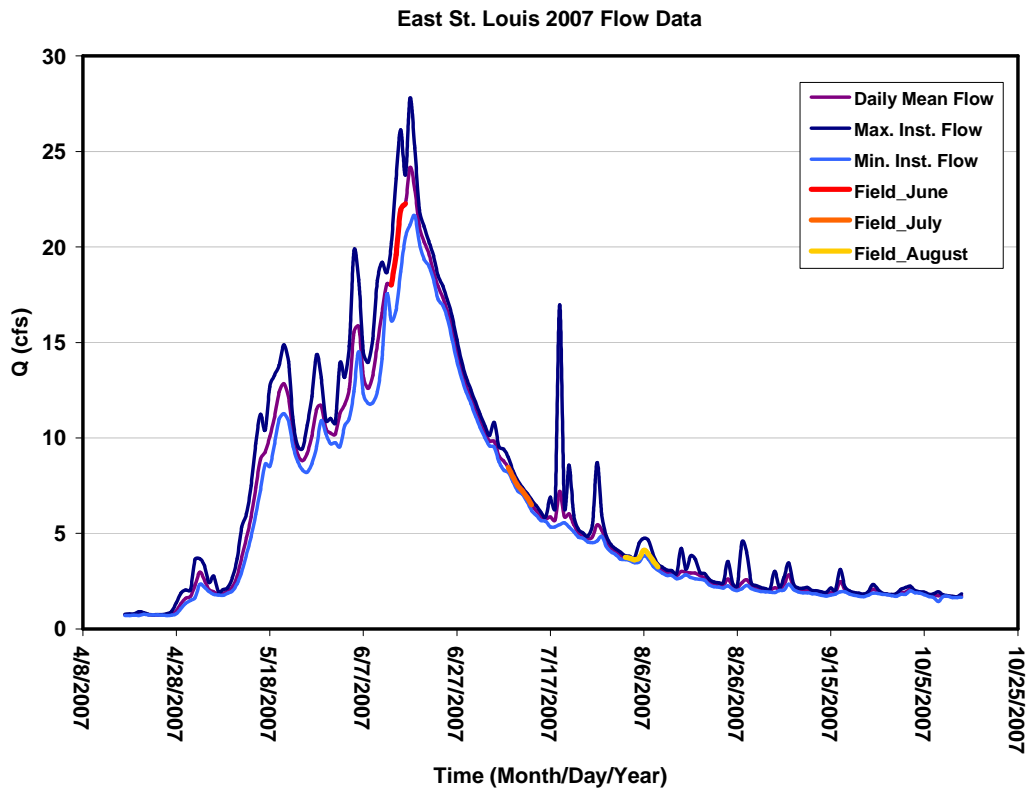


Figure 54: Daily mean flow and minimum and maximum instantaneous flow for East St. Louis in 2007. Red, orange, and yellow indicate days data were collected in the field.

Lower Fool Creek Flow Data 2007

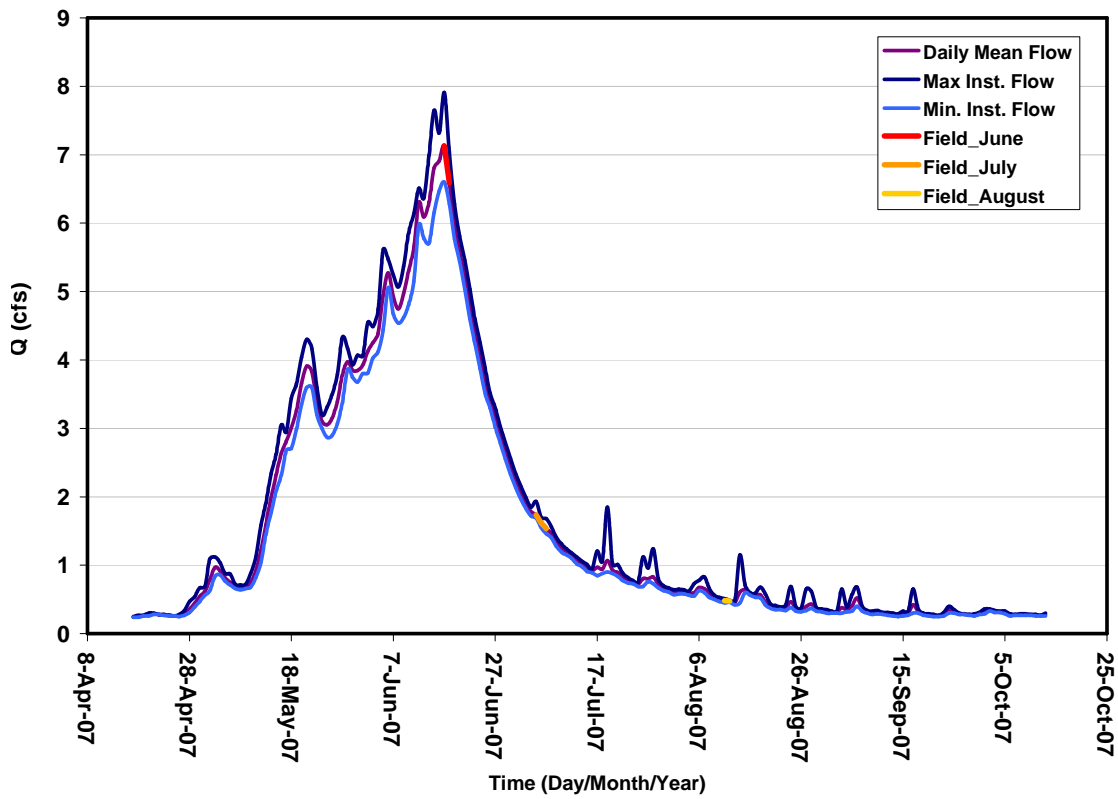


Figure 55: Daily mean flow and minimum and maximum flow data for Lower Fool Creek in 2007. Red, orange, and yellow indicate days field data were collected in stream.

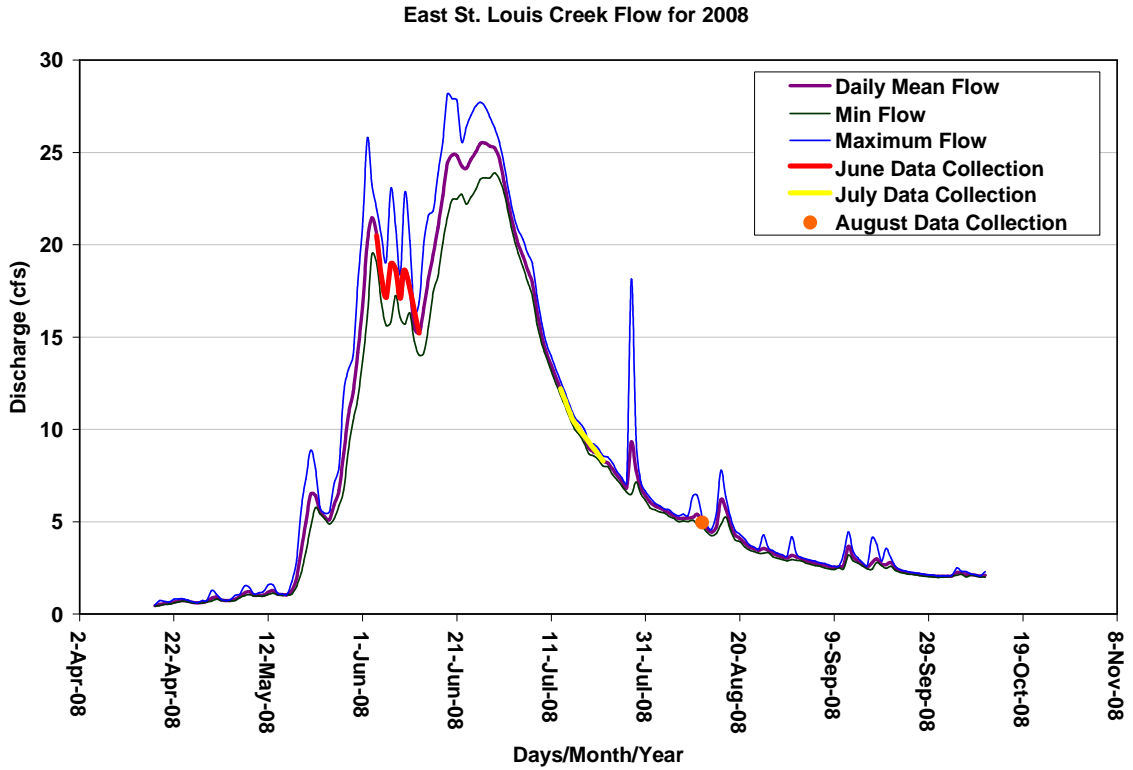


Figure 56: Daily mean flow and minimum and maximum flow for East St. Louis in 2008. Red, yellow, and orange sections indicate days field work was completed in the channel.

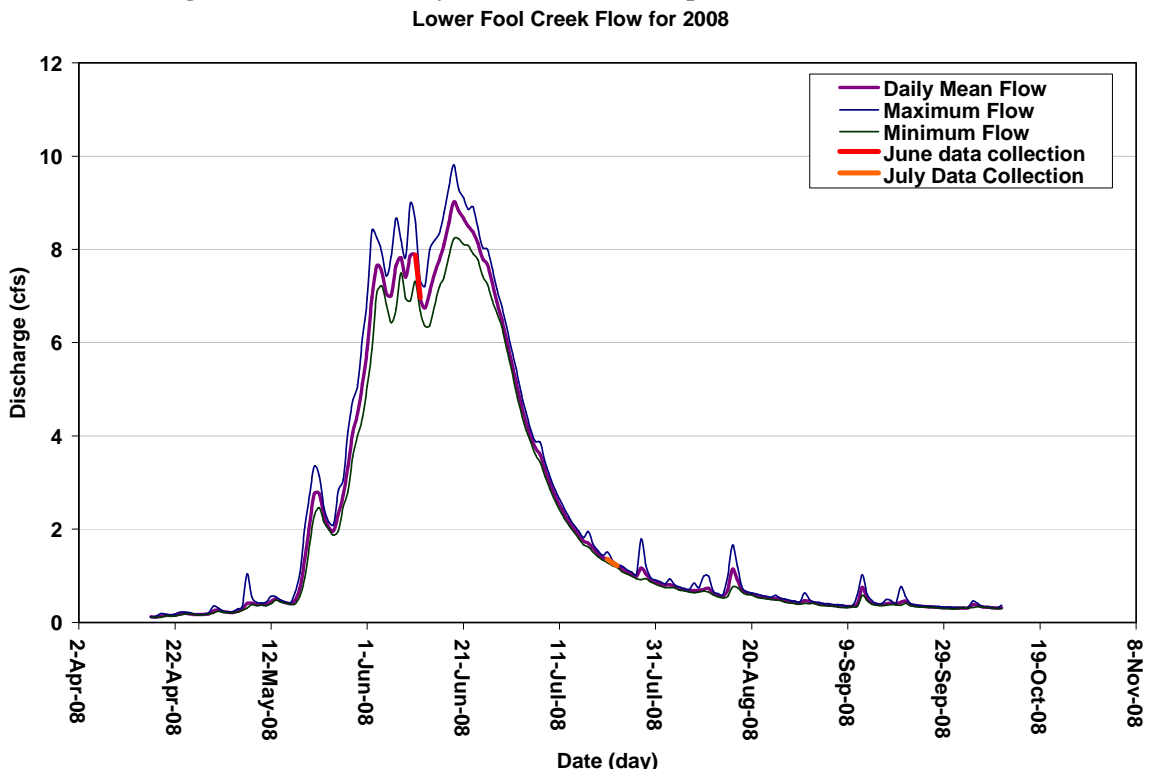


Figure 57: Daily mean flow and minimum and maximum flow for Lower Fool Creek in 2008. Red and orange sections indicate days field work was completed in the stream.

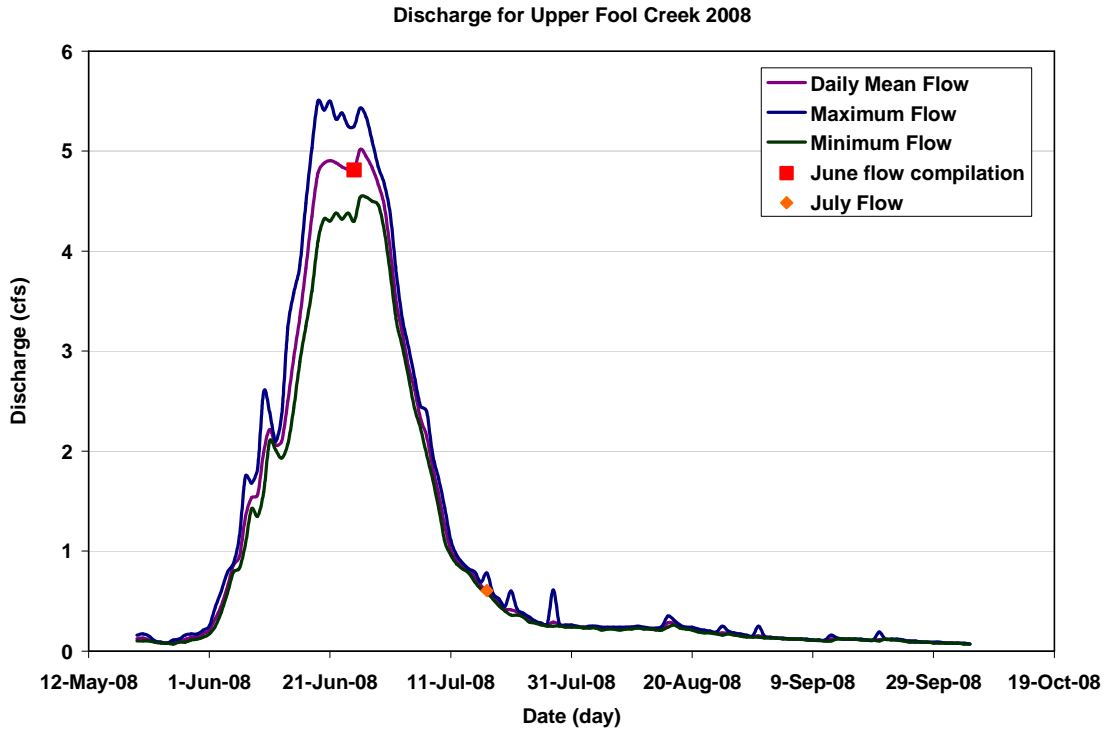
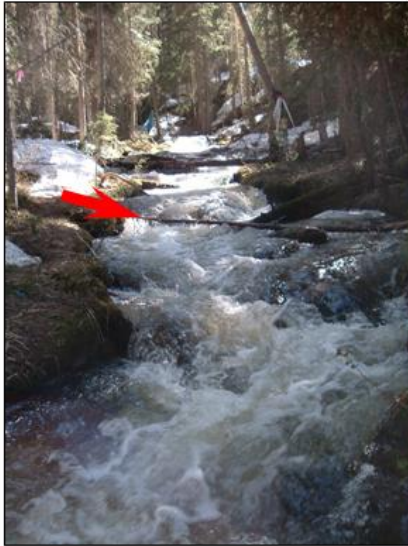


Figure 58: Daily mean flow and minimum and maximum flow for Upper Fool Creek in 2008. Red and orange dots indicate days that field work was completed in the channel.

9.3 Appendix C: Detailed Pictures and Descriptions of Each Reach

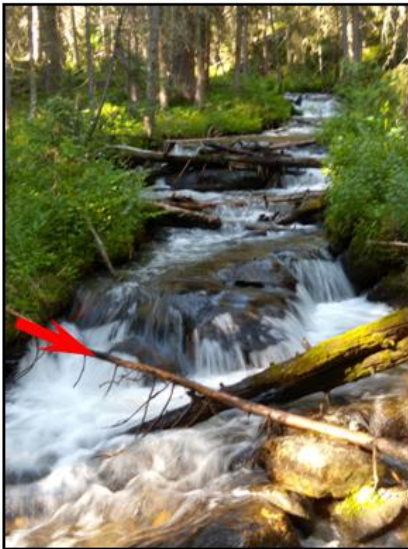
ESL1: Step-pool



June 10, 2008
 $Q = 0.66 \text{ m}^3/\text{s}; V = 0.66 \text{ m/s};$
 $ff = 4.23; S_{0=} = 0.093$



August 2, 2007
 $Q = 0.06 \text{ m}^3/\text{s}; V = 0.22 \text{ m/s};$
 $ff = 16.32; S_{0=} = 0.086$



July 22, 2008
 $Q = 0.29 \text{ m}^3/\text{s}; V = 0.41 \text{ m/s};$
 $ff = 9.81; S_{0=} = 0.104$

Figure 59: Photographs and summary of measured and calculated hydraulic variables for ESL1. Red arrow indicates same location in the reach in each photograph.

ESL2: Step-pool

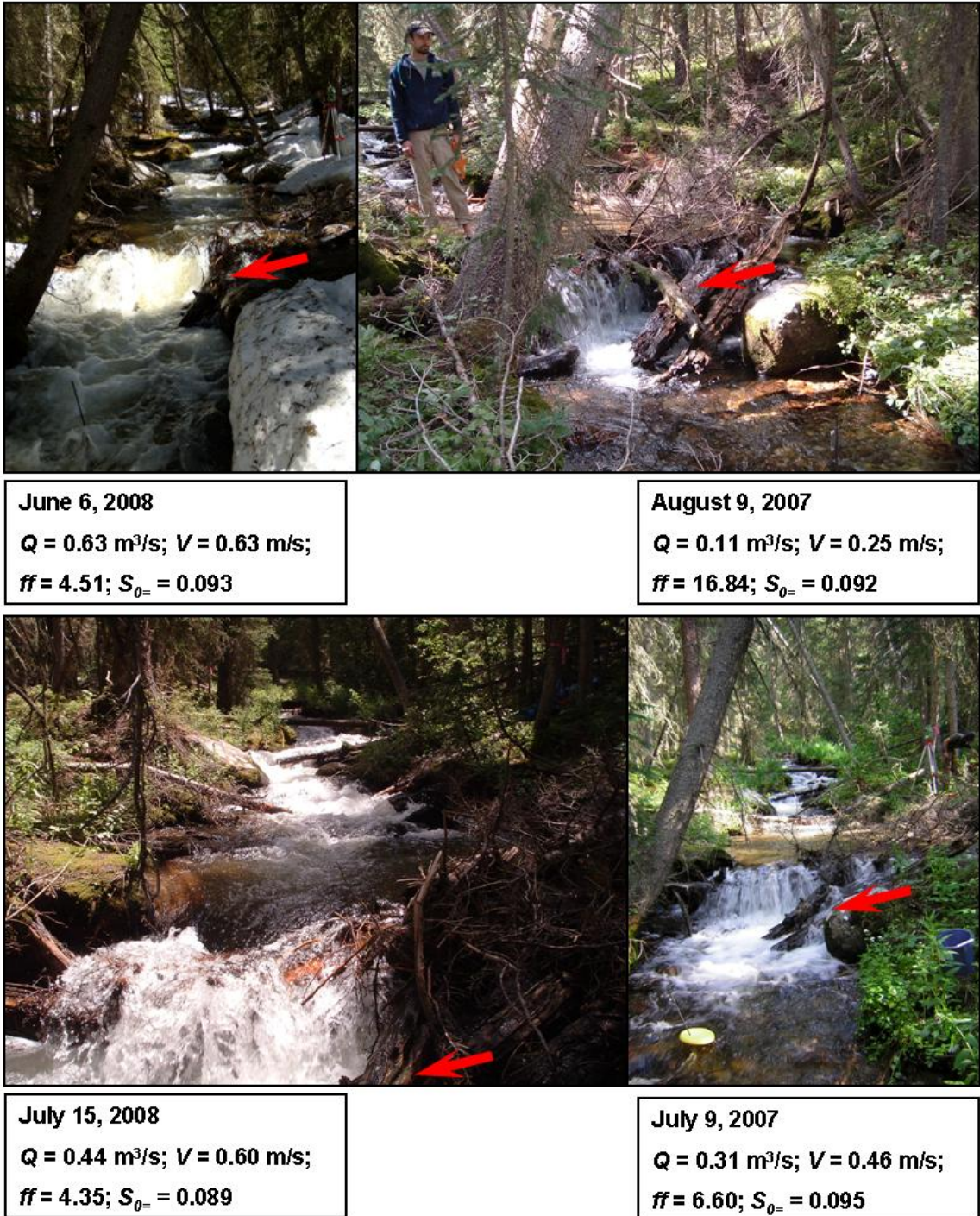
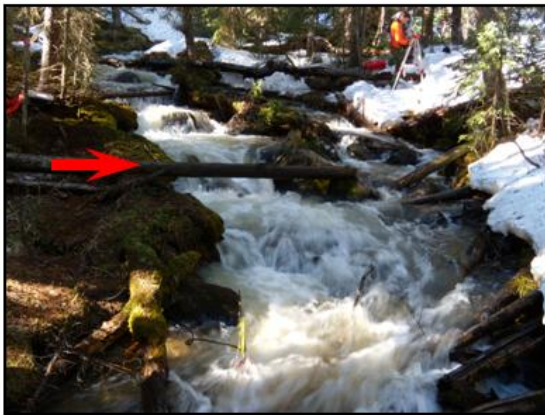


Figure 60: Photographs and measured and calculated hydraulic variables for each flow period in ESL2. Red arrows indicate same location in each photograph.

ESL3: Cascade



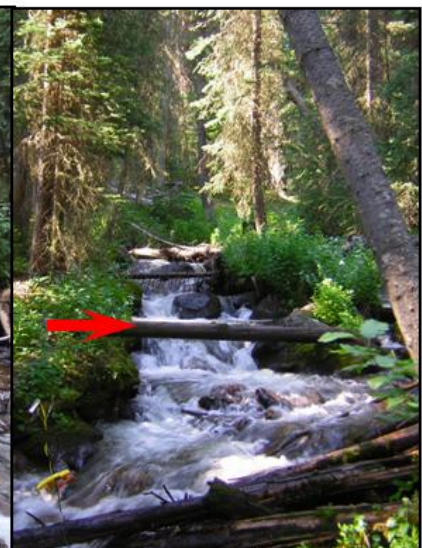
June 7, 2008
 $Q = 0.64 \text{ m}^3/\text{s}$; $V = 0.73 \text{ m/s}$;
 $ff = 3.75$; $S_{0=} = 0.140$



August 9, 2007
 $Q = 0.16 \text{ m}^3/\text{s}$; $V = 0.39 \text{ m/s}$;
 $ff = 9.15$; $S_{0=} = 0.131$



July 15, 2008
 $Q = 0.48 \text{ m}^3/\text{s}$; $V = 0.60 \text{ m/s}$;
 $ff = 5.02$; $S_{0=} = 0.124$



July 10, 2007
 $Q = 0.30 \text{ m}^3/\text{s}$; $V = 0.50 \text{ m/s}$;
 $ff = 6.34$; $S_{0=} = 0.131$

Figure 61: Photographs and measured and calculated hydraulic variables for ESL3. Red arrows indicate same location in each photograph.

ESL4: Step-pool



June 7, 2008
 $Q = 0.68 \text{ m}^3/\text{s}; V = 0.69 \text{ m/s};$
 $ff = 5.17; S_{0=} = 0.128$



August 6, 2007
 $Q = 0.16 \text{ m}^3/\text{s}; V = 0.33 \text{ m/s};$
 $ff = 13.15; S_{0=} = 0.102$



July 10, 2007
 $Q = 0.26 \text{ m}^3/\text{s}; V = 0.45 \text{ m/s};$
 $ff = 8.85; S_{0=} = 0.121$



July 14, 2008
 $Q = 0.40 \text{ m}^3/\text{s}; V = 0.51 \text{ m/s};$
 $ff = 7.56; S_{0=} = 0.110$

Figure 62: Photographs and measured and calculated hydraulic variables for ESL4. Red arrows indicate same location in each photograph.

ESL5: Cascade



June 9, 2008

$Q = 0.63 \text{ m}^3/\text{s}; V = 0.52 \text{ m/s};$

$ff = 10.66; S_{0-} = 0.155$



August 8, 2007

$Q = 0.15 \text{ m}^3/\text{s}; V = 0.25 \text{ m/s};$

$ff = 22.85; S_{0-} = 0.123$



July 14, 2008

$Q = 0.49 \text{ m}^3/\text{s}; V = 0.45 \text{ m/s};$

$ff = 11.22; S_{0-} = 0.130$



July 12, 2007

$Q = 0.29 \text{ m}^3/\text{s}; V = 0.38 \text{ m/s};$

$ff = 13.46; S_{0-} = 0.143$

Figure 63: Photograph and measured and hydraulic variables for ESL5. Red arrows indicate same location in each photograph.

ESL6: Plane-bed



June 9, 2008

$Q = 1.85 \text{ m}^3/\text{s}$; $V = 1.67 \text{ m/s}$;

$ff = 0.16$; $S_{0-} = 0.018$



August 8, 2007

$Q = 0.18 \text{ m}^3/\text{s}$; $V = 0.42 \text{ m/s}$;

$ff = 1.31$; $S_{0-} = 0.023$



July 14, 2008

$Q = 1.13 \text{ m}^3/\text{s}$; $V = 1.43 \text{ m/s}$;

$ff = 0.14$; $S_{0-} = 0.020$



July 13, 2007

$Q = 0.34 \text{ m}^3/\text{s}$; $V = 0.60 \text{ m/s}$;

$ff = 1.02$; $S_{0-} = 0.017$

Figure 64: Photograph and measured and hydraulic variables for ESL6. Red arrows indicate same location in each photograph.

ESL7: Cascade



June 8, 2008

$Q = 0.71 \text{ m}^3/\text{s}$; $V = 0.73 \text{ m/s}$;
 $ff = 3.34$; $S_{0=} = 0.099$



August 4, 2007

$Q = 0.18 \text{ m}^3/\text{s}$; $V = 0.43 \text{ m/s}$;
 $ff = 5.23$; $S_{0=} = 0.086$



July 15, 2008

$Q = 0.46 \text{ m}^3/\text{s}$; $V = 0.54 \text{ m/s}$;
 $ff = 5.18$; $S_{0=} = 0.093$



July 12, 2007

$Q = 0.29 \text{ m}^3/\text{s}$; $V = 0.51 \text{ m/s}$;
 $ff = 4.74$; $S_{0=} = 0.094$

Figure 65: Photograph and measured and hydraulic variables for ESL7. Red arrows indicate same location in each photograph.

ESL8: Step-pool



June 9, 2008
 $Q = 0.57 \text{ m}^3/\text{s}; V = 0.62 \text{ m/s};$
 $ff = 4.22; S_{0-} = 0.099$



August 5, 2007
 $Q = 0.17 \text{ m}^3/\text{s}; V = 0.36 \text{ m/s};$
 $ff = 8.05; S_{0-} = 0.082$



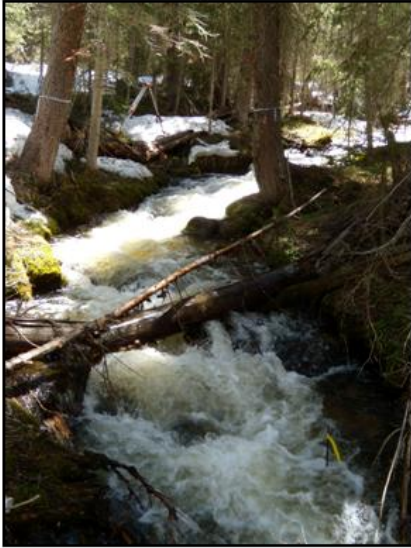
July 16, 2008
 $Q = 0.43 \text{ m}^3/\text{s}; V = 0.55 \text{ m/s};$
 $ff = 4.82; S_{0-} = 0.086$



July 11, 2007
 $Q = 0.27 \text{ m}^3/\text{s}; V = 0.46 \text{ m/s};$
 $ff = 6.22; S_{0-} = 0.091$

Figure 66: Photograph and measured and hydraulic variables for ESL8. Red arrows indicate same location in each photograph.

ESL9: Step-pool



June 4, 2008
 $Q = 0.57 \text{ m}^3/\text{s}$; $V = 0.62 \text{ m/s}$;
 $ff = 5.60$; $S_{0-} = 0.115$



August 6, 2007
 $Q = 0.16 \text{ m}^3/\text{s}$; $V = 0.34 \text{ m/s}$;
 $ff = 10.78$; $S_{0-} = 0.095$



July 16, 2008
 $Q = 0.33 \text{ m}^3/\text{s}$; $V = 0.46 \text{ m/s}$;
 $ff = 8.68$; $S_{0-} = 0.111$



July 11, 2007
 $Q = 0.16 \text{ m}^3/\text{s}$; $V = 0.34 \text{ m/s}$;
 $ff = 10.00$; $S_{0-} = 0.117$

Figure 67: Photograph and measured and hydraulic variables for ESL9. Red arrows indicate same location in each photograph.

FC1: Step-pool



June 11, 2008
 $Q = 0.33 \text{ m}^3/\text{s}$; $V = 0.86 \text{ m/s}$;
 $ff = 1.07$; $S_{0-} = 0.062$

August 12, 2007
 $Q = 0.02 \text{ m}^3/\text{s}$; $V = 0.20 \text{ m/s}$;
 $ff = 7.58$; $S_{0-} = 0.058$



July 23, 2008
 $Q = 0.05 \text{ m}^3/\text{s}$; $V = 0.29 \text{ m/s}$;
 $ff = 5.18$; $S_{0-} = 0.060$

July 5, 2007
 $Q = 0.08 \text{ m}^3/\text{s}$; $V = 0.41 \text{ m/s}$;
 $ff = 2.90$; $S_{0-} = 0.060$

Figure 68: Photograph and measured and hydraulic variables for FC1. Red arrows indicate same location in each photograph.

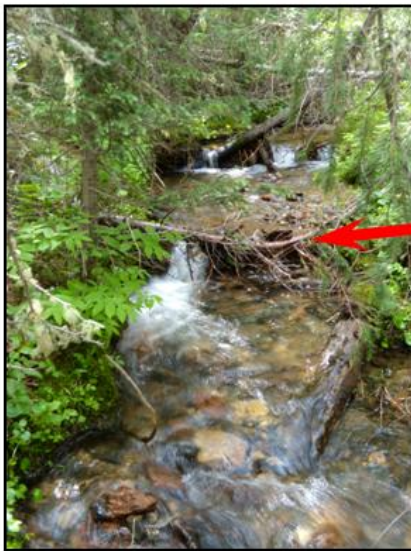
FC2: Step-pool



June 11, 2008
 $Q = 0.26 \text{ m}^3/\text{s}$; $V = 0.68 \text{ m/s}$;
 $ff = 2.23$; $S_{0=} = 0.074$



August 12, 2007
 $Q = 0.01 \text{ m}^3/\text{s}$; $V = 0.19 \text{ m/s}$;
 $ff = 9.39$; $S_{0=} = 0.071$



July 23, 2008
 $Q = 0.05 \text{ m}^3/\text{s}$; $V = 0.25 \text{ m/s}$;
 $ff = 9.59$; $S_{0=} = 0.077$

No Photograph

July 7, 2007
 $Q = 0.07 \text{ m}^3/\text{s}$; $V = 0.41 \text{ m/s}$;
 $ff = 3.49$; $S_{0=} = 0.073$

Figure 69: Photograph and measured and hydraulic variables for FC2. Red arrows indicate same location in each photograph.

FC3: Step-pool



June 12, 2008
 $Q = 0.24 \text{ m}^3/\text{s}; V = 0.43 \text{ m/s};$
 $ff = 7.24; S_{0-} = 0.093$

August 11, 2007
 $Q = 0.01 \text{ m}^3/\text{s}; V = 0.11 \text{ m/s};$
 $ff = 42.13; S_{0-} = 0.095$



July 22, 2008
 $Q = 0.04 \text{ m}^3/\text{s}; V = 0.18 \text{ m/s};$
 $ff = 26.92; S_{0-} = 0.092$

No Photograph

July 6, 2007
 $Q = 0.06 \text{ m}^3/\text{s}; V = 0.27 \text{ m/s};$
 $ff = 10.04; S_{0-} = 0.079$

Figure 70: Photograph and measured and hydraulic variables for FC3. Red arrows indicate same location in each photograph.

FC4: Step-pool



June 12, 2008
 $Q = 0.37 \text{ m}^3/\text{s}$; $V = 0.75 \text{ m/s}$;
 $ff = 3.82$; $S_{0-} = 0.141$



August 11, 2007
 $Q = 0.02 \text{ m}^3/\text{s}$; $V = 0.15 \text{ m/s}$;
 $ff = 39.89$; $S_{0-} = 0.132$



July 21, 2008
 $Q = 0.06 \text{ m}^3/\text{s}$; $V = 0.27 \text{ m/s}$;
 $ff = 16.20$; $S_{0-} = 0.130$

No Photograph

July 7, 2007
 $Q = 0.06 \text{ m}^3/\text{s}$; $V = 0.25 \text{ m/s}$;
 $ff = 19.90$; $S_{0-} = 0.136$

Figure 71: Photograph and measured and hydraulic variables for FC4. Red arrows indicate same location in each photograph.

FC5: Cascade



June 25, 2008
 $Q = 0.12 \text{ m}^3/\text{s}; V = 0.60 \text{ m/s};$
 $ff = 4.64; S_{0-} = 0.163$



August 10, 2007
 $Q = 0.01 \text{ m}^3/\text{s}; V = 0.12 \text{ m/s};$
 $ff = 39.22; S_{0-} = 0.143$



July 17, 2008
 $Q = 0.02 \text{ m}^3/\text{s}; V = 0.24 \text{ m/s};$
 $ff = 17.64; S_{0-} = 0.163$



July 8, 2007
 $Q = 0.02 \text{ m}^3/\text{s}; V = 0.23 \text{ m/s};$
 $ff = 18.12; S_{0-} = 0.159$

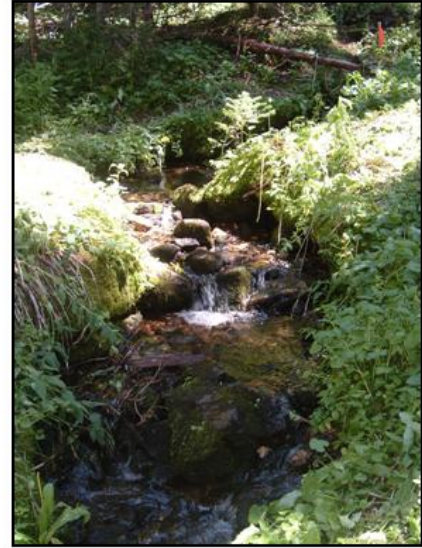
Figure 72: Photograph and measured and hydraulic variables for FC5. Red arrows indicate same location in each photograph.

FC6: Cascade



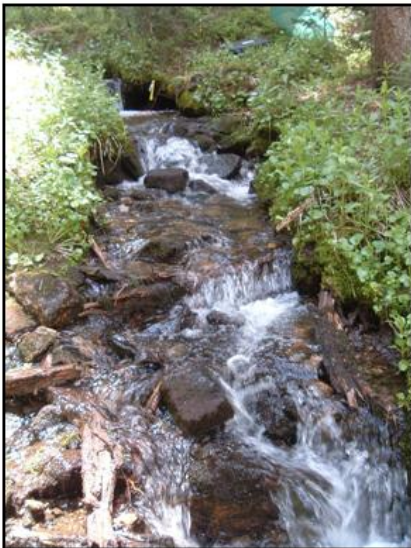
June 25, 2008

$Q = 0.10 \text{ m}^3/\text{s}$; $V = 0.61 \text{ m/s}$;
 $ff = 4.73$; $S_{0-} = 0.195$



August 10, 2007

$Q = 0.01 \text{ m}^3/\text{s}$; $V = 0.13 \text{ m/s}$;
 $ff = 36.16$; $S_{0-} = 0.166$



July 17, 2008

$Q = 0.02 \text{ m}^3/\text{s}$; $V = 0.23 \text{ m/s}$;
 $ff = 19.33$; $S_{0-} = 0.181$

No Photograph

July 8, 2007

$Q = 0.02 \text{ m}^3/\text{s}$; $V = 0.27 \text{ m/s}$;
 $ff = 15.29$; $S_{0-} = 0.185$

Figure 73: Photograph and measured and hydraulic variables for FC6. Red arrows indicate same location in each photograph.

9.4 Appendix D: Grain size distribution graphs for each reach

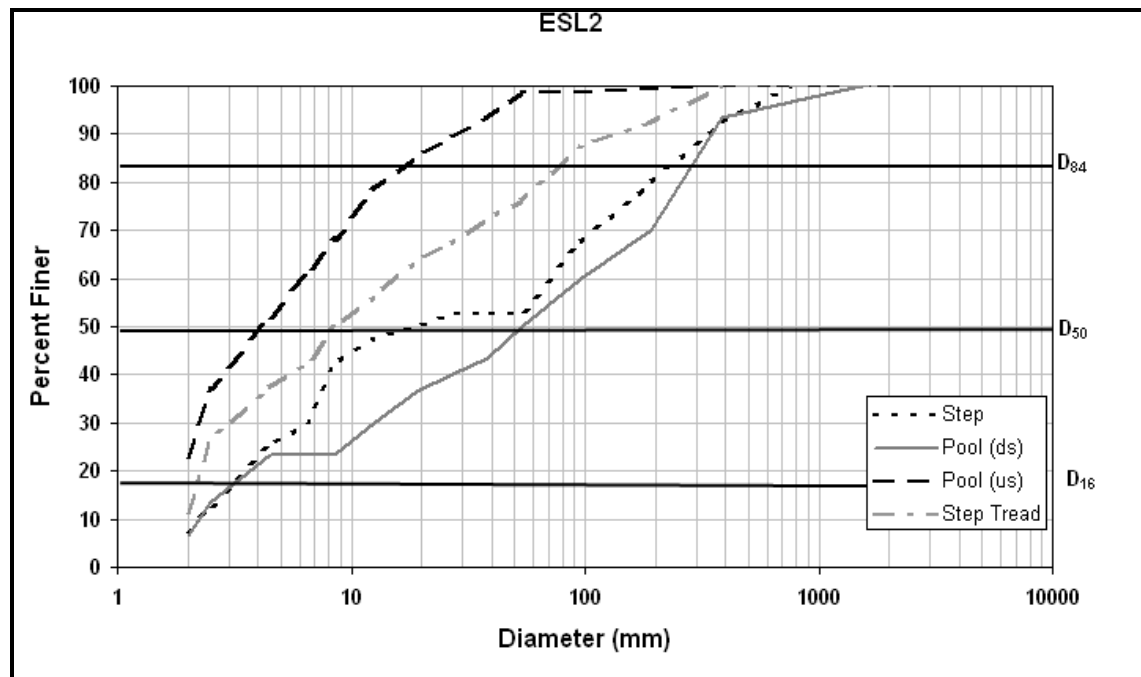
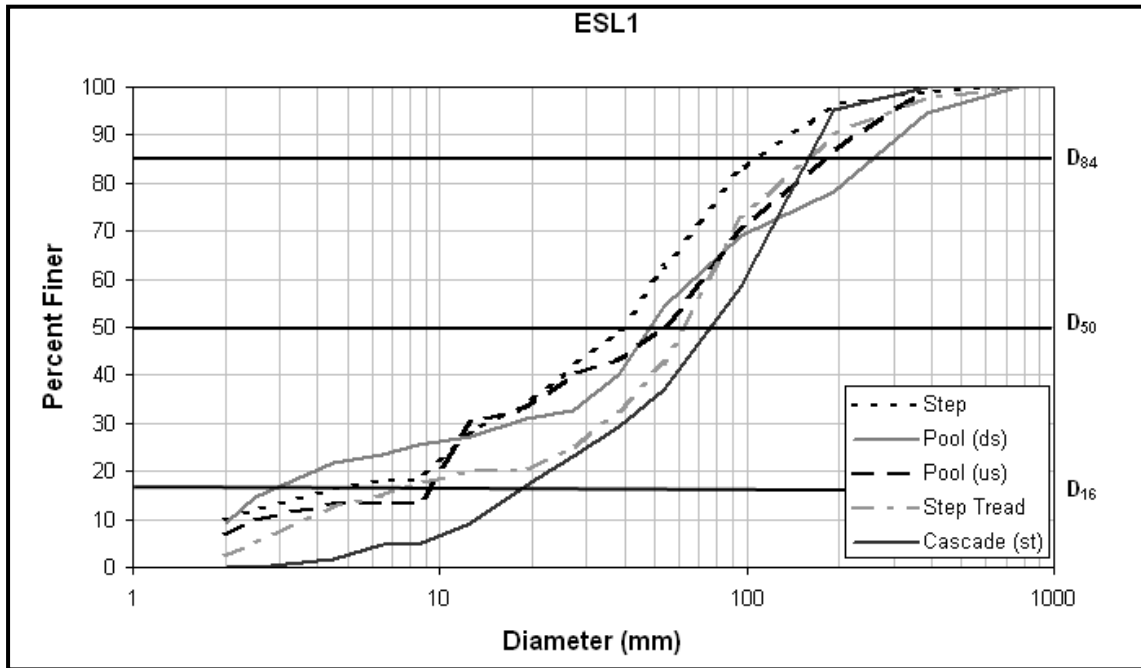
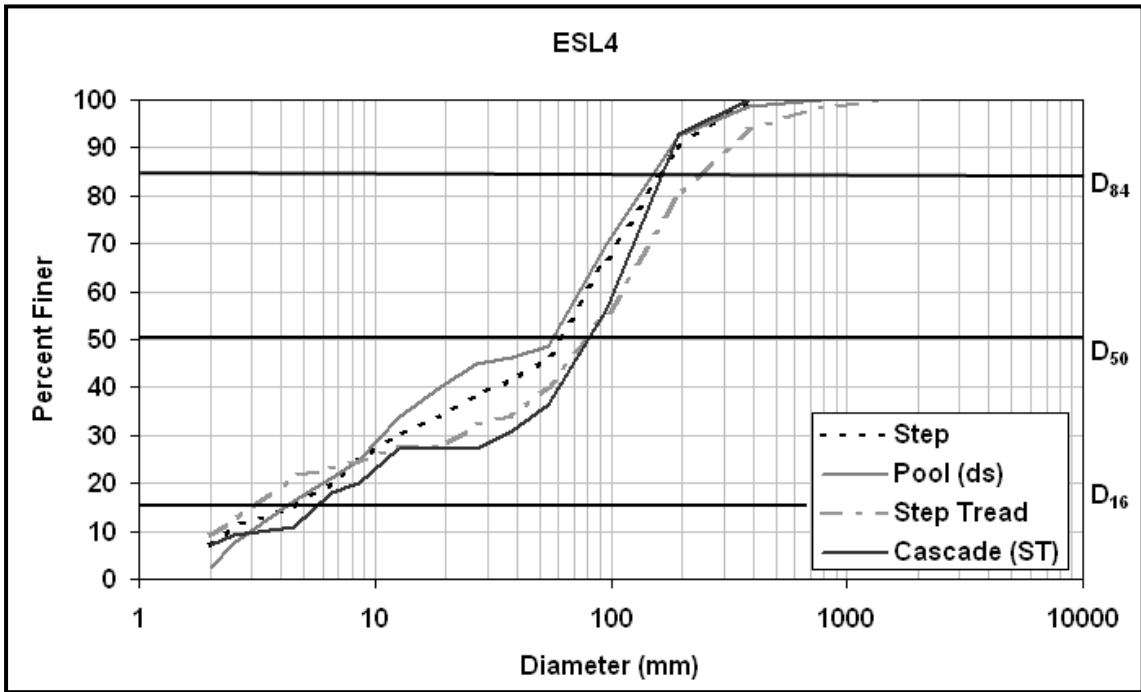
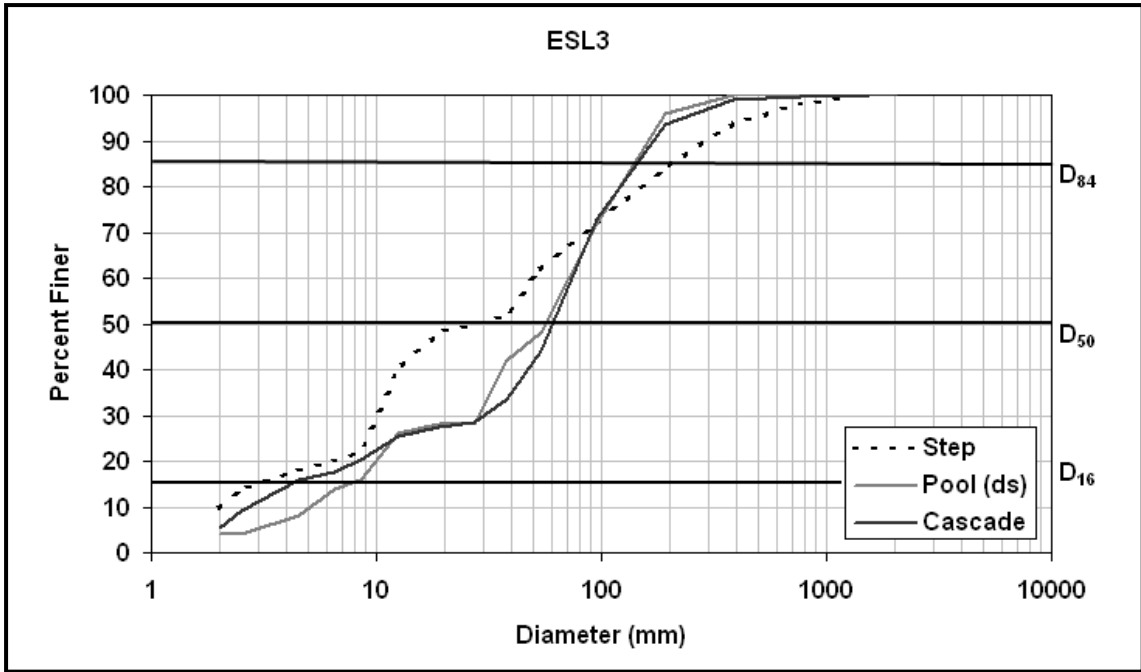


Figure 75: Grain size distribution for entire reach and separated by section for ESL2.



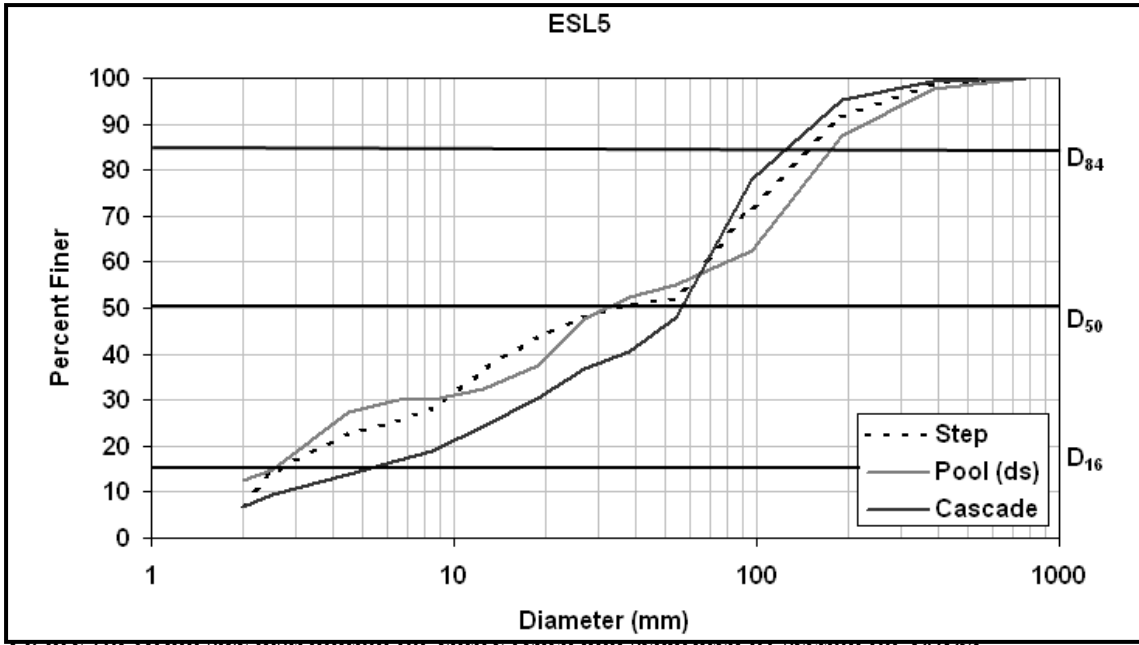


Figure 78: Grain size distribution for entire reach and separated by section for ESL5.

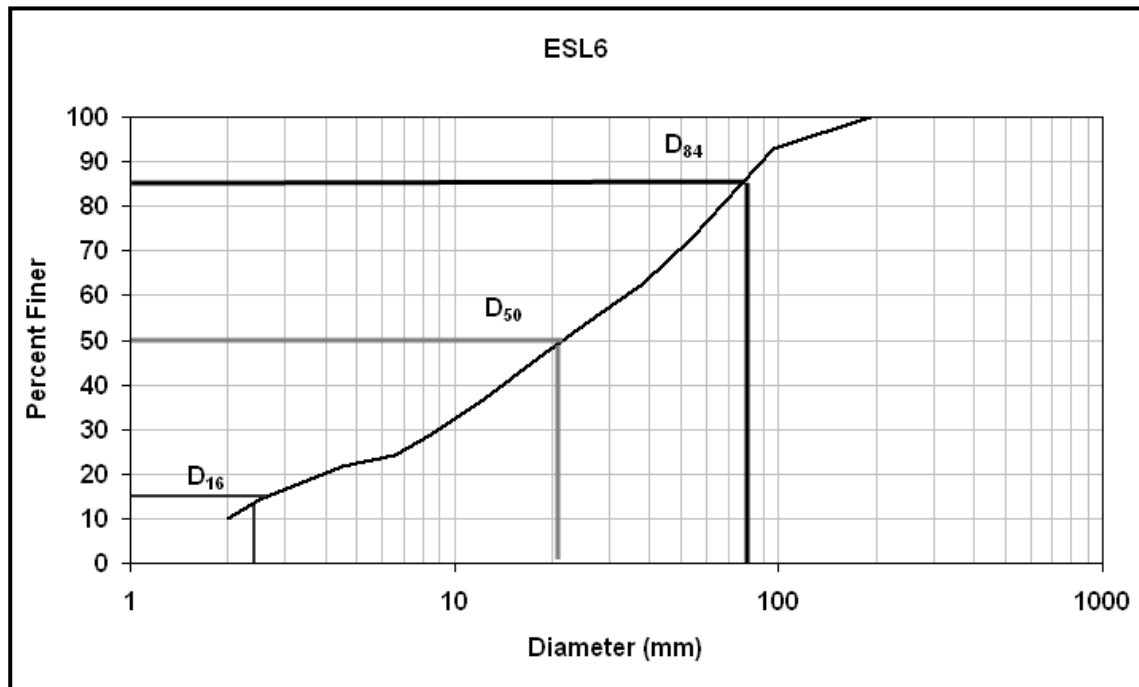


Figure 79: Grain size distribution for entire reach for ESL6.

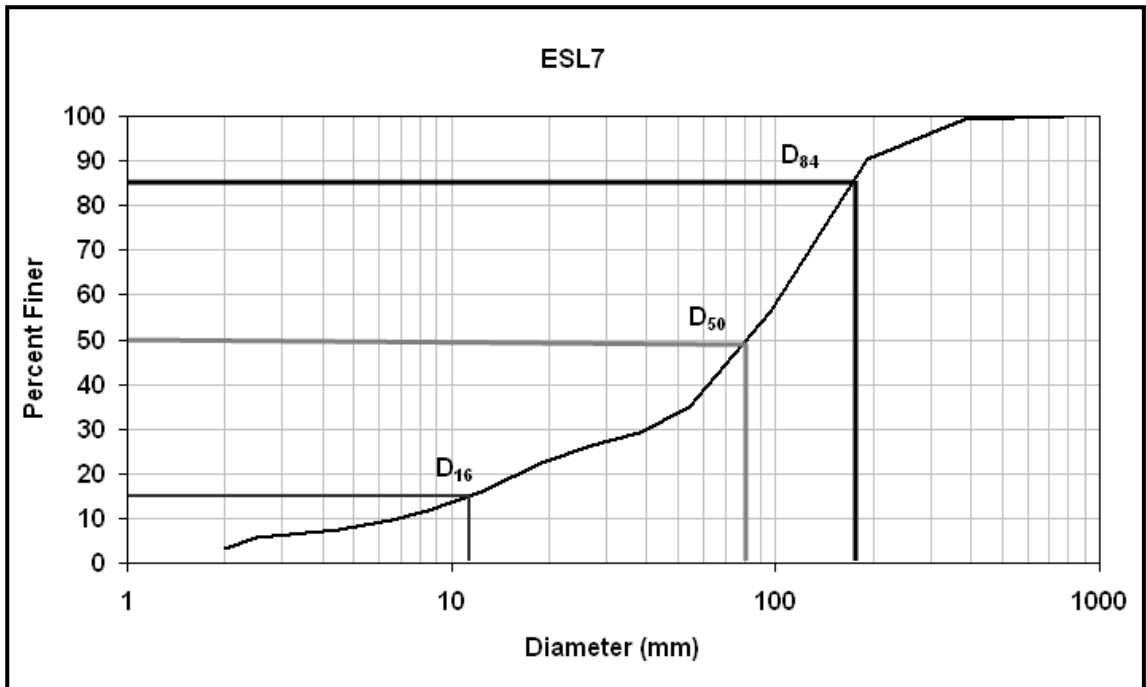


Figure 80: Grain size distribution for entire reach for ESL7.

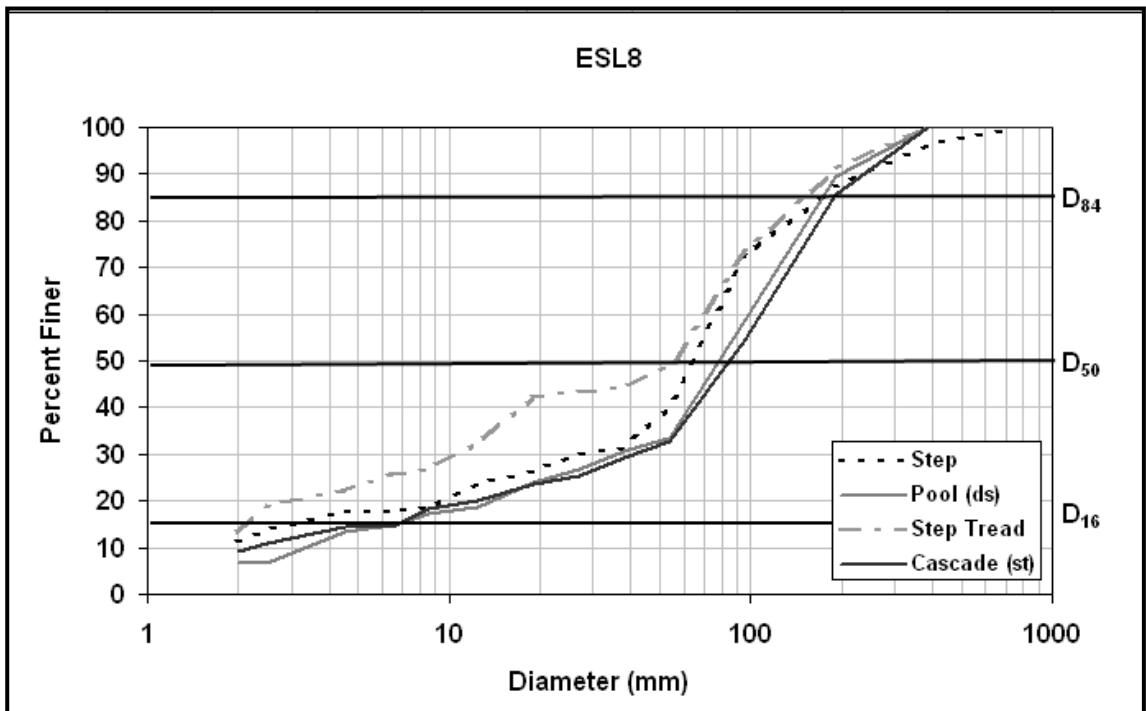


Figure 81: Grain size distribution for entire reach and separated by section for ESL8.

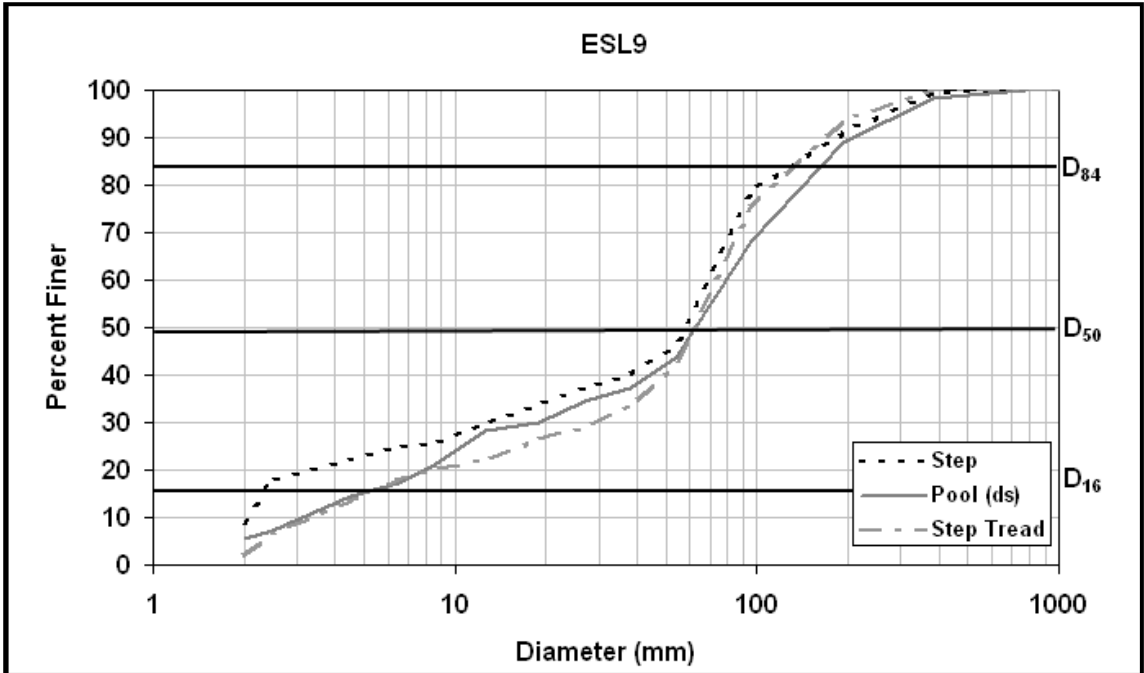


Figure 82: Grain size distribution for entire reach and separated by section for ESL9.

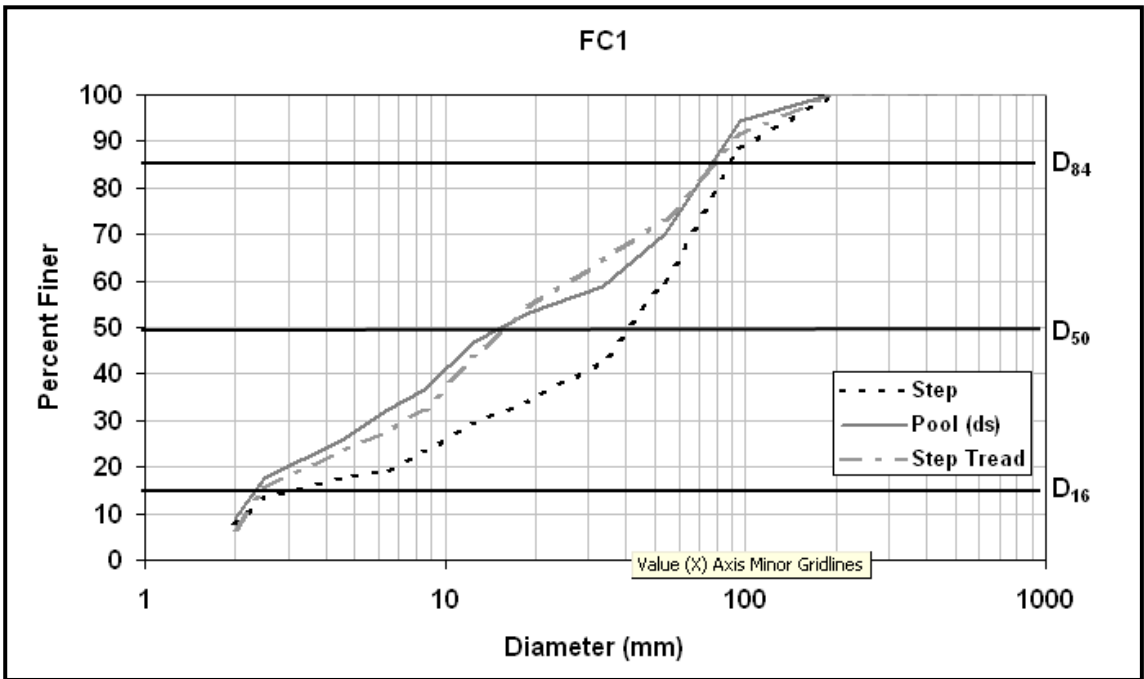


Figure 83: Grain size distribution for entire reach and separated by section for FC1.

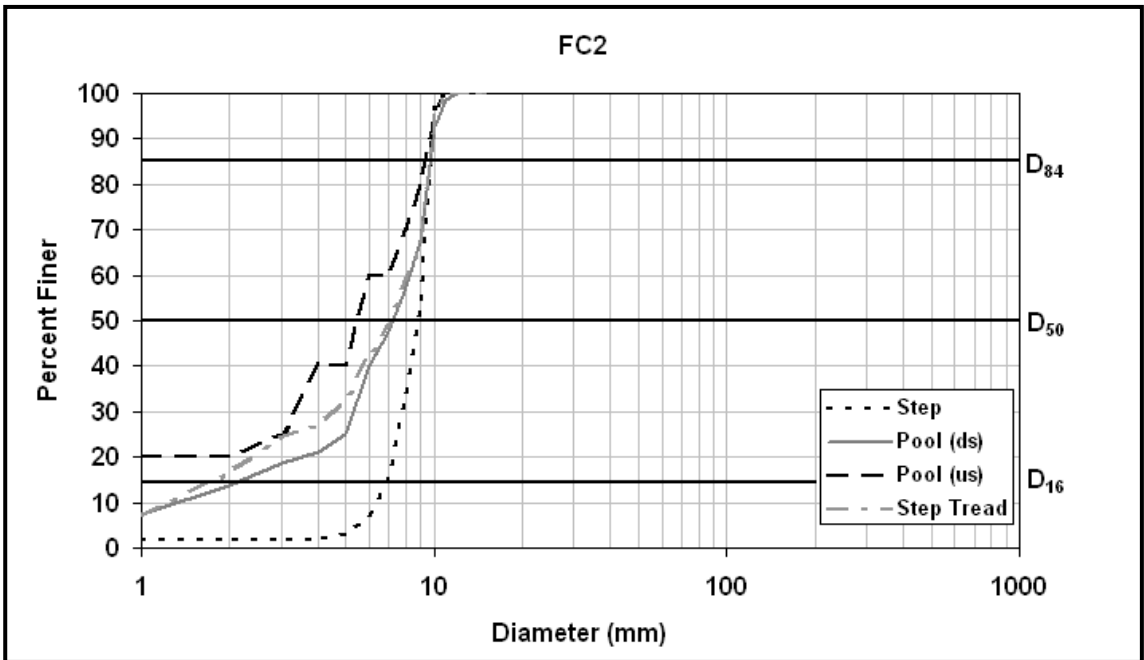


Figure 84: Grain size distribution for entire reach and separated by section for FC2.

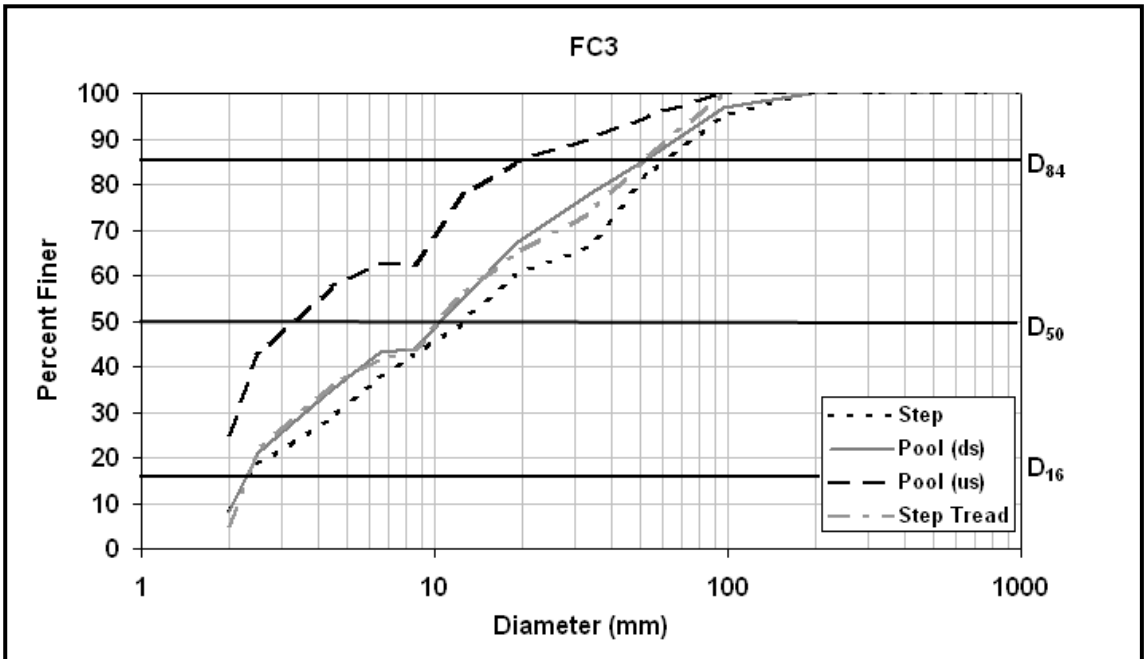


Figure 85: Grain size distribution for entire reach and separated by section for FC3.

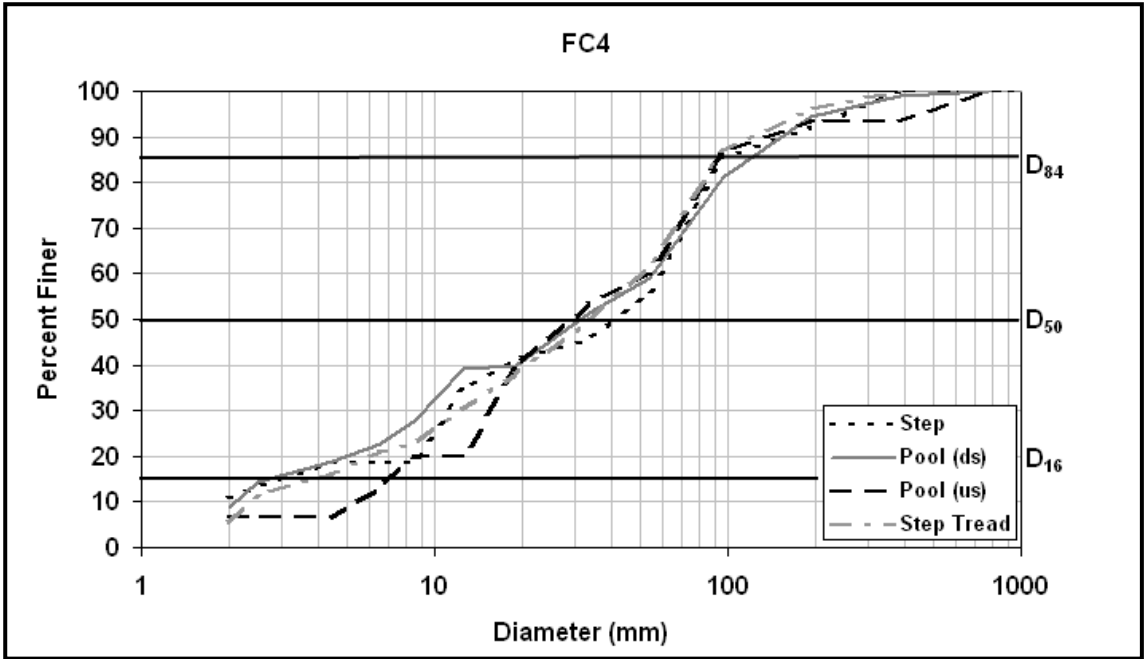


Figure 86: Grain size distribution for entire reach and separated by section for FC4.

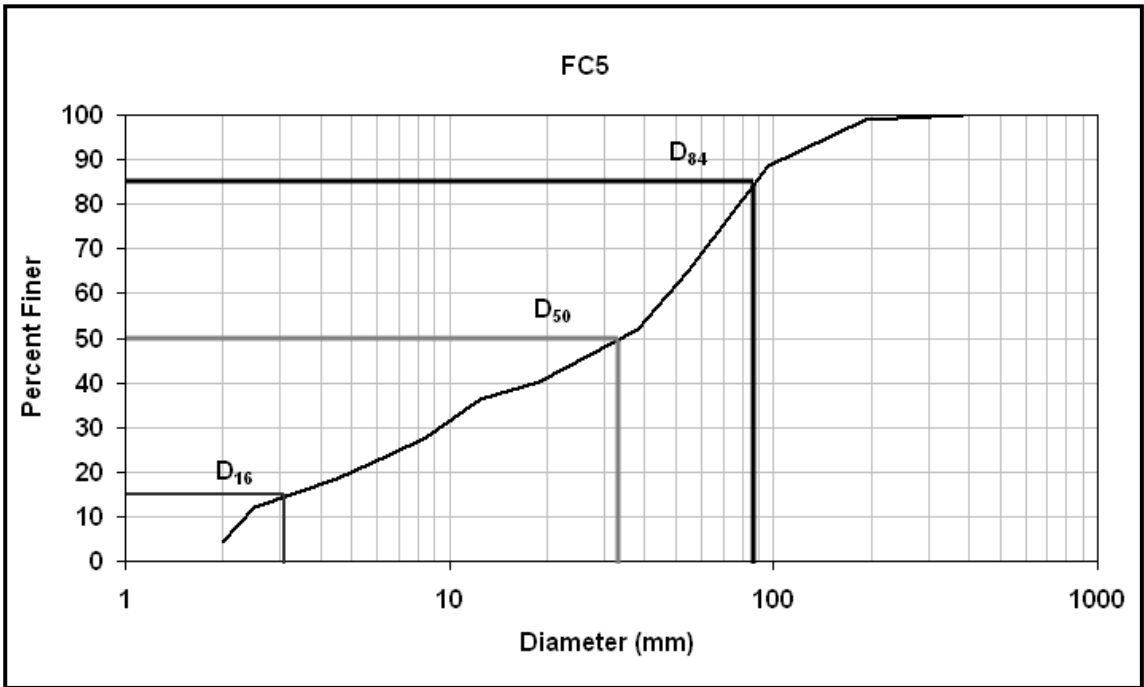


Figure 87: Grain size distribution for entire reach and separated by section for FC5.

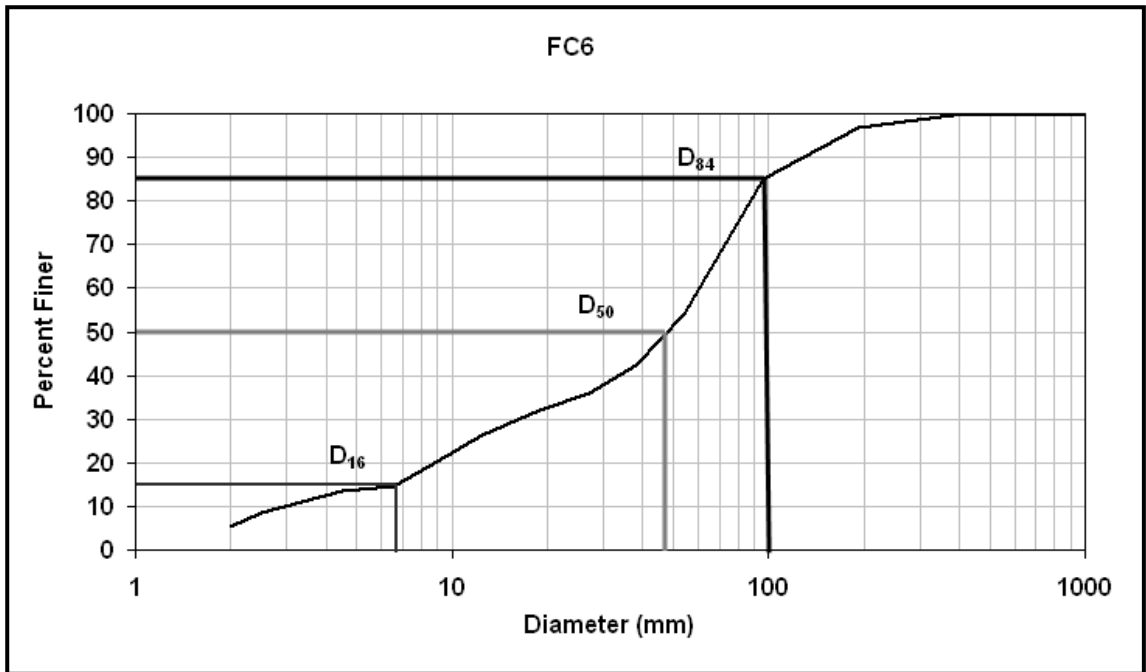


Figure 88: Grain size distribution for entire reach and separated by section for FC6.

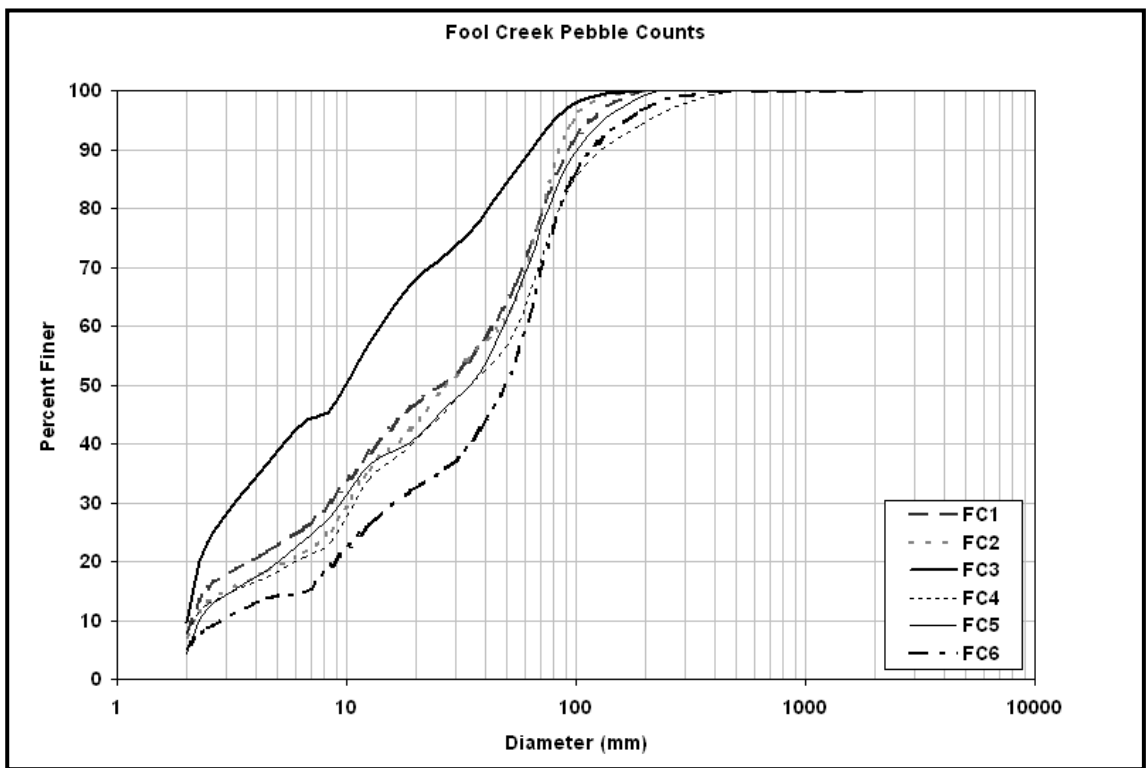


Figure 89: Cumulative grain size distribution for all Fool Creek reaches.

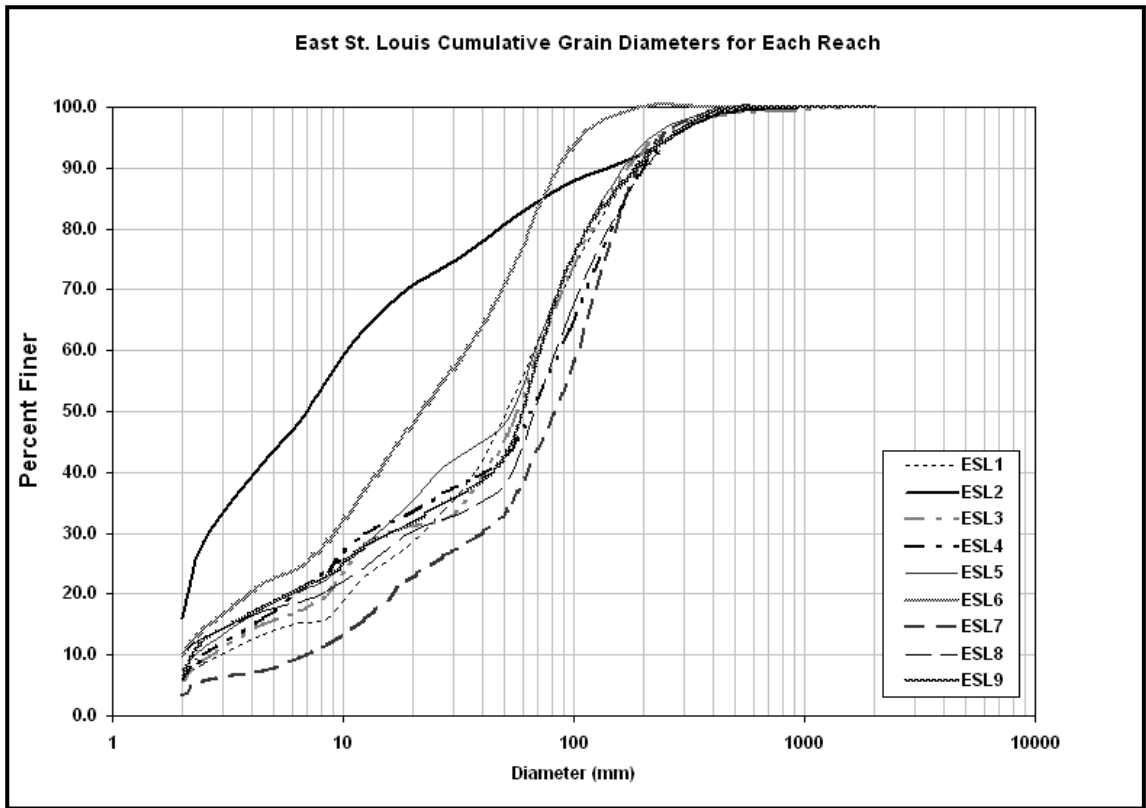


Figure 90: Cumulative grain size distribution for all East St. Louis reaches.

9.5 Appendix E: In-channel wood photographs and location in each reach.

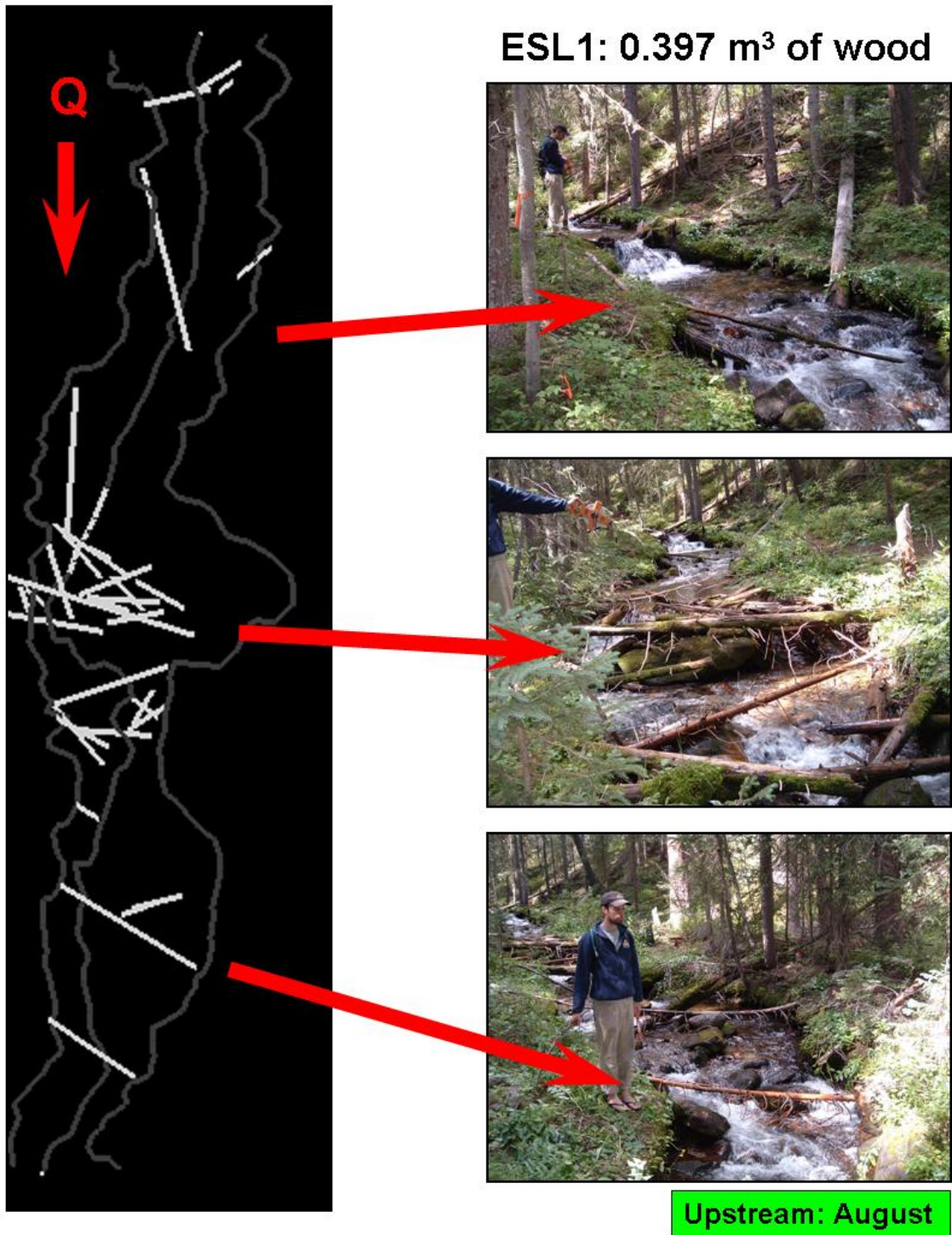


Figure 91: Location and photographs of wood in ESL1.

ESL2: 0.946 m³ of wood

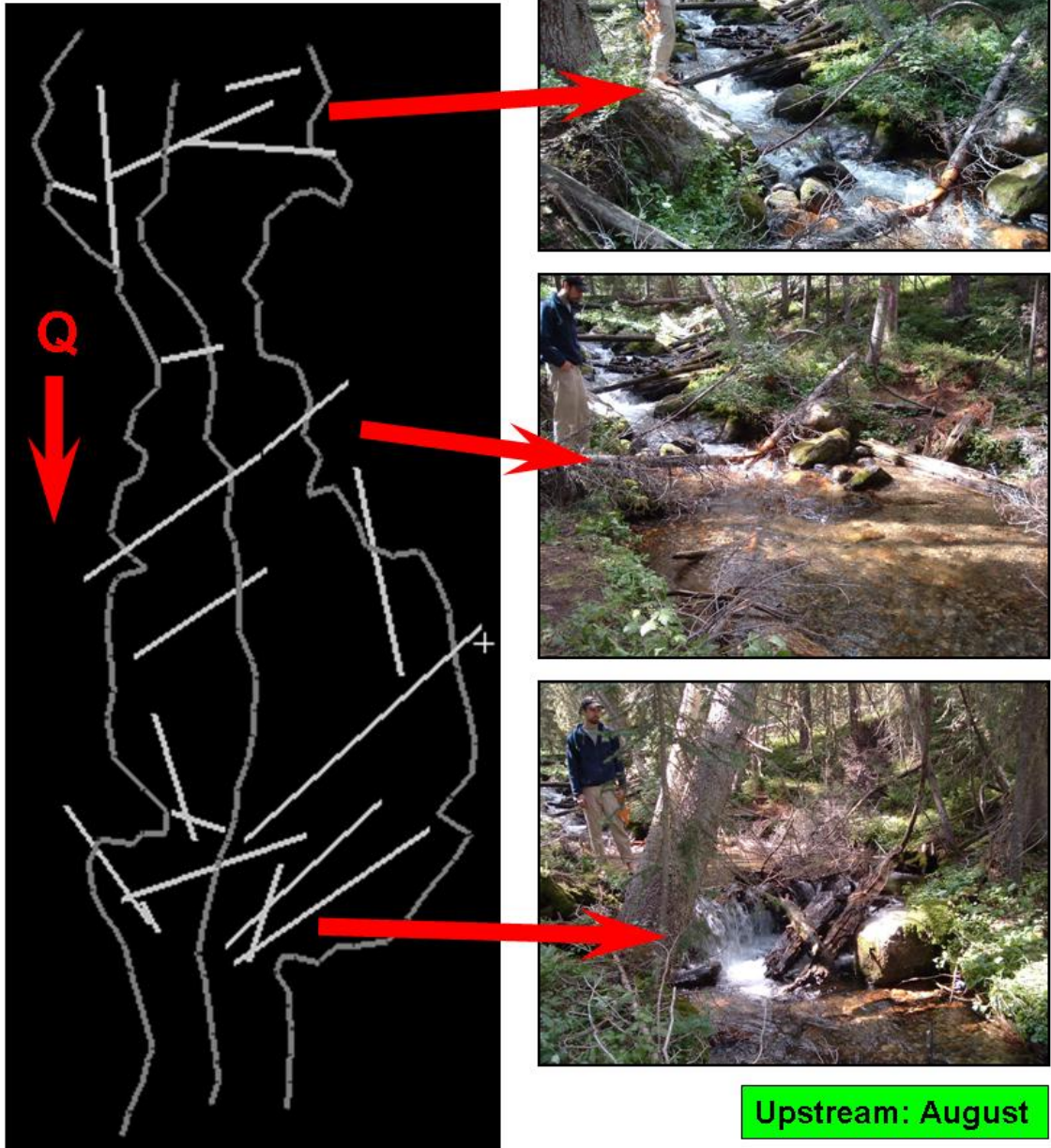


Figure 92: Location and photographs of wood in ESL2.

ESL3: 0.033 m³ of wood

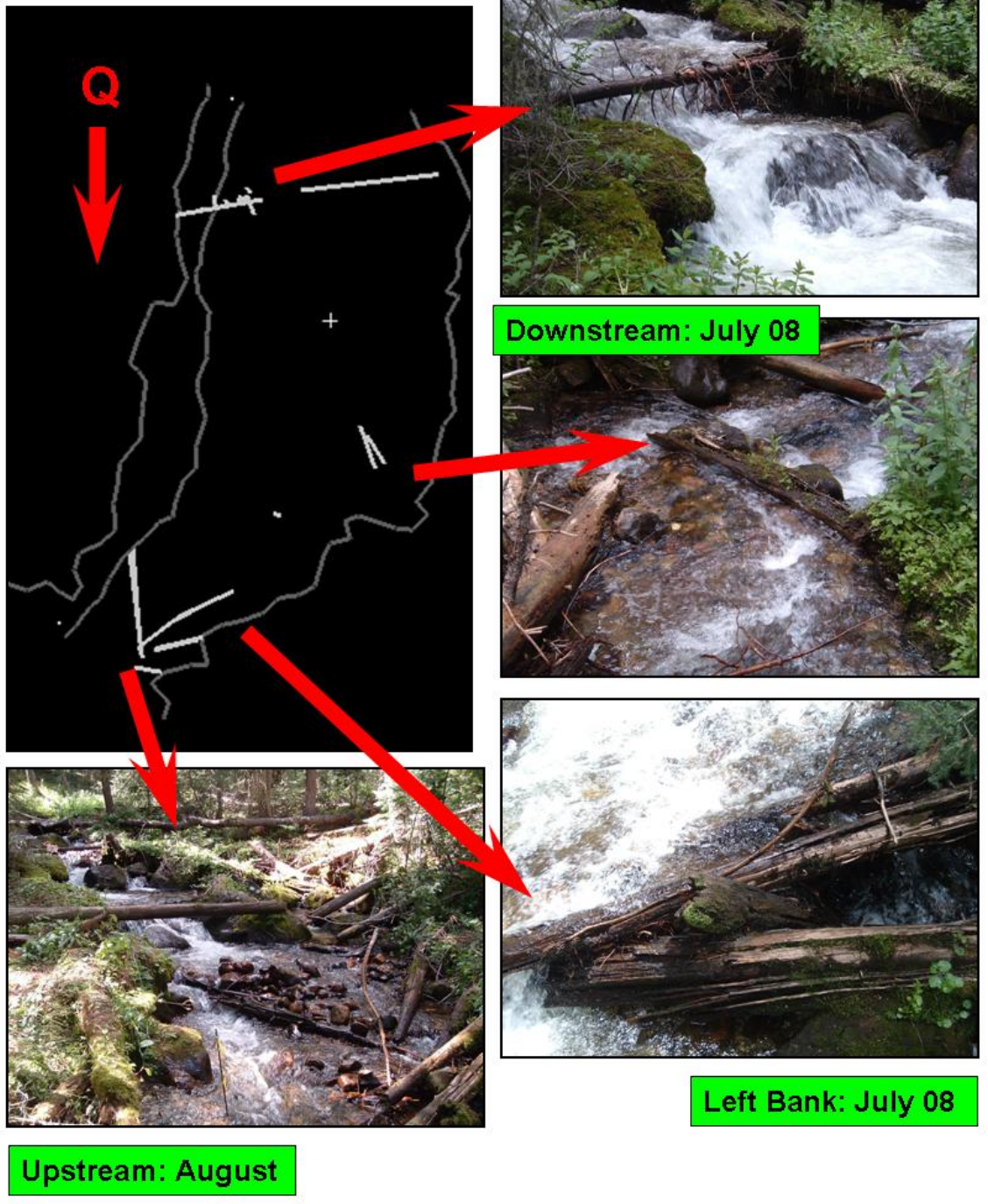


Figure 93: Location and photographs of wood in ESL3.

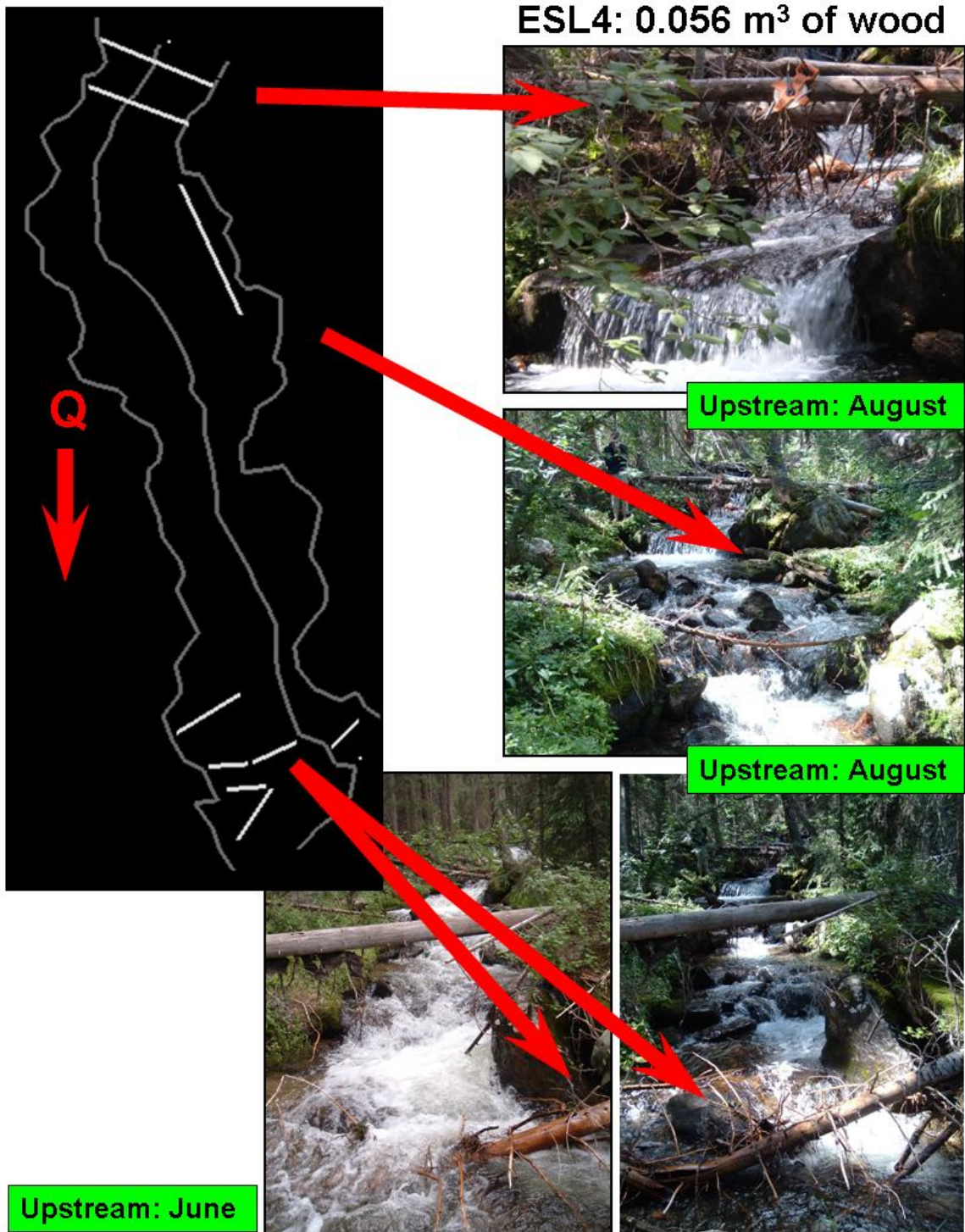


Figure 94: Location and photographs of wood in ESL4.

ESL5: 0.335 m³ of wood

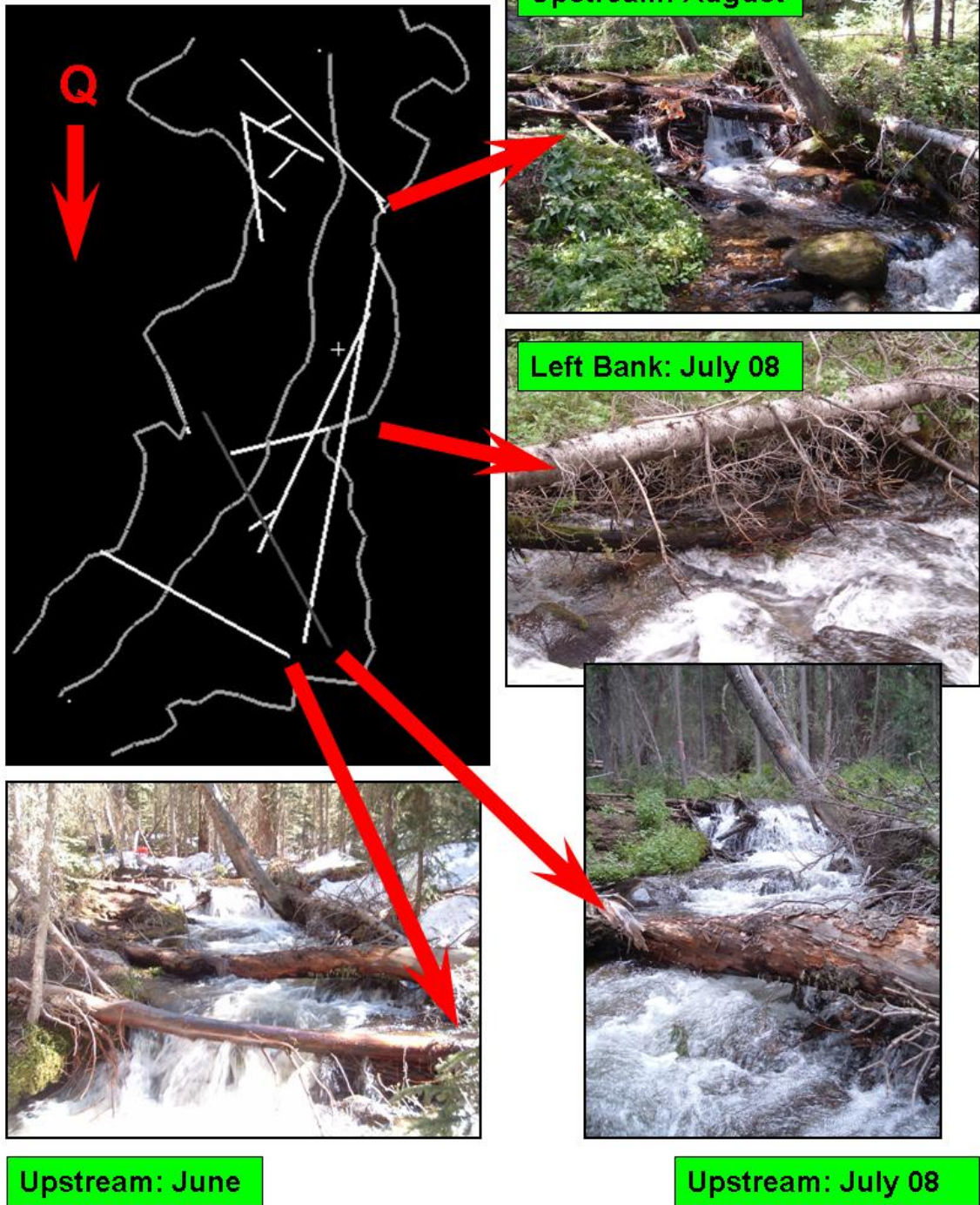
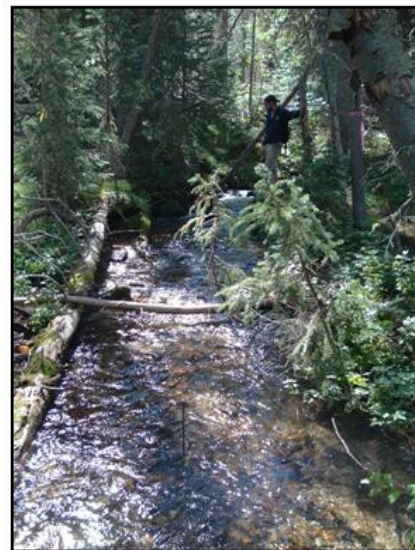
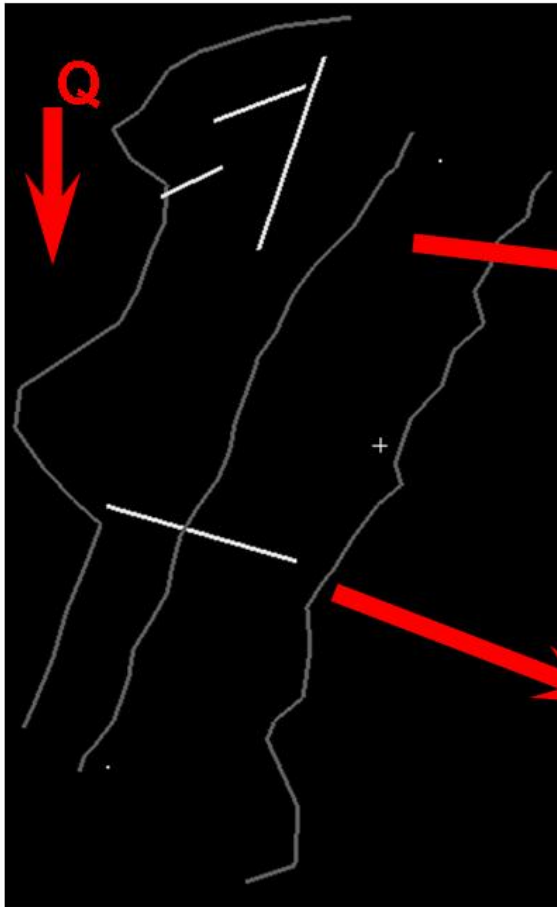


Figure 95: Location and photographs of wood in ESL5.

ESL6: 0.044 m³ of wood

Downstream: August



Upstream: August

Figure 96: Location and photographs of wood in ESL6.

ESL7: 0.069 m³ of wood

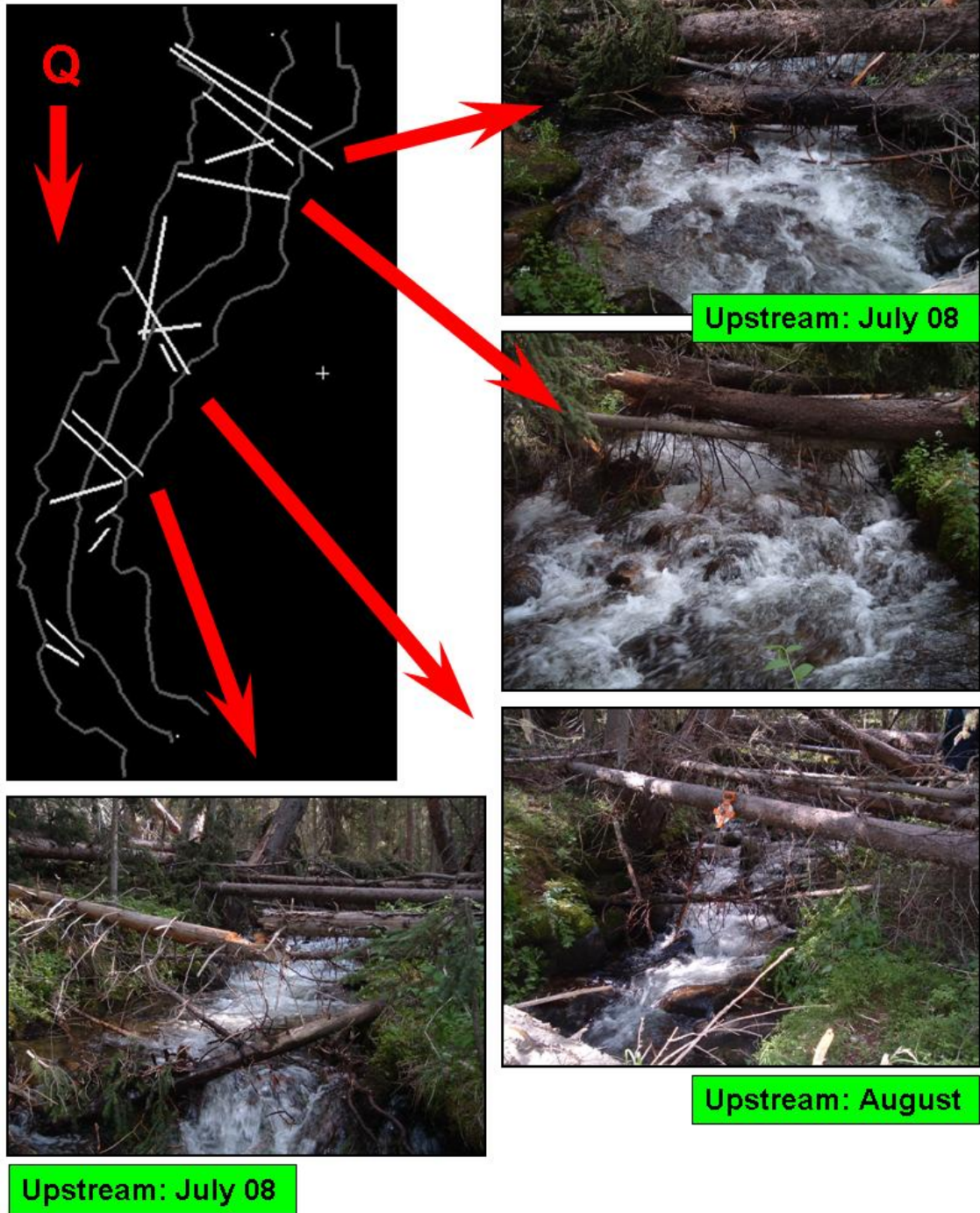
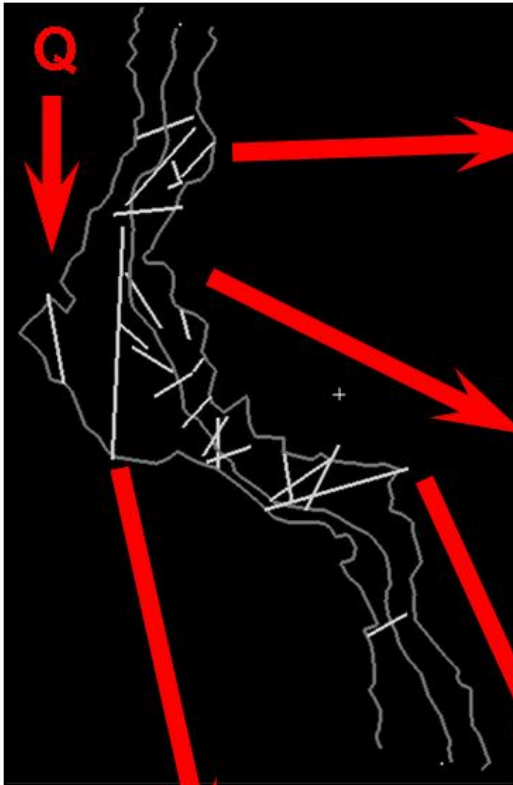


Figure 97: Location and photographs of wood in ESL7.

ESL8: 0.502 m³ of wood

Right Bank: August



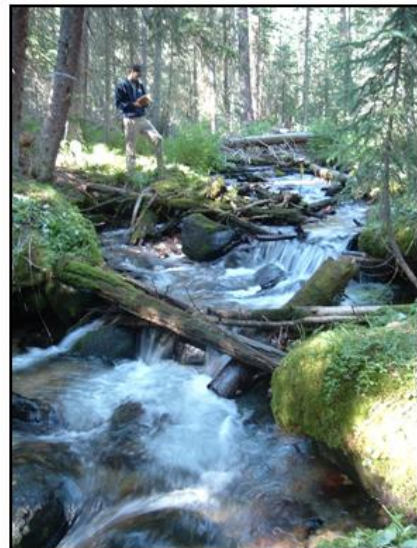
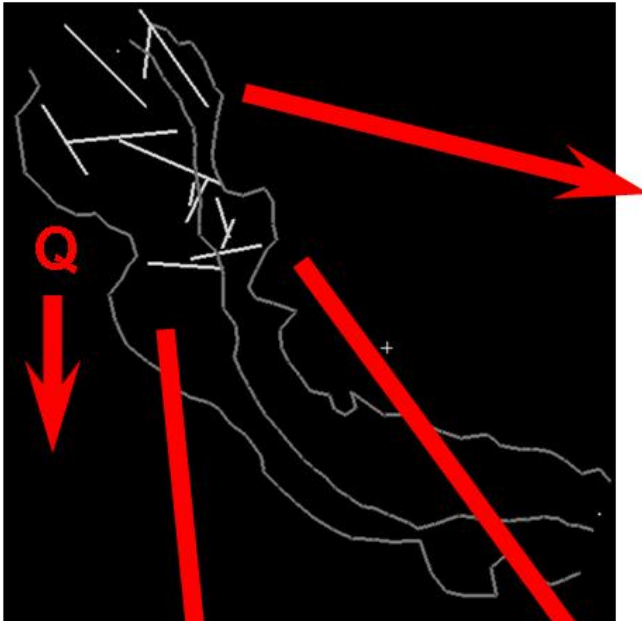
Upstream: July 08

Upstream: July 08

Figure 98: Location and photographs of wood in ESL8.

ESL9: 0.304 m³ of wood

Upstream: August



Upstream: July 08

Upstream: August

Figure 99: Location and photographs of wood in ESL9.

FC1: 0.006 m³ of wood

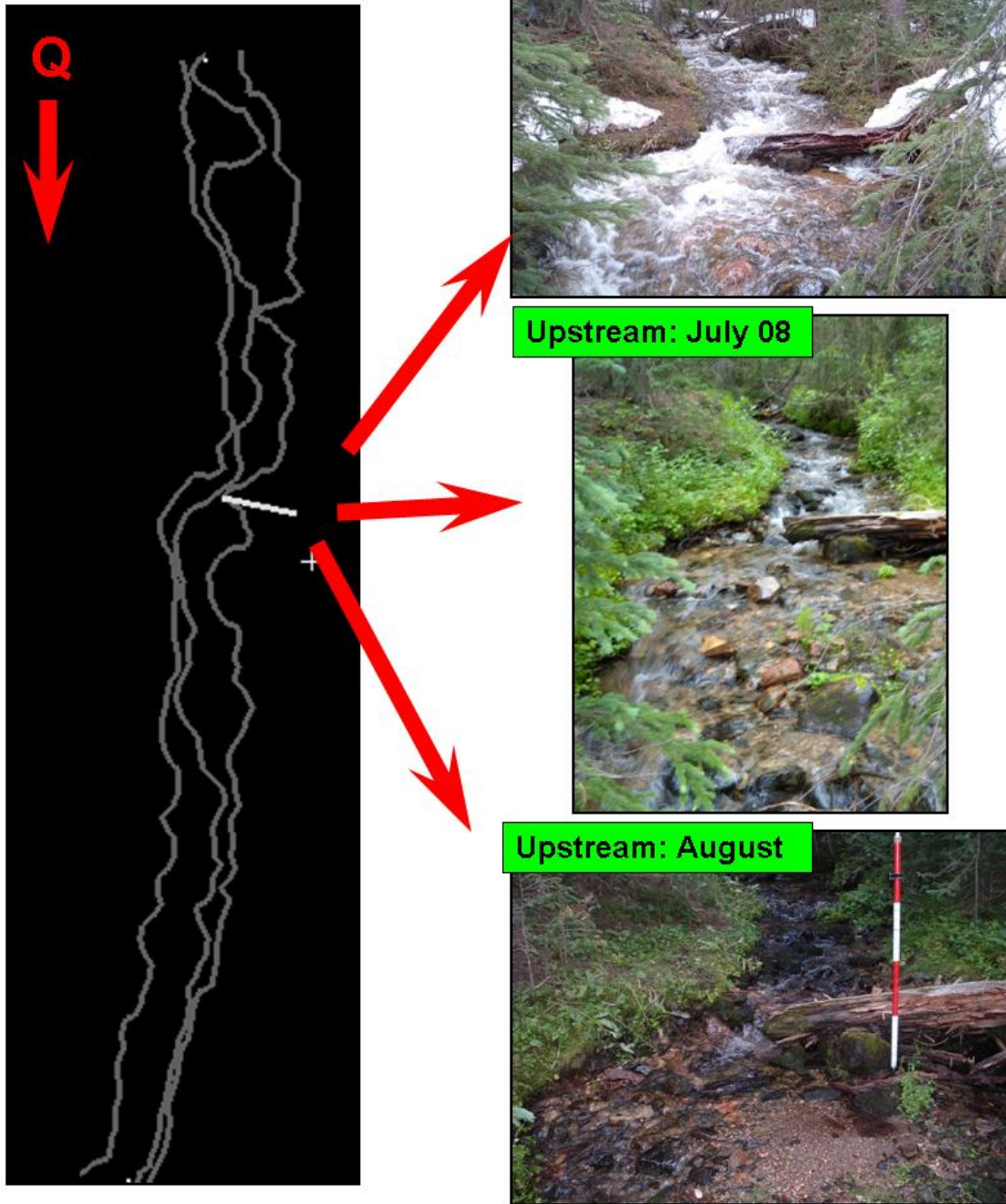


Figure 100: Location and photographs of wood in FC1.

FC2: 0.055 m³ of wood

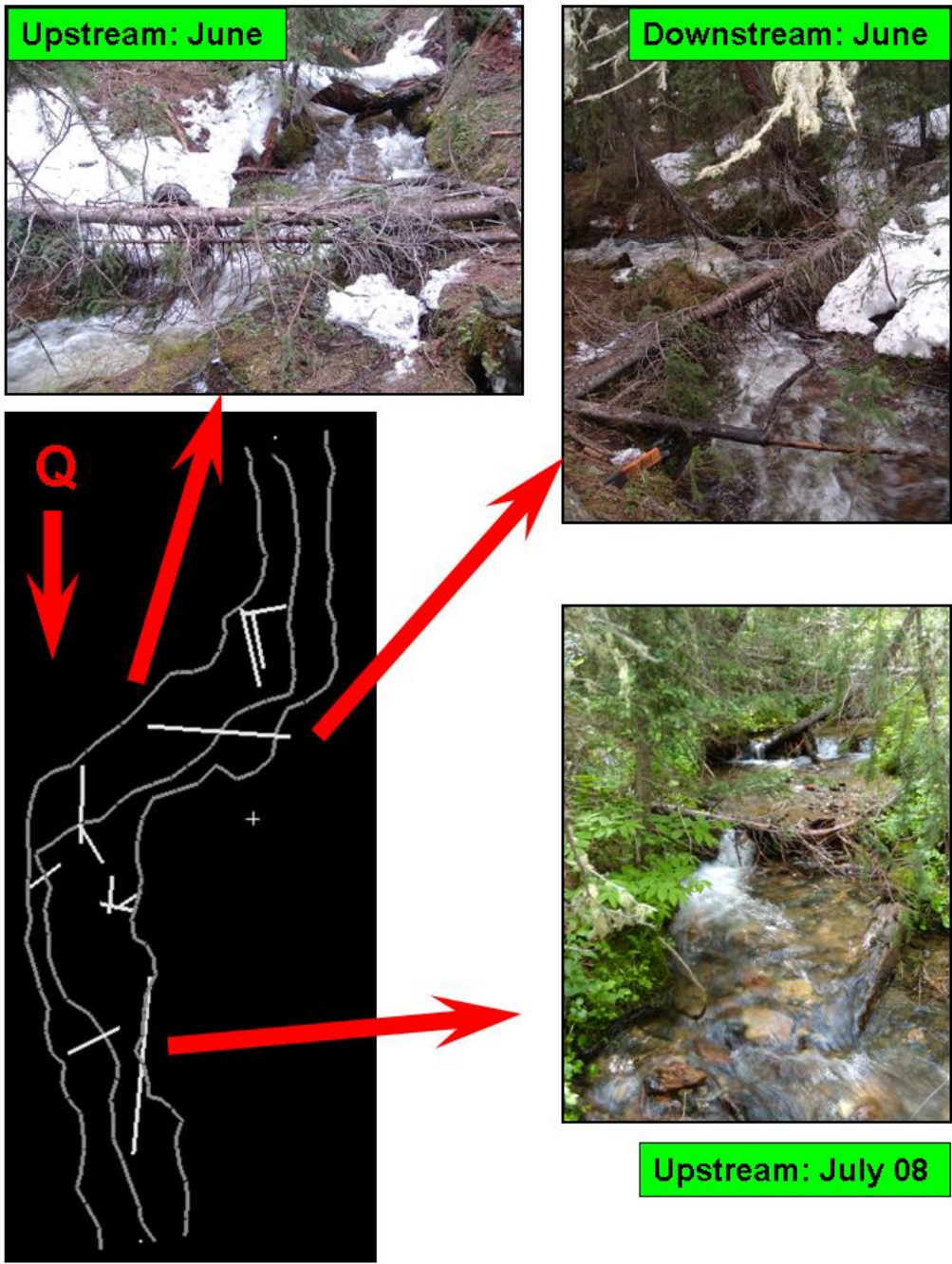


Figure 101: Location and photographs of wood in FC2.

FC3: 0.174 m³ of wood

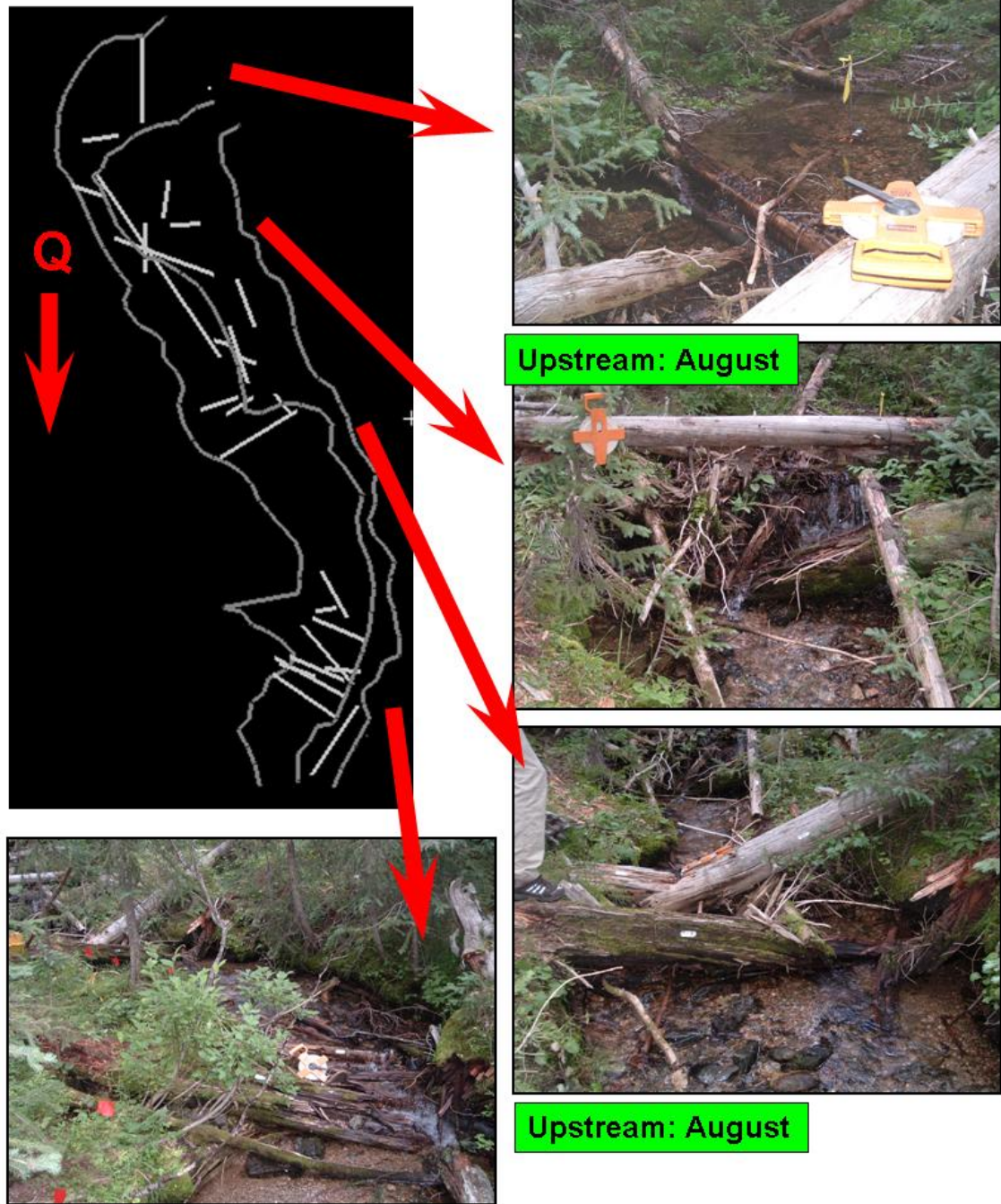


Figure 102: Location and photographs of wood in FC3.

FC4: 0.183 m³ of wood

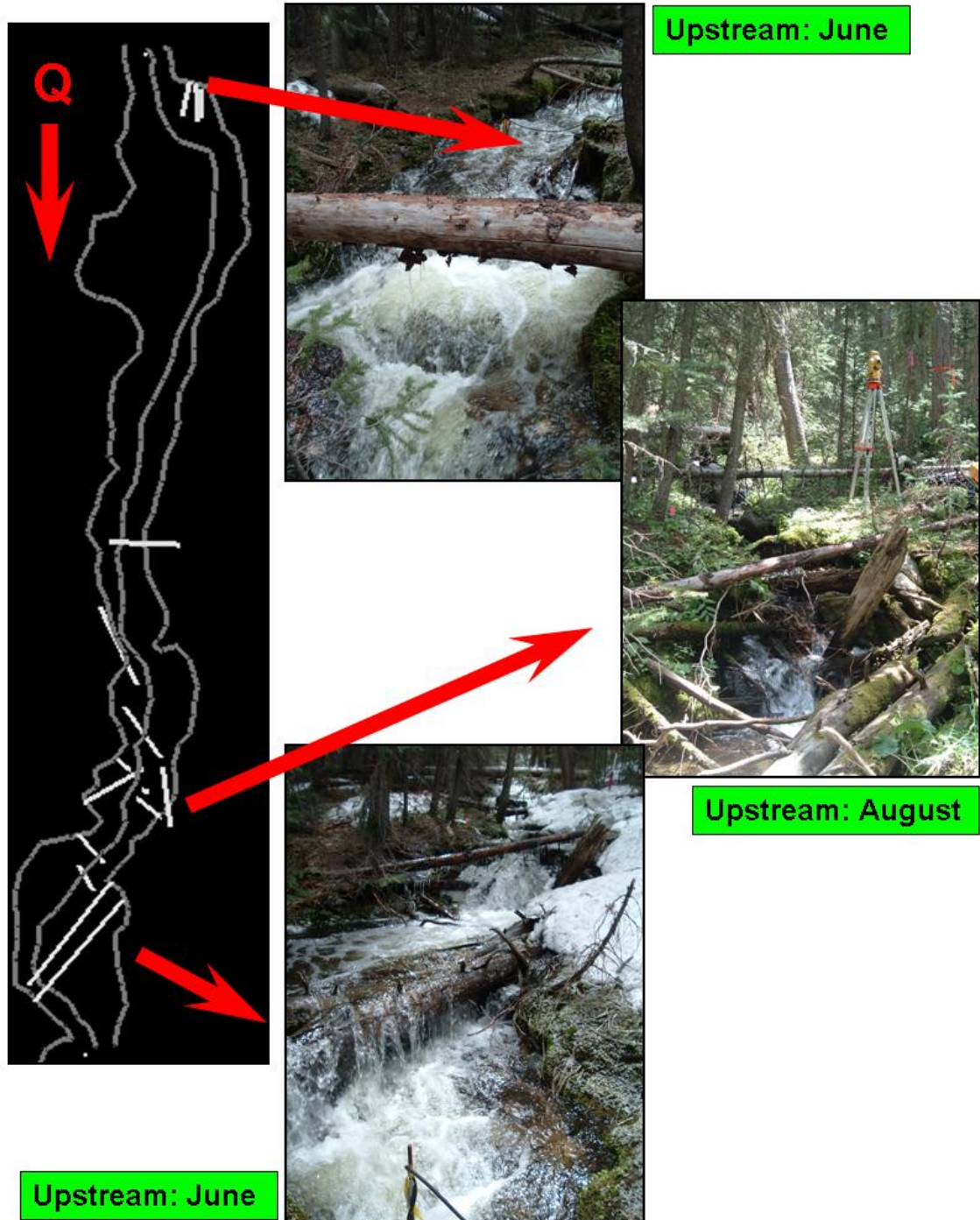


Figure 103: Location and photographs of wood in FC4.

FC5: 0.099 m³ of wood

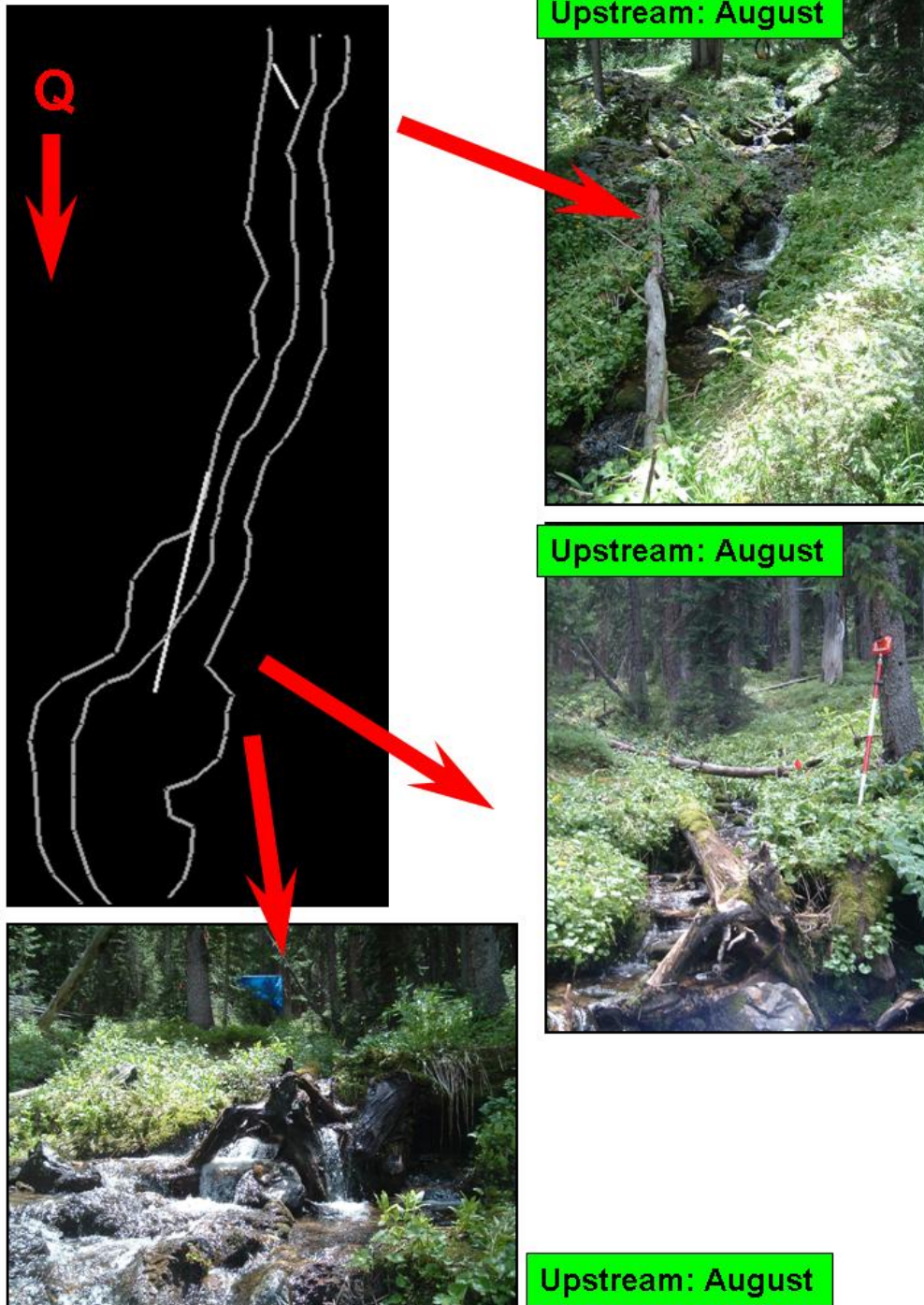


Figure 104: Location and photographs of wood in FC5.

FC6: 0.011 m³ of wood

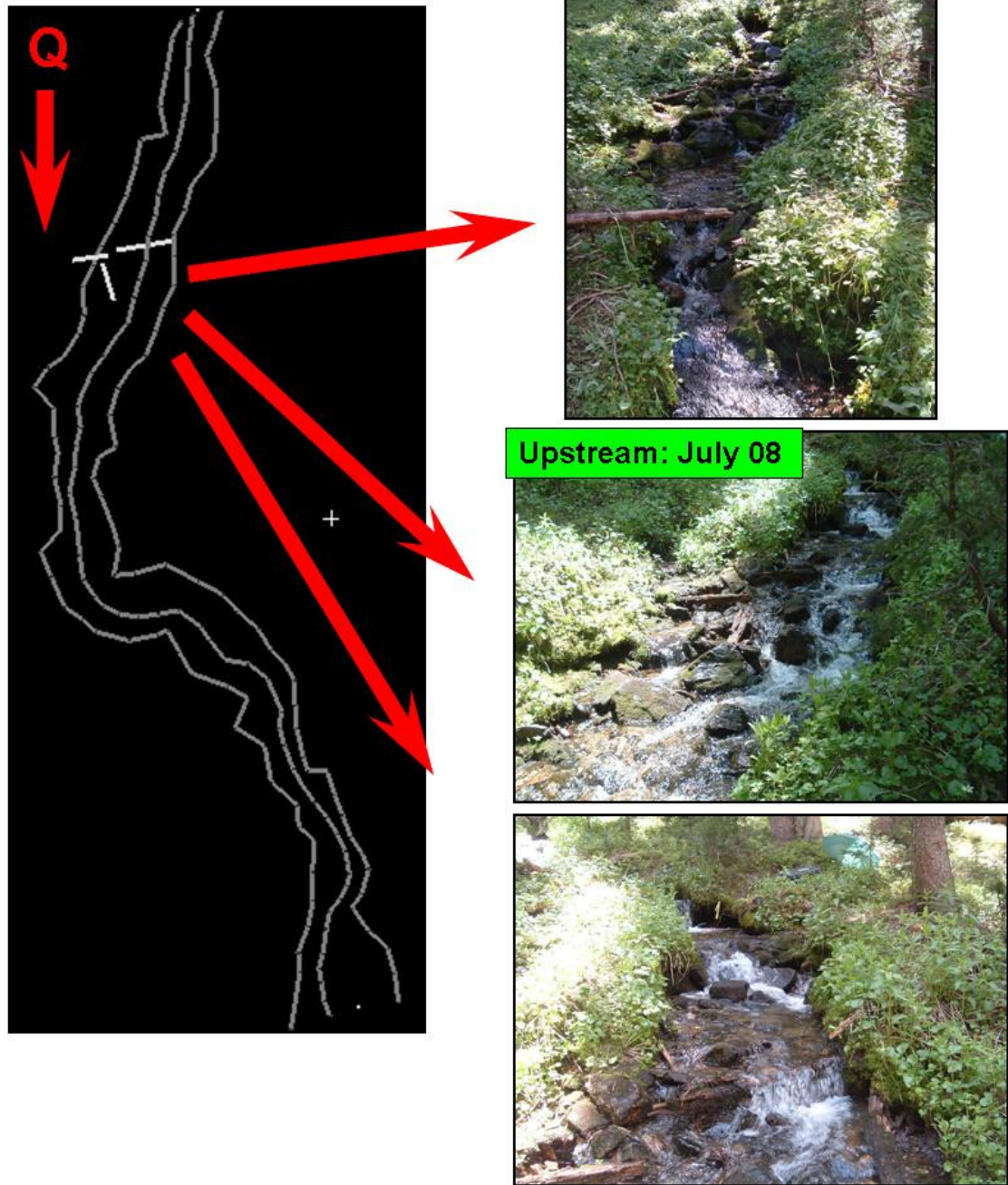


Figure 105: Location and photographs if wood in FC6.

Table 20: Summary table for wood: No. cyl = number of pieces counted in each reach as an individual cylinder that influences roughness; L_w = average length of individual cylinders in each reach; D_w = average diameter of individual cylinders; V_T = total volume of wood counting both wood as individual pieces and wood in steps; V_C = total volume of individual cylinders in each reach; V_{WS} = total volume of wood in steps in each reach; % Steps = percent of wood in steps; % Cyl. = percent of wood as individual cylinders; ff_{wood} = partitioned friction factor for wood (only using wood as individual cylinders in each reach).

Reach	Channel Type	Flow Period	No. Cyl.	L_w	D_w	V_T	V_C	V_{WS}	Wood per m ² of channel	Wood Density (all)	Wood Density (ind)	% Steps	% Cyl.	ff_{wood}
ESL1	Step-Pool	June2008	15	1.563	0.088	0.397	0.119	0.278	4.63E-03	0.170	0.065	70.1	29.9	3.11
		July2008	11	1.108	0.094	0.351	0.073	0.278	4.94E-03	0.172	0.046	79.3	20.7	2.27
		Aug2007	6	0.425	0.097	0.296	0.017	0.278	4.65E-03	0.153	0.012	94.1	5.9	1.52
ESL2	Step-Pool	June2008	5	2.274	0.123	0.948	0.258	0.689	2.15E-02	0.459	0.128	72.7	27.3	1.77
		July2008	5	1.643	0.121	0.862	0.172	0.689	2.08E-02	0.446	0.095	80.0	20.0	1.45
		July2007	5	1.505	0.117	0.833	0.143	0.689	2.09E-02	0.451	0.086	82.8	17.2	0.63
		Aug2007	4	1.610	0.113	0.786	0.096	0.689	2.18E-02	0.475	0.072	87.7	12.3	0.38
ESL3	Cascade	June2008	5	0.689	0.074	0.033	0.021	0.012	8.93E-04	0.039	0.023	36.2	63.8	3.14
		July2008	4	0.298	0.079	0.023	0.011	0.012	6.10E-04	0.027	0.011	52.1	47.9	2.78
		July2007	4	0.251	0.074	0.020	0.008	0.012	6.10E-04	0.028	0.010	61.0	39.0	2.77
		Aug2007	none	none	none	0.012	0.000	0.012	4.42E-04	0.022	0.000	100.0	0.0	0.00
ESL4	Step-Pool	June2008	9	1.041	0.062	0.056	0.056	0.000	1.26E-03	0.053	0.053	0.0	100.0	1.47
		July2008	8	0.636	0.054	0.023	0.023	0.000	5.16E-04	0.025	0.025	0.0	100.0	2.00
		July2007	7	0.303	0.040	0.004	0.004	0.000	1.08E-04	0.008	0.008	0.0	100.0	1.22
		Aug2007	2	0.258	0.041	0.001	0.001	0.000	1.83E-05	0.002	0.002	0.0	100.0	0.14
ESL5	Cascade	June2008	6	1.821	0.110	0.335	0.084	0.251	6.64E-03	0.161	0.054	74.9	25.1	2.00
		July2008	4	2.111	0.075	0.287	0.037	0.251	5.24E-03	0.133	0.036	87.2	12.8	1.07
		July2007	3	0.659	0.045	0.255	0.004	0.251	5.27E-03	0.117	0.006	98.3	1.7	0.42

ESL6	Plane-Bed	Aug2007	3	1.846	0.042	0.270	0.019	0.251	5.48E-03	0.132	0.023	93.0	7.0	0.62
		June2008	2	1.587	0.118	0.044	0.044	0.000	2.30E-03	0.066	0.066	0.0	100.0	0.08
		July2008	2	1.221	0.111	0.034	0.034	0.000	1.88E-03	0.053	0.053	0.0	100.0	0.09
ESL7	Cascade	July2007	2	0.598	0.091	0.016	0.016	0.000	8.81E-04	0.024	0.024	0.0	100.0	0.02
		Aug2007	none	none	none	0.000	0.000	0.000	0.00E+00	0.000	0.000	0.0	0.0	0.00
		June2008	14	1.173	0.071	0.069	0.069	0.000	1.04E-03	0.051	0.051	0.0	100.0	2.90
		July2008	10	1.350	0.055	0.026	0.026	0.000	3.64E-04	0.024	0.024	0.0	100.0	1.75
		July2007	8	1.454	0.042	0.015	0.015	0.000	2.37E-04	0.018	0.018	0.0	100.0	1.35
ESL8	Step-Pool	Aug2007	2	1.414	0.058	0.017	0.017	0.000	2.87E-04	0.012	0.012	0.0	100.0	1.78
		June2008	12	1.381	0.086	0.502	0.153	0.349	5.18E-03	0.141	0.050	69.5	30.5	3.62
		July2008	8	1.227	0.079	0.391	0.042	0.349	3.96E-03	0.110	0.020	89.2	10.8	3.01
		July2007	7	1.496	0.066	0.397	0.048	0.349	4.63E-03	0.129	0.026	88.0	12.0	2.73
ESL9	Step-Pool	Aug2007	1	0.281	0.050	0.350	0.001	0.349	3.82E-03	0.097	0.001	99.8	0.2	0.14
		June2008	3	1.997	0.118	0.304	0.071	0.233	6.69E-03	0.188	0.051	76.6	23.4	2.18
		July2008	3	1.997	0.071	0.260	0.028	0.233	6.01E-03	0.173	0.030	89.3	10.7	1.10
		July2007	3	1.997	0.061	0.250	0.017	0.233	6.10E-03	0.176	0.026	93.0	7.0	0.92
FC1	Step-Pool	Aug2007	1	1.122	0.048	0.235	0.002	0.233	5.51E-03	0.149	0.004	99.1	0.9	0.24
		June2008	1	1.454	0.070	0.006	0.006	0.000	1.23E-04	0.007	0.007	0.0	100.0	0.37
		July2008	none	none	none	0.000	0.000	0.000	0.00E+00	0.000	0.000	0.0	0.0	0.00
		July2007	none	none	none	0.000	0.000	0.000	0.00E+00	0.000	0.000	0.0	0.0	0.00
FC2	Step-Pool	Aug2007	none	none	none	0.000	0.000	0.000	0.00E+00	0.000	0.000	0.0	0.0	0.00
		June2008	3	0.413	0.096	0.055	0.028	0.028	2.36E-03	0.071	0.029	49.8	50.2	0.50
		July2008	2	0.405	0.087	0.035	0.008	0.028	1.75E-03	0.063	0.014	78.5	21.5	1.12
		July2007	1	0.579	0.138	0.036	0.009	0.028	1.71E-03	0.060	0.013	76.1	23.9	1.14

FC3	Step-Pool	Aug2007	1	0.579	0.050	0.029	0.001	0.028	1.69E-03	0.063	0.006	96.0	4.0	0.95
		June2008	6	0.459	0.075	0.174	0.015	0.159	6.10E-03	0.224	0.026	91.2	8.8	1.58
		July2008	2	0.577	0.059	0.164	0.005	0.159	8.09E-03	0.292	0.014	96.8	3.2	0.34
		July2007	2	0.577	0.059	0.164	0.005	0.159	6.75E-03	0.244	0.011	96.8	3.2	0.34
FC4	Step-Pool	Aug2007	1	0.881	0.085	0.164	0.005	0.159	1.02E-02	0.365	0.015	97.0	3.0	0.27
		June2008	2	0.732	0.210	0.183	0.007	0.176	5.90E-03	0.175	0.017	96.1	3.9	0.65
		July2008	2	0.732	0.120	0.179	0.002	0.176	6.49E-03	0.188	0.009	98.7	1.3	0.38
		July2007	2	0.732	0.111	0.177	0.001	0.176	6.45E-03	0.185	0.006	99.4	0.6	0.23
FC5	Cascade	Aug2007	1	1.446	0.021	0.177	0.001	0.176	7.38E-03	0.209	0.004	99.7	0.3	0.18
		June2008	1	0.554	0.053	0.099	0.001	0.097	7.25E-03	0.149	0.007	98.8	1.2	0.14
		July2008	1	0.364	0.015	0.097	0.000	0.097	8.74E-03	0.174	0.002	99.9	0.1	0.03
		July2007	1	0.364	0.015	0.097	0.000	0.097	8.37E-03	0.167	0.002	99.9	0.1	0.03
FC6	Cascade	Aug2007	none	none	none	0.097	0.000	0.097	9.20E-03	0.182	0.000	100.0	0.0	0.00
		June2008	2	0.516	0.044	0.011	0.002	0.010	5.44E-04	0.024	0.007	86.4	13.6	1.49
		July2008	2	0.492	0.024	0.010	0.000	0.010	5.30E-04	0.022	0.004	95.6	4.4	0.92
		July2007	2	0.492	0.024	0.010	0.000	0.010	5.68E-04	0.024	0.004	95.6	4.4	0.95
		Aug2007	2	0.610	0.008	0.010	0.000	0.010	6.58E-04	0.026	0.002	99.4	0.6	0.26

9.6 Appendix F: Plan view of each reach showing location of large boulders and cobbles used to calculate ff_{grain} with the drag approach

ESL1

$ff_{grain} = 0.46$ (Jun08), 3.58 (Aug07)

$\Gamma = 0.028$ to 0.037

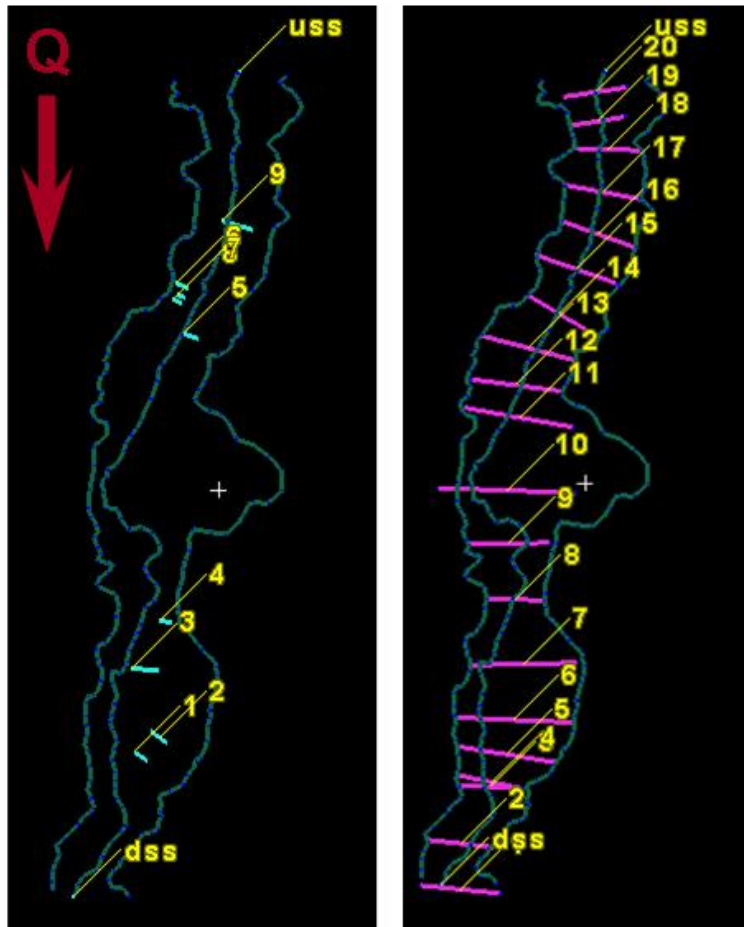


Figure 106: Plan view of ESL1 showing each boulder measured for the drag approach and for calculating the boulder concentration (left). The value of ff_{grain} shown above was calculated using the drag approach. The cross-sections on the right indicate the locations where the reach was traversed for pebble counts, which are shown in Appendix D.

ESL2

$ff_{grain} = 0.09$ (Jun08), 3.64 (Aug07)

$\Gamma = 0.032$ to 0.038

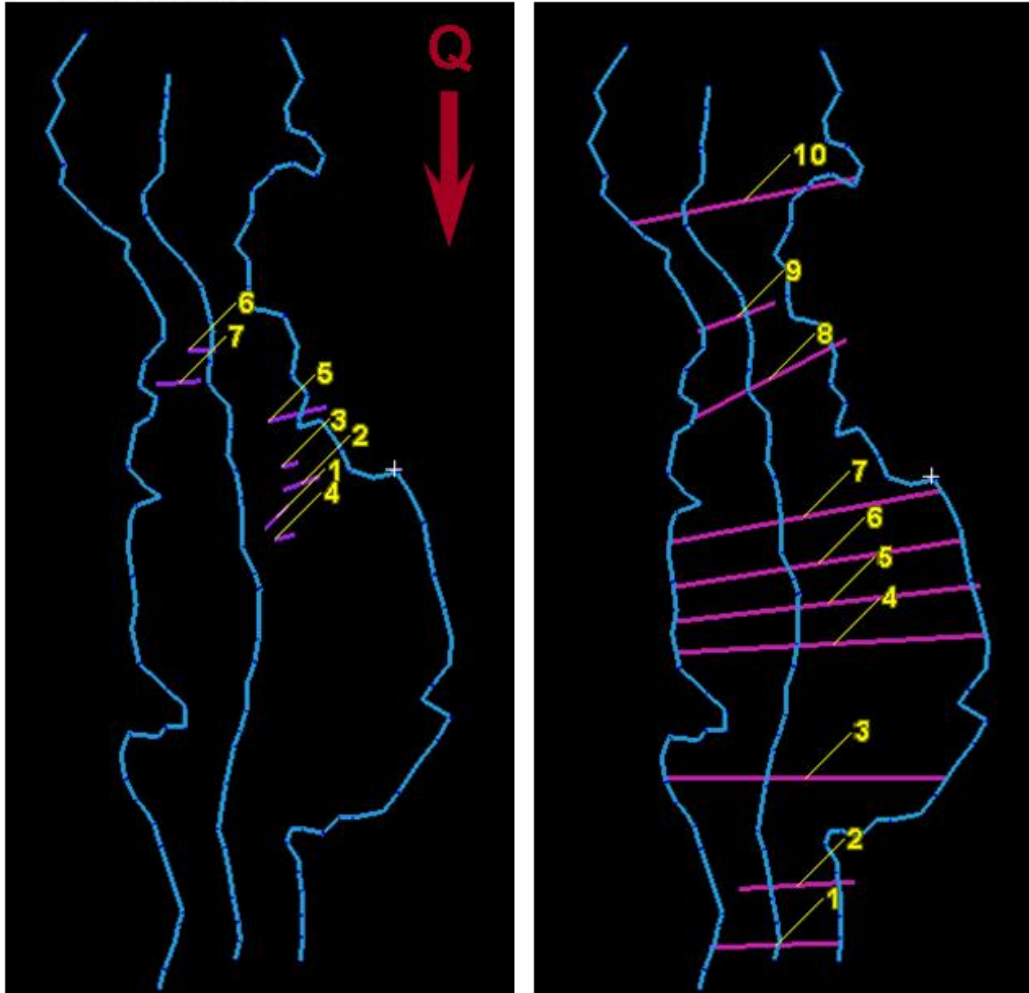


Figure 107: ESL2 boulders (left) and pebble count cross-sections (right)

ESL3

$ff_{grain} = 0.29$ (Jun08), 2.62 (Aug07)

$\Gamma = 0.163$ to 0.222

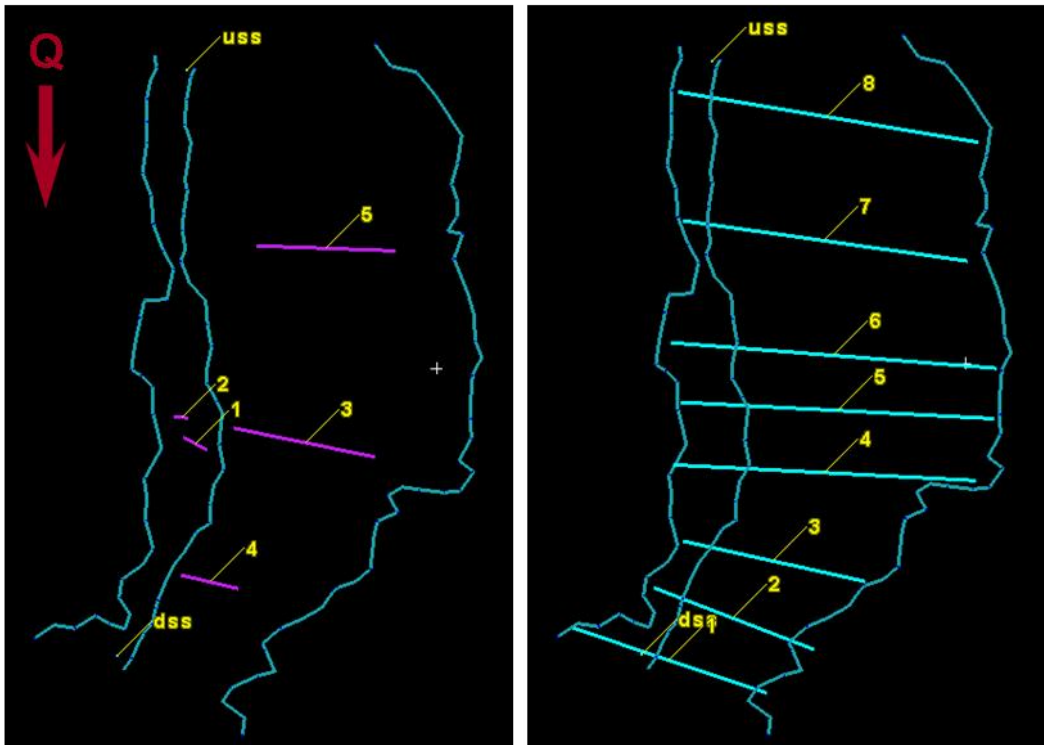


Figure 108: ESL3 boulders (left) and pebble count cross-sections (right)

ESL4

$ff_{grain} = 0.08$ (Jun08), 1.73 (Aug07)

$\Gamma = 0.037$ to 0.043

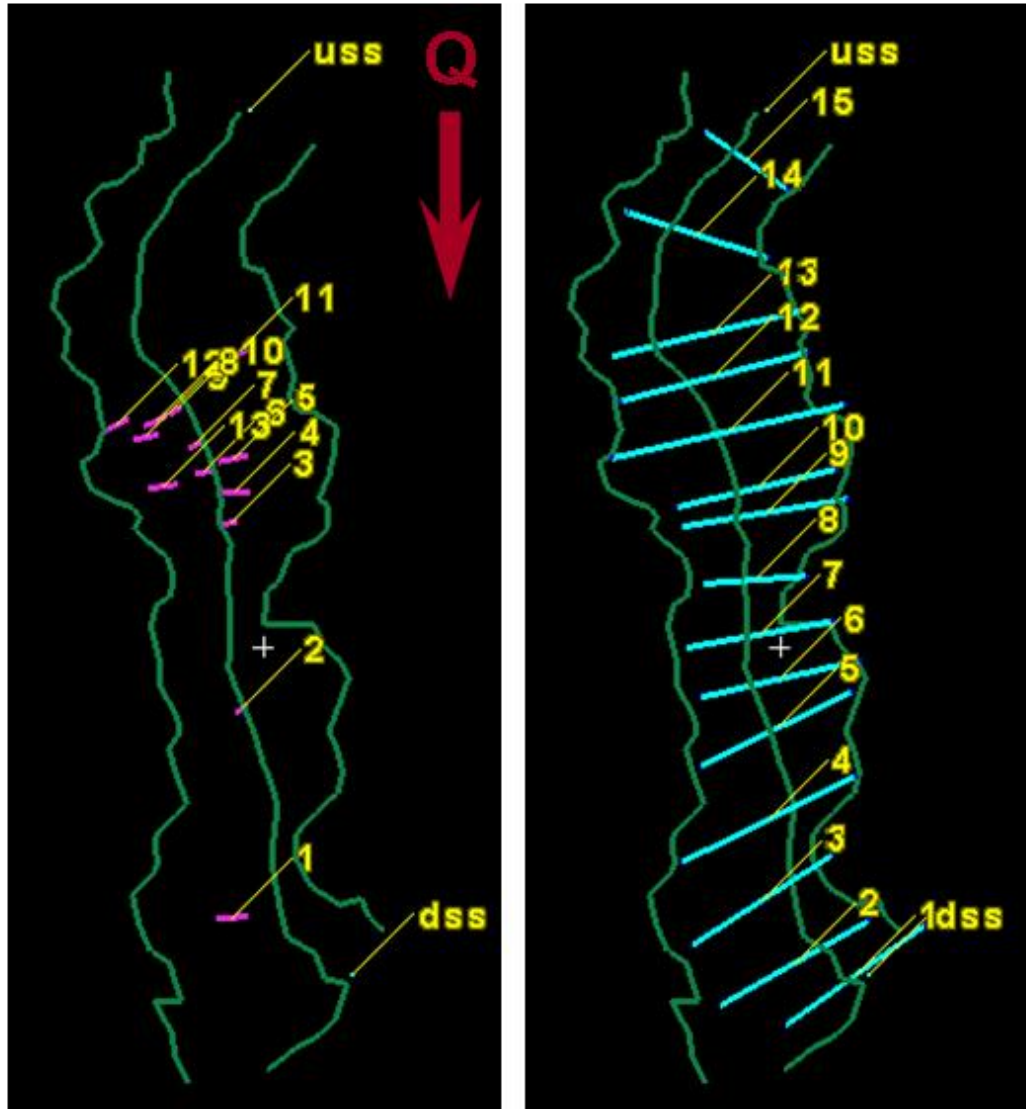


Figure 109: ESL4 boulders (left) and pebble count cross-sections (right).

ESL5

$ff_{grain} = 0.64$ (Jun08), 4.35 (Aug07)

$\Gamma = 0.065$ to 0.068

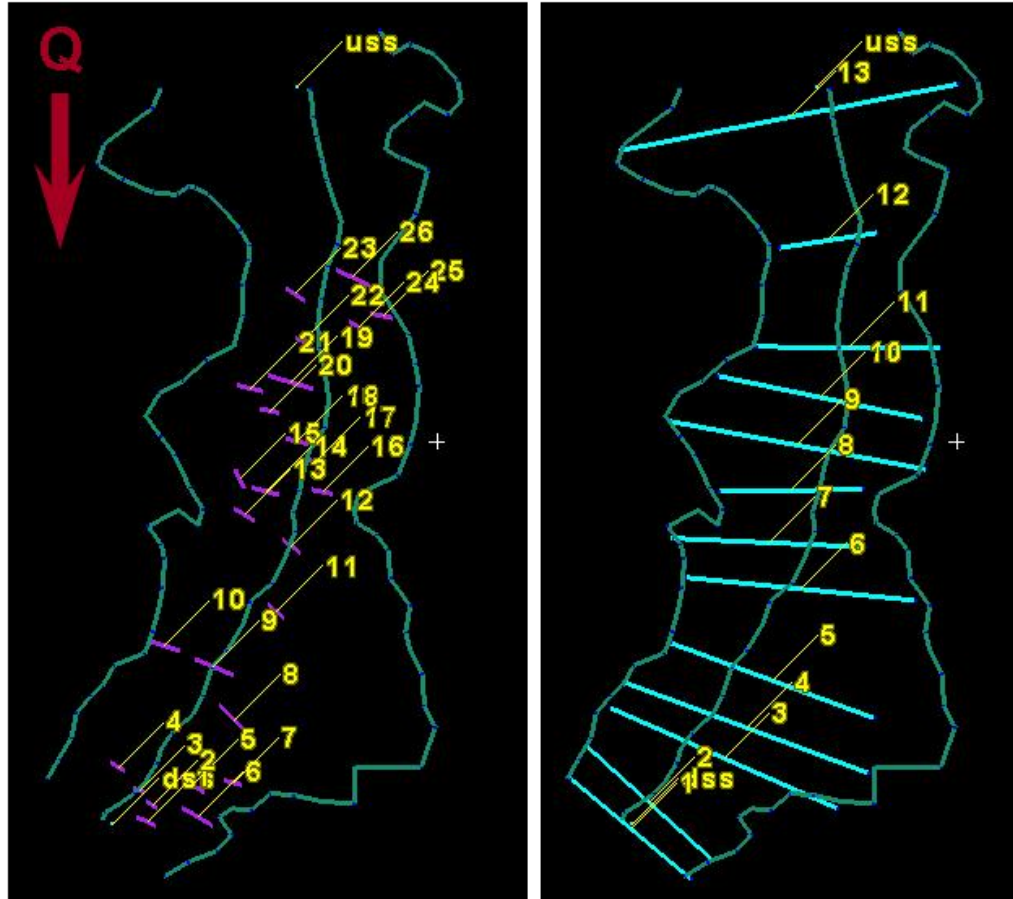


Figure 110: ESL5 boulders (left) and pebble count cross-sections (right)

ESL6

$ff_{grain} = 0.13$ (Jun08), 0.49 (Aug07)

$\Gamma = 0.020$ to 0.023

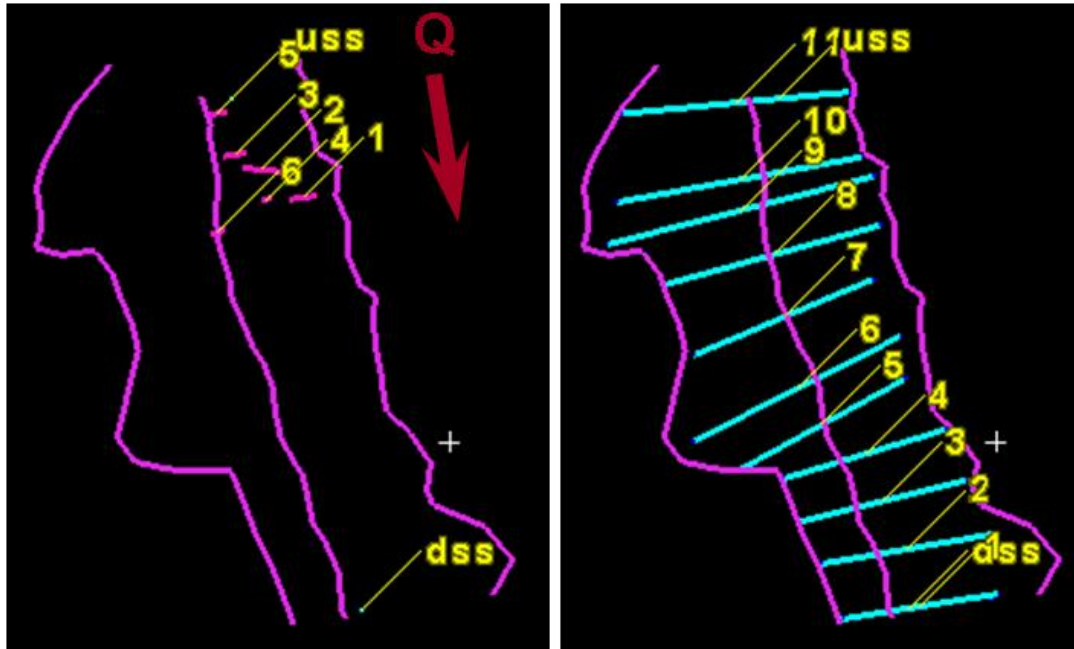


Figure 111: ESL6 boulders (left) and pebble count cross-sections (right)

ESL7

$ff_{grain} = 1.10$ (Jun08), 5.64 (Aug07)

$\Gamma = 0.048$ to 0.056

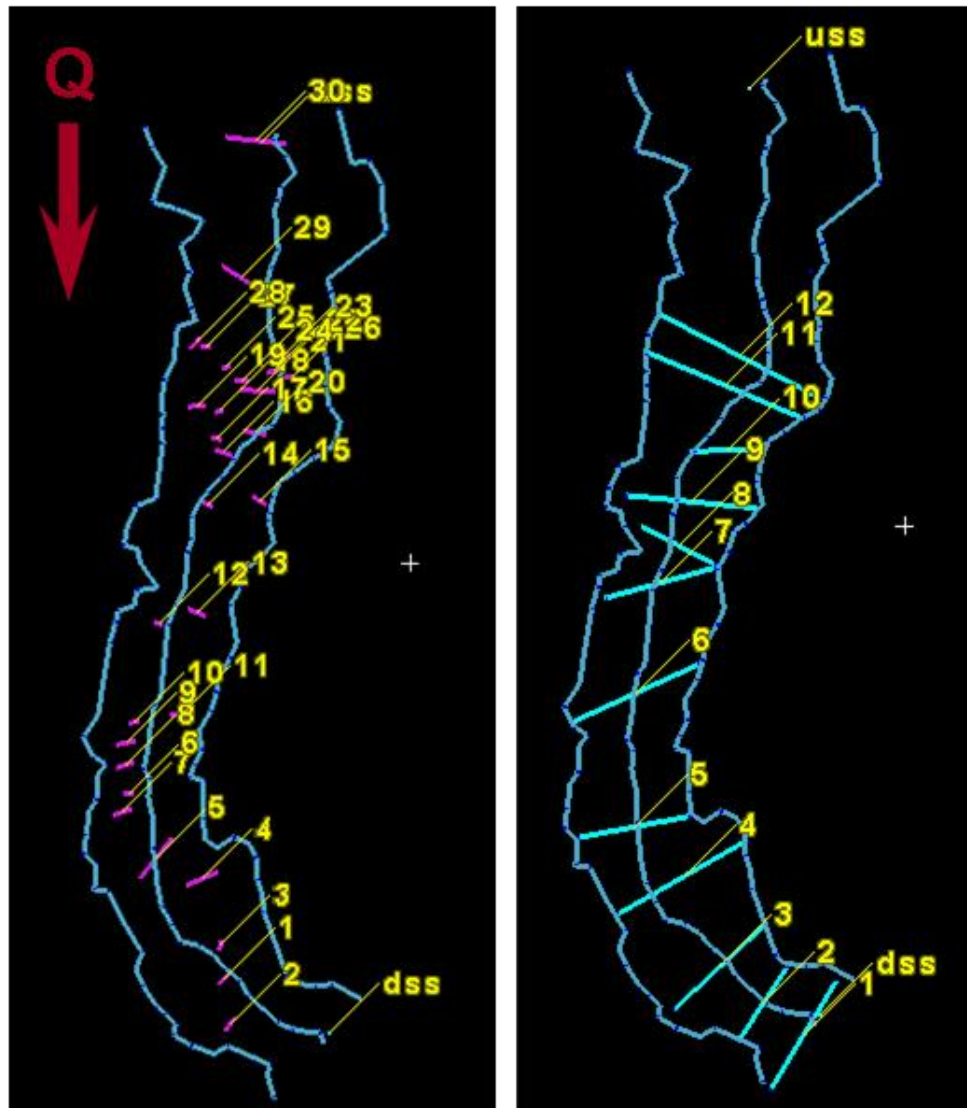


Figure 112: ESL7 boulders (left) and pebble count cross-sections (right)

ESL8

$ff_{grain} = 0.76$ (Jun08), 4.15 (Aug07)

$\Gamma = 0.027$ to 0.031

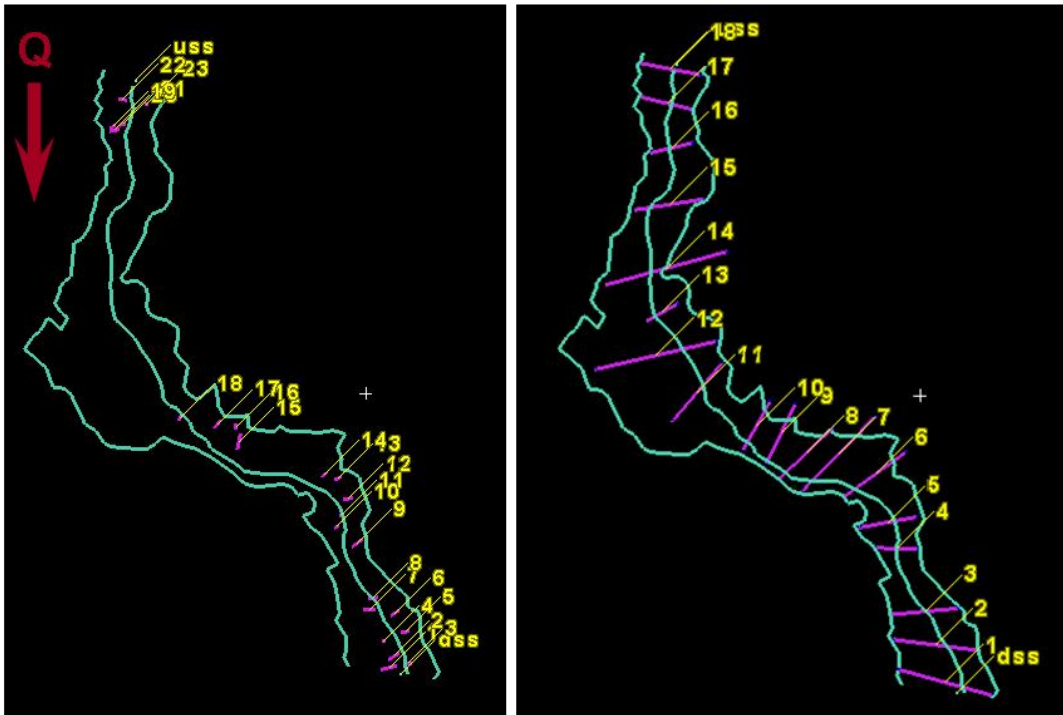


Figure 113: ESL8 boulders (left) and pebble count cross-sections (right)

ESL9

$ff_{grain} = 1.01$ (Jun08), 10.07 (Aug07)

$\Gamma = 0.083$ to 0.092

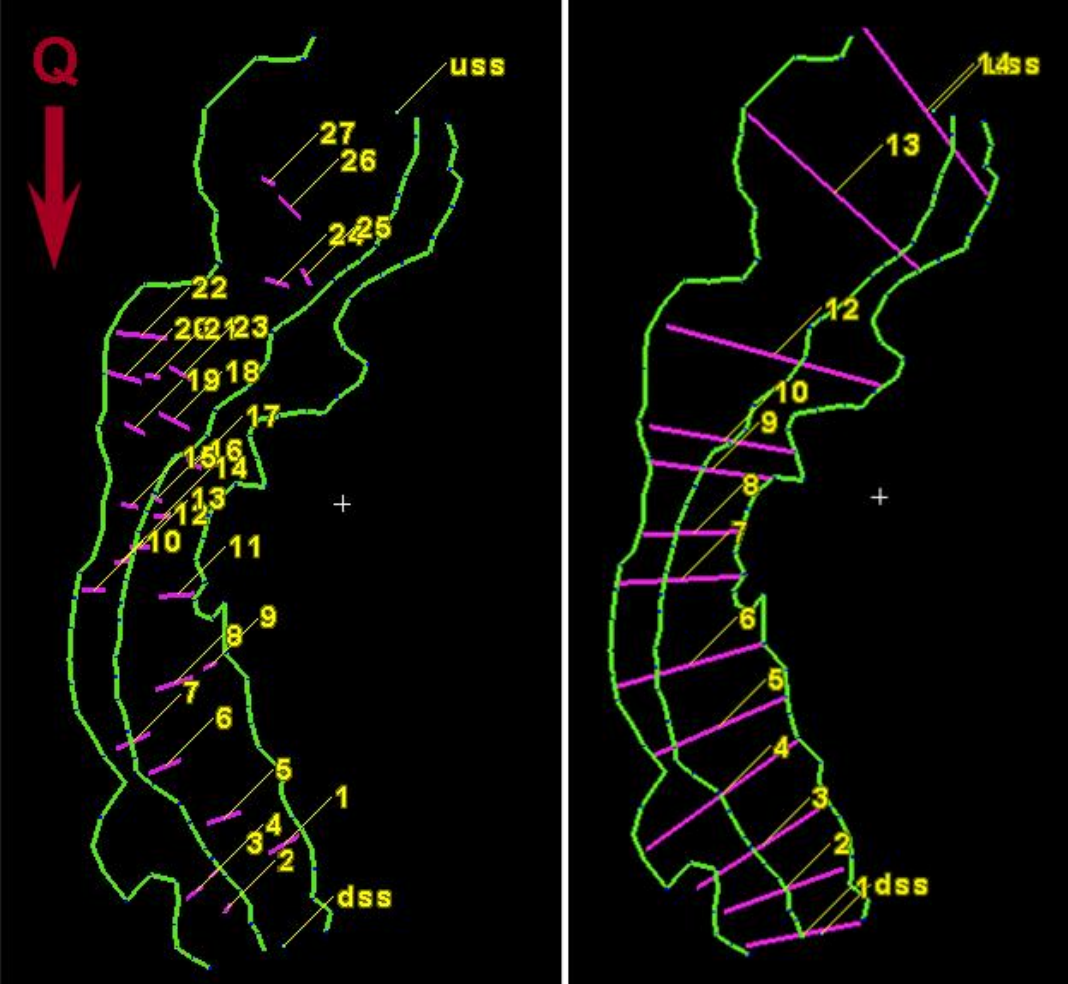


Figure 114: ESL9 boulders (left) and pebble count cross-sections (right)

FC1

$ff_{grain} = 0.07$ (Jun08), 0.51 (Aug07)

$\Gamma = 0.007$ to 0.009

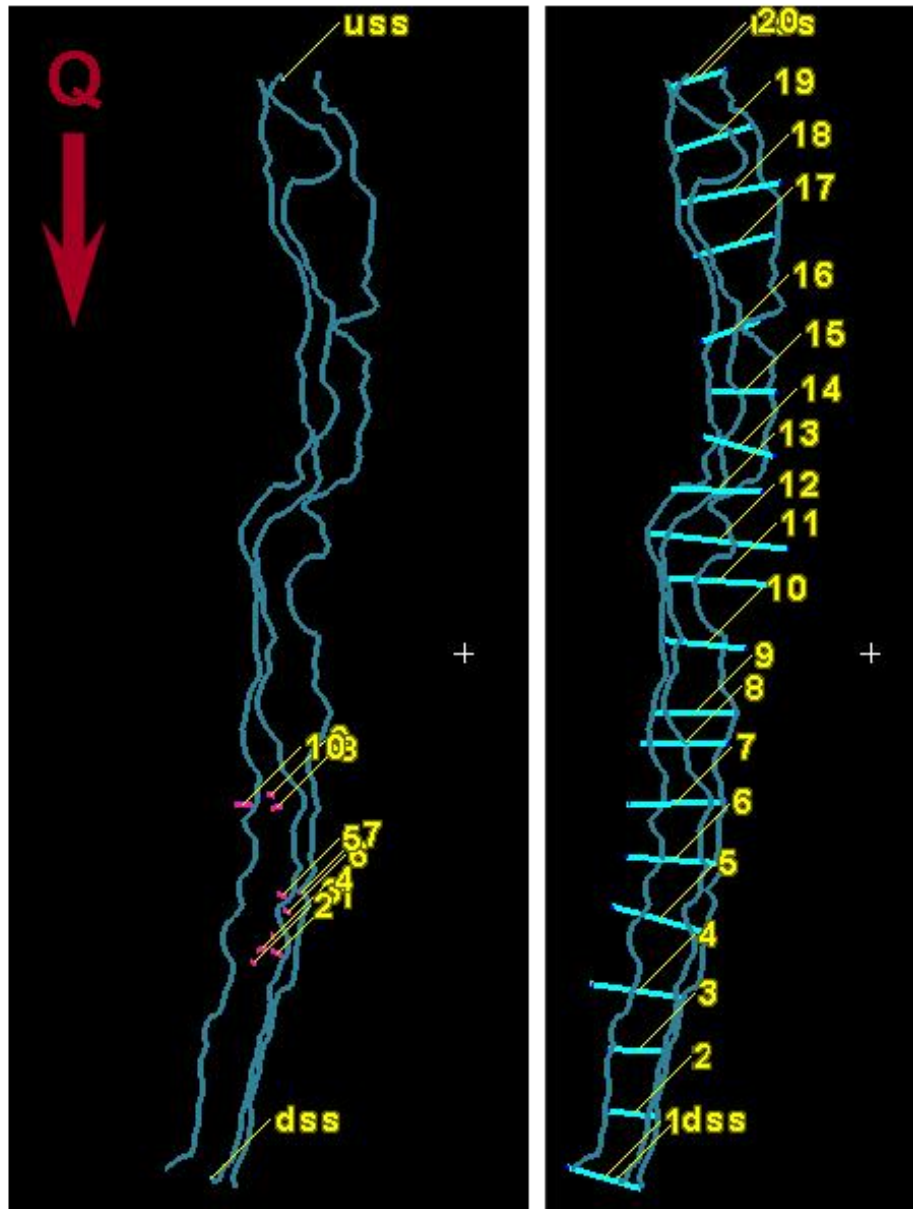


Figure 115: FC1 boulders (left) and pebble count cross-sections (right)

FC2

$ff_{grain} = 0.46$ (Jun08), 0.74 (Aug07)

$\Gamma = 0.019$ to 0.026

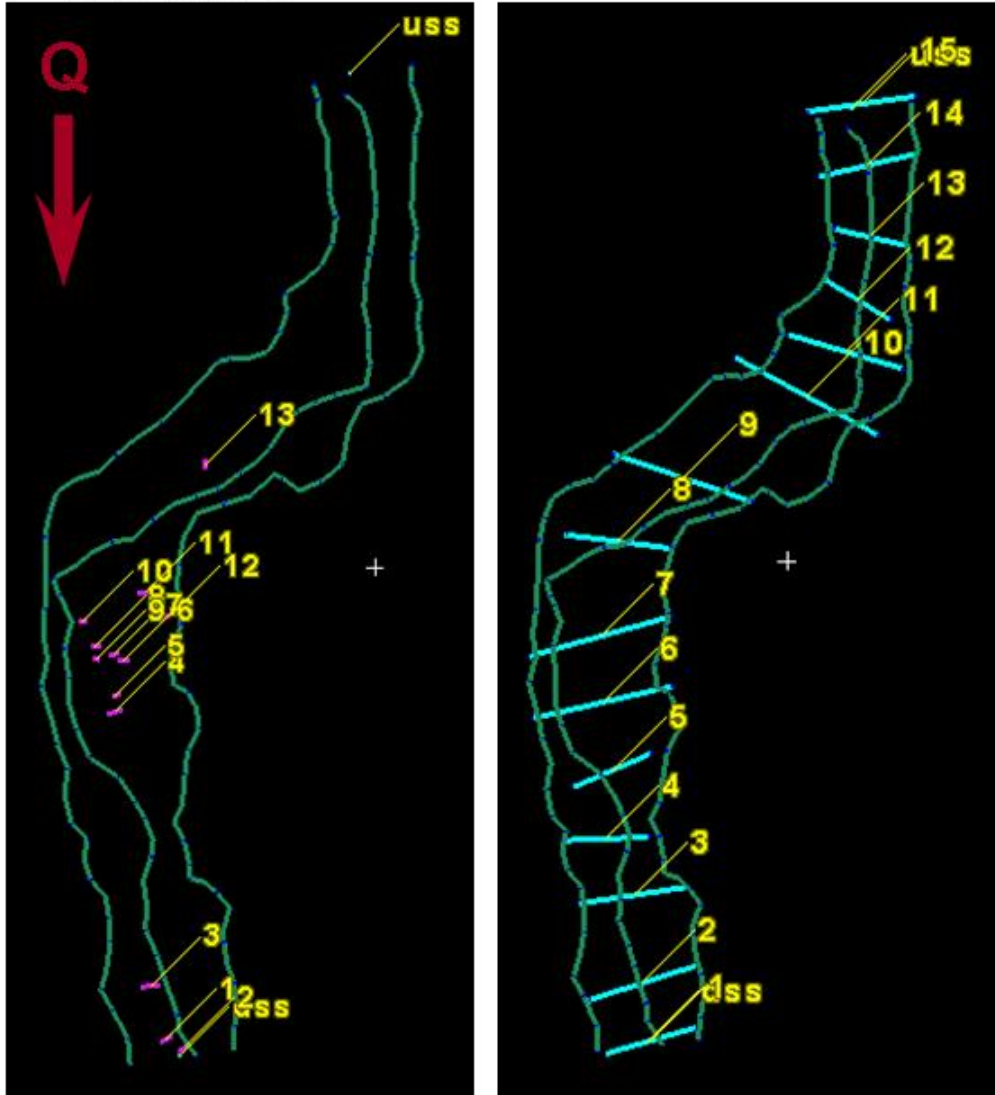


Figure 116: FC2 boulders (left) and pebble count cross-sections (right)

FC3

$ff_{grain} = 0.17$ (Jun08), 1.37 (Aug07)

$\Gamma = 0.008$ to 0.014

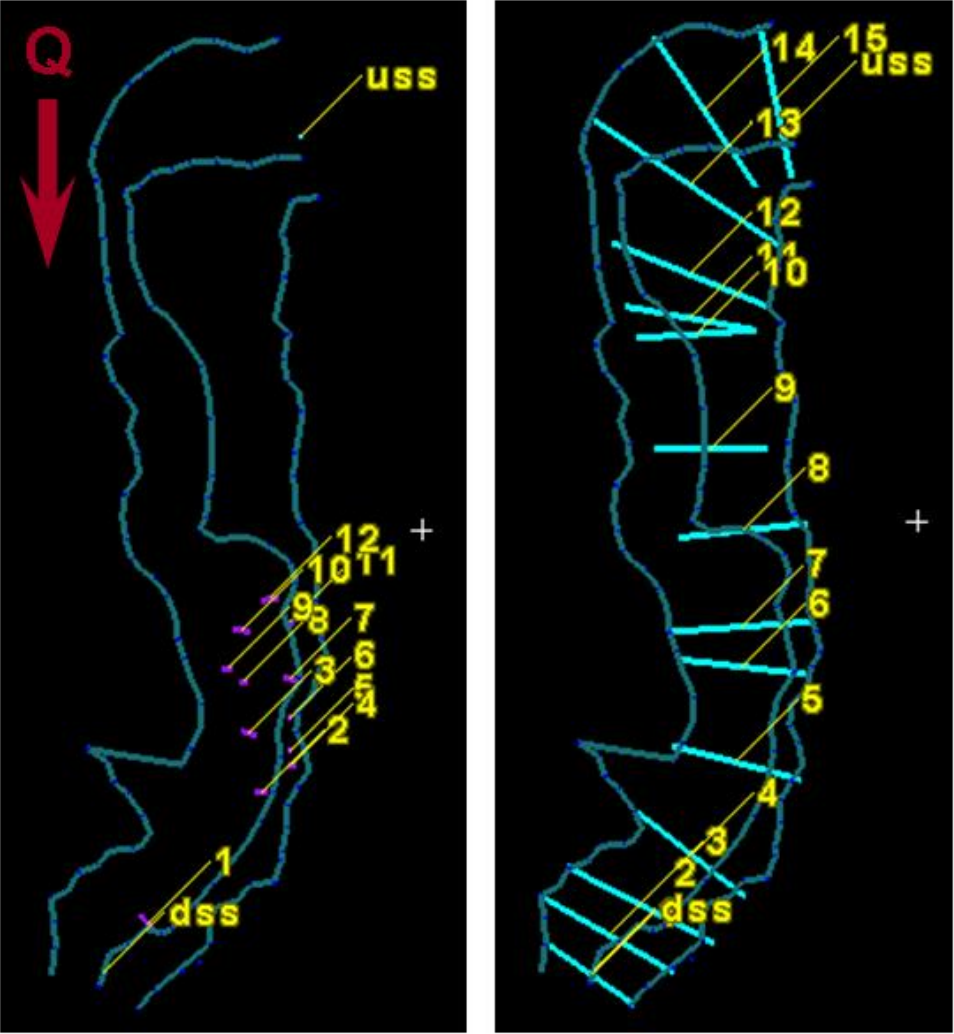


Figure 117: FC3 boulders (left) and pebble count cross-sections (right)

FC4

$ff_{grain} = 1.08$ (Jun08), 5.35 (Aug07)

$\Gamma = 0.050$ to 0.064

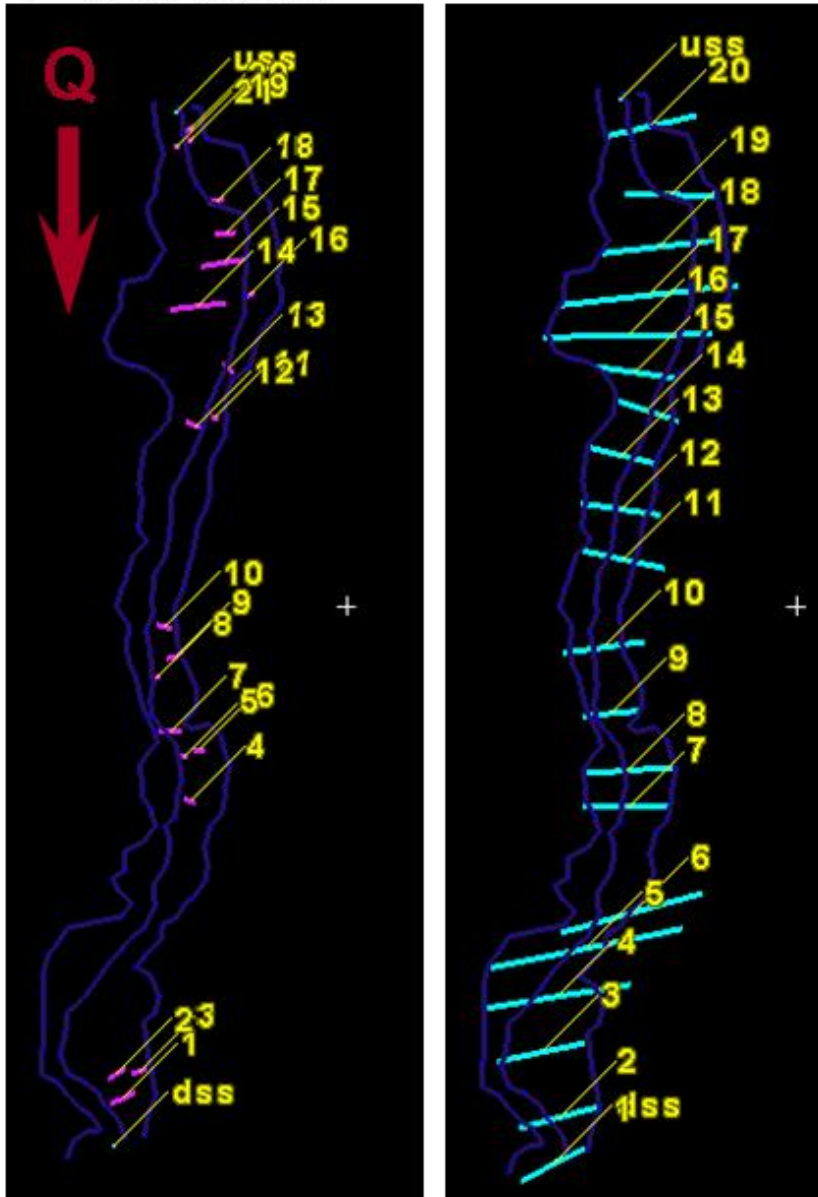
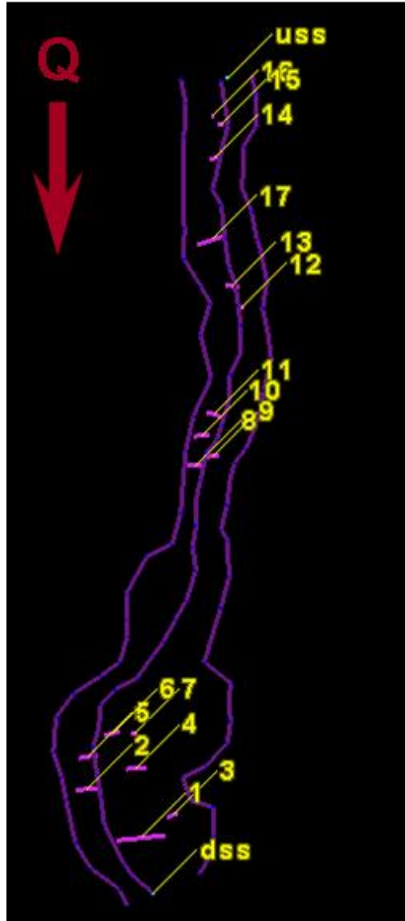


Figure 118: FC4 boulders (left) and pebble count cross-sections (right)

FC5

$ff_{grain} = 1.00$ (Jun08), 4.54 (Aug07)

$\Gamma = 0.050$ to 0.064



FC6

$ff_{grain} = 1.00$ (Jun08), 8.28 (Aug07)

$\Gamma = 0.049$ to 0.068

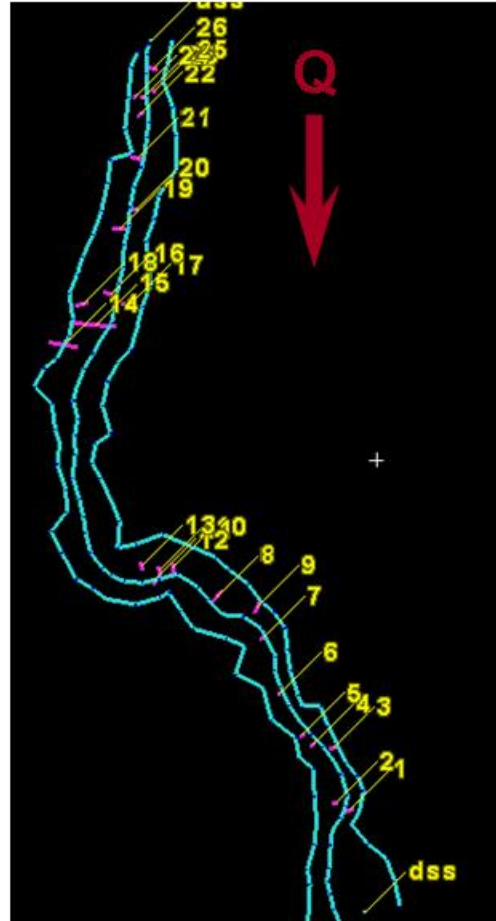


Figure 119: Plan view of FC5 (right) and FC6 (left) showing each boulder measured for the drag approach and for calculating the boulder concentration. Cross sections were not used for pebble counts in these reaches, since the reaches were so small that almost every pebble was counted.

9.7 Appendix F: Longitudinal Profiles and plan view of thalweg for East St. Louis, Lower Fool Creek, and Upper Fool Creek

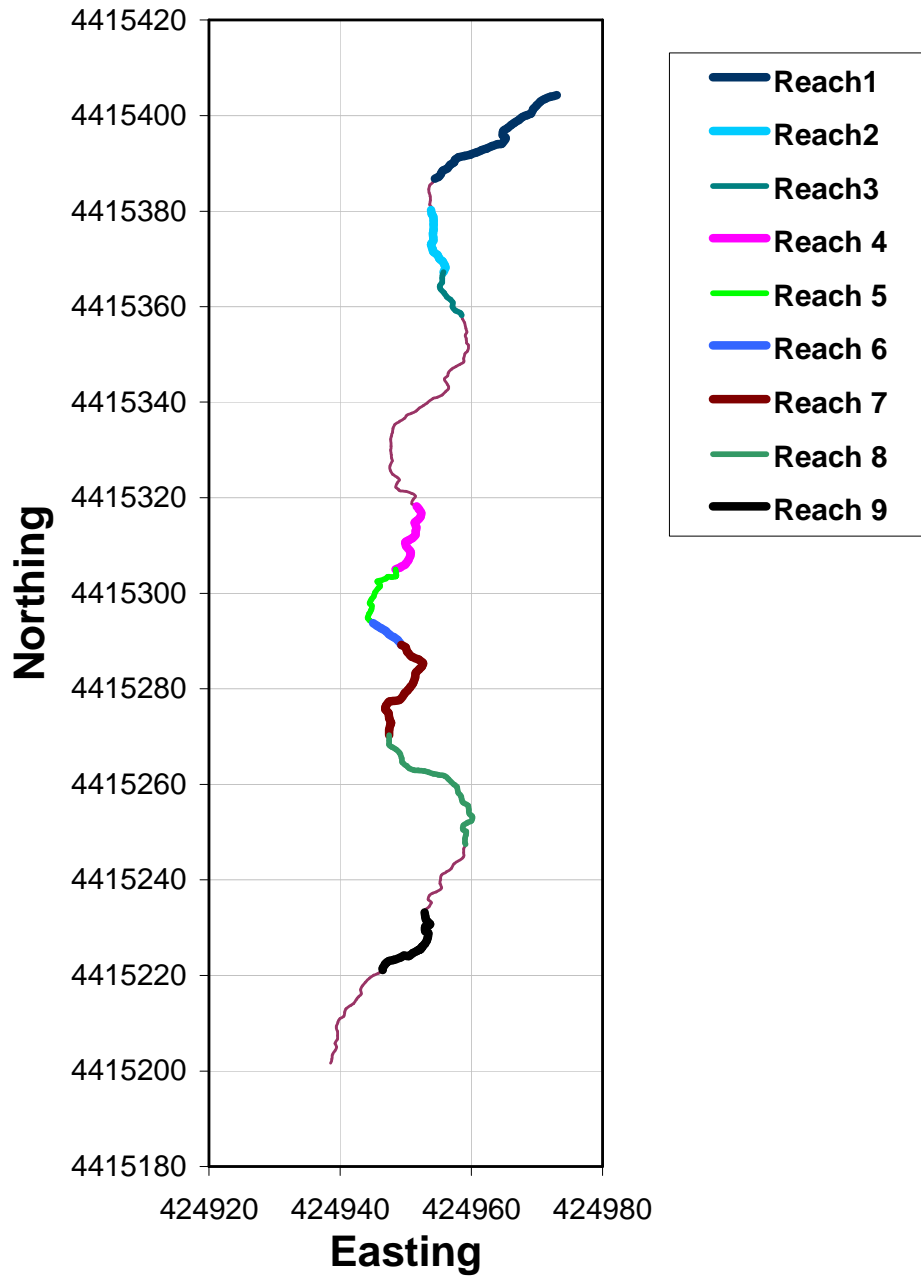


Figure 120: Plan view of thalweg trace of East.St. Louis Creek showing the location of ESL1 to ESL9.

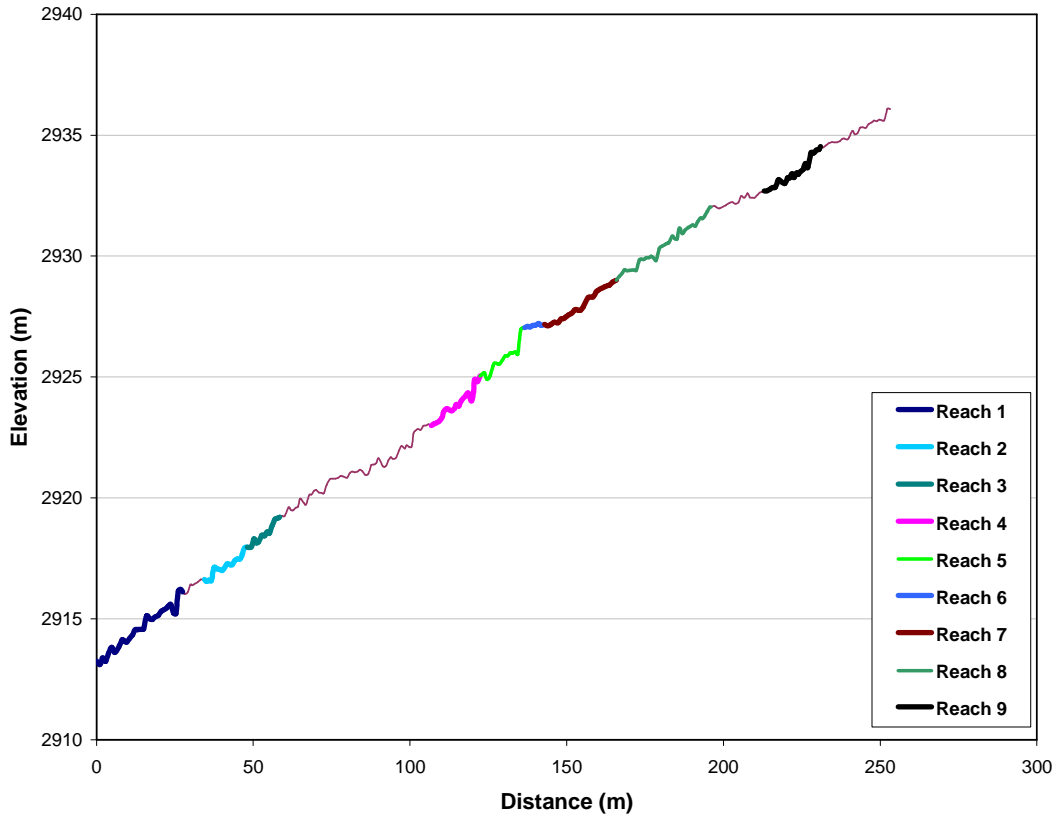


Figure 121: Longitudinal profile of East St. Louis Creek. Points were collected every 0.5 to 1 m.

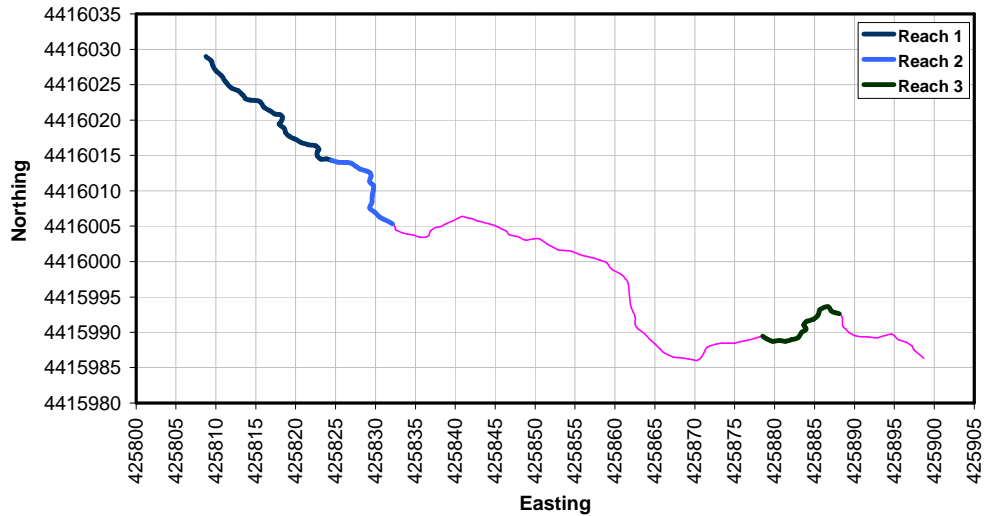


Figure 122: Plan view of thalweg trace of Lower Fool Creek showing the location of FC1 to FC3. FC4 is much further upstream from these reaches.

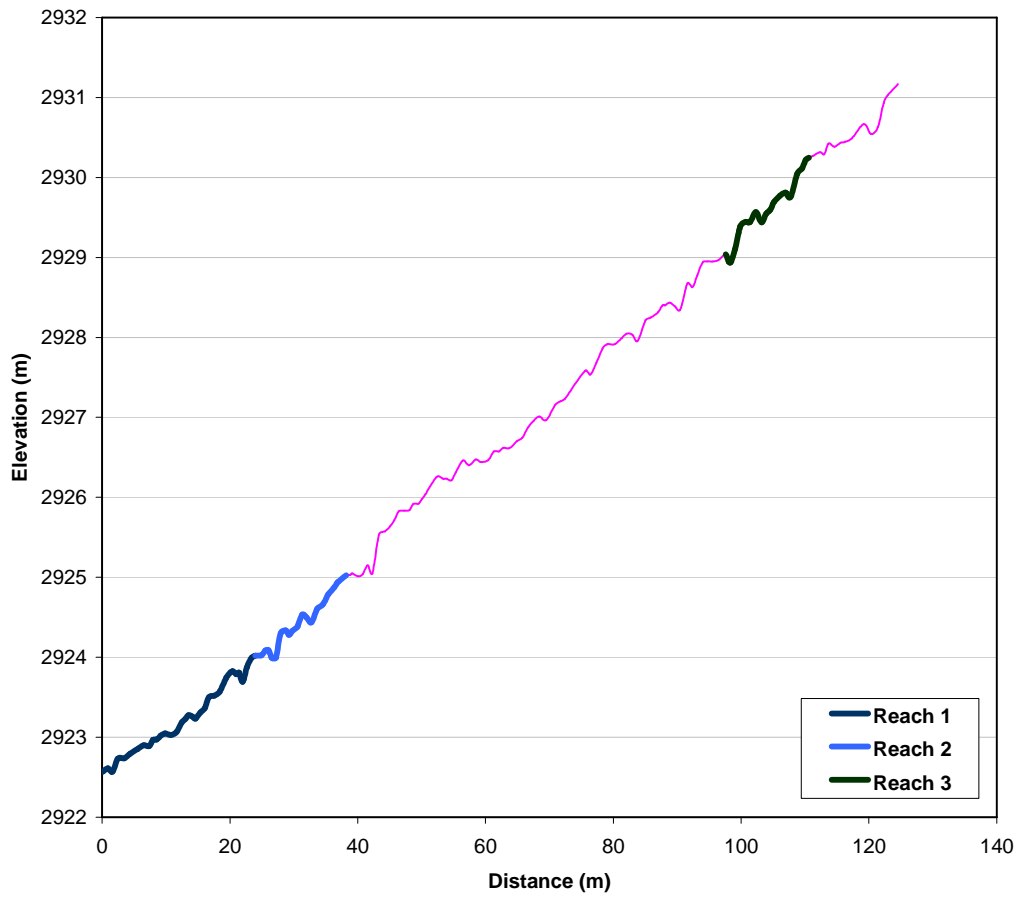


Figure 123: Corresponding longitudinal profile of Lower Fool Creek.

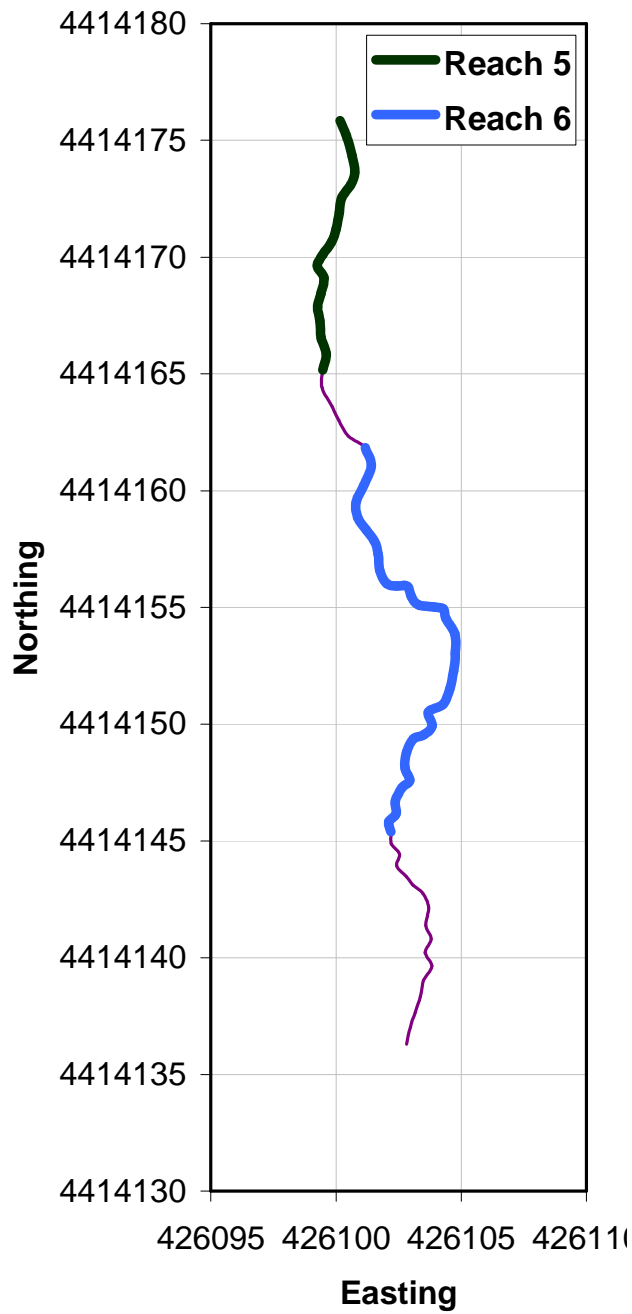


Figure 124: Plan view of Upper Fool Creek, showing the locations of FC5 and FC6.

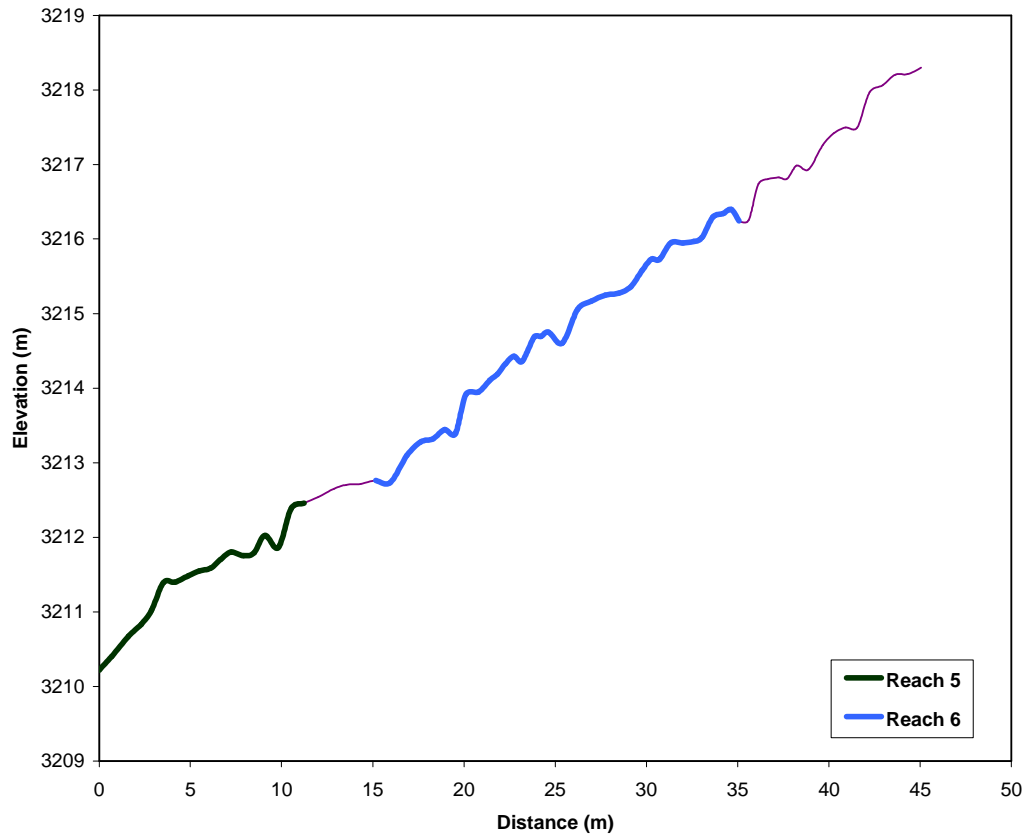


Figure 125: Corresponding longitudinal profile for Upper Fool Creek.